Transition Metal Complexes with Imine-phenolate and Imino-benzosemiquinone Ligands; Synthesis, Characterization and Their Catalytic Reactivity

Dissertation for the degree of
Doktor der Naturwissenschaft
in the Fakultät für Naturwissenschaften
(Department Chemie)
at the Universität Paderborn

presented by

Soumen Mukherjee

Mülheim an der Ruhr 2003

To my Parents

Knowledge, the object of knowledge
and the knower are the three factors
which motivate action; the senses,
the work and the doer comprise the
threefold basis of action.

" *Bhagavad Gita* "

This work was independently carried out between December 1999 and July 2003 at the **Max-Planck-Institut für Bioanorganische Chemie,** Mülheim an der Ruhr, Germany.

Papers published:

1. S. Mukherjee, T. Weyhermüller, E. Bothe, K. Wieghardt , P. Chaudhuri;
Single-atom O-bridged Urea in a Dinickel(II) Complex together with Ni^{II}_4, Cu^{II}_2 and Cu^{II}_4 Complexes of a Pentadentate Phenol-containing Schiff Base with (O,N,O,N,O)-Donor Atoms.
Eur. J. Inorg. Chem. **2003**, 863.

2. S. Mukherjee, T. Weyhermüller, E. Bothe, P. Chaudhuri;
Structural, Magnetochemical and Electrochemical Studies of Dinuclear Complexes Containing the $[V^{V}O]_2$, $[V^{IV}O]_2$, Cr^{III}_2, Mn^{III}_2 and Fe^{III}_2 Cores of a Potentially Pentadentate Phenol-Containing Ligand with (O,N,O,N,O)-Donor Atoms.
Eur. J. Inorg. Chem. **2003**, 1956.

3. S. Mukherjee, E. Rentschler, T. Weyhermüller, K. Wieghardt , P. Chaudhuri;
A unique series of dinuclear transition metal-polyradical complexes with a m-phenylenediamine spacer and their catalytic reactivity.
Chem. Comm., **2003**, 1828.

4. S. Mukherjee, T. Weyhermüller, K. Wieghardt, P. Chaudhuri
The Molecular and Electronic Structure of $[Fe^{III}_2(^{t\text{-}bu}L^{ISQ})_4(\mu\text{-}O)]$ - a Dinuclear Ferric Complex Containing Four, *O,N*-Coordinated *o*-Iminobenzosemiquinonate(1-) π Radical Anions
Dalton Trans., **2003**, 3483.

Examination Committee:

Prof. Dr. N. Risch
Prof. Dr. K. Huber
Prof. Dr. G. Henkel
Prof. Dr. P. Chaudhuri

Examination: 31st October, 2003.

Acknowledgements

I would like to acknowledge everyone who extended their support and help during the course of this work. My deep sense of gratitude goes to:

- Prof. Dr. P. Chaudhuri, for his encouragement, invaluable guidance, frequent suggestions, continuous support and hour-long discussions.
- Prof. Dr. K. Wieghardt, for the opportunity of working in his research group and providing with all needed laboratory facilities.
- Dr. T. Weyhermüller and Mrs. H. Schucht for their excellent work with the X-ray crystallography.
- Dr. E. Bothe , Mrs. P. Höfer and Mr. H. Schmidt for their help during electrochemical measurements.
- Dr. E. Rentschler and Dr. U. Schatzschneider for assistance with the fitting of some magnetochemical data.
- Dr. E. Bill, Mr. A. Göbels, Mr. F. Reikowski and Mr. B. Mienert for discussions and measurements of EPR, SQUID and Mössbauer spectroscopy.
- Dr. K. Hildenbrand for the measurement and simulation of room temperature EPR.
- Mr. U. Pieper and Mrs. R. Wagner for their help in the laboratory.
- Mrs. U. Westhoff, Mrs. G. Schmidt and Mrs. M. Trinoga for skilful GC and LC analyses.
- Mrs. J. Teurich, Mrs. E. Hollander, Mrs. T. Montenbruck and Mrs. B. Deckers for their helpfulness in general.
- Mr. K. Chlopek, Dr. N. Aliaga-Alcalde, Dr. U. Beckmann, Dr. C. N. Verani, Dr. R. Schumacher, Dr. S. Kimura and Dr. T. Kruse for their interest and friendship during this work.
- Dr. T.K. Paine, Mr. K. Ray, Dr. D. Ray, Mr. S. Khanra, Mrs. R. Kapre and Mr. S. Kinge for a nice atmosphere in- and outside the laboratory.
- My parents for their constant inspiration and encouragement.
- Family Basak, Family Göhl, Family Gupta-Nehring, Family Ghosh and Dr. S. Chatterjee for providing a nice atmosphere outside the laboratory.
- Deutsche Forschungsgemeinschaft (DFG) and Max-Planck-Gesellschaft (MPG) for financial support.

CONTENTS

Abbreviations:

technical terms:

aCU: antiferromagnetic coupler

AF : antiferromagnetic

Ag / $AgNO_3$: reference electrode

av. : average

B : magnetic field

CT : charge transfer

D : zero-field splitting

deg. : degree (°)

e^- : electron

E : total energy

E.C. : enzyme classification

EHMO : extended Hückel molecular orbital

exp. : experimental

fCU: ferromagnetic coupler

F : ferromagnetic

fac. : facial

Fc^+/Fc : internal electrochemical standard

g : Landé factor

H : Hamiltonian

HS /h.s: high spin

I : nuclear spin

IS : intermediate spin

J : coupling constant (cm^{-1})

LS : low spin

m/z : mass per charge

$[M]^+$: molecular ion peak

M : molar magnetization

m- : meta-

mer.: meridional

MP : melting point

PI : paramagnetic impurity

RT : room temperature (293K)

S : electron spin

SCE : standard calomel electrode

sh. : shoulder

sim. : simulated

TIP : temperature independent paramagnetism

TON : turnover number

techniques:

CV : cyclic voltammetry

EA : elemental analysis

EI : electron ionisation

EPR : electron paramagnetic resonance

ESI : electrospray ionization

FTIR : Fourier transform infrared spectroscopy

GC : gas chromatography

HPLC : high performance liquid chromatography

IR : infrared spectroscopy

LC : liquid chromatography

MS: mass spectroscopy

NMR : nuclear magnetic resonance

OTTLE : optically transparent thin layer electrochemical

SQUID : superconducting quantum interface device

SQW : square wave voltammetry

UV-Vis : ultraviolet-visible spectroscopy

XRD : X-Ray Diffractometry

units:

Å : angstrom (10^{-10} m)

cm : centimeter

emu : electromagnetic unit

G : gauss

h : hour

K : Kelvin

m : meter

M : molar

min. : minute

mm : millimeter

nm : nanometer (10^{-9} m)

ppm : part per million

s : second

T : tesla

V : volts

μ_B : bohr magnetron

latin expressions:

ca. : around

et al : and coworkers

e.g. : for example

i.e. : that is

tert- : tertiary

vs. : versus, against

viz. namely

symbols:

λ : wavelength (nm)

ε : extinction coefficient ($M^{-1}cm^{-1}$)

θ : Theta- Weiss parameter

IS : isomer shift (mms^{-1})

μ_{eff} : magnetic moment (μ_B)

ΔE_Q : quadrupole splitting (mm/s)

δ : isomer shift (mm/s)

solvents and reagents:

Bu_4NOMe : tetrabutylammoniummethoxide

cat.: catechol

CH_2Cl_2 : dichloromethane

$CDCl_3$: deuteriated chloroform

DTBP : 2,6-di-tert-butylphenol

3,5-DTBC : 3,5-di-tert-butylcatechol

3,5-DTBQ : 3,5-di-tert-butyl-o-benzoquinone

Et_2O : diethylether

Et_3N : triethylamine

EtOH : ethanol

H_2O_2 : hydrogen peroxide

KBr : potassium bromide

MeCN : acetonitrile

MeOH : methanol

$TBAPF_6$: tetrabutylammonium hexafluorophosphate

THF : tetrahydrofuran

TMS : tetramethylsilane

TTBD : 3,3´-5,5´-Tetra-tert-butyldiphenoquinone

ligands used in this work:

H_3L^1 :- 2,4-Di-tert-butyl-6-[(5-methyl-3H-imidazol-4-ylmethyl)-amino]-phenol

H_3L^2 :- 2,6-Bis-iminomethyl-(4,6-di-tertbutyl-2-iminophenol)-4-methyl-phenol

H_4L^3 :- 1,3-bis-(4,6-di-tert-butyl-2-iminophenol)benzene

H_4L^4 :- 4,4´-bis-(4,6-di-tert-butyl-2-iminophenol)diphenyl methane

$H_2L^{6\text{-}12}$:- 2-(mono- to di- substituted)anilino-4,6-ditert-butylphenol

List of complexes synthesized with their numbers:

$Ni^{II}_4L^1_4$	**(1)**
$Cu^{II}_4L^1_4$	**(2)**
$[Ni^{II}_2 (L^2)(NH_2CONH_2)(OAc)(MeOH)_2]$	**(3)**
$[Ni^{II}_4 (L^2H)_2(OMe)_2(OAc)_2(MeOH)_2]$	**(4)**
$[Cu^{II}_2 L^2 (MeO) (THF)_2]$	**(5)**
$[Cu^{II}_4L^2_2 (\mu_4\text{-}O)]$	**(6)**
$Fe^{III}_2 L^2_2$	**(7)**
$Mn^{III}_2L^2_2$	**(8a)**
$[Mn^{III}_2L^2_2 (THF)_2]$	**(8b)**
$Cr^{III}_2L^2_2$	**(9)**
$[(V^{IV}=O)_2 (\mu\text{-}O^{isoprop}) L^2)]$	**(10)**

$[(V^{V}=O)_2\ L^{2}_{2}]$ **(11)**

$Cu^{II}_{2}L^{3}_{2}$ **(12)**

$Ni^{II}_{2}L^{3}_{2}$ **(13)**

$Co^{III}_{2}L^{3}_{3}$ **(14)**

$Fe^{III}_{2}L^{3}_{3}$ **(15)**

$Mn^{IV}_{2}(L_A{}^{3})_2L^{3}$ **(16)**

$Co^{III}_{2}L^{4}_{3}$ **(17)**

$Mn^{IV}(L_A{}^{6})(L^{6})_2$ **(18)**

$Mn^{IV}(L_A{}^{7})(L^{7})_2$ **(19)**

$Mn^{IV}(L_A{}^{8})(L^{8})_2$ **(20)**

$Mn^{IV}(L_A{}^{9})(L^{9})_2$ **(21)**

$Mn^{IV}(L_A{}^{10})(L^{10})_2$ **(22)**

$Co^{III}(L^{6})_3$ **(23)**

$Fe^{III}(L^{6})_3$ **(24)**

$Fe^{III}(L^{11})_3$ **(25)**

$[Fe^{III}_{2}(\mu\text{-}O)(L^{12})_4]$ **(26)**

Chapter 1

OBJECTIVES AND INTRODUCTION

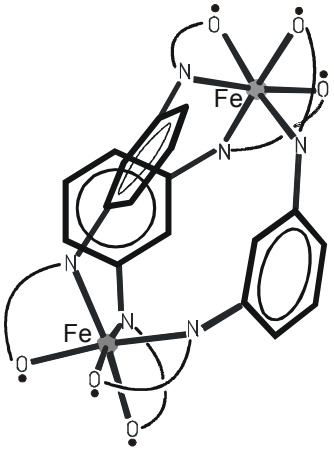

OBJECTIVES AND OUTLINE OF THE THESIS

Two apparently dissimilar subjects viz. molecular magnetism and metal sites in biology are at the center of this thesis. The principles of coordination chemistry e.g. ligand field theory constitute a common ground for molecular magnetism, biomimicking and bioinspired chemistry. Summarily, this thesis describes model complexes both of structural and functional types, for various metalloprotiens containing paramagnetic metal ions, with particular emphasis on the interactions of ligand radicals with transition metal ions using different spectroscopic techniques which help one to learn how nature has employed common transition metals in a number of intriguing catalytic transformations.

This work is divided in five chapters. The first chapter gives an introduction relevant to this work and consists of two parts. The first part (Chapter1) considers the importance of metals and radicals in biology. The importance of ligands as a backbone for metal centers and also as an activation center for catalysis is discussed. A few examples of metalloenzymes, whose structural and functional models are relevant to this thesis, is outlined. The second part (Chapter1) discusses the building up of polynuclear "parallel spin coupled" system using "accidental ferromagnetism" and "planned ferromagnetism" both governed by the common principle of orthogonal orbital overlap.

The second and fourth chapters are relevant to "metallobiochemistry" and the third and fifth chapters to "molecular magnetism". The second chapter deals with the synthesis and characterization of 3d- di- and tetranuclear homometallic complexes bridged by imidazolate, phenolate and urea ligands. Some of the complexes act as structural models for enzymes like the Cu-Zn superoxide dismutase and the dinickel containing enzyme urease. In the fourth chapter, a functional model of the dicopper containing enzyme catechol dioxygenase, which catalyses the oxidation of catechols to quinones , is discussed.

The third chapter concerns the synthesis and characterization of transition metal containing imino-semiquinone radical complexes. All the complexes consists of homodimetallic centers with ***four*** or ***six*** ligand-based radical centers. Here the concept of *spin polarization* was used in an attempt to bring the metal or radical centers in spin aligned arrangement i.e. coupling between the metal-metal or radical-radical centers are **ferromagnetic**. Continuing with polyradical based metal complexes the fifth chapter highlights the effect of substitution at different position in tuning the spin ground state of a metal center. The complexes synthesized are mono- and dinuclear with ***three*** or ***four*** imino-benzosemiquinone radicals.

1.1 METALS AND RADICALS IN BIOLOGICAL SYSTEMS

One of the major roles played in biochemistry is by the *metalloenzymes*. Metalloenzymes are those enzymes, which require a metal center not only as an active site to function but bind that metal ion (or ions) strongly even in the resting state. There are several hundred metalloenzymes and they belong to the subclass of metalloprotiens i.e. proteins, which incorporate one or more metal atoms as a normal part of the structure.[1]

As these metalloenzymes are large macromolecules with molecular weights ranging in kilodaltons (1 dalton ≈ weight of 1 proton) the interest for the synthesis of smaller molecular weight compounds, which can act as structural, and, perhaps as functional model, grew. These smaller molecules can serve as good mimics for the metalloenzymes and can help in understanding their nature and characteristics. The amino acid containing bases like histidine, tyrosine and cystine sparked and fueled the synthesis of a large number of low molecular weight ligands containing imidazole, phenol and thiol respectively. It is observed that the active center of a metalloenzyme constitutes either a single metal center (e.g. Galactose oxidase with a single copper center) or multi-metal centers (e.g. Urease with a dinickel center). Thus, in order to mimic the structural model of the respective metalloenzyme, the nature of ligand plays an important role.

Ligands should, therefore, be designed in such a way that the amino acid residue can be replaced by commonly occurring donor groups and also fit multimetal centers. The most common ligands used by bioinorganic chemists are based on phenolate (tyrosinase mimic) and imidazolate (histidine mimic). In order to mimic metalloenzymes containing two metal centers (the simplest!), dinucleating ligands have been used. The importance of these three types of ligands, which are pertinent to this work, in bioinorganic chemistry is outlined below.

With the advancement about the knowledge of metals in biochemistry, the role of radicals, both stable and transient, started to gather interest. Table 1.1 shows some of the protein radicals along with some of their characteristics.[2]

Radical type	Structure	Examples (found in)	UV-vis, λ_{max} (nm) [ε_{max} (M^{-1} cm^{-1})]	Reference
Tyrosyl	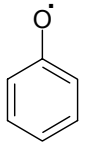	Class I Ribonucleotide Reductase (RNR) Galactose oxidase Plasma amine oxidase	407 [3200]	3
Thiyl	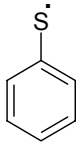	Class II RNR	300-330 [400-1200]	4
Glycyl	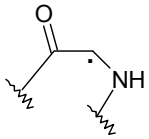	Class III RNR Pyruvate formate lyase	365 [8000]	5
Trptophan	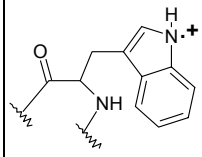	Cytochrom peroxidase	320 [2800]	6

Table 1.1:- Some protein radicals in enzymatic systems

1.1.1 Phenol; the tyrosine mimic

The better stability and easy detection of tyrosyl radicals in comparison to other radical systems invoked the bioinorganic chemists to synthesize model complexes where phenol based ligands were used. Phenoxyl radicals have been generated either chemically or electrochemically and studied extensively. Electronic spectra of phenoxyl radicals show that irrespective of the substitution pattern, the absorption maximum lies at ~380 nm($\varepsilon \approx 1.5 \times 10^3$ M^{-1} cm^{-1}) and 400 nm ($\varepsilon > 1.8 \times 10^3$ M^{-1} cm^{-1}) with a weak maximum at 600-700 nm ($\varepsilon \sim 500$ M^{-1} cm^{-1}).[7] The absorption range of phenoxyl radical at 380-400 nm can be compared to that of tyrosyl radicals, which has absorbance at 407 nm [Table 1.1]. Electrochemical data (cyclic voltametry) for phenoxyl-phenolate and phenoxyl-phenol couples in water have been obtained. Presence of electron donating substituents at 2 or 4 positions decreases the oxidative potentials of phenols making the phenoxyl radicals much

more easily available.[6,8] Tertiary butyl group has been a good choice as it provides excellent electronic stability to the phenoxyl radicals by increasing the electron density at oxygen. The most noteworthy observation was in electrochemistry where the oxidative peaks of the cyclic voltammogram tend towards reversibility as one increases the electron donating properties of the 2 and 4 substituent groups.

The main research goal of this group is to synthesize simple molecular models, which can act both as structural and functional models for metalloenzymes. Most of the synthesized ligands were phenol based and were redox active or "non-innocent" in character. By redox active it is meant that the ligand itself is easily oxidized in mild conditions. Using "non-innocent" ligands to bind to metal centers were first used for magnetism but once the role of radicals in enzymatic catalysis *skyrocketed* [2], new complexes were synthesized which act as possible functional model for metalloenzymes. One such metalloenzyme, which has been studied in detail, is Galactose Oxidase (GO) [EC 1.1.3.9]. It is a copper-containing enzyme, which catalyzes the two-electron oxidation of primary alcohols to their corresponding aldehydes.[10]

$$RCH_2OH \xrightarrow{\textbf{GO , } \mathbf{O_2}} RCHO + H_2O_2$$

The X-ray structure at 1.9 Å resolution shows that the copper is in a square pyramidal geometry with two tyrosine residues, two histidine residues and a water or acetate at the 5th position[11]. From a mechanistic view tyrosyl radical is generated in presence of substrate, which actually catalyzes the oxidation[12]. Stack et. al.[13] and Chaudhuri et. al.[14,17] have synthesized copper complexes with phenol containing ligands, which act as functional models of Galactose Oxidase (Figure1.1). The ligand H_3L^N, originally reported by Girgis and Balch[15],

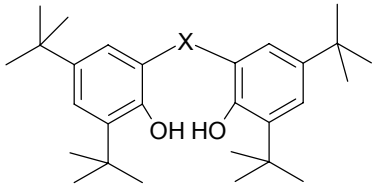

H_3L^N when X =NH
H_2L^S when X =S
H_2L^{Se} when X =Se

Figure 1.1:- Ligands used by Chaudhuri et. al. as functional models of Galactose Oxidase

was found to be redox active as it forms air stable free radical in presence of metal centers and air. The copper complex of the ligand H_2L^S forms transient phenoxyl radicals in solution as observed was found to by UV and EPR spectroscopy.

Another copper enzyme containing a tyrosinase residue is plasma amine oxidase. This enzyme catalyzes the two electron oxidation of primary amines to the corresponding aldehydes.

$$RCH_2NH_2 \xrightarrow[\text{Amine Oxidase}]{O_2} RCHO + H_2O_2 + NH_3$$

However, the tyrosine is in a modified form acting as a co-factor and bound independently from the copper center. The copper center lies in a distorted square pyramidal geometry bounded to 3 histidine bases and two water molecules [16]. The copper complex with both the ligands H_2L^S and H_2L^{Se} were found to be good functional models for amine oxidases.[17]

Tyrosine residue and subsequently tyrosyl radicals were found to play important roles in other metalloenzymes e.g. the iron containing enzyme class I Ribonucleotide Reductase [18] or in the $Y_z^{\cdot}$ component in manganese containing Photosystem II[19] where a tyrosine residue is oxidized to an intermediate tyrosyl radical which subsequently reduces back to tyrosine before the next turnover.[20]

1.1.2 Imidazole-bridged ligands

The role of imidazole, a five membered nitrogen hetrocycle, is well known in chemical and biological systems[21]. It occurs in proteins as part of the side chain in the amino acid histidine, in nucleic acid structures as part of the purine ring of adenosine and guanine and in the vitamin B_{12} coenzyme as benzimidazole. A good example where imidazole acts as bridging ligand is the bovine erythrocyte superoxide dismutase (BESOD)[22] in which it bridges a Cu(II) and a Zn(II) ions. The main function of this enzyme is to protect animals from microbial infection by destroying superoxides to yield molecular oxygen and hydrogen peroxide. There are quite a number of imidazolate bridged metal complexes which provides functional models[23] for various enzymes but these complexes have been more actively studied in order to understand the extent of exchange coupling between the two paramagnetic metal centers through the imidazolate bridge.[24,25] Unfortunately only a few of these structurally characterized compounds have been subjected to a combined EPR and magnetic susceptibility study.[25]

1.1.3 Dinucleating ligands

Since the first report by Robson[26] in 1970 of a dinucleating Schiff-base ligand obtained by condensation of 2,6-diformyl-4-methylphenol with 2-aminophenol, many examples of

similar compartmental ligands have been reported.[27] The dinucleating ability of these ligands stems from the readiness of the phenol to deprotonate and bridge two metal ions. Recently trinuclear and tetranuclear complexes with the ligands derived from the condensation of 2,6-diformyl-4-methylphenol and selected diamine or hydroxylamine were reported, which yield heteronuclear complexes of the type $M_AM_BM_C$ and $M_AM_BM_BM_A$.[28] Dinucleating ligands are also helpful in providing the backbone for the synthesis of structural and functional models for metalloenzymes having a *homodinuclear* center at the active site. Two such enzymes, which are relevant to this work, are the dinickel containing hydrolase enzyme urease [E.C. 3.5.1.5][29] and the dicopper enzyme catechol oxidase[30] [E.C. 1.10.3.1].

Urease, which is present in bacteria, fungi and higher plants, catalyzes the hydrolysis of urea to ammonia and carbon dioxide. The structure of urease shows that each nickel ion is coordinated to two histidine residues from the protein, and a carbamylated lysine residue bridges the two metal ions. The second nickel ion is additionally ligated by an aspartate

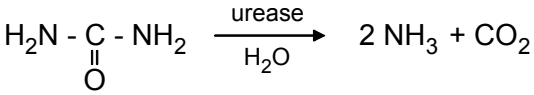

residue. Two terminally coordinated water molecules and one bridging water molecule results in a distorted square pyramidal environment for one nickel site and pseudooctahedral for the other nickel site [Figure 1.2].[29b,29c,29e,31]

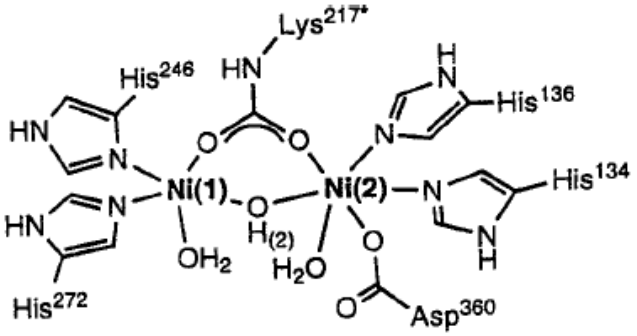

Figure 1.2:- Schematic view of the active site of urease from *K. aerogenes*.

There are quite a few dinickel complexes relevant to the active site of urease[32]. Several dinuclear nickel(II) complexes with urea[33] have been reported as models for possible binding modes of urea in urease. But none of the complexes except one[34] reported so far contains a carbonyl single-atom bridging urea. In this work, a dinuclear nickel(II) complex with a bridging urea through a single-atom O-bridging of the carbonyl oxygen is reported[35a]. Unfortunately, presence of strong hydrogen bonding in the molecule inhibits the attack of

nucleophile (here ethanol) to allow any hydrolysis. This type of models indicates that there might be an alternative mechanistic pathway for the hydrolysis of urea.

As mentioned earlier, the role of radicals in biological electron transfer processes surged the interest for the synthesis of radical containing metal complexes. The ligand reported by Girgis and Balch [15](H_3L^N) oxidizes in air with the formation of free radical. Later on, Pierpont and coworkers synthesized a variety of complexes using 3,5-di-*tert* butyl catechol[37]. Chaudhuri et. al.[38] reported a new aminophenol containing ligand 2-anilino-4,6-di-*tert* butylphenol, which oxidizes sequentially to imino-benzosemiquinato monocation (S_R = ½) and finally the neutral o-imino-benzoquinone.

As a natural and obvious progression, a dinucleating redox active ligand is reported here based on *meta*-phenylenediamine. Using the dimetallic complexes of this ligand, an oxidative reactivity study was carried out in order to mimic the function of catechol oxidase[39,40], a type III copper protein that catalyzes the two-electron oxidation of catechols to quinones in presence of air.

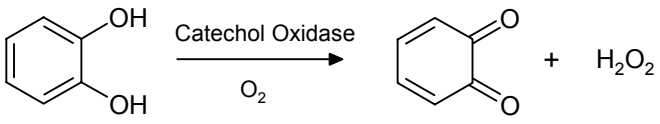

1.2 MOLECULAR MAGNETISM

It is now clear that magnetic property of a material can be determined by a way in which the unpaired electrons interact with each other. In case of a ferromagnet, the unpaired spins are parallely "high-spin" coupled to each other. From Pauli's principle, electrons of like spins are forbidden to occupy the same region of space i.e. nature always prefers antiferromagnetic coupling of two weakly interacting electrons. So, on designing ferromagnets, one cannot create a large number of spins, crystallize or condense them and then hope for the best! The challenge for the chemist is therefore to go against nature and create parallel spin coupled systems against common natural law.

The exchange pathway for magnetic interactions between metal centers are dependent on the nature of pathway linking the centers.[41,42] If the metal based orbitals are not close enough to overlap directly, the nature of spin interactions are formalized by the Goodenough-Kanamouri rules.[43] A number of complexes with predictable magnetic properties have been synthesized using this principle.[42,44] However, if the metal centers are far apart to overlap directly, the bridging ligand mediates in the interaction (superexchange process) i.e. even if the pure metal orbitals cannot overlap directly, mixing of these orbitals with the orbitals of the bridging ligands means that the magnetic orbitals may not be purely metal centered but also have a significant ligand-based component, and in such cases direct overlap of the magnetic orbitals can still occur. Thus the bridging ligand plays an important part by mediating in the electronic interactions. This type of interactions was seen in organic radicals[45] where it was shown that special topology and structure was needed. For long range interactions, the topological importance grew with the generation of the McConnell "spin-polarization" mechanism.[46]

1.2.1 Accidental ferromagnetism

The Goodenough-Kanamouri rules is based on the nature of overlap between the orbitals of the different magnetic centers via the intervening ligand orbitals. Two orbitals can overlap either in an orthogonal fashion or a non-orthogonal fashion. If the orbitals interact with each other in a non-orthogonal fashion, the interaction is anti-ferromagnetic. However, if there is overlap between half filled orbital of one ion with either an empty or filled orbital of another, ferromagnetic interaction occurs. This concept has been employed in controlling the magnetic properties of polynuclear coordinated complexes. A good example is the magnetostructural correlation associated with an octahedral coordinated dinickel center

bridged by an oxygen atom.[47a] There are several complexes reported with the $[Ni_4(OR)_4]$ (R = H, alkyl) cubane structure along with their magnetochemical property. It has been observed that ferromagnetic exchange between the two nickel centers are generated when the Ni-O-Ni angle tends towards orthogonality. Such type of "accidental ferromagnetism" of superexchange transmitted through bridging atoms can also be observed through different donor atoms e.g. nitrogen in azide [48b].

1.2.2 Planned orthogonality by spin polarization

The concept of spin polarization[46,48] was first applied to organic conjugated di-radicals and was first observed in trimethylenemethane (**1,** Fig. 1.3) by Dowd.[45b,46] Later on 1,2 and 1,4 connected diradicals were also synthesized. Unfortunately both of them turned out to have antiferromagnetic interactions between them. Calculation for **1** showed that the single triplet energy gap is +15 Kcal/mol.[49] If *m*- benzoquinonedimethane diradical moiety is taken, calculation predicts that the interaction is ferromagnetic and the energy between the singlet and triplet state is +10 Kcal/mol [Figure 1.3][50].

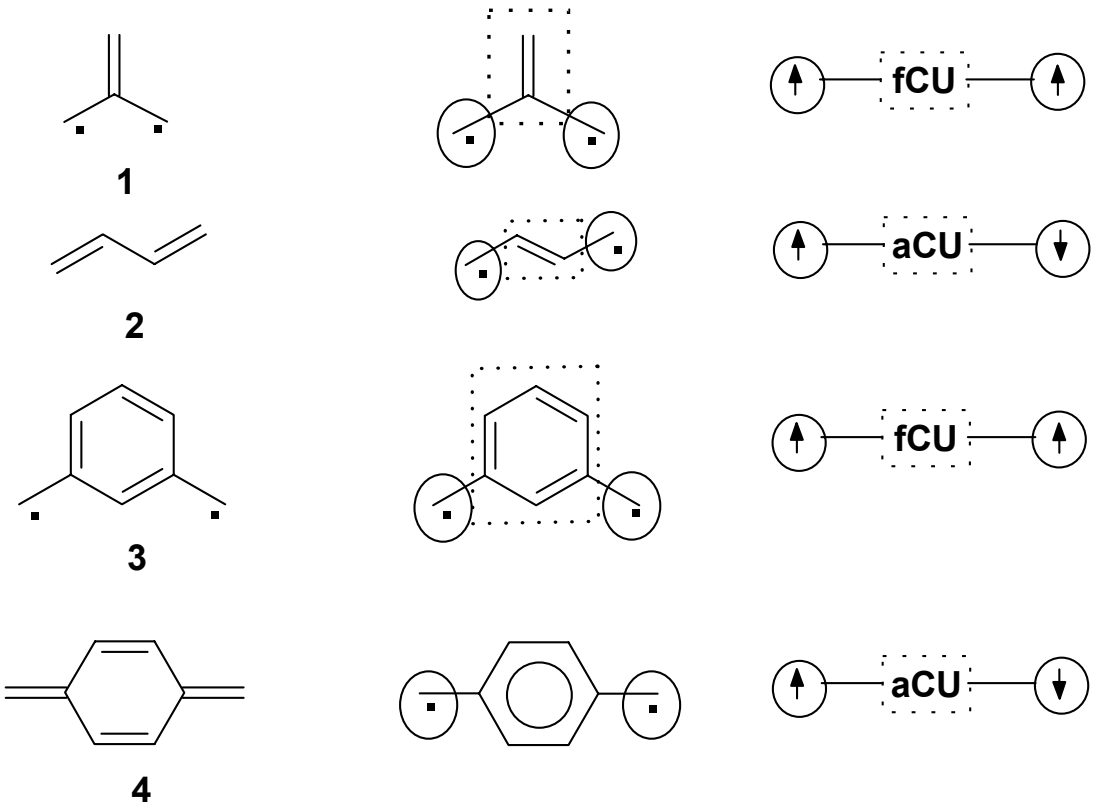

Figure 1.3 :- Different organic π–conjugated di-radical systems with their coupling scheme

aCU :- antiferromagnetic coupler ; fCU :- ferromagnetic coupler

A plausible reason for such type of behavior can be given by spin polarization. It describes how an unpaired electron polarizes the electron cloud on the adjacent atom in the opposite sense. Spin densities at the adjacent atomic centers in a π-conjugated system always prefer opposite signs α and β. This leads to an αβαβαβ spin pattern [Figure 1.4]. This concept of spin polarization was adopted by the inorganic chemist although it lagged behind in the

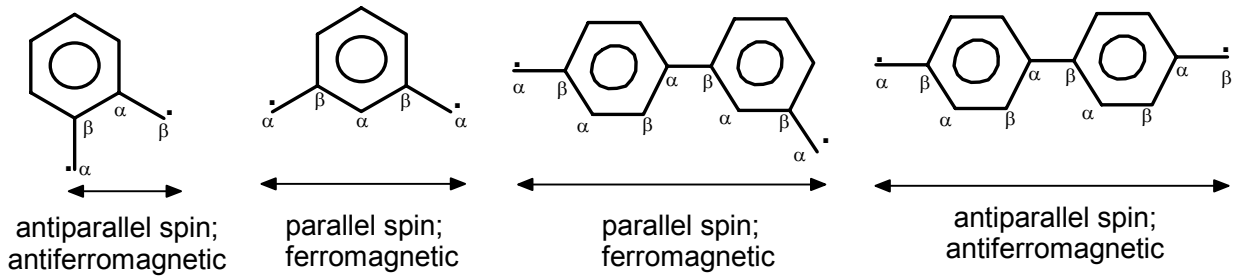

Figure 1.4:- Spin propagation along substituted benzene moiety

development of organic ferromagnets. The advantages of inorganic over organic paramagnetic centers include high spin density, improved chemical stability (organic radicals tends to polymerize) and the possibility of reversible redox activity (for switching). Soon high spin binuclear transition metal complexes with suitable bridging ligands as ferromagnetic coupler were reported. Ferromagnetism was ascribed mainly to i) the meta-substitution pattern of the ligand and ii) d(π) – p (π) overlap between metal and ligand which allowed propagation of the exchange interaction by a simple spin polarization mechanism involving the d(π) unpaired electrons in the metal centers and the p (π) electrons in the bridging ligand.[51]

There are a number of complexes, which have been synthesized using the spin polarization mechanism. Different bridging ligands like 1,3 bipyridine, polypyridines, 1,3 substituted phenols and 1,3,5 substituted phenols have been used as ferromagnetic couplers and are listed in Table 1.2.

Another ligand which acts as a ferromagnetic coupler is the *meta*-phenylenediamine moiety. Here again, the 1,3 position helps in αβαβαβ spin propagation forcing the electron centers in the metal to be spin parallel. Fernández et. al.[52] synthesized a copper(II) dimer with the ligand, a parent acid of N,N′-1,3-phenylenediaminebis(oxamate) where the electrons in the copper atoms were aligned in a spin parallel orientation. From the susceptibility measurement the value of magnetic interactions between the two copper centers were +8.4 cm^{-1}. This was further supported by theoretical calculations which showed that the single-triplet energy gap was +7.1 cm^{-1} [Figure 1.5].

Bridging ligands used as ferromagnetic coupler	Reference
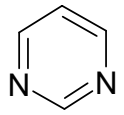	51b, 51c, 51d, 51f, 51g, 51h, 51i
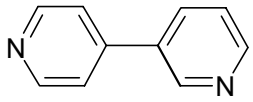	51d, 51j
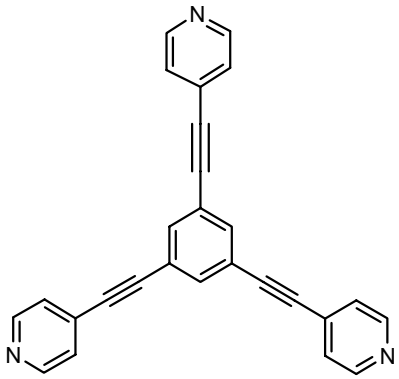	51d
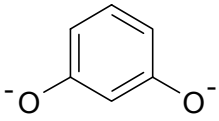	51a, 51b, 51j
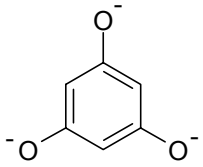	51j, 51e

Table 1.2:- Different substituted ligands used as ferromagnetic couplers

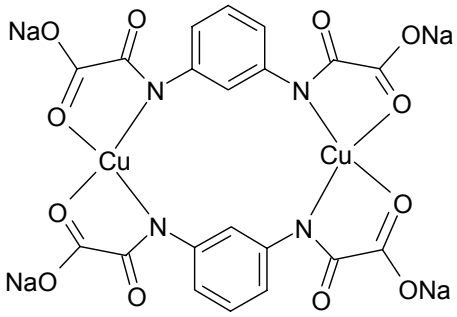

Figure 1.5 :- The dicopper(II) complex synthesized by Fernández et. al.[52]

Keeping a view on the above aspects, it is clear that in order to synthesize molecules with ferromagnetic interactions between the two paramagnetic centers, the derivatization of 1,3 position is important. As mentioned earlier, it is also clear that imino-semiquinone radicals are easily stabilized by a 3d-metal. These two aspects were conjoined and a new ligand was synthesized based on a 1,3 diaminobenzene moiety where the ligand oxidizes easily in presence of air and the radicals are stabilized by the 3d-metals. The 1,3 position necessitates ferromagnetism between the paramagnetic centers.

1.2.3 Spin-crossover of Iron(III) compounds

The magnetic properties of mononuclear iron (III) complexes are now well understood. Fe(III) has an electronic configuration of $3d^5$ and the complexes can be high spin ($S=^5/_2$, HS), intermediate spin ($S=^3/_2$, IS) or low spin (S= ½, LS). In an octahedral geometry, presence of strong crystal field increases 10Dq (the energy difference between the e_g and the t_{2g} set of orbitals) leading to the formation of low spin electronic ground states whereas in presence of weak crystal field strength ligand, the e_g states are also populated due to weakening of 10Dq leading to the formation of high spin electronic ground states. Thus the majority of the complexes are either high spin or low spin. Only a few complexes are known where the iron is in the intermediate spin state.[53]

The spin state of a metal can also change within the same molecule. In Fe(II)[55a,55d] and Co(II)[54b] systems this "spin crossover" can be observed. For Fe(III) the most widespread example known is the iron(III) dithiocarbamate[55c] where a $^6A_{1g}$ (HS) $\Leftrightarrow$ $^2T_{2g}$(LS) crossover is observed. In this work, an iron complex has been described which shows a HS $\Leftrightarrow$ LS spin crossover. The iron is in an six-coordinated or distorted octahedral geometry and the ground state for iron is $^1/_2$.

References

1) S.J.Lippard, J.M.Berg, *Principles of Bioinorganic Chemistry*;University ScienceBooks:,1994.

2) J.Stubbe, W. A. v. d. Donk, *Chemical Reviews,* **1998**, 98, 705.

3) K. Bansal, R. W. Fessenden, *Radiat. Res.,* **1976**, 67, 1.

4) M. I. Hoffman, E. Hayon, *J. Phys. Chem* , **1973**, 77, 990.

5) H. Conradt, M. Hohmann-Berger, H. Hohmann, H. P. Blaschkowski, J. Knappe, *Arch. Biochem. Biophy.,* **1984**, 228, 133.

6) M. R. DeFilippis, C. P. Murthy, M. Faraggi, M. R. Klappe, *Biochemistry,* **1989**, 28, 4847.

7)(a) C.D. Cook, R. C. Wood, *J.Am.Chem.Soc.,* **1953**, 75, 6242. (b) Cook C.D, Depathi C.B., English E.S., *J.Org.Chem.,* **1959**, 24, 1356 (c) Müller E., Ley K., *Ber.,***1954**,87, 922

8)(a) Y. A .Ilan, G. Czapski, D. Meisel, *BioChim. Biophys. Acta.*, **1976**, 430, 209 (b) S. Steenken, D. Neta, *J. Phy. Chem*., **1979**, 83, 1134 (c) S.Steenken, D. Neta, *J. Phy. Chem*., **1982**, 86, 3661

9)(a) A. Caneschi, D. Gatteschi, R. Sessoli, *Acc. Chem. Res*., **1989**, 22, 392 (b) A. Aukauloo, X. Ottenwaelder, R. Ruiz, S. Poussereau, Y. Pei, Y. Journaux, P. Fleurat, F. Volatron, B. Cervera, M. C. Muñoz, *Eur. J. Inorg. Chem.,* **1999**, 7, 1067

10) J. W. Whittaker, In *Metal Ions in Biological Systems*; H. Sigel, A. Sigel, Eds.; Marcel Dekker: New York, 1994; Vol. 30, 315

11)(a) N. Ito, S. E. V. Phillips, C. Stevens ,Z. B. Ogel, M. J. McPherson, J. N. Keen, K. D. S. Yadav, P. F. Knowles, *Nature,* **1991**, 350, 87.(b) N. Ito, S. E. V. Phillips, K. D. S. Yadav, P. F. Knowles, *J. Mol. Biol.,* **1994**, 238, 794.

12) R. M. Wachter, M. P. Montagne-Smith, B. P. Branchaud, *J.Am. Chem. Soc.* **1997**, 119, 7743.

13) Y. Wang, J. L. DuBois, B. Hedman, K. O. Hodgson, T. D. P. Stack, *Science* **1998**, 279, 537.

14)(a) P. Chaudhuri, M. Hess, U. Flörke, K. Wieghardt, *Angew. Chem., Int. Ed.* **1998**, *37*, 2217 (b) P. Chaudhuri, M. Hess, T. Weyhermüller, K. Wieghardt, *Angew. Chem.,Int. Ed.,***1999**, 38, 1095.(c) P. Chaudhuri, M. Hess, J. Müller, K. Hildenbrand, E. Bill, T. Weyhermüller, and K. Wieghardt, *J. Am. Chem. Soc.* **1999,** 121*,* 9599.

15) A. Y . Girgis , A. L. Balch, *Inorg. Chem.*, **1975,** 14, 2724.

16)(a) D.M. Dooley, M.A. McCruise, C.E. Cote, P.F. Knowles, J. Singh, M. Spiller, R.D. Brown, S. H. Koenig, *J. Am. Chem. Soc.* **1991,** 113, 654.(b) J. McCracken, J. Peisach, D. M. Dooley, *J. Am. Chem. Soc.* **1987**, 109, 4064.(c) D. Collison, P. F. Knowles, F. E. Mabbs, F. X. Rius, I. Singh, D. M. Dooley, C. E. Cote, M. McGuirl, *Biochem. J.* **1989**, 264,663. (d) D. M. Dooley, W. S. McIntire, M. A. McGuirl, C. E. Cote, J. L. Bates, *J. Am .Chem. Soc.* **1990**, 112, 2782 (e) R. A. Scott, D. M. Dooley, *J. Am. Chem.Soc.* **1985**, 107, 4348. f) C. M. Wilmot, J. Hajdu, M. J. Mcpherson, P.F. Knowles, S.E.V. Phillips., *Science*, **1999**, 286, 1724.

17) T. K. Paine ,Ph.D Thesis, Universität-Paderborn, 2003

18) P. Nordlund, B.M. Sjöberg, H. Eklund, *Nature* **1990**, 345, 593.

19)(a) V. K. Yachandra, V. J. DeRose, M. J. Latimer, I. Mukerji, K. Sauer, M. P. Klein, *Science* **1993**, 260, 675.(b) V. J.; DeRose, I.; Mukerji, M. J.; Latimer, V.K. Yachandra, K. Sauer, M. P. Klein, *J. Am. Chem. Soc.* **1994**, 116, 5239.(c) P. J. Riggs-Gelasco, R. Mei, J. E.Penner- Hahn, *In Mechanistic Bioinorganic Chemistry*; Thorp, H. H., Pecoraro, V. L., Eds.; American Chemical Society: Washington, DC, 1995; Vol. 246, pp 219-248.(d) G. W. Brudvig, In *Mechanistic Bioinorganic Chemistry*; H. H. Thorp, V. L.

Pecoraro, Eds.; American Chemical Society: Washington, DC, 1995; Vol. 246, pp 249

20) C. W. Hoganson, N. Lydakis-Simantiris, X.-S. Tang, C. Tommos, K. Warncke, G. T. Babcock, B. A. Diner, J. McCracken, S. Styring, *Photosynth. Res.* **1995**, 46, 177.

21(a) T. E.Creighton, *Proteins, Structures and Molecular Properties;* W. H. Freeman: New York, 1984. (b) W. Saenger, *Principles of Nuclei Acid Structure;* Springer- Verlag: New York, 1984. (c) J. M. Pratt, *Inorganic Chemistry of Vitamin B_{12}*; Academic Press: New York, 1972.

22) (a) J. A. Tainer, E. D. Getzoff, K. M. Beem, S. J. Richardson, D. C. Richardson, *J. Mol. Biol.* **1982**, 160, 181. (b) W. R. Rypniewski, S. Mangani, S. Bruni, P. L. Orioli, M. Casati, K. Wilson, *J. Mol. Biol.* **1995**, 251, 282. (c) I. Bertini, S.Mangani, M. S. Viezzoli, *Ad*v.. *Inorg. Chem.* **1998**, 45, 127. (d) T. J. Lyons, B. B.Gralla, J. S.Valentine, *Met. Ions Biol. Syst.* **1999**, 36, 125.

23)(a) W.A. Alves, I. A. Bagatin , A. M. D. C. Ferreira, *Inorg. Chim. Acta*, **2001**, 321, 1 (b) J. Gao, J. H. Reibenspies, A. E. Martell, *Inorg. Chim. Acta* , **2003**, 346, 67 and references therin

24)(a) N. Matsumoto, T. Nozaki, H. Ushio, K. Motoda, M. Ohba, G. Mago, H. Okawa, *J. Chem. Soc., Dalton Trans.* **1993**, 2157.(b) T. Nozaki, H. Ushio, G. Mago, N. Matsumoto , H. Okawa, Y. Yamakawa, T. Anno, T. Nakishima, *J. Chem. Soc., Dalton Trans.* **1994**, 2339. (c) N. Matsumoto, Y. Mizuguchi, G. Mago, S. Eguchi, H. Misayaka, T. Nakashima, J. P. Tuchagues, *Angew. Chem., Int. Ed. Engl.* **1997**, 36, 1860.(d) M. Mimura, T. Matsuo, T. Nakashima, N. Matsumoto, *Inorg. Chem.* **1998**, 37, 3553 and references therein.(e) J. M. Domýnguez-Vera, F. Ca´mara, J. M. Moreno, E. Colacio, H. Stoeckli-Evans, *Inorg. Chem.* **1998**, 37,3046.(f) N. Matsumoto, Y. Motoda, T. Matsuo, T. Nakashima, N. Re, F. Dahan, J. P. Tuchages, *Inorg. Chem,* **1999**, 38,1165 and references therein. (g) J. L. Pierre, P. Chautemps, S. Refaif, C. Beguin, C. A. El Marzouki , G. Serratrice, E. Saint-Aman, P. Rey, *J. Am. Chem. Soc.* **1995**, 117,1965. (h) R. Wang, G. Brewer, *Inorg. Chim. Acta* **1993**, *206*,117. i) J. P. Costes, J. F. Serra, F.. Dahan, J. P. Laurent, *Inorg.Chem.* **1986**, 25, 2790. (j) Z. W. Mao, M. Q. Chen, X. S. Tan, J. Liu, W. X. Tang, *Inorg. Chem.* **1995**, 34, 2889. (k) N.Matsumoto, H. Okawa, S. Kida, T. Ogawa, A. Ohyoshi, *Bull. Chem. Soc. Jpn* .**1989**, 62, 3812. (l) C. A. Koch, C. A. Reed, G. A. Brewer, Rath,N. P.; W. R. Scheidt, G. Gupta, G. Lang, *J. Am. Chem. Soc.* **1989**, 111, 7645. (m) E. Colacio, J. M. Domý´nguez-Vera, M. Ghazi, R. Kivekäs, M. Klinga, J. M. Moreno, *Inorg. Chem.***1998**, 37, 3040.

25) P. Chaudhuri, I. Karpenstein, M. Winter, M. Lengen, C. Butzlaff, E. Bill, A. Trautwein, U. Flörke, H. J. Haupt, *Inorg.Chem.* **1993**, 32, 888 and references therein

26)(a) R.Robson, *J. Inorg. Nucl. Chem. Lett.* **1970**, 6, 125.(b)R. Robson, *Aust. J. Chem.***1970**, 23, 2217. (c) A. M. Bond, M. Haga, I. S. Creece, R. Robson, J. C. Wilson, *Inorg. Chem.* **1988**, 27, 712 (d) A. M. Bond, M. Haga, I. S. Creece, R. Robson, J. C. Wilson, *Inorg. Chem.* **1989**, 28, 559.

27) H. Okawa, H. Furutachi, D. E. Fenton, *Coord. Chem. Rev.* **1998**, 174, 51 and references therein.

28)(a) C. N. Verani, T. Weyhermüller, E. Rentschler, E. Bill, P. Chaudhuri, *Chem. Commun.***1998**, 2475. b) C.N. Verani, E. Rentschler, T. Weyhermüller, E. Bill, P. Chaudhuri, *J. Chem. Soc., Dalton Trans.* **2000**, 4263.(c)C. Krebs, M. Winter, T. Weyhermüller, E. Bill, K. Wieghardt, P. Chaudhuri, *J. Chem. Soc., Chem. Commun.* **1995**, 1913.

29)(a) K. Andrews, R. L. Blakeley, B. Zerner, in *"The Bioinorganic Chemistry of Nickel"*, ed. J. R. Lancaster, VCH, New York 1988.(b) E. Jabri, M. B. Carr, R. P. Hausinger, P. A. Karplus, *Science* **1995**, 268, 998.(c) M. A. Pearson, L. O. Michel, R. P. Hausinger, P. A. Karplus, *Biochemistry* **1997**, 36, 8164.(d) S. Benini, W. R. Rypniewski, K. S. Wilson, S. Ciurli, S. Mangani, *J. Biol. Inorg. Chem.* **1998**, 3,

268.(e) S. Benini, W. R. Rypniewski, K. S. Wilson, S. Miletti, S. Ciurli, S. Mangani, *Structure* **1999**, 7, 205. (e) S. Ciurli, S. Benini, W. R. Rypniewski, K. S. Wilson, S. Miletti, S. Mangani, *Coord. Chem. Rev.* **1999**,190-192, 331.

30) C. Gerdemann, C. Eicken and B. Krebs, *Acc. Chem. Res.,* **2002**, 35, 183

31)(a) S. Benini, W. R. Rypniewski, K. S. Wilson, S. Ciurli, S. Mangani, *JBIC,***1998**, *3*, 268.(b) S. Benini, W. R. Rypniewski, K. S. Wilson, S. Miletti, S. Ciurli, S. Mangani,*Structure* **1999**, *7*, 205.

32)(a) P. Chaudhuri, H.-J. Küppers, K. Wieghardt, S. Gehring, W. Haase, B. Nuber, J. Weiss,*J. Chem. Soc., Dalton Trans.* **1988**,1367.(b) A. J. Stemmler, J.W. Kampf, M. L. Kirk, V. L. Pecoraro, *J. Am.Chem. Soc.* **1995**, 117, 6368 .(c) M. Ito, Y. Takita *Chem. Lett.*,**1996**, 929.(d) D. Volkmer, A. Hörstmann, K. Griesar, W. Haase, B. Krebs, *Inorg. Chem.* **1996**, 35, 1132. (e) D. Volkmer, B. Hommerich, K. Griesar, W. Haase, B. Krebs, *Inorg. Chem.* **1996**, 35, 3792.(f) Y. Hosokawa, H. Yamane, Y. Nakao, K. Matsumoto, S. Takamizawa, W. Mori, S. Suzuki, *Chem. Lett.* **1997**, 891. (g) B.Hommerich, H. Schwo¨ppe, D. Volkmer, B. Krebs, *Z. Anorg .Allg. Chem.* **1999**, 625, 75.

33)(a) H. E. Wages, K. L. Taft, S. J. Lippard, *Inorg. Chem.* **1993**, 32,4985.b) T.Koga, H. Furutachi, T. Nakamura, N. Fukita, M. Ohba, K. Takahashi, H. Okawa, *Inorg. Chem* . **1998**, 37, 989.b) F. Meyer, H. Pritzkow, *Chem. Commun.* **1998**,1555

34) A. Barrios, S. J. Lippard, *J. Am. Chem. Soc.* **2000,** 122*,* 9172

35)(a) S. Mukherjee, T. Weyhermüller, E. Bothe, K. Wieghardt, P. Chaudhuri, *Eur. J. Inorg. Chem.* **2003**, 863. (b) S. Mukherjee, T. Weyhermüller, E. Bothe, P. Chaudhuri, *Eur. J. Inorg .Chem.,***2003**, 1956.

36)(a) W. R. Fearon, *Biochem. J.* **1923**, 17, 84.(b) E. Mack, D. S. Villars, *J. Am. Chem. Soc.* **1923**, 45, 505.(c) R.L. Blakeley, A. Treston, R. K. Andrews, B. Zerner, *J. Am. Chem. Soc.* **1982**, 104, 612.(d) K. Yamaguchi, S. Koshino, F. Akagi, M. Suzuki, A. Uehara, S. Suzuki, *J. Am. Chem. Soc.* **1997**, 119, 5752.(e) M. Konrad, F. Meyer, A. Jacobi, P. Kircher, P. Rutsch, L. Zsolnai, *Inorg. Chem.* **1999**, 38, 4559.

37)(a) C. G. Pierpont , C. W. Lange, *Progr. Inorg. Chem.,* **1994**, 41, 331;(b) C. G. Pierpont, *Coord. Chem. Rev.,* **2001**, 216, 99.

38)(a) C. N. Verani, S. Gallert, E. Bill, T. Weyhermüller, K. Wieghardt and P. Chaudhuri, *Chem. Commun.,* **1999**, 1747;(b) P. Chaudhuri, C. N. Verani, E. Bill, E. Bothe, T. Weyhermüller and K. Wieghardt, *J. Am. Chem. Soc.,* **2001**, 123, 2213;(c) H. Chun, C. N. Verani, P. Chaudhuri, E. Bothe, E. Bill, T. Weyhermüller, K. Wieghardt, *Inorg. Chem.,* **2001**, 40, 4157.

39) Hughes, A. L. *Immunogenetics* ,**1999**, 49, 106-114.

40) E. I. Solomon, U. M. Sundaram, T. E. Machonkin, *Chem. Rev*.,**1996**, 96, 2563.

41) C.M. Hurd, Contemp. Phys. **1982,** 23, 469

42)(a) O. Kahn Molecular Magnetism; VCH Publishing, Inc.,New York, 1993 b) R.J. Bushby; J.L. Pailland, Molecular magnets in Introduction to Molecular Electronics, M.C. Petty, M.R. Bryce, D. Bloor, Eds.; Edward Arnold ; London,1995, pg. 72-91

43)(a) J.B. Goodenough, *Phys. Rev.,***1955**,100,564.(b) J.B. Goodenough , *J. Phys. Chem. Solids,* **1958**, 6, 287 (c)J. Kanamori, *J. Phys. Chem. Solids* **1959**, 10,87(d)A. P Ginsberg,*Inorg. Chim. Acta Rev.* **1971**, 5,45.

44(a) O. Kahn, *Struct. Bonding,* **1987**, 68, 89.(b) Gordon-Wylie, S. W.; Bominaar, E. L.; T. J. Collins, J. M. Workman, B. L. Claus, R. E. Patterson, S. A. Williams, B. J. Conklin, G. T. Yee, S. T. Weintraub, *Chem. Eur. J.* **1995**, 1, 528-537.

45(a) J. S. Miller, A. J. Epstein, *Angew. Chem., Int. Ed. Engl.* **1994**, 33, 385.(b) H. Iwamura, *Pure Appl. Chem.*

1993, 65, 57.(c) A. Rajca, *Chem. Rev.* **1994**, 94, 871.(d) S. Rajca, A. Rajca, *J. Am. Chem. Soc.* **1995**, 117, 9172.(e) K.; Yoshizawa, *Chem. Eur. J.* **1995**, 1, 403. (f) H. Iwamura, N. Koga, *Acc. Chem. Res.* **1993**, 26, 346.

46) H.M. McConnell, *J. Chem. Phys.*,**1963**, 39, 1910.

47)(a) K. E. Andrew, A. B. Blake, *J. Chem. Soc. A*, **1969**, 1456 (b) M. A. Halcrow, J.-S. Sun, J.C. Huffman, G. Christou, *Inorg. Chem.* **1995**, 34, 4167.

48) H.C. Longuet-Higgins, *J. Chem. Phys*, **1950**,18,265.

49)(a) P. Dowd, *J. Am. Chem. Soc.* **1966**, 88,2587.(b) R. J. Baseman, D. W. Pratt, M. Chow, P. Dowd, *J. Am. Chem. Soc*. **1976**,98,5726.(c) R. J. Baseman, D. W. Pratt, M.Chow, P. Dowd, *Angew. Chem. Int. Ed. Engl*., **1993**, 32, 119.(d) D. A. Dixon, T.A. Dunning, R. A. Eades, D. A. Kleier, *J. Am. Chem. Soc.* **1981**,103, 2878.

50)(a)J. A. Beraon, In *The Chemistry of Quinoid Compounds*; S. Petai, Z. Rappaport, Eds.;Wiley: **1988;** Vol. 11, Chapter 10. (b) M. Rule, A. R. M a t h , D. E. Seeger, E. F. Hilinski, D. A. Dougherty, J. A. Berson, *Tetrahedron* **1982**,38,787. **(**c) J. L. Goodman , J. A. Berson, *J. Am. Chem. Soc.* **1985**,107,5409. (d) B. B. Wright, M. Platz, *J. Am. Chem. Soc.* **1983**, 105, 628.(e) E. Migirdicyan, J. Baudet, *J. Am. Chem. Soc*. **1975**,97,7400.(f) R. C. Jr. Fort, S. J. Getty, D. A. Hrovat, P. M. Lahti, W. T. Borden, *J. Am. Chem. Soc.* **1992**,114,7549. **(**g) S. Kato, K. Morokuma, D. Feller, E. R. Davidson, W. T. Borden, *J. Am. Chem. Soc.* **1983**,105, 1791.

51)(a) H. Oshio, *Chem. Comm.*, **1991**,240 (b)H. Oshio, H. Ichida, *J Phys. Chem.*, **1995**, 99, 3294 (c) S. Mitsubai, T. Ishida, T. Nogai, H. Iwamura, *Chem. Lett.*,**1994**,285(d) J. A. McCleverty, M. D. Ward, *Acc. Chem. Res.,* **1998**, 31, 842. (e) T. Glaser, M. Gerenkamp, Roland Fröhlich, *Angew. Chem. Int. Ed.,* **2002,** 41, 3828.(f) T. Ishida, S. Mitsubori, T. Nogami, N. Takeda, M. Ishikawa, H. Iwamura, *Inorg. Chem.* **2001**, 40,7059.(g) F.Lloret, G. De Munno, M. Julve, J. Cano, R. Ruiz, A. Caneschi, *Angew. Chem. Int. Ed.* **1998**, 37, 135. h)V. Ä. Ung, S. M. Couchman, J. C. Jeffery, J. A. McCleverty, M. D.Ward, F. Totti, D. Gatteschi, *Inorg. Chem*. **1999**, 38, 365.(i) L.C. Francesconi, D.R. Corbin, A.W Clauss, D.N. Hendrickson, G.D. Stucky, *Inorg. Chem*., **1981**, 20, 2078.(j) V. Ä. Ung, A. M.W. Cargill Thompson, D. A. Bardwell, D. Gatteschi, J.C. McCleverty, F. Totti, M. D. Ward, *Inorg. Chem.* **1997**, 36, 3447.

52) I. Fernández, J. Faus, M. Julve, F. Lloret, J. Cano, X. Ottenwaelder, Y.Journeaux, M. C. Muňeoz, *Angew. Chem. Int. Ed.* **2001**, 40, 3039.

53)(a) R. L. Martin, A. H. White, *Inorg. Chem.* **1967**, 6, 712. (b) B. F. Hoskins, A. H. White, *J. Chem. Soc. A* **1970**, 1668. (c) K. L. Kostka, B. G. Fox, M. P. Hendrich, T. J. Collins, C. E. F. Richard, L. J. Wright, E. Munck, *J. Am. Chem. Soc*. **1993**, 115, 6746.(d) S. Koch, R. H. Holm, R. B. Frankel, *J. Am. Chem. Soc.* **1975**, 97, 6714. (e) D. H. Dolphin, J. R. Sams, T. B. Tsin, *Inorg. Chem.* **1977**, 16, 711.(f) D. A. Summerville, I. A. Cohen, K. Hatano, W. R. Scheidt, *Inorg.Chem.* **1978**, 17, 2906. (g) D. Mansuy, I. Morgenstern-Baradau, M. Lange, P. Gans, *Inorg. Chem.* **1982**, 21, 1427. (h) J.P. Fritzgerald, B. S. Haggerty, A. L. Rheingold, L. May, G. A. Brewer, *Inorg.Chem* **1992**, 31, 2006. (i) B. J. Kennedy, K. S. Murray, P.R. Zwack, H. Homborg, Kalz, W. *Inorg. Chem.* **1986**, 25, 2539. (j) H. Chun, T. Weyhermüller, E. Bill, K. Wieghardt, *Angew. Chem. Int. Ed.* **2001**,40,2489.

54. O. Koch, V. Schünemann, M. Gerdan, A. X. Trautwein, H.J. Krüger, Chem. Eur. J.,**1998,**4,686.

55(a) H.A. Goodwin, *Coord. Chem. Rev*, **1976**, 18, 293 (b) C.L. Rasta, A.H. White, *J. Chem. Soc. Dalton Trans.*,**1974**, 1803 (c) C.L. Rasta, A.H. White, *J. Chem. Soc. Dalton Trans.*, 1976,7 (d) H.L. Nigam, K.B. Pandeya, H. Singh, *J. Ind. Chem. Soc.*, **2001**, 78,525 (e) P.Gültich , J. Jung , *Nuovo Cimento*, **1996**, 18, 107.

Chapter 2

TRANSITION METAL COMPLEXES WITH IMINE-PHENOLATE LIGANDS

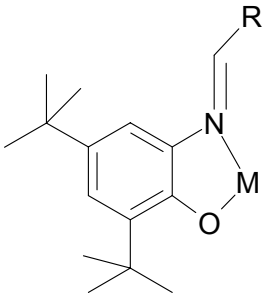

2.1 INTRODUCTION

The homopolynuclear complexes are of interest to the inorganic chemists for their relevance to biology and magnetism (Chapter 1). This chapter describes some 3d-transition metal containing di- and tetranuclear complexes which are relevant to some metalloenzymes and their importance in magnetostructural correlation. The ligands chosen are phenol based with either imidazole- or imine-containing side chain.

2.2 SYNTHESIS AND CHARACTERIZATION OF LIGANDS

The interest for the synthesis of redox-active aminophenol ligands paved the way in preparing H_3L^1 (2,4-Di-tert-butyl-6-[(5-methyl-3H-imidazol-4-ylmethyl)-amino]-phenol). When 2,4-di-*tert*-butyl-6-aminophenol is condensed with 5-Methyl-3H-imidazole-4-carbaldehyde and then further reduced by $NaBH_4$ in methanol, the ligand H_3L^1 precipitates as a white solid in an aqueous medium (Figure 2.1). It has a molecular peak at m/z 315 (EI-MS) with the characteristic peaks at IR (Table 2.1). NMR spectroscopy unambiguously proves the presence of 26 protons (3 protons are exchangeable).

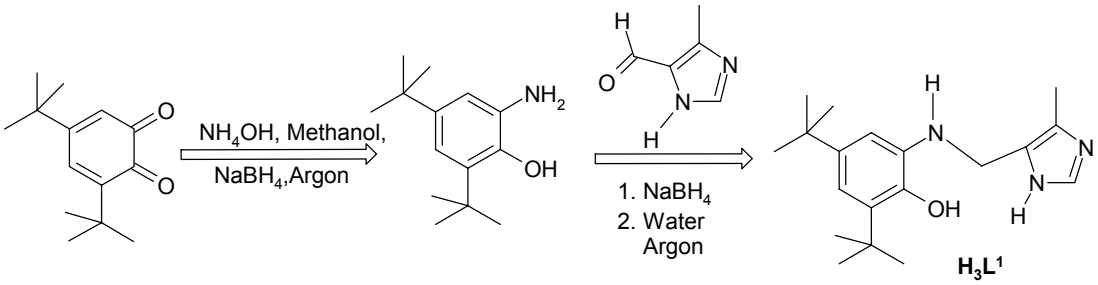

Figure 2.1 :- Synthetic procedure for the preparation of H_3L^1

In a methanolic solution containing a few drops of triethylamine, this ligand is redox active i.e. it forms radicals in presence of air. When this solution is subjected to EPR studies, a six line hyperfine spectrum appears[Figure 2.2]. The radical center couples with the nitrogen center (I = 1) and the proton centers (I= ½), giving rise to the six hyperfines. A simulation of this spectrum shows that the coupling constants for nitrogen is 4.74 G and for the two protons 9.30 G and 3.59 G respectively. The *g* value is centered at 2.0049 which clearly shows that the ligand is "non-innocent" and forms imino-semiquinone radical in air.

It has already been reported that *tert*-butyl substituents at the *ortho* and *para* positions of the phenolates facilitate one-electron oxidation to the corresponding phenoxyl radicals,

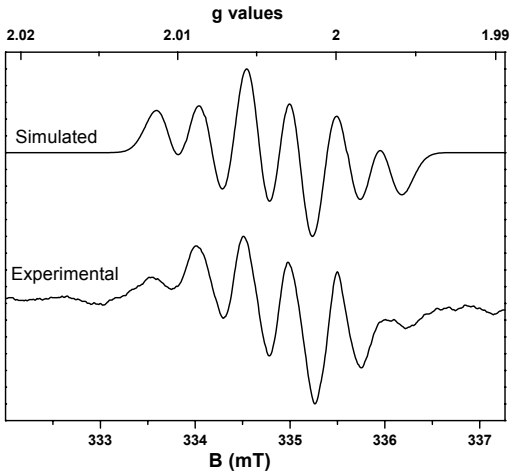

Figure 2.2 :- EPR spectrum of H_3L^1 in methanol in presence of triethylamine.

because these substituents decrease the oxidation potential of the phenolates and provide enough steric bulk to suppress bimolecular decay reactions of the generated phenoxyl radicals. Accordingly, the Schiff-base ligand, H_3L^2, derived from the (1+2) condensation of 2,6-diformyl-4-methylphenol and 2,4-di-*tert*-butyl-6-aminophenol, was synthesized [Figure 2.3]. This ligand has been already reported by Robson [1] but other than a dimeric cobalt complex[2], no other crystal structure was reported. This ligand acts as a dinucleating ligand with a pentadentate (O, N, O, N, O)-donor atoms and is as expected "innocent" i.e. non-redox active. The ligand shows characteristic peaks in IR spectroscopy (Table 2.1). Mass spectroscopy in the EI-mode shows the molecular peak at m/z 570 and NMR data reveals the presence of 47 protons (3 are exchangeable).

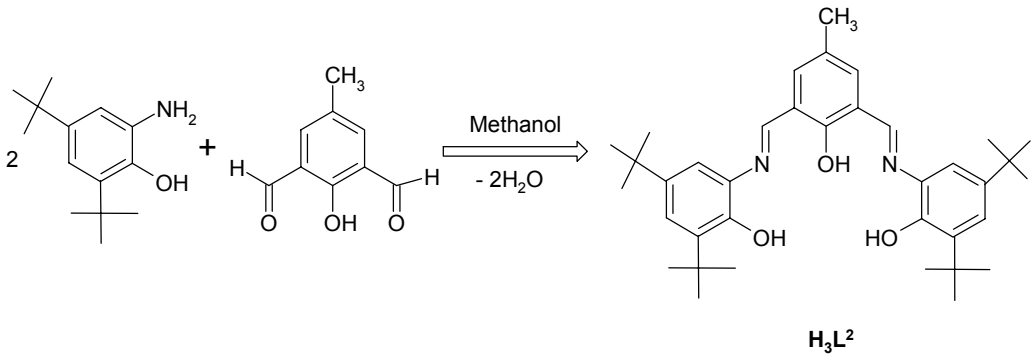

Figure 2.3 :- Synthetic procedure for the preparation of H_3L^2

2.3 TRANSITION METAL COMPLEXES WITH H_3L^1 AND H_3L^2

Using the ligand H_3L^1 , Ni(II) (**1**) and Cu(II) (**2**) complexes have been synthesized using the corresponding metal salts and in the presence of triethylamine as base. The complexes obtained were characterized by Infrared spectrometry, Mass spectrometry, Elemental Analysis and Single-crystal X-ray diffractometric study. Magnetic susceptibility and EPR studies were performed with the copper complex.

The dinucleating Schiff-base, H_3L^2 form complexes with all the 3d transition metals ions. Figure 2.4 shows the complexes prepared and thus exemplifies the diversity of this ligand. Reaction of metal salts and the ligand H_3L^2 in presence of the base triethyl amine or tetrabutylammonium methoxide affords all the complexes in moderate yield.

When nickel acetate and H_3L^2 in presence of sodium acetate are allowed to react with a slight excess of urea in methanol, complex **3** is obtained. In the absence of urea, the tetranuclear complex **4** is obtained. Complex **4** can also be transformed to **3** by adding urea to the red solution of **4** in methanol. Formation of **3** from **4** implies that the driving force for formation of **3** lies in the strong tendency of urea to be incorporated in the dinickel center embedded in the dinucleating ligand $[L^2]^{3-}$.

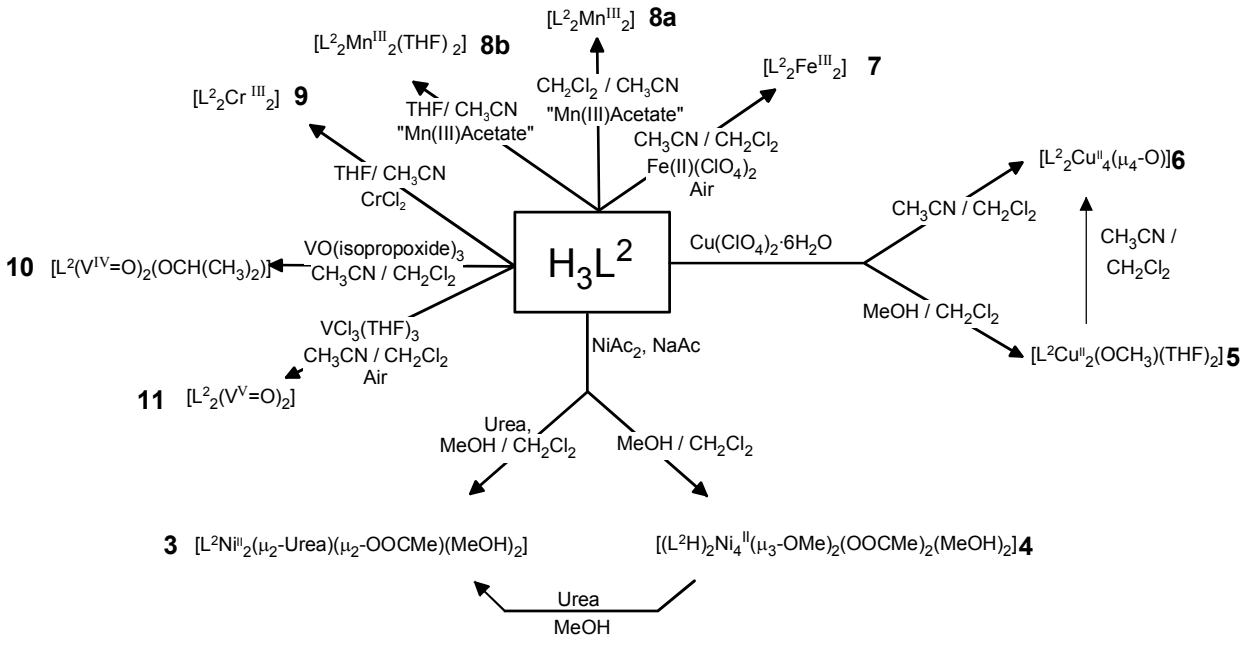

Figure 2.4 :- Complexes prepared with ligand H_3L^2.

The reaction of copper perchlorate and the Schiff-base ligand H_3L^2 afforded either **5** or **6**, depending on the solvent system, in relatively high-yield. Lacking protic solvents, complex **5**, a methoxo-bridged dicopper(II) species, is transformed easily to **6**, a μ_4-oxo-tetracopper(II) complex, in presence of the solvent-mixture CH_3CN/CH_2Cl_2 indicating the stability of **6**. Adventitious water in the solvent serves as a source for the μ_4-oxo ligand.

The complexes **7-11** were obtained by using the salts shown in Figure 2.4. All these dinuclear complexes were easily isolated and characterized by different methods. Remarkably $[L^2{}_2Mn^{II}{}_2]$ (**8a)**, which is considered to possess identical coordination sphere and atom connectivity as with the structurally characterized $[L^2{}_2Fe^{III}{}_2]$ (**7)**, yields on recrystallization from THF $[L^2{}_2Mn^{III}{}_2(THF)_2]$ (**8b)**, in which the phenolate-bridging between two manganese centers prevailing in **8a** does not persist any more, and thus resulting in a comparatively long Mn•••Mn separation (6.45 Å).

2.3.1 INFRARED AND MASS SPECTROSCOPY OF COMPLEXES 1-11

The solid state FTIR spectra of the ligand H_3L^1 shows characteristic stretching peaks for ν(OH) and ν(NH) in the region 3100 to 3400 cm^{-1} which is missing in **1** as well as for **2**. This indicates that that the phenol and amine character of the ligand is lost upon complexation. The weak band at 1615 cm^{-1} due to (-C-N) stretch shifts to 1600 cm^{-1} in the

Compound	ν (cm^{-1})
H_3L^1	3299 (-NH), 2959(tert-butyl), 1615(C-N) ,1591(C=C,aromatic), 1233(C-O)
H_3L^2	3523, 3492, 3348w, 2954, 2868s, 1625m, 1580m, 1482s, 1456s, 1361s, 1250s, 987s, 960s, 867m
1	2952, 1600, 1474, 1399, 1253,1130, 861
2	2951, 1595, 1470, 1398, 1257, 1126, 857, 647
3	3586w, 3382m, 3139m, 1670m, 1654m, 1568s, 1469s, 1444s, 1410s, 1250s, 1159m, 831m
4	3440br, 1624s, 1552m, 1477s, 1446s, 1410s, 1259s, 1039s, 805m
5	1597m, 1557m, 1474s, 1445s, 1256s, 1077m, 830m
6	1593m, 1557m, 1467s, 1254s, 1200m, 1077m, 829m, 564m, 539m, 510m
7	1610m, 1591m, 1565m, 1471s, 1408m, 1255s, 1163m, 834m, 537m, 492m
8	1610m, 1587m, 1442m, 1406m, 1360m, 1246s, 1161m, 836m, 561m, 537m
9	1598m, 1565m, 1445s, 1406m, 1256s, 1162m, 832m, 569m, 539m, 517m
10	1614m, 1569m, 1476s, 1446m, 1250s, 1161s, 990vs, 948m, 831s, 567m, 546s
11	1616m, 1591m, 1544s, 1476s, 1443s, 1361s, 1244s, 996s, 838m

Table 2.1 :- *Characteristic FTIR peaks for the ligands H_3L^1 and H_3L^2 and complexes **1-11**.*

case of **1** and 1595 cm^{-1} for **2**. Quite interestingly, these two peaks are stronger and sharper than the weak peak observed at 1615 cm^{-1} for the ligand. Characteristic IR peaks are summarized in Table 2.1.

The sharp peaks in the solid state FTIR spectrum due to ν(OH) of the ligand H_3L^2 occur at 3523, 3492 and 3348 cm^{-1}. These bands are missing in **3** and **5-11**, indicating that on complexation the phenol-character of the ligand has been lost. For complex **4**, the presence of two phenolic protons, as evidenced from the crystal structure, could not be observed due to the broadness of the bands at 3440 cm^{-1} . The solid state FTIR spectrum of complex **3** exhibits a shift in the carbonyl stretching frequency of urea from 1690 to 1670 cm^{-1} upon coordination to the dinickel center. For **6** the sharp band of medium intensity at 510 cm^{-1} is associated with the ν_{Cu-O} frequency in the Cu_4O core. Support for this assignment is obtained by comparison with the vibrational spectrum of **5**, which exhibits, similar to that for **6**, two sharp bands of medium intensity at 564 and 539 cm^{-1} attributable to ν(Cu-O) vibrations for bonds to the phenolate groups. These three bands are missing in the spectrum of the free ligand. Selected IR data for complexes **3 - 11** are given in the Table 2.1. There are several peaks in the region 3000 - 2800 cm^{-1} due to the *tert*-butyl groups along with the other ν(C-H), ν(C=C), ν(C=N) and ν(C-O) vibrations found in the normal range for these types of linkages. For **10** the sharp strong-band at 990 cm^{-1} is associated with the ν(V=O) vibration. The corresponding band for **11** occurs at 996 cm^{-1}.

When **1** and **2** were subjected to mass spectrometry in EI and ESI mode, it is clear that the Ni (in **1**) and Cu (in **2**) are bounded to the ligand center. However, a large number of peaks were observed ranging from mononuclear to tetranuclear complexes. Elemental analysis of both **1** and **2** shows the metal to ligand ratio as 1:1. It is therefore probable that the complexes are not monomers which is furthur proved by single crystal X-Ray diffractometric studies.

Mass spectrometry in the EI mode indicates unambiguously the presence of urea and acetate ion in **3**. In the ESI positive mass spectrum of **3** the peak with an abundance of 100 % is observed centered around *m/z* 743, corresponding to $[L^2Ni_2(OOCCH_3)]^+$, with expected isotope pattern. EI-MS for **4** did not provide much useful information regarding its tetranuclear nature, but exhibits signals around *m/z* 714-720 (100 %) with expected isotope pattern for a dinickel compound, indicating clearly the presence of $[L^2Ni_2(OCH_3)]^+$ in the gas phase. In the EI mass spectrum of **5** the molecule peak at *m/z* 724 with an abundance of 100% corresponding to the $LCu_2(OCH_3)$-species is observed. Additionally, a clear indication of the presence of THF in **5** is found at *m/z* 72. Mass spectrometry in the EI mode has been proved

to be very useful for **6**, for which the molecule peak at *m/z* 1404 with expected isotope pattern confirming the presence of $[L^{2}_{2}Cu_4(O)]$ is observed. For complexes **7-11** mass spectrometric analysis were also performed. In the EI mode for **7** exhibits the molecular ion peak centered around *m/z* 1247 with expected isotope pattern, indicating unambiguously the composition to be $L^{2}_{2}Fe_2$. For **8a** the parent ion peak corresponds to a small peak centered around *m/z* 1244; the peaks with dominating intensities are observed at *m/z* 206, 351 and 568. MS-EI indicates unambiguously the presence of THF in **8b**. Compound **9** shows the main peak at *m/z* 1239 in the MS-ESI (positive) spectrum in CH_2Cl_2, indicating the composition to be $L^{2}_{2}Cr_2$ like that of **7**. In the EI mass spectrum of **10** the parent ion peak with an abundance of ~21 % is observed at *m/z* 760 with expected isotope pattern. The peak at *m/z* 718 with an abundance of 100 % corresponding to the $L^{2}V_2O_3$ species is also observed. In addition there are other peaks including at *m/z* 702 corresponding to the $L^{2}V_2O_2$ species. MS-EI for **11** does not leave any doubt about the composition $L^{2}_{2}V_2O_2$ with the molecule ion peak at *m/z* 1268; the strongest peak (100 %) with *m/z* 1251 corresponds to $L^{2}_{2}V_2O$. The other significant peaks at *m/z* 1236 and 618 are attributed to $L^{2}_{2}V_2^{+}$ and $L^{2}_{2}V_2^{2+}$ ions.

2.3.2 CRYSTAL STRUCTURE AND CHARACTERIZATION OF COMPLEXES

$[L^{1}_{4}\ Ni^{II}_{4}]$ (1)

Orange-red single crystals of **1**, afforded from a dichloromethane-methanol solvent mixture, was subjected to X-ray diffractometric studies. The structure (Figure 2.5) shows the formation of a neutral tetranuclear nickel complex along with 9 dichloromethane molecules. Each of the nickel center is in a distorted square planer geometry with N_2O co-ordination from the ligand and the 4th coordination sphere being occupied by the nitrogen atom of the adjacent imidazolate ring. A closer look at the bond length of one of the ligand shows that the C(8)-N(7) bond distance has shortened considerably to 1.297 (11) Å i.e. a double bond has been formed. This indicates oxidation occurs at this bond, instead of the phenyl ring. The average Ni-O(phenol), Ni-N (imine), Ni-N (imidazolate nitrogen) and Ni-N (imidazolate nitrogen of adjacent ligand) bond lengths are 1.856Å, 1.850Å, 1.891Å and 1.850Å, respectively which are comparable to other square planer Ni(II) complexes[3a]. The four nickel centers forms a "butterfly structure"[3b-d] with Ni(1)-Ni(1A)-Ni(1B) making one plane and Ni(1C)-Ni(1A)-Ni(1B) the other (shown in dashed line in Figure 2.5(b)). The dihedral angle between these two planes is 107.7 °. All the adjacent Ni-Ni were equidistant with a value of 5.851 Å. Selected bond distances and angles are given in Table 2.2.

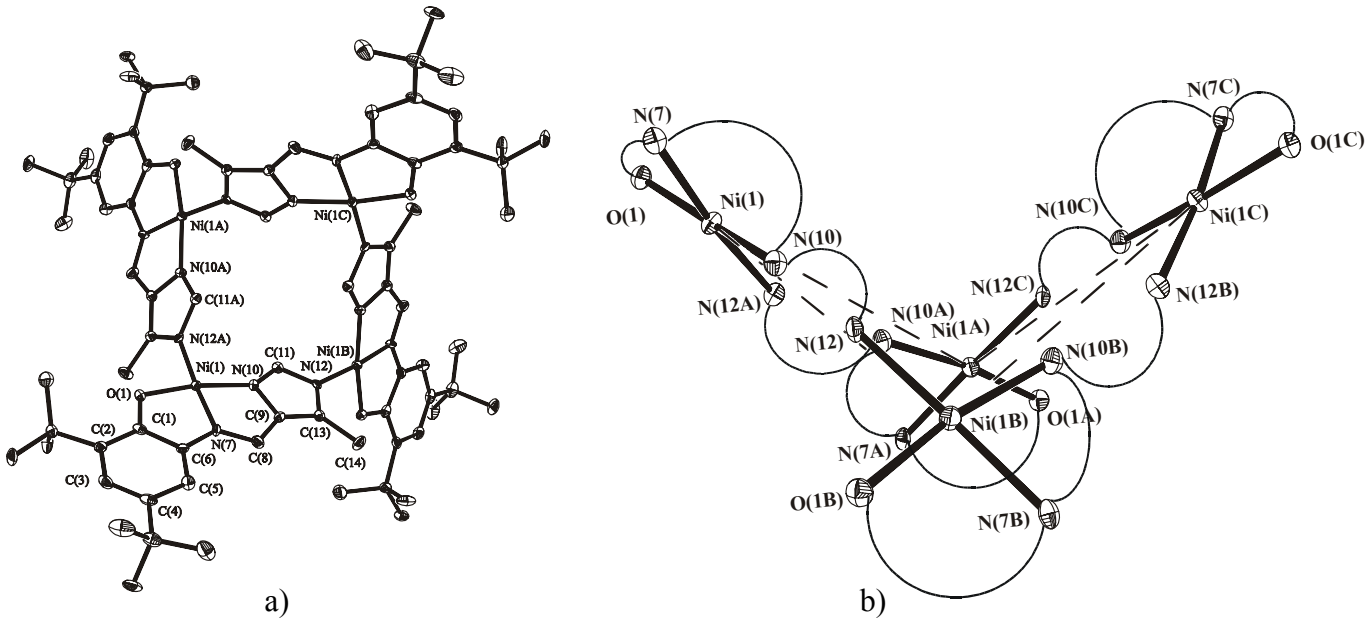

Figure 2.5:- a) ORTEP diagram of **1** b) A view of **1** highlighting the "butterfly structure" of the four nickel centers. The ligand L^1 is denoted only by the donor atoms joined by the curved lines.

Table 2.2:- *Selected bond distances (Å) and angles (degree) for **1***

Ni(1)-N(7)	1.850 (7)	C(4)-C(5)	1.405 (12)
Ni(1)-N(12A)	1.891 (6)	C(5)-C(6)	1.405 (11)
Ni(1)-N(10)	1.885 (7)	C(1)-C(6)	1.407 (12)
Ni(1)-O(1)	1.856 (5)	C(9)-N(10)	1.381 (10)
C(1)-O(1)	1.355 (9)	N(12)-C(11)	1.332 (11)
C(6)-N(7)	1.391 (10)	C(13)-N(12)	1.362 (10)
N(7)-C(8)	1.297 (11)	C(11)-N(10)	1.297 (11)
C(1)-C(2)	1.396 (11)	C(8)-C(9)	1.447 (11)
C(2)-C(3)	1.411 (12)	C(9)-C(13)	1.370 (11)
C(3)-C(4)	1.368 (13)	C(13)-C(14)	1.489 (11)
Ni(1)…Ni(1A)	5.851	Ni(1C)…Ni(1A)	5.851
Ni(1)…Ni(1B)	5.851	Ni(1C)…Ni(1B)	5.851
Ni(1A)…Ni(1B)	7.351	Ni(1)…Ni(1C)	7.351
Ni(1A)-Ni(1)-Ni(1B)	77.8	Ni(1B)-Ni(1C)-Ni(1A)	77.8
Ni(1)-Ni(1B)-Ni(1C)	77.8	Ni(1C)-Ni(1A)-Ni(1)	77.8
O(1)-Ni(1)-N(7)	86.5 (3)	N(12A)-Ni(1)-N(10)	94.1 (3)
N(7)-Ni(1)-N(10)	84.0 (3)	N(12A)-Ni(1)-O(1)	95.6 (3)
N(7)-Ni(1)-N(12A)	174.6 (3)	N(10)-Ni(1)-O(1)	170.2 (3)
C(1)-O(1)-Ni(1)	111.8 (5)	Ni(1)-N(10)-C(9)	112.4 (5)
C(8)-N(7)-C(6)	129.8 (7)	C(11)-N(12A)-Ni(1)	123.8 (5)
Ni(1)-N(10)-C(11)	142.8 (6)	C(13)-N(12A)-Ni(1)	130.5 (5)
C(8)-N(7)-Ni(1)	117.3 (6)	C(6)-N(7)-Ni(1)	112.8 (5)

The tetramer Ni(II) complex is as expected diamagnetic and is proved by magnetic susceptibility as well as ^{1}H NMR studies. In ^{1}H NMR spectra, the ratio of -CH proton (tert-butyl, twice), -CH (Methyl), -CH (-N=CH-), -CH (aromatic proton) and –CH (imidazolate ring) is 9:9:3:1:2:1 as expected from the deprotonated ligand.

$[L^{1}_{4}Cu^{II}_{4}(THF)_{4}]$ (2)

The crystal structure determination of **2** confirms that it is isostructural to **1** (Figure 2.6). However, even at low temperature, the crystal decomposes and as a result the R value is high. Due to this high R value, it is not clear how many THF molecules are embedded in the unit cell. Other solvent mixtures gave microcrystalline solid. Only a THF and Methanol or THF and Ethanol mixture affords X-Ray quality crystals.

The relevant interatomic distances and angles are given in Table 2.3. As observed in **1**, oxidation of ligand occurs at the same position (C(8)-N(7)= 1.31 Å). The structure consists of a distorted square pyramidal tetranuclear neutral molecule with the Cu centers forming a "butterfly structure" [Figure 2.6 (b)]. The fifth position of the coordination site in each copper center is occupied by a THF molecule. The dihedral angle between the plane made by connecting Cu(1)-Cu(2)-Cu(4) and Cu(3)-Cu(2)-Cu(4) is 150.1°. The average Cu-O (phenol), Cu-N (imine), Cu-N (imidazolate nitrogen) and Cu-N (imidazolate nitrogen of adjacent ligand) bond lengths are 1.942Å, 1.942Å, 1.992Å and 1.948Å, respectively which are comparable to other square planer Cu (II) complexes [4]. It is observed that the Cu(1)-N(10) bond is elongated than the other coordinating atoms. This tendency is same for the other copper centers and is due to Jahn-Teller effect which is present for d^{9} systems thus making **2** less symmetric than **1**, a d^{8} system. The Cu(1) is displaced by 0.11 Å from the mean basal plane of the three nitrogen [N(7), N(10), N(42)] and one oxygen atom [O(1)]. The dihedral angles made between the plane N(42)O(1)N(7)N(10) containing the Cu(1) ion and the planes N(42)C(43)C(39)N(40)C(41) and N(10)C(9)C(13)N(12)C(11) describing the two imidazolate bridging groups are 47.2° and 82.2° respectively. It is interesting to note that angle between the Cu(1)-N_{im}(42) and Cu(2)-N_{im}(40) vectors is 142.2° and that made between the Cu(1)-N_{im}(10) and Cu(4)-N_{im}(12) vector is 132.6°. The plane made by Cu(1)O(1)N(7)N(10)N(42) and Cu(2)O(31)N(37)N(40)N(72) makes an angle 139.1° between them.

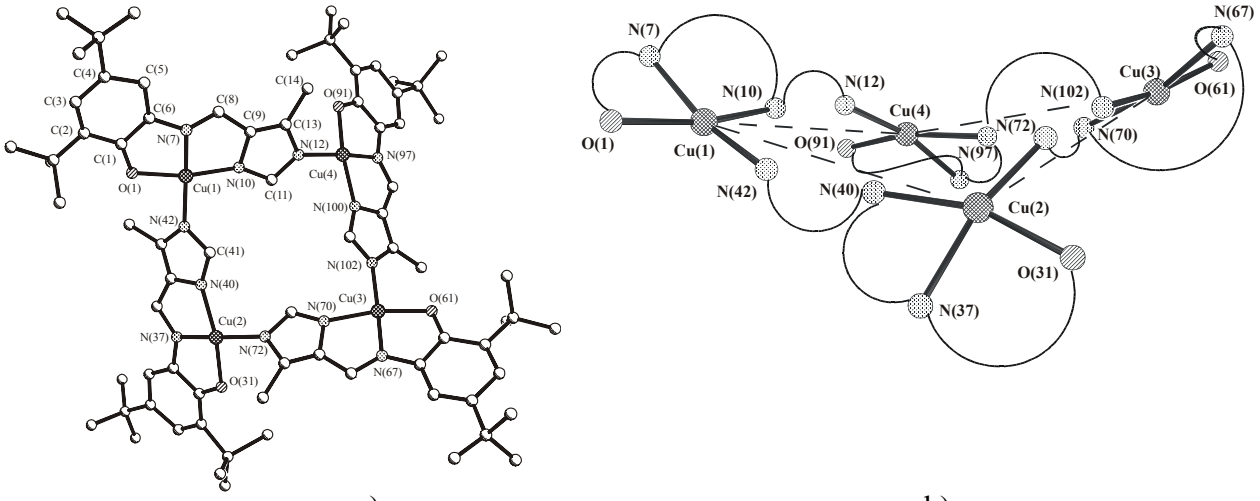

a) b)

Figure 2.6:- a) ORTEP diagram of **2** b) A view of **2** highlighting the "butterfly structure" of the four copper centers. The ligand L^1 is denoted only by the donor atoms joined by the curved lines.

Table 2.3:- *Selected bond distances (Å) and angles (degree) for **2***

Cu(1)-N(7)	1.913 (17)	Cu(2)-N(37)	1.964 (16)
Cu(1)-N(42)	1.925 (17)	Cu(2)-N(72)	1.957 (16)
Cu(1)-N(10)	1.952 (16)	Cu(2)-N(40)	2.020 (16)
Cu(1)-O(1)	1.955 (12)	Cu(2)-O(31)	1.965 (13)
C(1)-O(1)	1.316 (25)	C(9)-N(10)	1.462
C(6)-N(7)	1.420	N(12)-C(11)	1.347
N(7)-C(8)	1.310	C(13)-N(12)	1.408
C(1)-C(2)	1.422	C(11)-N(10)	1.381
C(2)-C(3)	1.399	C(8)-C(9)	1.461
C(3)-C(4)	1.365	C(9)-C(13)	1.341
C(4)-C(5)	1.399	C(13)-C(14)	1.525
C(5)-C(6)	1.409		
C(1)-C(6)	1.377		
Cu(1)…Cu(2)	6.054	Cu(3)…Cu(4)	6.034
Cu(1)….Cu(4)	6.044	Cu(1)…Cu(3)	8.524
Cu(2)…Cu(3)	6.019	Cu(2)…Cu(4)	8.245
Cu(1)-Cu(2)-Cu(3)	89.8	Cu(3)-Cu(4)-Cu(1)	89.8
Cu(2)-Cu(3)-Cu(4)	86.3	Cu(4)-Cu(1)-Cu(2)	85.9
O(1)-Cu(1)-N(7)	82.6	O(31)-Cu(2)-N(37)	81.6
N(7)-Cu(1)-N(10)	83.4	N(37)-Cu(2)-N(40)	81.7
N(7)-Cu(1)-N(42)	164.7	N(37)-Cu(2)-N(72)	163.2
N(42)-Cu(1)-N(10)	99.5	N(72)-Cu(2)-O(31)	93.8
N(42)-Cu(1)-O(1)	94.2	N(72)-Cu(2)-N(40)	100.9
N(10)-Cu(1)-O(1)	166.0	N(40)-Cu(2)-N(31)	162.7
Cu(1)-N(10)-C(11)	146.14 (16)	Cu(2)-N(40)-C(41)	142.8 (17)
Cu(1)-N(42)-C(41)	123.59 (16)	Cu(4)-N(12)-C(11)	123.89 (16)

The magnetic susceptibility data for polycrystalline sample of **2** was measured from 2-290 K in an applied magnetic field of 1 T to characterize the nature and magnitude of the exchange interaction propagated by the bridging ligands. The Heisenberg spin Hamiltonian in the form $H = -2J\ \vec{S}_A \bullet \vec{S}_B$ for an isotropic exchange coupling was used. The experimental magnetic data were simulated using a least-square fitting computer program [5] with a full-matrix diagonalization of exchange coupling, Zeeman splitting, and axial single-ion zero-field interactions ($D\vec{S}_z^2$), if necessary. The susceptibility data were corrected for diamagnetism (Pascal corrections), temperature-independent paramagnetism (TIP) and the presence of paramagnetic monomer impurity (P) in the following way: $\chi_{calc} = (1-P)\chi + \chi_{TIP} + P\chi_{mono}$. It is to be noted here that the conditions which are mentioned above are taken as the standard for all the magnetic susceptibility measurements related to this work and their simulation. For all the complexes, other than for magnetization measurements at different field strength, the magnetic field applied was 1T.

The nature of the plot of **2** (Figure 2.7(a)) shows a behavior typical for antiferromagnetic spin coupling. The μ_{eff} decreases monotonically with the decrease in temperature; the values of μ_{eff} are 3.051 μ_B at 290 K and 0.180 μ_B at 2 K. Thus the magnetic data reveal an energetically well-isolated ground state of total spin $S_t = 0$, discernible from the decline of effective moments at temperatures below 100 K. The residual moment of 0.180 μ_B at 2 K could be attributed to a monomeric (S =½) impurity (2.0%). Monomeric species appeared also in weak abundance in the EPR spectra, as will be mentioned later.

The susceptibility data could be simulated between adjacent Cu(II) pairs with local spins (S=½), as sketched in Figure 2.7(a)(inset). The multiplets $|S_A S_B S_t>$ are labeled by the "pair spins", S_A ($\vec{S}_A = \vec{S}_1 + \vec{S}_3$) and S_B ($\vec{S}_B = \vec{S}_2 + \vec{S}_4$), and the total spin S_t ($\vec{S}_t = \vec{S}_A + \vec{S}_B$). The ground state is a singlet |110> and the first excited state at energy 2J is a triplet |111> [Figure 2.7(b)]**.** The states |011>, |000> and |101> are degenerate at energy 4J and the highest state at energy 6J is a quintet |112>. In zero field the multiplets remain degenerate in magnetic quantum numbers, according to their multiplicity. The simulation of the experimental susceptibility data for the tetramer yielded an exchange coupling constant $J = -49\ cm^{-1}$, g = 2.022 , a paramagnetic impurity (P) of 2% and a temperature independent paramagnetism (TIP) of 240 $x10^{-3}$. In an imidazolate bridged system, there can be two type of pathways in explaining the magnetic interaction viz. the σ and the π-exchange pathway. Generally, it is agreed that the π-orbitals are not involved in the coupling[6,4b,7]. It has been stated that, since

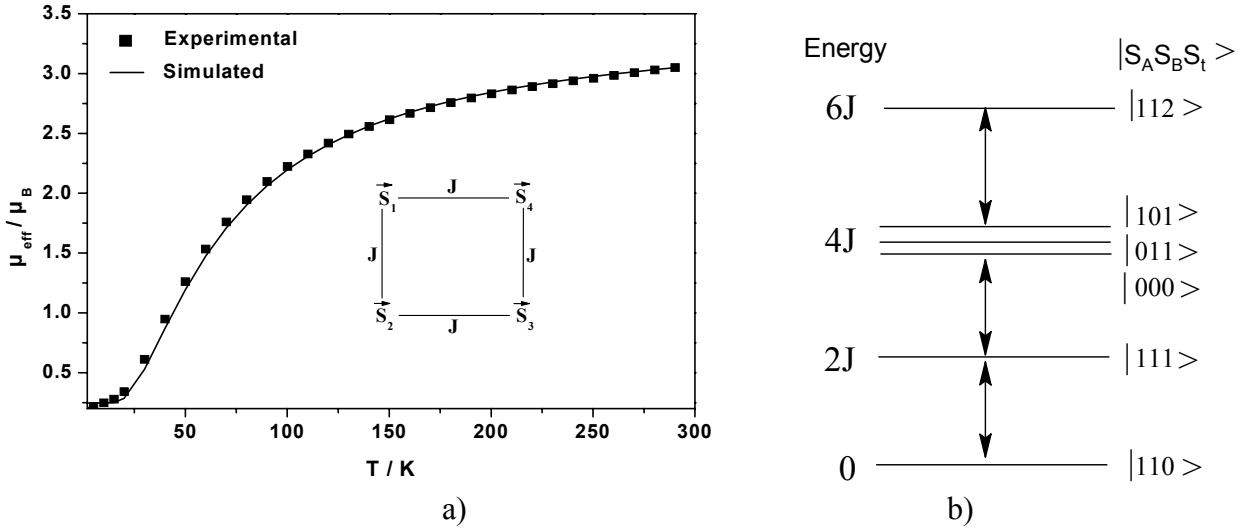

a) b)

Figure 2.7:- a) Magnetic measurement of **2** with the model of spin coupling.b) Corresponding spin states in Zero Applied Field

the magnetic orbitals are σ -antibonding for square planar and square pyramidal complexes, the relevant exchange pathway through the imidazolate bridge is of the σ -type. The imidazolate orbitals that are responsible for this sort of interaction are of the type sketched in Figure 2.8(a), and they are essentially parallel to the N-N' (or C-C) direction.

Several studies have already been reported[4a,4b,7], in which structural data have been used to find correlations between structure and exchange coupling in imidazolate-bridged copper(II) complexes. In Table 2.4, the structural parameters which appear to be responsible for the exchange coupling constant are listed for several structurally characterized imidazolate-bridged complexes. Different angles listed in the Table 2.4 are defined in Figure 2.8(b). Comparison of the numerical data shows that a simple magnetostrutural correlation for imidazolate bridged Cu complexes does not exist. However, as the values of J is independent of θ, a π–exchange pathway can be discarded. However it has been concluded from EHMO calculations[7] that the extent of anti-ferromagnetic coupling will increase when

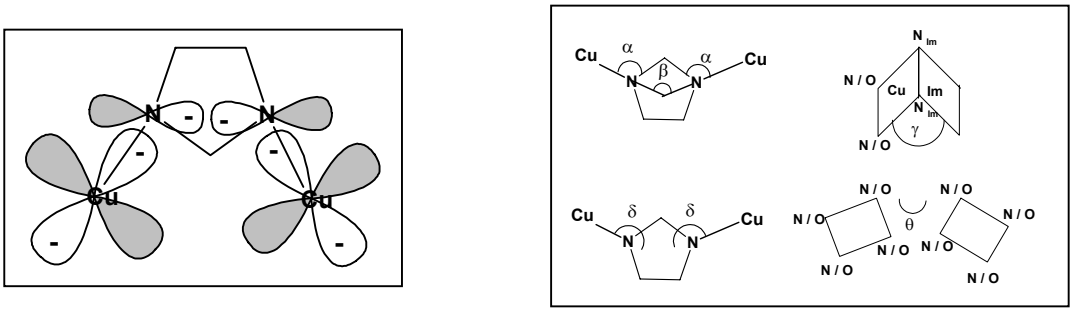

a) b)

Figure 2.8 a) Schematic representation of the orbital orientations for the Cu-Im-Cu unit.
b) Different angles used in the magnetostructural correlation.

Table 2.4 *Exchange Coupling Constants and Structural Parameters for Imidazolate-Bridged Copper(II) Complexes*

Complex	J /cm^{-1}	α	β	γ	δ	θ	reference
catena- $[Cu_3(Im)_2(ImH)_8(Cl0_4)_4]$	-58.5	130.0		70.0	162.9		4e,7
		129.8		60.0	160.9		
catena- [Cu (Im)$(ImH)_2$Cl]	-42	135.3		90.0	169.4		4f,7
		128.5		90.0	168.8		
$[L'_3Cu_3(Im)_3](ClO_4)_3$	-37.5	127.0	131.1	91.2	154.0	74.3	4a,4g
		123.0	135.3	74.3	157.4	61.0	
		120.5		56.2	154.5	56.2	
						91.2	
$[L_4Cu_4(Im)_4](ClO_4)_4$	-35	130.4	134.6	76.9	157.7	63.8	4g
		126.6	142.1	50.2	164.4		
		126.7		95.7	156.9		
				26.9	157.6		
$[Cu_4(Bpim)_2(Im)_2](NO_3)_4$	-35	120.0		97.3		153	4b
		128.0		100			
$[Cu_2(TMDT)_2(Im)_2](ClO_4)_3$	-26	129.0	143.0	91.8	161.9		4b
		129.0		90.0	160.2		
$[Cu_2(Pip)_2(Im)](NO_3)_3$	-27	121.0		95.0	166.3		4b
		120.0		80.1	158.9		
		124.0		90.0			
		128.0		77.4			
$[Cu_2(Macro)(Im)](Cl0_4)_3$	-21	134.4		79.1			4j
		129.1		68.8			
$[Cu_2$(Schiff Base)(Im)$](CF_3SO_3)_3$	-19.3	126.5	133.0	91.4		45.2	4k
		128.9	128.0	93.4			
			140.0				
$Na[Cu_2(Gly\text{-}Glyo)_2(Im)]$	-19	124.5	135	5.8	157.5	5.9	4l
		124.1		10.4	157.2		
$[Cu_3(IH)_2(hfca)_4]$	-30.3	145.6				11.7	4h
		166.3				41.6	
$[Cu_3(IP)_2(hfca)_4]$	-18.6	126.5					4i
		143.6					
$[L^1{}_4Cu_4(THF)_4]$	-49	146.14	142.2	44		139.1	this work
		142.80	132.6				

Im=imidazolate (1-), L=1,4,7-triazacyclononane, L' = 1.4,7-trimethyl-1,4,7- triazacyclononane, Bpim =4,5-bis[2-[[(2-pyridyl)ethyl]imino]-methyl] imidazolate, TMDTN, N,N',N'-tetramethyldiethylene triamine, Pip= 2-[2-[[(2 pyridyl) ethyl] imino] methyl] pyridine, Macro = a 30-membered macrocyclic ligand derived from 2,6-diacetylpyridine and 3,6-dioxaoctane-1,I-diamine,Gly-Glyo = glycylglycinate(2-), Schiff Base = macrocycle prepared from 2 molecules of 2,6-diacetylpyridine and 2 molecules of m-xylenediamine, IH = Schiff Base prepared from the condensation of 2.-imidazolecarboxaldehyde and histamine, IP = Schiff Base prepared from the condensation of 2.-imidazolecarboxaldehyde and 2-amino ethyl pyridine, hfca = hexafluroacetylacetonate anion.

the N-N and other Cu-N bonds are parallel to the imidazolate carbon-carbon bond, thus favoring a σ-exchange pathway. Although the coupling constant for **2** is strong compared to the other complexes, the values of J cannot be strictly attributed to the values of α and γ. This indicates that only σ-superexchange cannot be the only mechanism for the exchange coupling

for this compound. The presence of ligand-ligand interaction may also play a part in this type of exchange coupling.

X-band EPR spectra for **2** in solid state, from 11.7 K to 62.1 K , shows a isotropic signal at g =2.08 which remains constant for the given temperature range. This is attributed to the monomeric paramagnetic impurity (2%) present in the solid state. On increasing the temperature additional changes in the spectra is observed between the 15-263 mT and between 380-600 mT [Figure 2.9(a)]. Below 10 K no significant change in spectra was observed between 380-600 mT; however, on increasing the temperature, the intensity of the signal increases and reaches a maximum at 34.5 K.

In order to elucidate the correlation between the EPR spectra and the spin multiplets of the coupled system, the change of intensity(I) at 480 mT was analyzed for all the temperature (T) range. As the population of the excited state in first order is dependent on the Boltzmann function of resonating levels , an IT vs. T was plotted [Figure 2.9 (b)]. The fading below 10 K and the strong rise at elevated temperatures prove that the signals arise from excited states and that the ground state is diamagnetic and EPR silent, in accordance with the susceptibility findings. For quantitative analysis, the experimental data was compared with the theoretical Boltzmann functions, derived from the spin coupling model (Figure 2.7(b)). It is to be noted that values till 40K were taken as saturation occurs above this temperature. The best agreement was obtained for $I_{111}T$, describing the thermal population of the first excited triplet state |111>

$$I_{111}\ T \approx (\exp(-J/kT))/Z$$

$$\text{where } Z = 1+3\exp(-J/kT) + 7\exp(-J/kT)$$

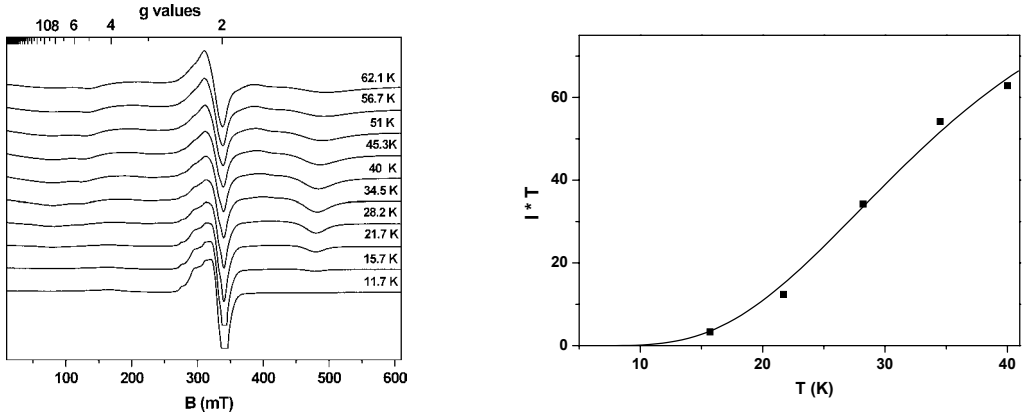

a) b)

Figure 2.9:- a) EPR spectra of **2**. b)Temperature dependence of the temperature- weighted intensity of the EPR spectra. The solid line are calculated Boltzmann functions: $I_{111}T$ with J = - 42 cm^{-1}.

The solid line is a fit with J = - 42 cm^{-1}, which is close to the exchange coupling constant of J = - 49 cm^{-1} evaluated from the susceptibility measurements. Therefore, the complex EPR spectra arising from 380-600 mT are assigned to the first excited triplet state |111> of the tetramer.

$[L^2Ni^{II}_2(\mu_2\text{-Urea})(\mu_2\text{-OOCMe})(MeOH)_2]$ (3)

The structure of **3** (Figure 2.10) shows the formation of a dinickel(II) complex with a bridging urea through the carbonyl oxygen. Ni(1) and Ni(2) are additionally bridged by a phenolate oxygen O(10) and an acetate ion. Each nickel is in a distorted octahedral NO_5 environment, being equatorially bound to the NO_3 donor set [Ni-N av. 1.975 Å; Ni-O av. 2.01 Å], and with axial interactions to an carboxylic O-donor of a bridging $MeCO_2^-$ group [Ni-O av. 2.09 Å] and a methanol O-donor [Ni-O 2.165, 2.159 Å] trans to the $MeCO_2^-$ group. Hydrogen atoms of the hydroxide group in MeOH and urea molecules were located from a difference map and are shown as circles of arbitrary radii in Fig. 2.10. The hydrogen atoms on the NH_2 groups of urea enter into hydrogen bonding with the phenolate oxygens, O(1) and O(17) with O(1)•••N(71) 2.784 and O(17)•••N(70) 2.813 Å, thus making urea presumably nonsusceptible to alcoholysis (see later). The intramolecular hydrogen bond between the methanol molecules cis-ligated to two different nickel(II) ions, O(40)•••O(50) 2.928 Å, is shown as dotted lines. The metal-metal distance Ni(1)•••Ni(2) of 2.966(1) Å in **3** is

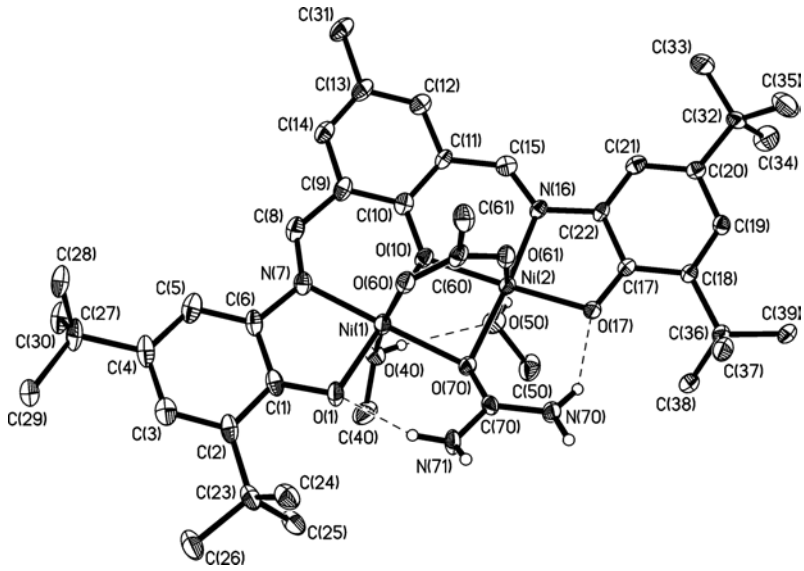

Figure 2.10 : - An ORTEP drawing of the neutral molecule **3**.

Table 2.5 *Selected bond distances (Å) and angles (degree) for* **3**

Ni(1)-O(1)	1.954(3)	Ni(2)-O(17)	1.967(3)
Ni(1)-N(7)	1.971(4)	Ni(2)-N(16)	1.978(4)
Ni(1)-O(10)	1.971(3)	Ni(2)-O(10)	1.986(3)
Ni(1)-O(70)	2.080(3)	Ni(2)-O(70)	2.065(3)
Ni(1)-O(60)	2.089(4)	Ni(2)-O(61)	2.088(4)
Ni(1)-O(40)	2.165(4)	Ni(2)-O(50)	2.159(4)
Ni(1)-Ni(2)	2.9656(11)	O(70)-C(70)	1.285(6)
N(70)-C(70)	1.323(7)	N(71)-C(70)	1.312(6)
	Ni(1)•••Ni(2)	2.966(1)	
O(17)-Ni(2)-N(16)	84.6(2)	O(1)-Ni(1)-N(7)	84.7(2)
O(17)-Ni(2)-O(10)	174.54(14)	O(1)-Ni(1)-O(10)	175.4(2)
N(16)-Ni(2)-O(10)	91.6(2)	N(7)-Ni(1)-O(10)	93.2(2)
O(17)-Ni(2)-O(70)	99.33(13)	O(1)-Ni(1)-O(70)	97.52(13)
N(16)-Ni(2)-O(70)	175.7(2)	N(7)-Ni(1)-O(70)	176.4(2)
O(10)-Ni(2)-O(70)	84.39(13)	O(10)-Ni(1)-O(70)	84.38(13)
O(17)-Ni(2)-O(61)	94.20(14)	O(1)-Ni(1)-O(60)	95.39(14)
N(16)-Ni(2)-O(61)	94.2(2)	N(7)-Ni(1)-O(60)	93.0(2)
O(10)-Ni(2)-O(61)	89.96(13)	O(10)-Ni(1)-O(60)	88.84(14)
O(70)-Ni(2)-O(61)	87.25(14)	O(70)-Ni(1)-O(60)	89.59(14)
O(17)-Ni(2)-O(50)	92.8(2)	O(1)-Ni(1)-O(40)	94.6(2)
N(16)-Ni(2)-O(50)	95.1(2)	N(7)-Ni(1)-O(40)	92.0(2)
O(10)-Ni(2)-O(50)	83.7(2)	O(10)-Ni(1)-O(40)	81.33(14)
O(70)-Ni(2)-O(50)	83.08(14)	O(70)-Ni(1)-O(40)	85.09(14)
O(61)-Ni(2)-O(50)	168.89(13)	O(60)-Ni(1)-O(40)	169.22(13)

significantly shorter than those observed in comparable complexes.[8,9] Bridging Ni-O (urea) distances, 2.080(3) and 2.065(3) Å, are significantly shorter than those in the only other single atom O-bridged urea compound, Ni-O (urea) 2.158(3) Å.[9] The Ni-O (urea) bond distances for compounds containing non-bridging urea lie within the range 2.05 - 2.13 Å.[8] The angle at bridging urea Ni(1)-O(70)-Ni(2) is 91.4(1)^{o} whereas the phenoxide bridging angle Ni(1)-O(10)-Ni(2) 97.1(2)^{o} is significantly greater. Relevant bond distances (Å) and angles (in degrees) are summarized in Table 2.5 .

The electronic spectra of **3** [Figure2.11(a)] show intense π-π* transitions below 480 nm, attributable to the ligand, as judged by their high absorption coefficients and comparison with the spectrum of the ligand (Table 2.6). Additionally, there are three broad, weak transitions in the visible-near IR region at 779, 858 and 1284 nm for **3**, indicating that the nickel ions are in an octahedral environment in solution as well as in the solid state (X-ray structure).

Table 2.6:- *Characteristic peaks in the electronic spectrum of* $[L^2]^{3-}$ *and* ***3.***

	Ligand with TBAOMe			**3**				
λ (nm)	300	350	496	330	464	779	858	1284
ε($M^{-1}cm^{-1}$)	6150	10,270	13,900	14,770	16,930	19	27	12

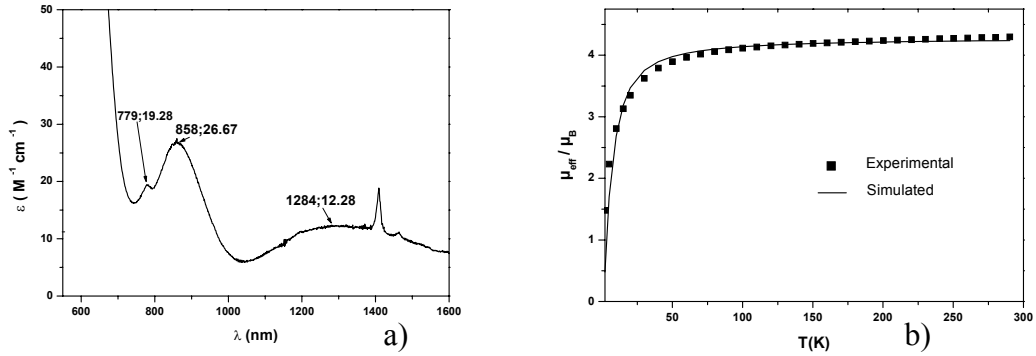

Figure 2.11 :- a) Electronic spectra of **3** showing the three lower energy bands. b)Magnetic measurements of **3**.

The magnetic susceptibility data for polycrystalline sample of **3** was collected to characterize the nature and magnitude of the exchange interaction propagated by the bridging ligands. The magnetic moment (μ_{eff}/molecule) for **3** of 4.280μ_B (χ_M•T=2.291 cm^3Kmol^{-1}) at 290 K decreases monotonically with decreasing temperature until it reaches a value of 1.474 μ_B (χ_M•T = 0.2717 cm^3 K mol^{-1}) at 2 K; this temperature dependence of μ_{eff} is a clear indication of an antiferromagnetic exchange coupling between two paramagnetic centers Ni(II) (S_{Ni} = 1) with a resulting diamagnetic ground state. Using only D (i.e. J = 0) a fit of a poor quality with unusually large D was obtained and hence discarded. Attempts to fit the data using both D and J yield physically meaningless D values. For example, a good fit was obtained with the following parameters: J = -2.6 cm^{-1}, D = +27.1 cm^{-1}, g = 2.13, P = 0.5%. As the zero-field splitting D is unusually large for a 6-coordinated Ni(II) ion, the solution was discarded. Finally, the solid line in Figure 2.11(b) represents the best fit with the following parameters: J = -3.5 cm^{-1}, $g_1 = g_2$ = 2.137, P = 0.5%. The quality of the fit is insensitive to D varying between 0 - 5 cm^{-1}.

The nickel complex **3** shows waves at +0.970 ,+0.470 V and preceded by one broad wave at +0.270 V in square wave voltammetry (SQW) mode (25 Hz) [Figure 2.12].

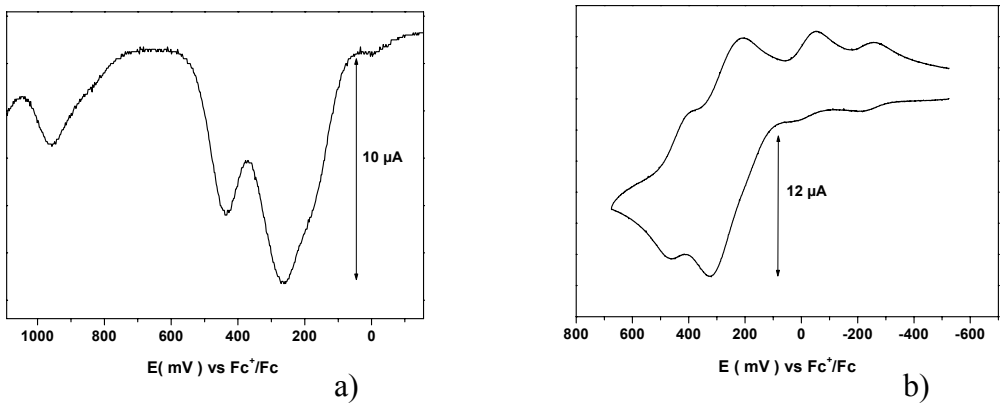

Figure 2.12 :- a) Square wave and b) Cyclic Voltammogram of **3.**

Additionally, with increasing scan rate the oxidation and re-reduction peaks in the cyclic voltammogram (CV) was found to split into two components. This complicated behavior was assigned to an involvement of the metal nickel(II)-ion in the redox processes leading to radical through oxidation. Ligand centered oxidation to radical is inferred from the occurrence of oxidation processes at potentials which are similar, irrespective of the nature of the central metal ion, and involvement of central nickel ions in oxidation processes of radical complexes was documented earlier[10] in detail, including digital simulations of complex cyclic voltammograms.

When an ethanolic solution of **3,** in presence of 50 times of urea, was refluxed at 80°C for 14 hours, a gas chromatography study showed that ethanol was converted to urethane (ethyl carbamate). However, calculation with undecane (C_{11}) as standard, showed that the turnover number, defined as the ratio of the number of moles of product to that of catalyst used, was one. This means that **3 does not** catalyze the ethanolysis of urea to urethane presumably due to hydrogen bonding network involving urea in **3**, which is also maintained in solution. Due to the presence of stable hydrogen bonded structure in solution, there is no possibility of intramolecular EtO^--delivery to the π^* orbital of urea, as has been proposed for the mechanism of action of urease (here OH^-).[11,9] It is noteworthy that the bond lengths within the coordinated urea,[8] bridging or non-bridging, are very similar, in contrast to the compound which exhibits catalytic activity.[8g]

$[(L^2H)_2Ni^{II}_4(\mu_3\text{-}OMe)_2(OOCMe)_2(MeOH)_2]$ (4)

The crystal structure of **4** is shown in Figure 2.13 with selected bond distances and angles provided in Table 2.7. The molecule is based on a roughly cubic Ni_4O_4[12] unit, consisting of two interpenetrating tetrahedra, one of four nickel atoms and one of four μ_3-oxygen atoms originating from cresol-phenolates (O10, O50) part of the ancillary ligand L^2 and methoxide groups (O81, O91). Each Ni(II) is in a distorted octahedral environment with an NO_5 donor set. For Ni(1) and Ni(4) a peripheral ligation is provided by a monodentate acetate ion, whereas for Ni(2) and Ni(3) a methanol molecule (O82 and O92, respectively) completes the sixth coordination position. The ancillary Schiff's base ligands are present in monoprotonted form HL^2 and protonated at O(1) and O(58) building hydrogen bonds with O(84) and O(94) of the acetate ions, respectively, O(1)•••O(84) 2.426 Å and O(58)•••O(94) 2.449 Å. Although it was not possible to locate all hydrogen atoms in the structure, the intra-molecular contacts between the oxygen atoms of the methanol molecules (O82 and O92) and

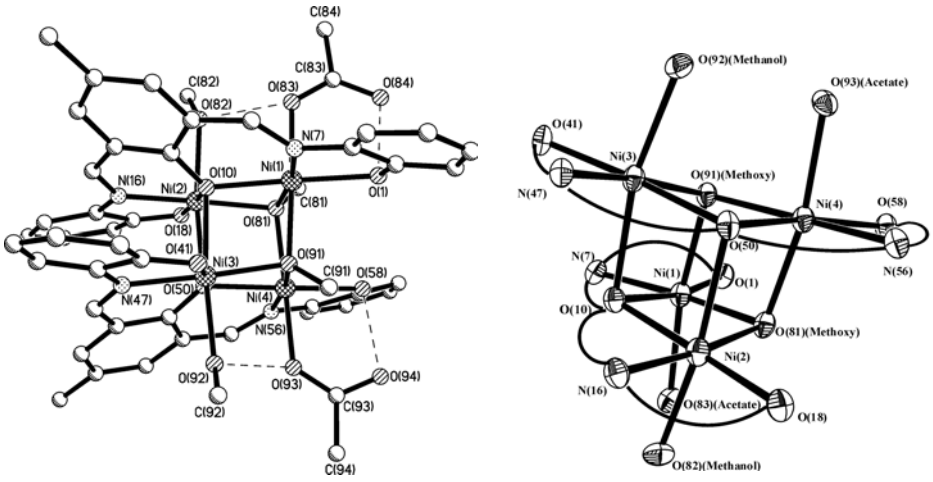

a) b)

Figure 2.13:-(a)Molecular structure of **4.** The tert-butyl groups have been removed for clarity. (b)A view of **4** highlighting the Ni_4O_4-cubane core. The pentadentate ligand $[HL^{2}]^{-2}$ is denoted only by the donor atoms joined by the curved lines.

Table 2.7 *Selected bond distances (Å) and angles (degree) for* **4**

Ni(1)-N(7)	1.988(7)	Ni(3)-O(41)	1.970(6)
Ni(1)-O(91)	2.050(6)	Ni(3)-N(47)	1.994(7)
Ni(1)-O(81)	2.052(6)	Ni(3)-O(91)	2.052(6)
Ni(1)-O(10)	2.081(6)	Ni(3)-O(50)	2.054(6)
Ni(1)-O(1)	2.089(6)	Ni(3)-O(92)	2.109(6)
Ni(1)-O(83)	2.112(6)	Ni(3)-O(10)	2.219(6)
Ni(2)-O(18)	1.970(6)	Ni(4)-N(56)	1.979(7)
Ni(2)-N(16)	1.984(7)	Ni(4)-O(91)	2.042(6)
Ni(2)-O(81)	2.024(6)	Ni(4)-O(81)	2.055(6)
Ni(2)-O(10)	2.049(6)	Ni(4)-O(50)	2.069(6)
Ni(2)-O(82)	2.123(6)	Ni(4)-O(93)	2.092(7)
Ni(2)-O(50)	2.229(6)	Ni(4)-O(58)	2.126(6)
	Ni(1)•••Ni(2)	3.047	
	Ni(3)•••Ni(4)	3.077	
	Ni(1)•••Ni(3)	3.191	
	Ni(2)•••Ni(4)	3.155	
	Ni(1)•••Ni(4)	3.102	
	Ni(2)•••Ni(3)	3.227	
O(91)-Ni(3)-O(50)	82.2(2)	O(10)-Ni(1)-O(83)	96.4(2)
O(41)-Ni(3)-O(92)	94.5(3)	O(1)-Ni(1)-O(83)	89.6(2)
N(47)-Ni(3)-O(92)	89.5(3)	O(18)-Ni(2)-N(16)	83.8(3)
O(91)-Ni(3)-O(92)	93.3(2)	O(18)-Ni(2)-O(81)	101.3(2)
O(50)-Ni(3)-O(92)	87.5(2)	N(16)-Ni(2)-O(81)	174.3(3)
O(41)-Ni(3)-O(10)	96.8(2)	O(18)-Ni(2)-O(10)	174.3(2)
N(47)-Ni(3)-O(10)	97.0(3)	N(16)-Ni(2)-O(10)	90.9(3)
O(91)-Ni(3)-O(10)	78.9(2)	O(81)-Ni(2)-O(10)	83.9(2)
O(50)-Ni(3)-O(10)	81.9(2)	O(18)-Ni(2)-O(82)	96.4(3)
O(92)-Ni(3)-O(10)	167.6(2)	N(16)-Ni(2)-O(82)	88.6(3)
N(56)-Ni(4)-O(91)	171.3(3)	O(81)-Ni(2)-O(82)	93.2(2)
N(56)-Ni(4)-O(81)	99.8(3)	O(10)-Ni(2)-O(82)	85.5(2)
O(91)-Ni(4)-O(81)	81.0(2)	O(18)-Ni(2)-O(50)	96.9(2)
N(56)-Ni(4)-O(50)	89.4(3)	N(16)-Ni(2)-O(50)	96.9(3)
O(91)-Ni(4)-O(50)	82.0(2)	O(81)-Ni(2)-O(50)	80.2(2)
O(81)-Ni(4)-O(50)	83.4(2)	O(10)-Ni(2)-O(50)	81.8(2)
N(56)-Ni(4)-O(93)	89.8(3)	O(82)-Ni(2)-O(50)	166.1(2)

N(7)-Ni(1)-O(91)	100.1(3)	O(81)-Ni(1)-O(83)	88.4(2)
N(7)-Ni(1)-O(81)	170.6(3)	O(91)-Ni(4)-O(93)	89.0(2)
N(7)-Ni(1)-O(1)	80.9(3)	O(81)-Ni(4)-O(93)	169.9(2)
O(91)-Ni(1)-O(1)	93.7(2)	O(50)-Ni(4)-O(93)	93.7(2)
O(81)-Ni(1)-O(1)	108.4(2)	N(56)-Ni(4)-O(58)	80.2(3)
O(10)-Ni(1)-O(1)	167.9(2)	O(91)-Ni(4)-O(58)	108.5(2)
N(7)-Ni(1)-O(83)	90.5(3)	O(81)-Ni(4)-O(58)	94.0(2)
O(91)-Ni(1)-O(81)	80.9(2)	O(50)-Ni(4)-O(58)	168.7(2)
N(7)-Ni81)-O(10)	88.5(3)	O(93)-Ni(4)-O(58)	90.7(2)
O(91)-Ni(1)-O(10)	82.3(2)	O(81)-Ni(1)-O(10)	82.4(2)
O(91)-Ni(1)-O(83)	169.3(2)		

the oxygen atoms of the acetate groups (O83 and O93, respectively) of 2.657 Å and 2.684 Å, can be interpreted as hydrogen bonds. Ni-O-Ni angles vary between 94.4(2) and 102.2(3)^{o}. Ni•••Ni distances on different cubic faces are also different, the shortest being Ni(1)•••Ni(2) 3.047 Å and the longest Ni(2)•••Ni(3) 3.227 Å. Average Ni-N and Ni-O bond distances of 1.99 and 2.10 Å, respectively, lie well within the range of reported values for the corresponding bond distances of the tetranuclear cubane-like Ni(II).[12] No substantial differences in bond lengths and angles are found between the two crystallographically independent molecules .

The electronic spectra of **4** shows similar intense π-π* transitions, like **3**, below 480 nm, which is again attributable to the ligand. Interestingly only one broad absorption in the range 917 nm for **4** [Figure 2.14] is observed as compared to **3.**

For **4**, the effective magnetic moment μ_B of 6.08 μ_B (χ_M•T = 4.629 cm^3 K mol^{-1}) at 290 K increases monotonically with decreasing temperature reaching a broad maximum at 20 - 30 K with μ_{eff} = 6.39 μ_B (χ_M•T = 5.1073 cm^3 K mol^{-1}). Below 20 K μ_{eff} starts to decrease reaching a value of 3.99 μ_B (χ_M•T = 1.992 cm^3 K mol^{-1}) at 2 K (Figure 2.15a); it is clear that the magnetic properties of **4** are dominated by a ferromagnetic exchange interaction between four $^3A_2$ nickel(II) ions as propagated by bridging phenoxides and methoxides. Structural

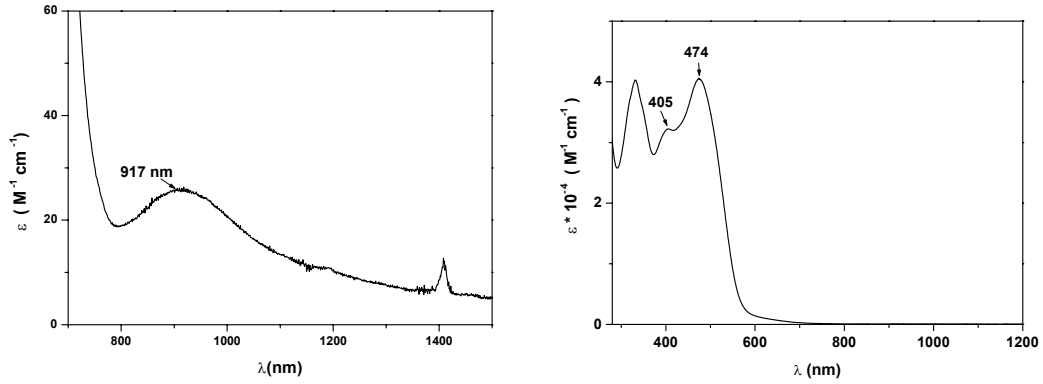

a) b)

Figure 2.14:- (a)Electronic spectra of **4** showing single band at 917 nm. (b) Electronic spectra from 280 to 1200.

parameters of **4** strongly suggest a lower symmetry than T_d (idealized D_{2d}) for the molecule. The magnetic analysis were carried out using either a two-J or three-J models based on the diagram shown in inset [Figure 2.15 (a)].

The data were fit initially by using a higher symmetry model, i.e. $J_{12} = J_{34}$ and $J_{13} = J_{14} = J_{24} = J_{23}$, which yielded a good fit (not shown) with $J_{12} = J_{34} = +1.5$ cm^{-1}, $J_{13} = J_{14} = J_{24} = J_{23} = +0.25$ cm^{-1}, g = 2.133, D = 14.8 cm^{-1}. This solution was discarded, as the zero-field splitting D is unusually large for a 6-coordinated $^3A_2$ Ni(II) ion.[13] Therefore the data was fitted with three different exchange parameters, which also corroborate with three different types of faces present in the Ni_4O_4 cubane core of **4**. The best fit parameters are: $J_{12} = J_{34} = +0.47$ cm^{-1}, $J_{13} = J_{24} = +4.25$ cm^{-1}, $J_{14} = J_{23} = -1.45$ cm^{-1}, g = 2.122 and D = 0 (fixed). The most important parameter in the magnetostructural correlation of the Ni_4O_4 cubane cores has been described in the literature[12] to be the averaged Ni-O-Ni angle of a cubane-face. A ferromagnetic exchange interaction is observed when this angle is close to orthogonality. On the other hand, the Ni-O-Ni angles in the vicinity of and larger than 99^o lead to antiferromagnetic interaction. Thus the strongest ferromagnetic coupling of $J_{13} = J_{24} = +4.25$ cm^{-1} should be associated with the average Ni(1)-O-Ni(3) angle of 99.0^o, which would be not in agreement with the magnetostructural correlation reported in the literature.[12] This suggested that a better fitting model should be used. So, the data was fitted again by using three different exchange parameters, but with the following constraints: J_{12}, J_{13} and $J_{14} = J_{24} = J_{23} = J_{34}$, as three different ranges of average Ni-O-Ni angles of 96^o, 97-98^o and 99^o are present in **4**. The best fit obtained with the parameter set, $J_{12} = +8.0$ cm^{-1}, $J_{14} = J_{24} = J_{23} = J_{34} = +0.9$ cm^{-1}, $J_{13} = -3.95$ cm^{-1}, g=2.120, D = 0 (fixed) is shown as a solid line in Figure 2.15(a). The differences and nature of the signs of the exchange parameters are in full accord with the Ni-O-Ni angle correlation and support the three-J model used, which takes into account the reduced symmetry of the cubane core observed in the X-ray structure of **4**. Thus these results for **4** predict a switch from ferromagnetic to antiferromagnetic coupling only for angles Ni-O-Ni above 98^o.

Recently it has been demonstrated[12i] that the major contributor to the superexchange constants observed in $[Ni_4(OR)_4]^{4+}$ cubanes is the Ni-O-Ni angle. A list of the nickel cubane complexes is listed in Table 2.8. Accordingly, a linear correlation between J and Ni-O-Ni angle has also been described[12i,12m]. A plot the observed J values for **4** and other structurally characterized $[Ni_4(OR)_4]^{4+}$ cubanes against average Ni-O-Ni angles [Figure2.15(b)] was done. The solid line drawn as a guide to the eyes shows a fairly good correlation between J and the

angles. The borderline between ferromagnetic and antiferromagnetic interaction, as seen here, is 98 ° which agrees well when compared to other nickel cubanes. This guide also allows one

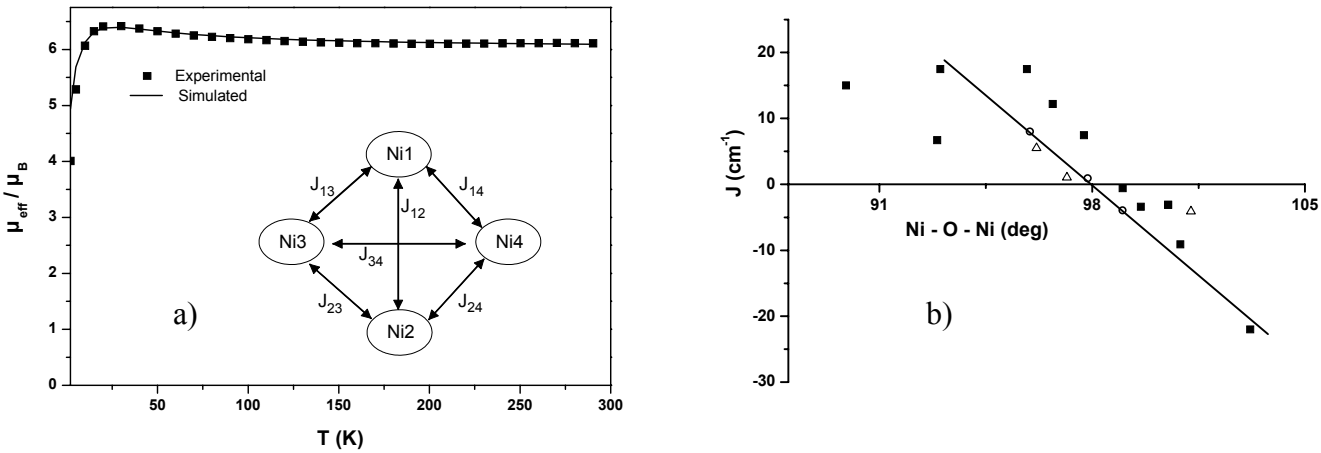

Figure 2.15 :- a) Magnetic measurement at 1T for **4**.(Inset:- The magnetic interaction (J) model used in simulating the experimental curve.) b) Plot of J vs Ni-O-Ni angle in $[Ni_4(OR)_4]$ cubanes. The values depicted by filled squares and open triangles are from literature and that of open circles are from this work.

Table 2.8 :- *J as a function of the Ni-O-Ni angles for the $[Ni_4(\mu_3\text{-}OR)_4]$ cubanes*

Complex	Ni-O-Ni$_{av}$ (deg)	J (cm^{-1})	Reference
$[Ni_4(\mu_3\text{-}OMe)_4\ (sal)_4(EtOH)_4]$	97.73	7.46	12a
$[Ni_4(\mu_3\text{-}OH)_4\ (chta)_4(NO_3)_4]$	99.0	-0.57	12b
$[Ni_4(\mu_3\text{-}OMe)_4\ (TMB)_4(\mu\text{-}O_2CMe)_4]$	93.0 100.9	17.5 - 9.1	12d
$[Ni_4(\mu_3\text{-}OH)_4\ (tzdt)_4(py)_4]$	95.89 103.2	17.5 -22.0	12f
$[Ni_4(\mu_3\text{-}OMe)_4\ (dbm)_4(MeOH)_4]$	96.7 99.6	2.2 -3.4	12i
$[Ni_4(\mu_3\text{-}OH)_2\ (pypentO)(pym)\ (\mu\text{-}Oac)_2\ (NCS)_2(OH_2)]$	89.9 92.9 100.5	15.0 6.7 -3.09	12m
$[Ni_4(\mu_3\text{-}OMe)_4\ (L^{Se})_2(MeOH)_2(MeCN)_2]$	96.17 97.17 101.25	5.50 1.05 -4.1	12n
$[Ni_4(L^2H)_2(\mu_3\text{-}OMe)_2\ (OAc)_2(MeOH)_2]$	95.94 97.85 99.0	8.0 1.0 -3.8	this work, 12o

salH = salicylaldehyde; chta = r-1-c-3-c-5 triaminocyclohexane; TMB=2,5-dimethyl-2,5-diisocyanohexane; dzdt = 1,3-thiazolidine-2-thione; dbmH = dibenzoylmethane; py = pyridine; pypentO = 1,5-bis[(2-pyridylmethyl)amino]-3-pentanolate; pym = 2-pyridylmethanolate; L^{Se} = 2,2′-seleno-bis(4,6-di-*tert*-butylphenol).

to notice that the antiferromagnetic interactions (-J) fall fairly well on the correlated line with respect to Ni-O-Ni angles. In contrast, the positive J values scatter appreciably. This is not surprising considering the high tolerance attached in general to the positive J values (ferromagnetic interactions) evaluated through simulation of the susceptibility data.

The non-zero magnetic moment of 3.99 μ_B at 2 K and the broad maximum with μ_{eff} = 6.39 μ_B at 20 - 30 K indicate that **4** has a complicated low-lying magnetic structure with a non-diamagnetic ground state smaller than the spin state of S_t = 4, expected for a ferromagnetically coupled tetranuclear nickel(II) (S_{Ni} = 1). The ground state can be determined by examining the magnetization of the compound at low temperatures as a function of the applied magnetic fields. Magnetization measurements have performed at applied magnetic fields of 1, 4 and 7 T. The field-dependent magnetizations as a function of temperature and their simulations are depicted in Figure 2.16. It is clear from Figure 2.16 that the saturated magnetization value reaches ~3.035 in the temperature range 2.0 - 2.8 K at the highest field of 7 T. The simulated parameters are: J_{12} = +8.0 cm^{-1}, J_{13} = -3.95 cm^{-1}, $J_{14} = J_{24} = J_{23} = J_{34}$ = +0.60 cm^{-1}, g = 2.12, $|D|$ = 3.0 cm^{-1}. These values corroborate well with those from the susceptibility measurements. As J_{12}, J_{13} and D are of similar magnitude, it is not possible to calculate the ground state in the form of an S_t value; S is not a good quantum number to describe the ground state, but rather M_S.

The compound **4** an irreversible oxidation wave at +0.163 V against Fc^+/Fc with other peaks at +0.44 V and 1.26 V [Figure 2.17]. At different scan rates, the peaks are scattered, the same observation as seen for **3**. Ligand center phenoxyl-radical formation is inferred.

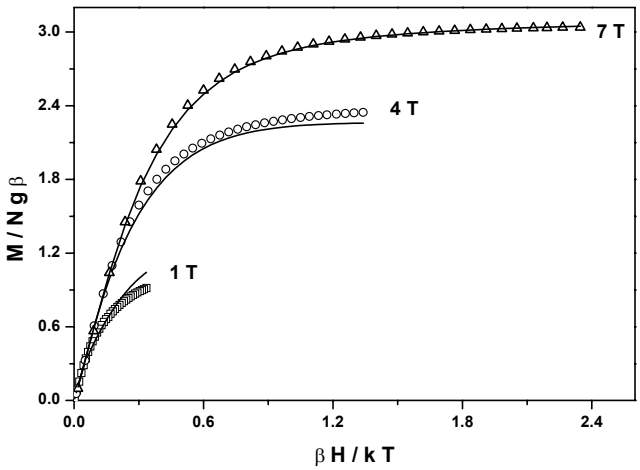

Figure 2.16 :- Field dependent magnetization curve of **4**.The open triangle, circle and square represents the experimental curve at 1,4 and 7 T respectively. The solid line is the simulated curve.

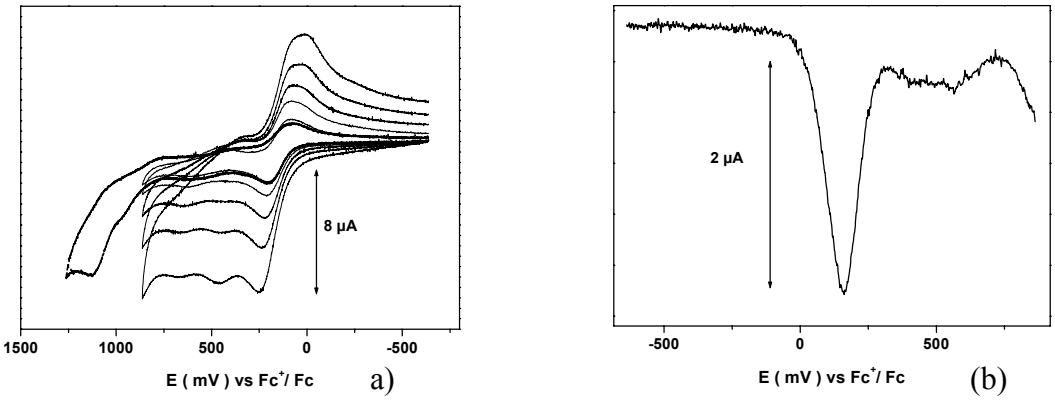

Figure 2.17 :- (a) Cyclic voltammogram of **4** at different scan rates b) Square wave voltammogram of **4** (10 Hz).

$[L^2Cu^{II}_2(OCH_3)(THF)_2]$ (5)

Although the analytical and spectroscopic data showed the presence of a dinuclear Cu_2 core as the smallest unit in **5**, an X-ray analysis was undertaken to remove the doubts regarding connectivity. Unfortunately, crystals of **5** diffract X-rays very weakly. In spite of the high R factor and large standard deviations, the crystal structure analysis of **5** confirmed its dinuclear structure. Selected bond lengths and angles are given in Table 2.9. The crystal structure reveals that the copper atoms are doubly bridged by the phenoxo and by a methoxide group (Figure 2.18). The penta-coordination of copper atoms is achieved by a tetrahydrofuran oxygen with Cu(1)-O(60) and Cu(2)-O(50) distances of 2.444 Å and 2.566 Å, respectively, which are oriented *trans* to each other in the dicopper complex. The coordination polyhedron for the copper centers is distorted square pyramid with O(1)N(7)O(10)O(40) for Cu(1) and O(10)N(16)O(17)O(40) for Cu(2) forming the equatorial planes, where Cu(1) and Cu(2) are respectively located at 0.102 Å and 0.134 Å out of the equatorial planes. The ring Cu(1)O(10)Cu(2)O(40) is not planar, the dihedral angle being 12.7°. The distances Cu-N and Cu-O are in the ranges reported for comparable complexes. [14]

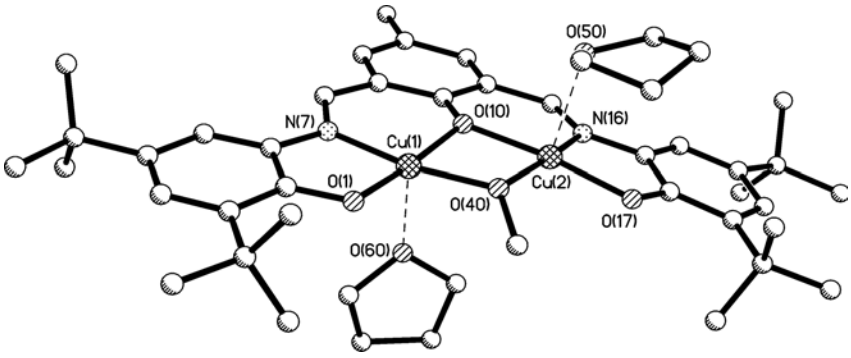

Figure 2.18:-A perspective view of the neutral complex **5.**

Table 2.9 *Selected bond distances (Å) and angles (degree) for* **5**

Cu(1)-O(1)	1.899(6)	Cu(2)-O(17)	1.880(7)
Cu(1)-O(40)	1.911(6)	Cu(2)-O(40)	1.905(6)
Cu(1)-N(7)	1.915(8)	Cu(2)-N(16)	1.931(8)
Cu(1)-O(10)	1.948(6)	Cu(2)-O(10)	1.952(7)
Cu(1)-O(60)		Cu(2)-O(50)	
	Cu(1)•••Cu(2)	2.974(2)	
Cu(1)-O(10)-Cu(2)	99.38(31)	O(10)-Cu(1)-N(7)	93.25(30)
Cu(1)-O(40)-Cu(2)	102.43(31)	O(40)-Cu(2)-O(10)	78.55(27)
O(1)-Cu(1)-O(10)	173.32(27)	O(40)-Cu(2)-N(16)	167.77(30)
O(40)-Cu(1)-N(7)	170.28(28)	O(40)-Cu(2)-O(17)	101.62(29)
O(1)-Cu(1)-O(40)	100.83(26)	O(10)-Cu(2)-N(16)	92.48(33)
O(1)-Cu(1)-N(7)	86.78(29)	N(16)-Cu(2)-O(17)	86.24(34)
O(40)-Cu(1)-O(10)	78.49(27)	O(10)-Cu(2)-O(17)	172.80(28)

The electronic spectra of **5** from 1000 to 200 nm shows strong π-π* band at 486nm with a high absorbance value (17,000 M^{-1} cm^{-1}) [Figure 2.19(a)]. These bands are all ligand based and can be compared with the absorbance bands for the deprotonated ligand .

Variable-temperature magnetic data for **5** exhibit a steady decrease of μ_{eff} from 1.634 μ_B (χ_M•T = 0.3338 cm^3 K mol^{-1}) at 290 K to 0.049 μ_B (χ_M•T = 0.03 x 10^{-3} cm^3 K mol^{-1}) at 2 K, which is indicative of very strong intramolecular antiferromagnetic coupling. The experimental data were simulated with the parameter set J = -192.1 cm^{-1}, g = 2.055, TIP =30 x 10^{-6}, P = 0 and is shown in Figure 2.19(b). The major factor controlling the exchange interactions in hydroxo-, alkoxo- and phenoxo-bridged copper(II) is the Cu-O-Cu bridge angle.[15,16] The average Cu-O-Cu bridge angle of 100.9° for **5** would result in an approximate J value of -250 cm^{-1} according to the empirical equation reported in the literature and it deviates appreciably from the experimentally evaluated value of -192 cm^{-1} for **5**. A possible reason for the weak exchange coupling in **5** may be the deviation from co-planarity within the central Cu_2O_2 ring. It seems plausible that the methoxide ion, with the shorter Cu(1)-O(40) 1.911 Å and Cu(2)-O(40) 1.905 Å distances and larger Cu(1)-O(40)-Cu(2) angle 102.43° than those with the phenoxide ion, provides a better pathway for antiferromagnetic exchange coupling.[14]

Electrochemical voltammetric measurements (cyclic voltammetry, CV, and square wave voltammetry, SQW) were performed with the complexes in CH_2Cl_2 solutions containing 0.1 M $TBAPF_6$ [Figure 2.20]. The copper(II) complex **5** exhibit an oxidation wave at +0.490 vs Fc^+/Fc for **5**. The waves have reversible appearance, however the peaks in CV and SQW are broad; the peak separation of the oxidative and reductive peaks in the CVs is relatively high(0.110 V even at low scan rates) and in SQW shoulders on the forward and reverse peaks

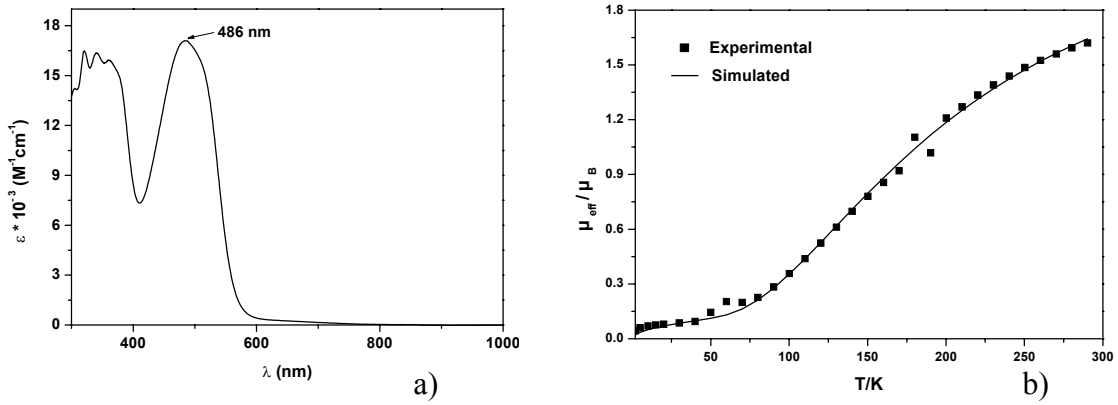

Figure 2.19 :- a) Electronic spectra of **5.** b) Magnetic data of **5**.

are discernible. Since a copper(II)-oxidation is not feasible at such low potentials, these redox processes were assigned to ligand centered oxidation yielding two phenoxyl radicals in the complex.

$[L^2{}_2Cu^{II}{}_4(\mu_4\text{-}O)]$ (6)

The molecular structure of **6** is shown in Figure 2.21. Selected interatomic distances and bond angles are listed in Table 2.10. Compound **6** consists of four copper(II) ions bridged by a central μ_4-oxygen atom in an approximately tetrahedral environment. The phenolate oxygen atoms, O(10) and O(50), of the cresol-part of the ligand bridge two copper centers, resulting in very similar angles Cu(1)-O(10)-Cu(2) and Cu(3)-O(50)-Cu(4) of 99.49(9)^o and 99.12(9)^o. Each copper center is coordinated by three oxygen atoms and one nitrogen atom, with the bond lengths ranging from 1.891(2) to 1.953(2) Å. There are considerable deviations

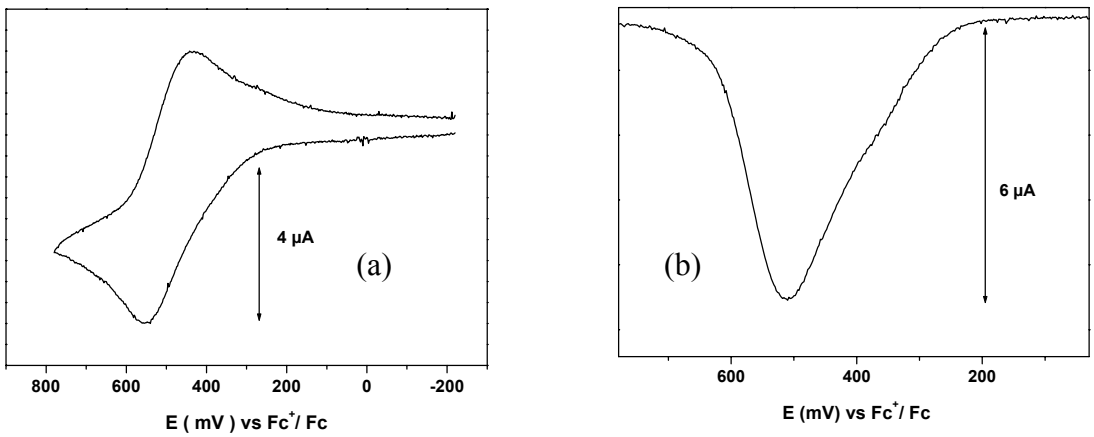

Figure 2.20:- (a) Cyclic and (b) square wave voltammogram (10 Hz) of **5**.

of the geometry of the copper center from the ideal square plane, as indicated by the basal plane angles (Table 2.10), although each CuO_3N portion is essentially planar. The dihedral angles between the Cu(1)/Cu(2) planes, and between the Cu(3)/Cu(4) planes are 8.5° and 3.2°, respectively. The two $Cu_2O_4N_2$ dinuclear units are nearly perpendicular as evidenced by the dihedral angle of 75.2° between the Cu(1)O(10)Cu(2)O(99) and Cu(3)O(50)Cu(4)O(99) planes. The copper tetrahedron around the μ_4-oxygen O(99) is distorted, as the bond angles Cu-O(99)-Cu range from 122.37(1)° for Cu(2)-O(99)-Cu(3) to 90.23(8) for Cu(4)-O(99)-Cu(1), the smallest among the six angles at O(99). Perhaps as a consequence, the Cu(2)•••Cu(3) distance of 3.356 Å is substantially longer than that of Cu(4)•••Cu(1), 2.759 Å. The remaining Cu•••Cu distances are Cu(1)•••Cu(2) 2.963, Cu(1)•••Cu(3) 3.368,

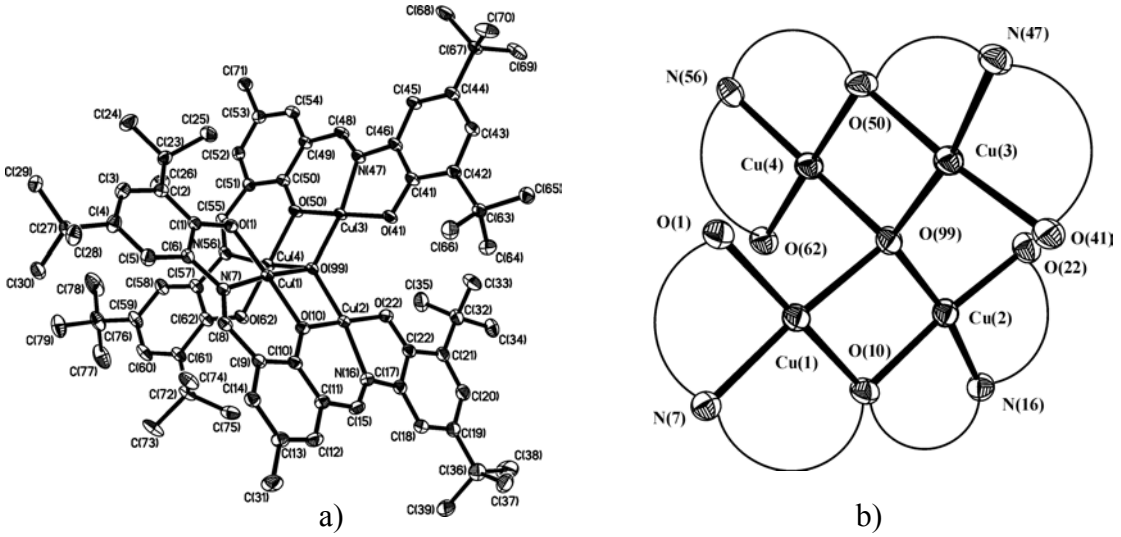

Figure 2.21:- a) Molecular structure of **6**. b) The atom connectivity in the core of complex **6**.

Table 2.10:- *Selected interatomic distances (Å) and angles (deg) for* ***6***

Cu(1)-O(1)	1.903(2)	Cu(3)-O(41)	1.897(2)
Cu(1)-N(7)	1.919(3)	Cu(3)-O(99)	1.915(2)
Cu(1)-O(10	1.925(2)	Cu(3)-N(47)	1.932(2)
Cu(1)-O(99)	1.953(2)	Cu(3)-O(50)	1.950(2)
Cu(2)-O(22)	1.897(2)	Cu(4)-O(62)	1.891(2)
Cu(2)-O(99)	1.915(2)	Cu(4)-N(56)	1.916(3)
Cu(2)-N(16)	1.927(3)	Cu(4)-O(50)	1.920(2)
Cu(2)-O(10)	1.956(2)	Cu(4)-O(99)	1.942(2)
Cu(1)•••Cu(4)	2.760(1)	Cu(1)•••Cu(3)	3.368(1)
Cu(1)•••Cu(2)	2.963(1)	Cu(2)•••Cu(4)	3.345(1)
Cu(3)•••Cu(4)	2.945(1)	Cu(2)•••Cu(3)	3.356(1)
Cu(2)-O(99)-Cu(3)	122.37(11)	N(7)-Cu(1)-O(99)	173.77(10)
Cu(2)-O(99)-Cu(4)	120.30(11)	O(10)-Cu(1)-O(99)	80.02(9)
Cu(3)-O(99)-Cu(4)	99.58(9)	O(1)-Cu(1)-Cu(4)	71.26(7)
Cu(2)-O(99)-Cu(1)	99.98(9)	N(7)-Cu(1)-Cu(4)	137.58(7)
Cu(3)-O(99)-Cu(1)	121.07(11)	O(10)-Cu(1)-Cu(4)	106.01(7)
Cu(4)-O(99)-Cu(1)	90.23(8)	O(99)-Cu(1)-Cu(4)	44.71(6)
Cu(4)-O(50)-Cu(3)	99.12(9)	O(1)-Cu(1)-Cu(2)	138.52(7)
Cu(1)-O(10)-Cu(2)	99.49(9)	N(7)-Cu(1)-Cu(2)	134.27(8)
O(1)-Cu(1)-N(7)	86.44(10)	O(10)-Cu(1)-Cu(2)	40.64(6)
O(1)-Cu(1)-O(10)	175.87(9)	O(99)-Cu(1)-Cu(2)	39.53(6)
N(7)-Cu(1)-O(10)	93.86(10)	Cu(4)-Cu(1)-Cu(2)	71.43(2)

O(1)-Cu(1)-O(99)	99.59(9)	O(22)-Cu(2)-O(99)	102.40(9)
O(22)-Cu(2)-N(16)	86.48(11)	N(47)-Cu(3)-Cu(4)	131.12(8)
O(99)-Cu(2)-N(16)	170.27(10)	O(50)-Cu(3)-Cu(4)	40.07(6)
O(22)-Cu(2)-O(10)	174.81(9)	O(62)-Cu(4)-N(56)	87.16(10)
O(99)-Cu(2)-O(10)	80.20(9)	O(62)-Cu(4)-N(50)	178.00(9)
N(16)-Cu(2)-O(10)	91.26(10)	N(56)-Cu(4)-O(50)	94.35(10)
O(22)-Cu(2)-Cu(1)	142.89(7)	O(62)-Cu(4)-O(99)	97.66(9)
O(99)-Cu(2)-Cu(1)	40.49(6)	N(56)-Cu(4)-O(99)	172.05(10)
N(16)-Cu(2)-Cu(1)	130.53(8)	O(50)-Cu(4)-O(99)	80.69(9)
O(10)-Cu(2)-Cu(1)	39.86(6)	O(62)-Cu(4)-Cu(1)	131.72(8)
O(41)-Cu(3)-O(99)	101.94(9)	N(56)-Cu(4)-Cu(1)	104.47(6)
O(41)-Cu(3)-N(47)	86.63(10)	O(50)-Cu(4)-Cu(1)	45.06(6)
O(99)-Cu(3)-N(47)	169.95(10)	O(99)-Cu(4)-Cu(1)	137.53(7)
O(41)-Cu(3)-O(50)	174.51(10)	O(62)-Cu(4)-Cu(3)	134.87(8)
O(99)-Cu(3)-O(50)	80.61(9)	N(56)-Cu(4)-Cu(3)	40.81(6)
N(47)-Cu(3)-O(50)	91.31(10)	O(50)-Cu(4)-Cu(3)	39.88(6)
O(41)-Cu(3)-Cu(4)	142.25(6)	O(99)-Cu(4)-Cu(3)	72.29(2)
O(99)-Cu(3)-Cu(4)	40.54(6)		

Cu(2)•••Cu(4) 3.345, Cu(3)•••Cu(4) 2.945 Å. Thus these differences can be explained by the steric forces of the chelating ligand $[L^{2}]^{3-}$ which contracts the Cu(1)-O(99)-Cu(4) angle with a concomitant expansion of the opposite angle Cu(2)-O(99)-Cu(3). Examples of tetranuclear copper(II) complexes with a μ_4-O kernel are abundant,[15,17,18] but all of them involve bridging ligands like halides or carboxylates between the edges of the tetrahedron. Compound **6** without any such bridging ligand is an exception. Figure 2.21(b) highlights the core structure for greater clarity and to emphasize the unique structure of the $Cu_4(\mu_4\text{-O})$-unit present in **6**.

The effective magnetic moment μ_{eff}/molecule for **6** of 2.768 μ_B ($\chi_M \bullet T$ = 0.9582 cm^3 K mol^{-1}) at 290 K decreases monotonically with decreasing temperature until it reaches a value of 0.133 μ_B ($\chi_M \bullet T$ = 0.0022 cm^3 K mol^{-1}) at 2 K indicating dominant antiferromagnetic interactions between four $^2B_2$ copper(II) ions; the data clearly show an $S_t = 0$ ground state for **6**.

Two different exchange pathways are envisagable for **6**: Cu-phenoxo-Cu and Cu-μ_4-oxo-Cu. Figure 2.22(a), shows the connection of the copper centers through the phenoxo and the oxo-group. As the pairs Cu(3)/Cu(4) and Cu(2)/Cu(1) are bridged by both phenoxo and oxo groups and the pairs Cu(4)/Cu(1), Cu(2)/Cu(3), Cu(2)/Cu(4) and Cu(1)/Cu(3) only through the oxo group, O(99), the experimental magnetic data were analyzed as a first approximation with a three-J model: $J_{12} = J_{34}$, $J_{14} = J_{23}$ and $J_{24} = J_{13}$. In this model the differences in the Cu- O-Cu angles has been neglected. A very good fit (not shown) was obtained with the following parameters: $J_{12} = J_{34} = -86.3$ cm^{-1}, $J_{14} = J_{23} = +40.8$ cm^{-1} and $J_{24} = J_{13} = -86.1$ cm^{-1}, g = 1.976, D = 0 (fixed), P = 0.7% and TIP = 240 x 10^{-6} which imply that the spin exchange is dominated by antiparallel coupling in **6**. The low g value and the positive coupling constants for both J_{14} and J_{23}, which represent the couplings between the copper

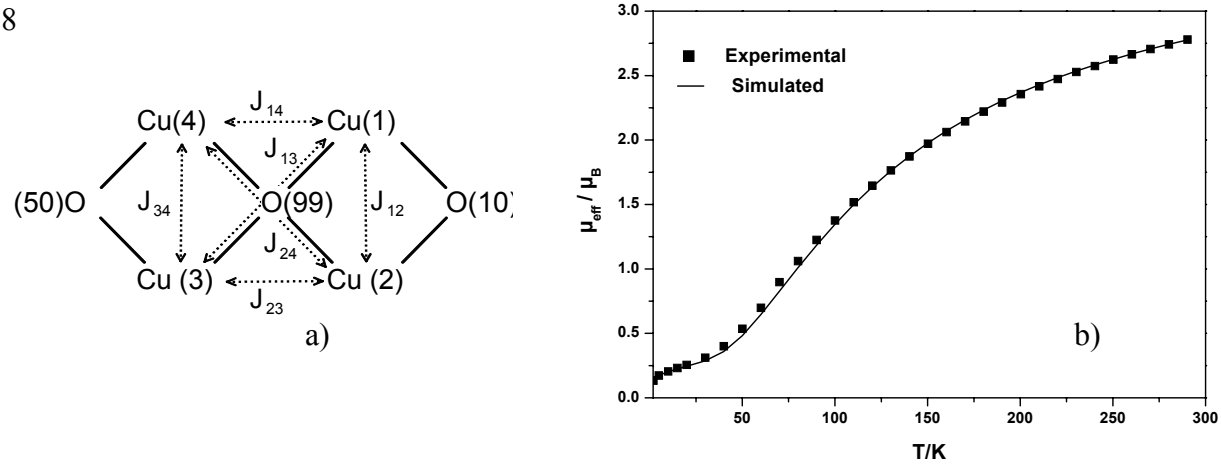

Figure 2.22:- a) Connection of the copper centers through the phenoxo and the oxo-groups.
b) Magnetic data of **6**.

centers with the angles Cu(4)-O(99)-Cu(1) 90.23° and Cu(2)-O(99)-Cu(3) 122.37°, however, suggest that a better fitting model should be used. The data were consequently fitted to a more accurate model. Therefore the data was fitted by using again a three-J model but with a different constraint based on the three ranges of Cu-O-Cu angles, 90.2, 99.12 - 99.98° and 120.30 – 122.37°. Thus, the following correlations between the six coupling constants depicted in Figure 2.22(a) were used to fit the experimental data: $J_{12} = J_{34}$, $J_{23} = J_{24} = J_{13}$ and J_{14}. The fit shown in Figure 2.22(b), was obtained with $J_{12} = J_{34} = -122.3$ cm^{-1}, $J_{23} = J_{24} = J_{13} = -90.0$ cm^{-1} and $J_{14} = 0$, g = 2.088, P = 0.3%, TIP = 240 x 10^{-6} and D = 0 (fixed). The susceptibility data consistent with this data set were found to be relatively insensitive to J_{14}, but very sensitive to J_{12} and J_{23}. J_{14}-values lying in the range -20 to +20 cm^{-1} have no influence on the quality of simulation.

For copper(II) centers bridged by a ligand oxygen atom (oxo, hydroxo, alkoxo, phenoxo, etc.), a linear relationship of exchange coupling J with the average Cu-O-Cu angles in the Cu_2O_2 ring has been reported.[17,20,23] It should be noted that although J_{12} of -122 cm^{-1} assigned to an angle of 99.5° does not deviate significantly from the reported linear relationship, the J_{23}-value of -90.0 cm^{-1} deviates remarkably. This is not very surprising as the electronic structures of the μ-OR and μ_4-O groups are clearly different. J_{14} is non-determinant for **6** within the measured temperature range 2 - 290 K.

The electronic spectra of **6** shows similar strong π-π* band at 485nm with a high absorbance value (35,700 M^{-1} cm^{-1}), similar to that as observed in **5** [Figure 2.23(b)]. These bands are all ligand based and can be compared with the absorbance bands for the deprotonated ligand . The tetranuclear copper complex (**6**) shows similar electrochemical behavior as observed for the dinuclear copper complex (**5**). An oxidation peak is observed at +0.523 mV against Fc^+/Fc [Figure 2.23(a)]. Coulometry of **6** at –25 °C in presence of 0.2 M

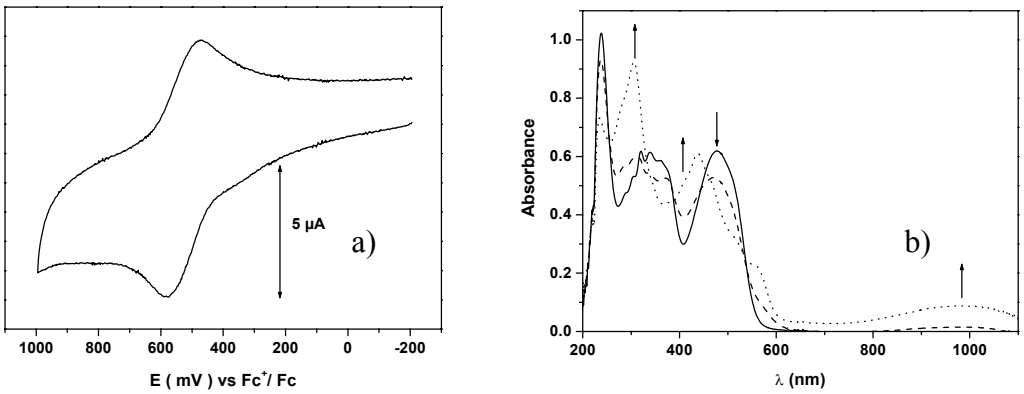

Figure 2.23 :- a) Cyclic voltammetry of **6** vs. Fc^{+}/Fc b) Electronic spectra of **6** (bold line) and its $1e^{-}$ oxidized species.

$TBAPF_6$ shows a single electron oxidation at +0.523 V with an increase in the intensity of the band at 410 nm and also at 990 nm. These two bands are the fingerprints for the formation of the phenoxyl radicals [Figure 2.23 (b)] (See 1.1.1).

$[L^{2}{}_{2}Fe^{III}{}_{2}]$ (7)

Although H_3L^{2} is estimably suited to form dinuclear complexes and the analytical and spectroscopic data are in accord with the presence of a dinuclear Fe_2L_2 unit as the smallest unit in **7**, an X-ray analysis was undertaken to remove the doubts regarding connectivity. Indeed, the structure analysis shows the presence of two 6-coordinated iron(III) centers with the $Fe_2O_6N_4$ coordination unit. An ORTEP drawing of the molecule is displayed in Figure 2.24 with selected bond distances and angles provided in Table 2.11.

The iron atoms, Fe(1) and Fe(2), are in distorted octahedral environments, having FeN_2O_4 coordination spheres. The two octahedra share a common edge and are bridged by two phenolate oxygen atoms O(50) and O(10). The six oxygen atoms of two ligands are roughly coplanar with the two Fe atoms. Thus, for two iron centers, the Fe(1)O(1)O(41)O(50)O(10) and Fe(2)O(62)O(22)O(50)O(10) atoms constitute the equatorial planes. Each iron center is coordinated to two nitrogen atoms, e.g Fe(1)-N(7) and Fe(1)-N(47), which are *trans* to each other with an angle N(47)-Fe(1)-N(7) of $162.7(2)^{o}$, and belong to two different $[L^{2}]^{3-}$ ligands.

The non-bridging Fe(1)-O(1)/O(41) av. 1.913(4) and Fe(2)-O(62)/O(22) av. 1.923(7) Å distances are distinctly different from the bridging Fe(1)-O(10)/O(50) av. 2.043(5) and Fe(2)-O(10)/O(50) av. 2.043 Å distances. The symmetry in the bridging bond lengths in the nearly planar Fe_2O_2 rhomb is noteworthy. Although the Fe-O-Fe angle of $108.9(2)^{o}$ for **7** fall

into the range 105 - 110^{o} observed for previously structurally characterized $Fe^{III}_2(OPh)_2$ bridge, the Fe•••Fe separation of 3.32 Å is one of the longest yet found for complexes with this bis(phenoxide) bridge.[19] In the previously reported $[Fe^{III}_2(salmp)_2]$,[19c] where $salmp^{3-}$ is the pentadentate ligand 2-bis(salicylideneamino)methylphenolate, the Fe-O-Fe angle of 97^{o} is the smallest yet found. As will be seen later, mostly because of the differences in the Fe-O-Fe angle, the magnetic properties of 1 differ considerably from that of $[Fe^{III}_2(salmp)_2]$, although **7** and $[Fe^{III}_2(salmp)_2]$ are otherwise very similar. The Fe-N and Fe-O bond distances are consistent with high-spin electron configuration of both Fe(III) centers in **7** with imine nitrogen and phenolate oxygen donor ligands. The d^5 h.s. electron configuration has also been confirmed both by Mössbauer and magnetic susceptibility measurements.

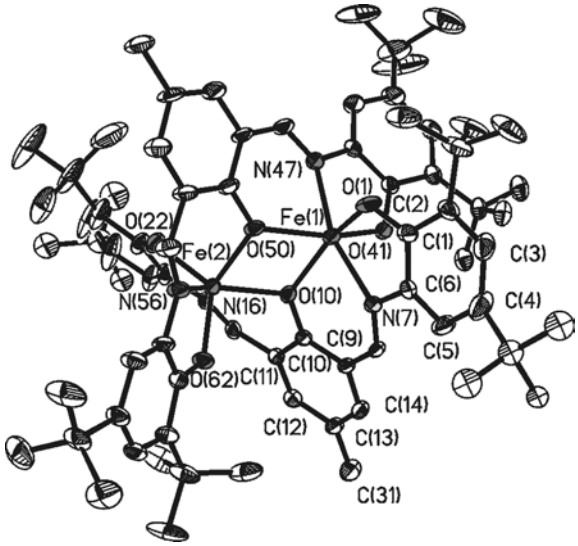

Figure 2.24 :- An ORTEP drawing of the neutral molecule **7.**

Table 2.11 *Selected Interatomic Distances (Å) and Angles (degrees) in* **7**

Fe(1)-O(1)	1.913(4)	Fe(2)-O(62)	1.920(4)
Fe(1)-O(41)	1.914(3)	Fe(2)-O(22)	1.927(4)
Fe(1)-O(10)	2.042(4)	Fe(2)-O(50)	2.041(4)
Fe(1)-O(50)	2.044(4)	Fe(2)-O(10)	2.044(3)
Fe(1)-N(47)	2.161(4)	Fe(2)-N(16)	2.167(5)
Fe(1)-N(7)	2.166(4)	Fe(2)-N(56)	2.174(5)
	Fe(1)•••Fe(2)	3.32(1)	
O(1)-Fe(1)-O(41)	100.2(2)	O(62)-Fe(2)-O(22)	122.5(2)
O(1)-Fe(1)-O(10)	150.9(2)	O(62)-Fe(2)-O(50)	135.4(2)
O(41)-Fe(1)-O(10)	99.8(2)	O(22)-Fe(2)-O(50)	94.3(2)
O(1)-Fe(1)-O(50)	99.9(2)	O(62)-Fe(2)-O(10)	93.4(2)
O(41)-Fe(1)-O(50)	150.8(2)	O(22)-Fe(2)-O(10)	135.9(2)
O(10)-Fe(1)-O(50)	71.1(2)	O(50)-Fe(2)-O(10)	71.2(2)
O(1)-Fe(1)-N(47)	89.6(2)	O(62)-Fe(2)-N(16)	88.8(2)
O(41)-Fe(1)-N(47)	79.1(2)	O(22)-Fe(2)-N(16)	77.2(2)
O(10)-Fe(1)-N(47)	114.9(2)	O(50)-Fe(2)-N(16)	126.3(2)
O(50)-Fe(1)-N(47)	80.0(2)	O(10)-Fe(2)-N(16)	79.1(2)
O(1)-Fe(1)-N(7)	79.2(2)	O(62)-Fe(2)-N(56)	77.6(2)
O(41)-Fe(1)-N(7)	89.9(2)	O(22)-Fe(2)-N(56)	88.9(2)
O(10)-Fe(1)-N(7)	79.9(2)	O(50)-Fe(2)-N(56)	79.1(2)
O(50)-Fe(1)-N(7)	114.6(2)	O(10)-Fe(2)-N(56)	126.3(2)
N(47)-Fe(1)-N(7)	162.7(2)	N(16)-Fe(2)-N(56)	151.3(2)

The Mössbauer spectrum of **7** , $[L_2Fe^{III}_2]$, at 80 K in zero applied magnetic field and the nonlinear least-squares fit is shown in Figure 2.25(a). The spectrum was fitted with a single quadrupole split doublet with an isomer shift of δ = 0.518 mm s^{-1} and a quadrupole splitting of ΔE_Q = 0.754 mm s^{-1}. The isomer shift is consistent with those observed for high spin iron(III) ions in an octahedral or distorted octahedral coordination.[20] The magnitude of the quadrupole splitting is a reflection of the unsymmetrical electric field gradient about each high-spin iron(III) site, although the two metal sites are equivalent.

The magnetic behavior of **7**, $L^{2}_2Fe^{III}_2$, is characteristic of an antiferromagnetically coupled dinuclear complex. At 290 K the μ_{eff} value of 6.784 μ_B (χ_M•T = 5.755 cm^3 K mol^{-1}) decreases monotonically with decreasing temperature until it reaches a value of 0.274 μ_B (χ_M•T = 9.380 x 10^{-3} cm^3 K mol^{-1}) at 2 K; this is a clear indication of exchange coupling between two paramagnetic Fe(III) centers (S_{Fe}=$^5/_2$) with a resulting S_t=0 ground state. The solid line in Figure2.25(b) represents the best fit with the following parameters:J = -12.7 cm^{-1}, g =2.00(fixed), P (S = $^5/_2$) = 0.3%. The evaluated antiparallel exchange is in keeping with the range observed for comparable diphenoxo-bridged ferric dimers. [19b-c,21]

Two semi-empirical magnetostructural correlations relating the magnitude of the exchange coupling to the iron-oxygen bond length in exchange coupled phenoxo-, alkoxo- and hydroxo-bridged dinuclear iron(III) compounds have been proposed.[19a-c] Using the empirical relationship J = -10^7 exp (-6.8 d),[19c] where d is the averaged iron-oxygen distance, 2.043 Å for **7**, the J value for **7** can be calculated to be -9.25 cm^{-1}, which differs from the experimentally observed value of -12.7 cm^{-1}. The second equation[19a]

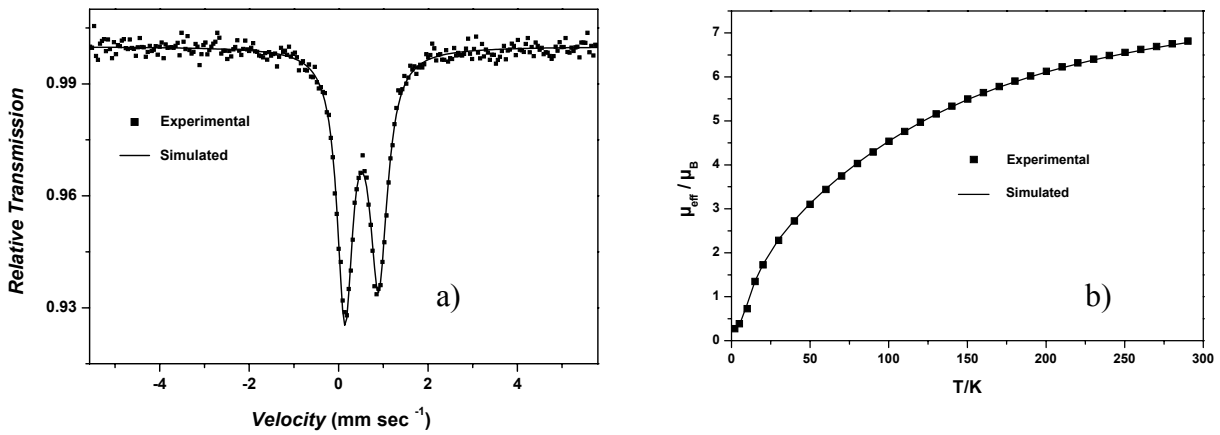

Figure 2.25 :- a) Mössbauer spectra for **7.** b) Magnetic data of **7**

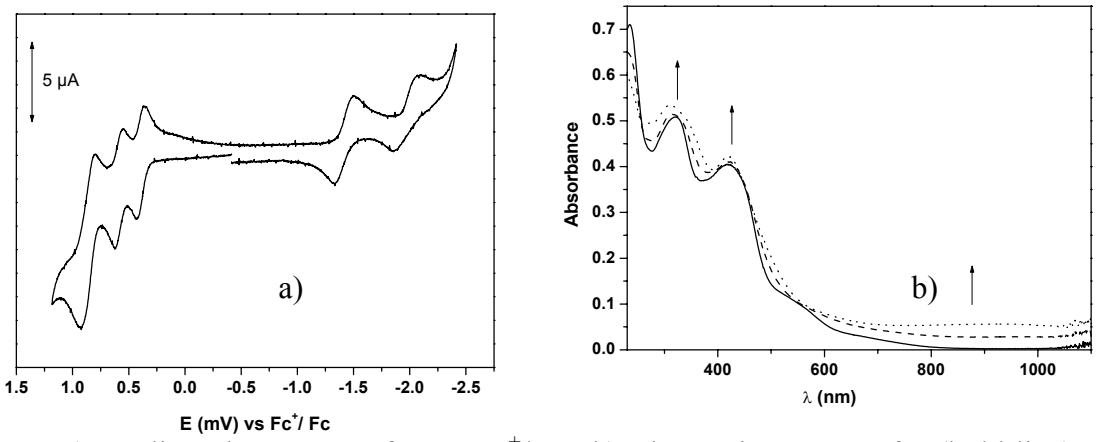

Figure 2.26 :- a) Cyclic voltammetry of **7** vs. Fc^{+}/Fc ; b) Electronic spectra of **7** (bold line) and its $1e^{-}$ oxidized species.

leads to a calculated value of -5.1 cm^{-1}. Regrettably none of these two correlations can satisfactorily reproduce the exchange interaction in the present ferric dimer, **7.**

The electrochemical properties of complex **7** was investigated in CH_2Cl_2 solutions containing 0.1 M TBA(PF_6). Voltammetric experiments (cyclic voltammetry, CV and square wave voltammetry, SQW) reveal that **7** can be oxidized thrice in three consecutive steps and reduced twice in two consecutive steps [Figure 2.26(a)]. The oxidation potential are found to be +0.870 V, +0.586 V and +0.390 V and the reduction peaks are found to be –1.42V and -1.95V against Fc^{+}/Fc. In the spectroelectrochemistry experiment with **7** in an OTTLE cell, increase in absorption at 350 - 450 nm and for >700 nm was observed during the first oxidation, as expected for formation of phenoxyl radicals [Figure 2.26(b)]. However, the maxima of the difference spectra were at 350 - 370 nm rather than at 400 - 420 nm. Most possibly these spectra are distorted by small oxidation-induced shifts in the very intense charge transfer bands of the complexes (the ε-values of the starting material are ten times higher than those of phenoxyl radicals at the respective wavelengths).

$[L^2{}_2Mn^{III}{}_2]$ (8a) and $[L^2{}_2Mn^{III}{}_2(THF)_2]$ (8b)

Single crystals of deep orange **8b** were obtained from a tetrahydrofuran solution of **8a** by slow evaporation. The structure of **8b** is shown in Figure 2.27 with selected bond distances and angles provided in Table 2.12. The molecule is based on two MnO_4N_2 octahedra, in which two triply deprotonated ligands $[O^{\frown}N^{\frown}O^{\frown}N^{\frown}O]^{3-}$ span between two manganese centers. The pentadentate ligand $[O^{\frown}N^{\frown}O^{\frown}N^{\frown}O]$ acts as a tridentate (O,N,O)-donor ligand for one manganese center, whereas the residual two donor atoms N,O coordinate to the second manganese center, thus each of the manganese center attains only pentacoordination through

the ligand. The sixth coordination position of each manganese center is occupied by the oxygen atom of a tetrahydrofuran molecule. That the manganese centers are in the +III oxidation state is evident from the axial elongation of the octahedra long the N(47)Mn(1)O(80) and the N(16)Mn(2)O(90) axes, as is expected for a Jahn-Teller distorted high-spin d^4 ion. The atoms Mn(1)N(7)O(1)O(41)O(14) and Mn(2)N(56)O(54)O(22)O(62) comprise the equatorial planes for each octahedron around Mn(1) and Mn(2) centers, respectively. The planarity of $MnNO_3$ fragment is good, the maximum deviation from the mean plane is 0.01 Å. Notable is the axial position of each coordinated tetrahydrofuran molecule. The average equatorial Mn-O and Mn-N distances of 1.896(16) and 2.006(3) Å, respectively, fall in the range reported for the structurally characterized d^4 Mn(III) complexes,[22] which also corroborate with the susceptibility measurements. The smallest acute bite angle between the phenolate O atom and the N atom of the L^{3-} ligand has been found for the Mn(1) center with the angle O(41)-Mn(1)-N(47) of 77.2(1)°.

*Compound **8b** is a rare example of a dinucleating ligand containing the central p-cresol group,[10] in which the central phenolate oxygen, O(54) or O(14), of the cresol ring does not coordinate as a bridging atom between two metal centers.*

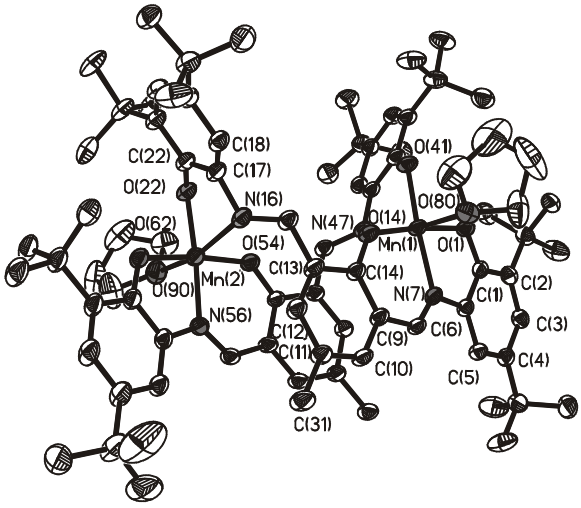

Figure 2.27:- Molecular structure of **8b**.

Table 2.12 *Selected Bond Distances (Å) and Angles (deg) for* **8b**.

Mn(1)-O(1)	1.879(2)	Mn(2)-O(62)	1.888(2)
Mn(1)-O(41)	1.899(2)	Mn(2)-O(22)	1.896(2)
Mn(1)-O(14)	1.907(2)	Mn(2)-O(54)	1.906(2)
Mn(1)-N(7)	2.005(2)	Mn(2)-N(56)	2.008(3)
Mn(1)-O(80)	2.291(3)	Mn(2)-O(90)	2.271(3)
Mn(1)-N(47)	2.310(3)	Mn(2)-N(16)	2.341(3)
	Mn(1)•••Mn(2)	6.448(2)	
O(1)-Mn(1)-O(41)	89.79(9)	O(54)-Mn(2)-N(56)	91.52(10)
O(1)-Mn(1)-O(14)	174.17(9)	O(62)-Mn(2)-O(90)	93.88(10)
O(41)-Mn(1)-O(14)	95.98(9)	O(22)-Mn(2)-O(90)	88.62(10)
O(1)-Mn(1)-N(7)	82.77(10)	O(54)-Mn(2)-O(90)	85.61(10)

O(41)-Mn(1)-N(7)	172.21(10)	N(56)-Mn(2)-O(90)	93.79(11)
O(14)-Mn(1)-N(7)	91.49(10)	O(62)-Mn(2)-N(16)	91.94(10)
O(1)-Mn(1)-O(80)	94.12(10)	O(22)-Mn(2)-N(16)	76.16(10)
O(41)-Mn(1)-O(80)	94.36(10)	O(54)-Mn(2)-N(16)	90.17(10)
O(14)-Mn(1)-O(80)	84.60(10)	N(56)-Mn(2)-N(16)	101.98(11)
N(7)-Mn(1)-O(80)	88.51(10)	O(90)-Mn(2)-N(16)	163.78(10)
O(1)-Mn(1)-N(47)	92.67(10)	O(80)-Mn(1)-N(47)	169.12(9)
O(41)-Mn(1)-N(47)	77.16(10)	O(62)-Mn(2)-O(22)	90.85(10)
O(14)-Mn(1)-N(47)	89.46(10)	O(62)-Mn(2)-O(54)	173.90(10)
N(7)-Mn(1)-N(47)	100.79(10)	O(22)-Mn(2)-O(54)	95.21(9)
O(62)-Mn(2)-N(56)	82.45(10)	O(22)-Mn(2)-N(56)	173.02(10)

The magnetic moment μ_{eff}/molecule for **8a** [$L^{2}_{2}Mn^{III}_{2}$] of 6.636 μ_B (χ_M•T = 5.507 cm^3 K mol^{-1}) at 290 K decreases monotonically with decreasing temperature until it reaches a value of 1.421 μ_B (χ_M•T = 0.2523 cm^3 K mol^{-1}) at 2 K; this temperature dependence of μ_{eff} is a clear indication of an antiferromagnetic exchange coupling between two paramagnetic Mn(III) (S_{Mn} = 2) centers. A least-squares fit, shown as the solid line in Figure 2.28, with J = - 2.95 cm^{-1}, g = 1.98 was obtained. Thus a weak exchange coupling is operating between the Mn(III) centers through the diphenoxo-bridge and as expected the exchange interaction is weaker in **8a** than that in **7**. The exchange coupling operating in **8b** [$L^{2}_{2}Mn^{III}_{2}(THF)_2$] is even weaker than that in **8a**, as is evident from the temperature-dependence of μ_{eff} for **8b**. The magnetic moment μ_{eff} varies only slightly (μ_{eff} = 6.94 to 6.54 μ_B) in the temperature range 290 - 40 K, but then starts to decrease monotonically reaching a value of 1.94 μ_B at 2 K. The simulation of the experimental magnetic data yields J = -0.66 cm^{-1}, g = 1.995 (the solid line in Figure 2.28). The weaker antiferromagnetic coupling in **8b** than that in **8a** is in accord with the dimeric solid state structure of **8b**, in which the manganese(III) centers are 6.45 Å apart from each other.

The electro- and spectroelectrochemistry of [$L^{2}_{2}Mn^{III}_{2}$](**8a**) and [$L^{2}_{2}Mn^{III}_{2}(THF)_2$](**8b**)

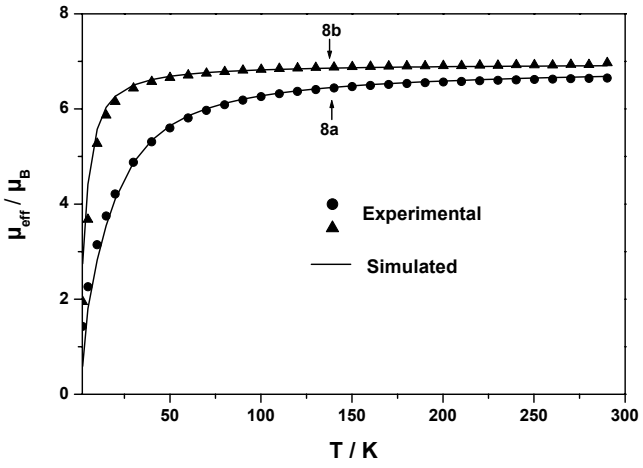

Figure 2.28 :- Magnetic study of **8a** and **8b.**

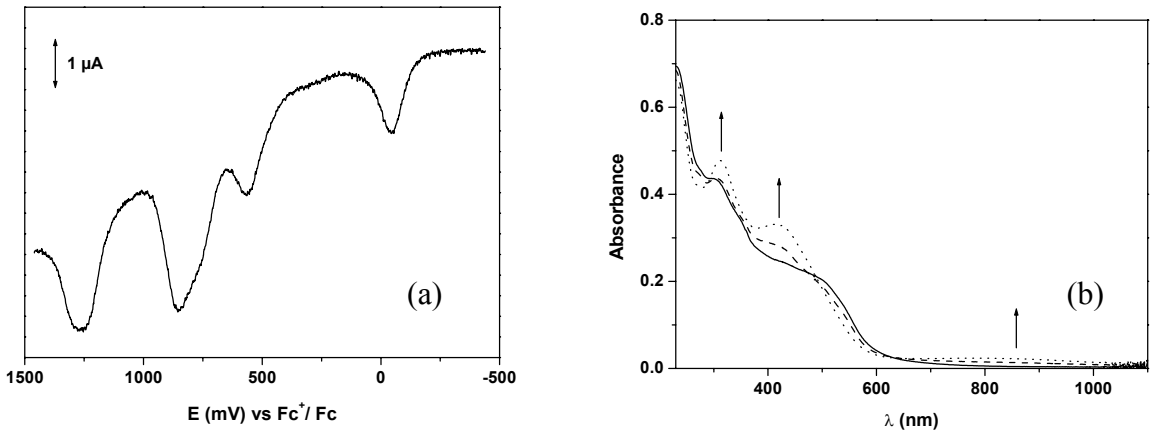

Figure 2.29:- a) Cyclic voltammetry of **8a** vs. Fc^{+}/Fc ; b)Electronic spectra of **8a** (bold line) and its $1e^{-}$ oxidized species.

was measured and it was found that both exhibits the same redox properties. The redox potentials of the first oxidations are spread over a somewhat larger range. The oxidative peaks in the square wave mode (Frequency 10Hz) are found to be +0.860V (irreversible), +0.542V (reversible) and -0.060V (reversible) and one reductive peak is found in -1.30V vs. Fc^{+}/Fc. In particular the redox potential at -0.06 V of the Mn-complex **8a** is low and could be due to formation of the Mn^{IV} form [Figure 2.29 (a)]. Therefore spectroelectrochemical measurements at -25 ^{o}C in an OTTLE cell was performed and it was found that the spectral changes upon the first oxidation of **8a** shows the fingerprints for phenoxyl radical formation.[18] In the difference spectrum a new peak with a maximum at 417 nm developed together with a broad band which extends from 650 - 950 nm and has a maximum at ~800 nm. Therefore, the first oxidation of **8a** can be clearly assigned to phenoxyl radical formation [Figure 2.29 (b)]. The reductions at potentials less than -1V are either electrochemically quasi-reversible (peak separation 0.15 - 0.25 V at 0.2 V/s scan rate) or chemically irreversible. They were not further investigated and are most feasibly metal-centered reductions to the M^{2+} oxidation states.

$[L^{2}_{2}\,Cr^{III}_{2}]$ (9)

The experimental magnetic moment of **9**, $L^{2}_{2}Cr^{III}_{2}$ decreases from 4.95 μ_B (χ_M•T = 3.064 cm^3 K mol^{-1}) at 290 K to an essentially diamagnetic value of μ_{eff} = 0.677 μ_B (χ_M•T = 0.05736 cm^3 K mol^{-1}) at 2 K, resulting from the antiferromagnetic interaction between two Cr(III) ions bridged by a diphenoxo-group in complex **9**. The solid line in Figure 2.30 represents the best fit with the following parameters: J = -7.6 cm-1, g = 1.893, P($S=^{3}/_{2}$)=1%. The evaluated antiparallel exchange falls in the range observed for comparable phenoxo-alkoxo-bridged chromium(III) dimers.[23]

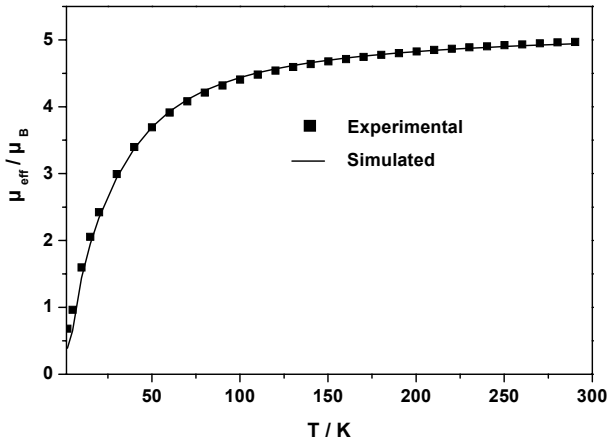

Figure 2.30 :- Magnetic measurement of **9**.

Electrochemical data of **9** in the square wave mode (25 Hz) shows the presence of three oxidative peaks at +0.905V, +0.410V and +0.144V and a single reductive peak at -1.99 V vs. Fc^{+}/Fc. The peaks at +0.905 and that of +1.99 V are irreversible in character with high peak current and the other two peaks are reversible [Figure 2.31(a)]. The nature of these peaks are similar to that obtained for **8** . The reductive peaks are attributed to the metal based reduction to M^{2+} state.

The electronic spectra of **9** shows a ligand based peak at 458 nm with a shoulder at 526 nm. When **9** is subjected to spectroelectrochemistry in an OTTLE cell, it is found there is an increase in the absorption at 350-450 nm and for >700 nm for the first oxidation as observed for **7** [Figure 2.31(b)].

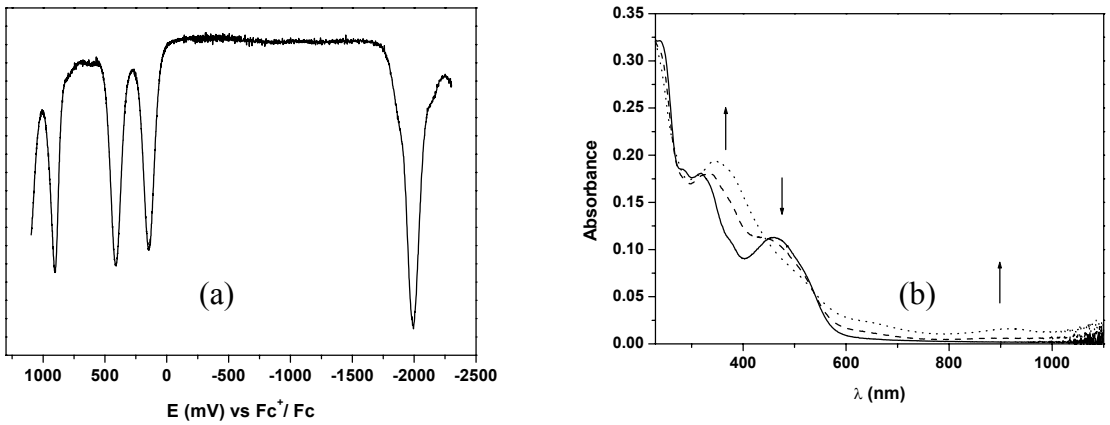

Figure 2.31:-a) Square wave voltammogram of **9**. b) Electronic spectra of **9** (bold line) and its $1e^{-}$ oxidized species.

$[L^2 (V^{IV}=O)_2(OCHMe_2)]$ (10)

The structure of **10** (Figure 2.32) shows the formation of a divanadyl(IV) complex with a bridging isopropoxide originating from the starting material vanadium isopropoxide. The atoms V(1) and V(2) are additionally bridged by a phenolate oxygen O(10). The penta-coordination of each vanadium atom is achieved by oxygen atoms O(12) and O(13), with V(1)-O(12) and V(2)-O(13) distances of 1.586(3) and 1.588(3) Å, respectively, indicating their double-bond character. The V=O groups are oriented *trans* to each other in the divanadium complex. The coordination polyhedron for the vanadium centers is distorted square pyramid with O(1)N(7)O(11)O(10) for V(1) and O(22)N(16)O(11)O(10) for V(2) forming the basal planes, in which both V(1) and V(2) are located at 0.60 Å out of the equatorial planes. The ring V(1)O(11)V(2)O(10) is not planar, the dihedral angle being 10.3°. The distances V-O and V-N are in the ranges reported for comparable complexes[24] and are in accord with the d^1 electron configuration for the vanadium centers. This electronic structure has also been confirmed by the magnetic susceptibility measurements. The separation V(1)•••V(2) of 3.063 Å necessitates consideration of direct interaction between the metal centers. Selected interatomic distances and bond angles are listed in Table 2.13.

The temperature dependence of the molar magnetic susceptibility χ_M for **10** shows a clear maximum around 230 K, consistent with the presence of significant antiferromagnetic coupling. That at low temperatures ($\leq$ 30 K) χ_M increases again has been often seen in

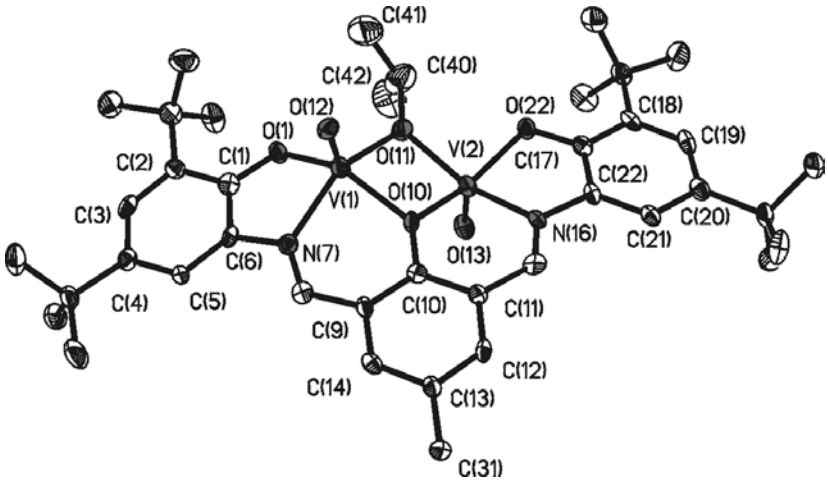

Figure 2.32 :- ORTEP diagram of **10.**

Table 2.13 *Selected Bond Distances (Å) and Angles (deg) for* **10**.

V(1)-O(12)	1.586(3)	V(2)-O(13)	1.588(3)
V(1)-O(1)	1.905(3)	V(2)-O(22)	1.919(3)
V(1)-O(11)	1.970(3)	V(2)-O(11)	1.953(3)
V(1)-O(10)	1.995(3)	V(2)-O(10)	1.994(3)
V(1)-N(7)	2.066(4)	V(2)-N(16)	2.065(4)

	V(1)•••V(2)	3.063(1)	
O(12)-V(1)-O(1)	109.3(2)	O(13)-V(2)-O(22)	107.3(2)
O(12)-V(1)-O(11)	110.6(2)	O(13)-V(2)-O(11)	110.9(2)
O(1)-V(1)-O(11)	95.45(13)	O(22)-V(2)-O(11)	94.61(13)
O(12)-V(1)-O(10)	107.86(14)	O(13)-V(2)-O(10)	106.1(2)
O(1)-V(1)-O(10)	142.13(14)	O(22)-V(2)-O(10)	146.22(13)
O(11)-V(1)-O(10)	77.92(12)	O(11)-V(2)-O(10)	78.36(12)
O(12)-V(1)-N(7)	102.6(2)	O(13)-V(2)-N(16)	105.7(2)
O(1)-V(1)-N(7)	80.16(14)	O(22)-V(2)-N(16)	79.87(14)
O(11)-V(1)-N(7)	146.03(14)	O(11)-V(2)-N(16)	142.89(14)
O(10)-V(1)-N(7)	85.12(13)	O(10)-V(2)-N(16)	86.15(13)
	V(2)-O(10)-V(1)	100.30(13)	
	V(2)-O(11)-V(1)	102.65(14)	

strongly antiferromagnetically coupled systems and arises from a small amount of paramagnetic impurity in the sample. The magnetic moment of **10** is 1.83 μ_B (χ_M•T = 0.4430 cm^3 K mol^{-1}) at 290 K, which is significantly lower than the spin-only value of (2.45 μ_B) for two uncoupled S = $^1/_2$ spins, and μ_{eff} gradually decreases on decreasing the temperature, reaching 0.15 μ_B at 2 K. The data were fitted by the following parameters: J = -128.5 cm^{-1}, g=1.90, PI (S = $^1/_2$) = 1.8%, TIP = 80 x 10^{-6} cm^3 mol^{-1}, θ = -3.0 K [Figure 2.33(a)]. The antiferromagnetic coupling constant of -128.5 cm^{-1} lies in the range of values found for other dinuclear vanadyl(IV) complexes[24,25] containing phenoxo, alkoxo and hydroxo-bridging ligands.

The complex **10** was subjected to electrochemical study and it was observed that broad, irreversible peaks at +0.436 V and +1.124V vs.Fc^+/Fc appear for the oxidative range in the square wave voltammogram. From the peak position, it can be inferred that the oxidations are all ligand centered with the formation of phenoxyl radicals. For the reductive range in the cyclic voltammogram multiple waves are observed at -0.830 V, -0.980 and –1.6 V vs. Fc^+/Fc [Figure 2.33(b)]. These peaks are probably due to the reduction of the metal centers to V^{+3}.

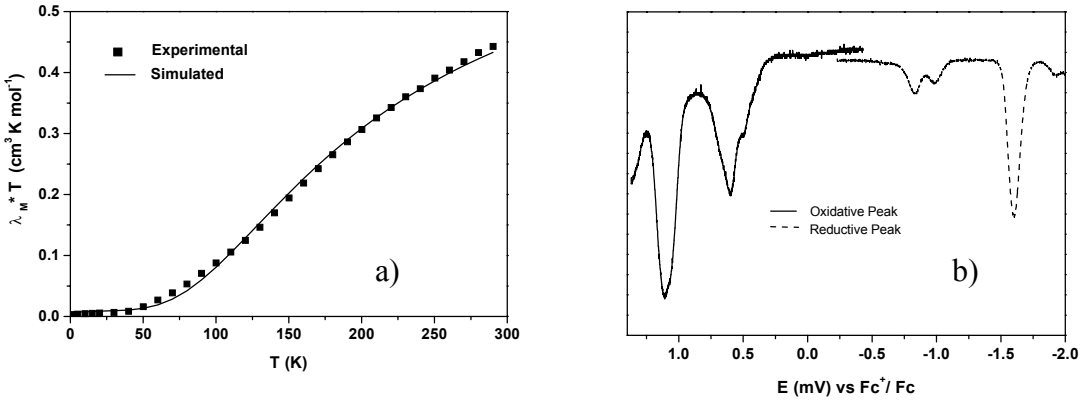

Figure 2.33 :- a)Magnetic susceptibility measurement of **10**. b) Square wave voltammogram of **10**.

$[L^2{}_2(V^V{=}O)_2]$ (11)

The crystals of $[L_2(VO)_2]\bullet 2CH_3CN$ obtained by crystallizing **11** from an acetonitrile solution were subjected to single-crystal X-ray crystallography at 100 K. Figure 2.34(a) shows a perspective view and atom-labeling scheme of **11**. Selected bond parameters are listed in Table 2.14.

In the distorted square pyramidal VO_4N coordination sphere the metal atom is displaced toward the O(1) or O(5) atom from the equatorial planes O(2)O(3)N(4)O(4) for V(1) and O(6)O(7)N(2)O(8) for V(2) by 0.33 and 0.31 Å, respectively. The V(1)-O(1) and V(2)-O(5) distances of 1.603(2) and 1.595(2) Å correspond to a vanadium-oxygen multiple bond and resemble closely vanadium(V) complexes containing a single V=O group.[26] Each ligand with its five donor atoms spans between two vanadium(V) centers and one N atom, N(1) or N(4), does not coordinate to any of the metal centers, rendering each of the ligand to be tetradentate. *This type of behaviour for the ligands based on 2,6-diformyl-p-cresol is observed for the first time.* A schematic drawing of the coordination sphere is shown [Figure 2.34(b)] to highlight the tetradentate coordination of the ligand. The V-O and V-N bond distances (Table 2.14) are comparable to those of vanadium(V) complexes with a monooxo- and cis-dioxo-vanadium moiety.[27] The C-O (average 1.34 Å) and the aromatic C-C

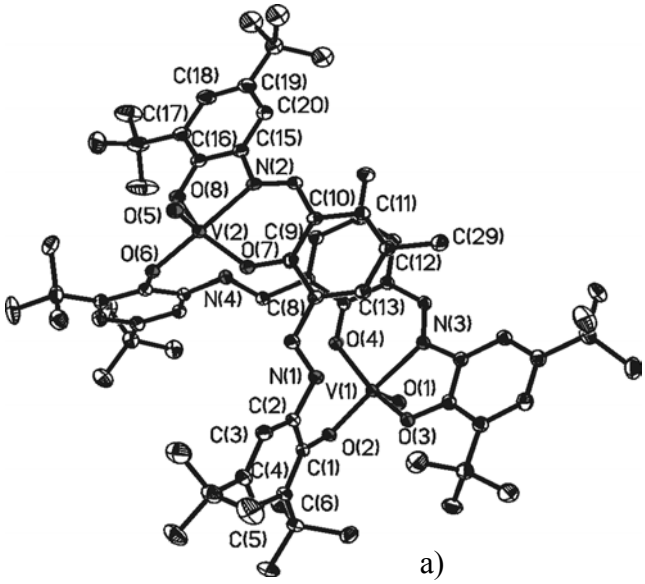

a)

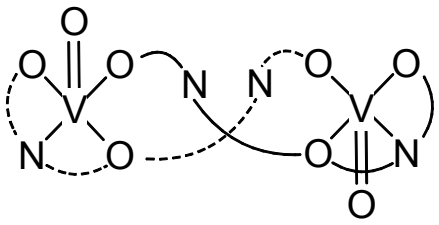

b)

Figure 2.34:-A perspective view of the neutral complex **11**.b)Schematic view of the coordination sphere of the deprotonated ligand $[L^2]^{-3}$ in **11.**

Table 2.14. *Selected Bond Distances (Å) and Angles (deg) for* **11**.

V(1)-O(1)	1.603(2)	V(2)-O(5)	1.595(2)
V(1)-O(2)	1.8202(13)	V(2)-O(6)	1.8340(14)
V(1)-O(4)	1.8787(14)	V(2)-O(7)	1.874(2)
V(1)-O(3)	1.883(2)	V(2)-O(8)	1.875(2)
V(1)-N(3)	2.108(2)	V(2)-N(2)	2.124(2)
	V(1)•••V(2)	6.882	
O(1)-V(1)-O(2)	100.01(7)	O(5)-V(2)-O(6)	98.01(7)
O(1)-V(1)-O(4)	101.12(7)	O(5)-V(2)-O(7)	100.17(8)
O(2)-V(1)-O(4)	102.23(6)	O(6)-V(2)-O(7)	102.69(6)
O(1)-V(1)-O(3)	105.51(7)	O(5)-V(2)-O(8)	104.38(8)
O(2)-V(1)-O(3)	88.66(6)	O(6)-V(2)-O(8)	89.26(7)
O(4)-V(1)-O(3)	148.96(7)	O(7)-V(2)-O(8)	150.87(7)
O(1)-V(1)-N(3)	93.26(7)	O(5)-V(2)-N(2)	95.41(7)
O(2)-V(1)-N(3)	163.17(7)	O(6)-V(2)-N(2)	163.20(7)
O(4)-V(1)-N(3)	85.14(6)	O(7)-V(2)-N(2)	84.75(6)
O(3)-V(1)-N(3)	77.78(6)	O(8)-V(2)-N(2)	77.61(7)

(average 1.40 Å) bond lengths are normal. The ligand is thus chelated in the trianionic phenolate form and the compound is correctly described with a physical oxidation state of +V for the vanadium ion with a d^0 electron configuration. This assignment also corroborates with the diamagnetism and ^{51}V NMR data for **11**.

Compound **11** containing V(V) with d^0 electron configuration is diamagnetic and was subjected to ^{51}V NMR measurements[28] with $VOCl_3$ in C_6D_6 as an internal standard. The compound gives rise to a single signal at δ = -420 ppm, suggesting that there is only one species in solution, as in the solid state.

A few electrochemical experiments were done with the Vanadium (V) compound $[L^2_2(V{=}O)_2]$ **(11)**. The square wave voltammogram exhibits three oxidations in the accessible potential range, two reversible ones at -0.136 V and +0.226 V. These oxidations, which proceed in the same potential range as those of **7** - **9**, and are assigned tentatively also to phenoxyl radical formation. Reductions do also occur, in the potential range -0.7 to -0.9 V which are most possibly metal-centered reductions to the V^{IV} state. The square wave voltammogram, however, exhibits complex multiple peak formations [Figure 2.35].

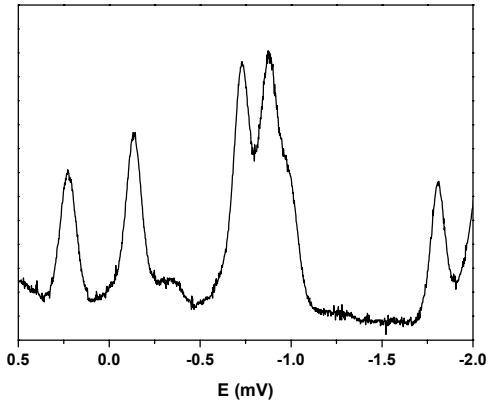

Figure 2.35:- Square wave voltammogram of 11.

References

1.a) R. Robson, *J. Inorg. Nucl. Chem. Lett.* **1970**, *6*, 125. (b) R. Robson, *Aust. J. Chem.* **1970**, *23*, 2217. (c) A. M.Bond, M. Haga, I. S. Creece, R. Robson, J. C. Wilson, *Inorg. Chem* **1988**, *27*, 712. (d) A. M. Bond, M. Haga, I.S. Creece, R. Robson, J. C. Wilson, *Inorg.Chem.* **1989**, *28*, 559.

2). B. F. Hoskins, R. Robson, D. Vince, *J. Chem. Soc., Chem. Commun.* **1973**, 392.

3) a)D.J.White, N. Laing, H. Miller, S. Parsons, S. Coles, P.A. Tasker, *Chem.Commun.,***1999**,2077 (b) C. J. Matthews, K. Avery, Z. Xu, L. K. Thompson, L. Zhao, D. O. Miller, K Biradha, K. Poirier, M.J. Zaworotko, C. Wilson, A.E. Goeta, J. A. K. Howard ,*Inorg. Chem.*, **1999,** *38,* 5266. (c)V. V. Pavlishchuk, S.V. Kolotilov, A. W. Addison, M. J. Prushan, D. Schollmeyer, L. K. Thompson, E. A. Goreshnik,Angew. Chem. Int. Ed., **2001**, 40, 4734. (d) M. Mimura, T.Matsuo, N. Matsumoto, S. Takamizawa, W. Mori, N. Re, Bull. Chem. Soc. Jpn., **1998**,71, 1831.

4) a)P. Chaudhuri, I. Karpenstein, M. Winter, C. Butzlaff, E. Bill, A. X**.** Trautwein, U. Flörke, H.-J. Haupt, *J. Chem. Soc*., *Chem.Commun.* **1992**, 321. b) G. Kolks, S. J. Lippard, J. Waszczak, H. R. Lilienthal, *J. Am. Chem. Soc.* **1982**, 104, 717. c) K. Matsumoto, S. Ooi, Y. Nakao, W. Mori, A. J . Nakahara, *J. Chem. Soc., Dalton Trans.* **1981**, 2045. d) P. K. Coughlin, S . J. Lippard, *Inorg. Chem.* **1984**, 23, 1446. e) G. Ivarsson, B. K. S. Lundberg, N. Ingri. *Acta Chem. Scand.***1972**, *26,* 3005. f) B. K. S. Lundberg, *Acta. Chem. Scand.* **1972**, *26,* 3902. g) P. Chaudhuri, I. Karpenstein, M. Winter, M. Lengen, C. Butzlaff, E. Bill, A. X. Trautwein, U. Flörke, H.-J. Haupt, *Inorg. Chem.,***1993**,32,888. h) E. Colacio, J. M. Dominguez-Vera, M. Ghazi, R. Kivekäs, M. Klinga, J. M. Moreno *Inorg. Chem.* **1998,** 37*,* 3040. i) E. Colacio, M. Ghazi, R. Kivekäs, M. Klinga, F. Lloret, J, M. Moreno, *Inorg. Chem.* **2000,** 39*,* 2770. j) M. G **.** B. Drew, M. McCann, S. M. Nelson,. *J.Chem. Soc., Dalton Trans.* **1981**, 1868. k) C. Salata, M. T. Youinou, C. J. Burrows, *Inorg. Chem.* **1991**,30,3454. l) N. Matsumoto, T. Akui, H. Murakami, J. Kanesaka, A. Ohyoshi, H. Okawa, *J. Chem. Soc.,Dalton Trans.* **1988**, 1021.

5) F. Birkelbach, C. Krebs, V. Staemmler, unpublished, Bochum, Germany, 1997.

6) a) M. S. Haddad, E. N. Duester, D. N. Hendrickson, *Inorg. Chem.* **1979**, 18, 141. b) M. S. Haddad, D. N. Hendrickson, *Inorg. Chem.* **1978**, 17, 2622.

7) (a) A. Bencini, C. Benelli, D. Gatteschi, C. Zanchini, *Inorg. Chem.* **1986**,25,398. (b) C. Benelli, R. K. Bunting, D. Gatteschi, C. Zanchini, *Inorg. Chem.* **1984**, 23, 3074.

8) (a) H. E. Wages, K. L. Taft, S. J. Lippard, *Inorg. Chem.* **1993**, 32, 4985. (b)Y. Hosokawa, H. Yamane, Y. Nakao, K. Matsumoto, S. Takamizawa, W. Mori, S. Suzuki, *Chem. Lett.* **1997**, 891. (c)M. Arnold, D. A. Brown,O. Deeg, W. Errington, W. Haase, K. Herlihy,T. J. Kemp, H. Nimir, R. Werner, *Inorg. Chem.* **1998**, 37, 2920. (d)T. Koga, H. Furutachi, T. Nakamura, N. Fukita, M. Ohba, K. Takahashi, H. Okawa, *Inorg. Chem.* **1998**, 37, 989. (e) F. Meyer, H. Pritzkow, *Chem. Commun.* **1998**, 1555. (f) F. Meyer, E. Kaifer, P. Kircher, K. Heinze, H. Pritzkow, *Chem. Eur. J.* **1999**, 5, 1617. (g) K.Yamaguchi, S. Koshino, F. Akagi, M. Suzuki, A. Uehara, S. Suzuki, *J. Am. Chem. Soc.* **1997**, 119, 5752. (h) H. Yamane, Y. Nakao, S. Kawabe, Y. Xie, N. Kanehisa, Y. Kai, M. Kinoshita, W. Mori, Y. Hayashi, *Bull. Chem. Soc. Jpn.* **2001**, 74, 2107.

9) A. M. Barrios, S. J. Lippard, *J. Am. Chem. Soc.* **2000**, 122, 9172.

10) P. Chaudhuri, C. N. Verani, E. Bill, E. Bothe, T. Weyhermüller, and K. Wieghardt, *J.Am. Chem. Soc.,* **2001,** 123*,* 2213.

11) S. Ciurli, S. Benini, W. R. Rypniewski, K. S. Wilson, S. Miletti, S. Mangani, *Coord. Chem. Rev.* **1999**, 190-192, 331.

12) (a)K. E. Andrew, A. B. Blake, *J. Chem. Soc. A*, **1969**, 1456. (b) B. Aurivillius, *Acta. Chem. Scand. A*, **1977**, 31, 501. (c)J.A. Bertrand, C. Marabella, D. G. Vanderveer, *Inorg. Chim. Acta* **1978**, 26, 113. (d) W. L. Gladfelter, M. W. Lynch, W.P. Schaefer, D.N. Hendrickson, H. B. Gray, *Inorg. Chem.* **1981**, *20*, 2390. (e) K. Bizilj, S. G. Hardin, B.F. Hoskins, P.J. Oliver, E. R. T. Tiekink, G. Winter, *Aust. J. Chem.* **1986**, 39, 1035. (f) L. Ballester, E. Coronado, A. Gutiérrez, A. Monge, M. F. Perpinán, E. Pinilla, T. Rico, *Inorg. Chem.* **1992**, 31, 2053. (g) A. J. Atkins, A. J. Blake, M. Schröder, *J.Chem. Soc.,Chem. Commun.* **1993**, 1662. (h) A. J. Blake, E. K. Brechin, A. Codron, R. O. Gould, C.M.Grant, S. Parsons, J. M. Rawson, R. E. P. Winpenny, *J. Chem. Soc., Chem. Commun* **1995**,1983. (i) M. A. Halcrow, J.-S. Sun, J.C. Huffman, G. Christou, *Inorg. Chem.* **1995**, 34,4167. (j) M. S. E. Fallah, E. Rentschler, A. Caneschi, D. Gatteschi, *Inorg. Chim. Acta* **1996**, 247, 231. (k) A. Escuer, M. Font-Bardiá, S. B. Kumar, X. Solans, R. Vicente,*Polyhedron* **1999**,18, 909. (l) M. L. Tong, H. K. Lee, S.-L. Zheng, X.-M. Chen, *Chem. Lett.* **1999**, 1087. (m)J. M. Clemente-Juan, B. Chansou, B. Donnadieu, J.-P. Tuchagues, *Inorg. Chem.* **2000**, 39, 5515. (n) T. K. Paine, E. Rentschler, T. Weyhermüller, P. Chaudhuri, Eur. J. Inorg. Chem., **2003**, 3167. (o) S. Mukherjee, T. Weyhermüller, E. Bothe, K. Wieghardt, P. Chaudhuri, *Eur. J. Inorg. Chem.* **2003**, 863.

13) S. A. Marshall, A. R. Reinberg, *J. Appl. Phys.* **1960**, 31, 3365.

14) (a) K. D. Karlin, A. Farooq, J. C. Hayes, B. I. Cohen, T. M. Rowe, E. Sinn, J. Zubieta, *Inorg. Chem.* **1987**, 26,1271.(b)M. Sakamoto, S. Itose, T. Ishimori, N. Matsumoto, H. Okawa, S. Kida, *J. Chem. Soc., Dalton Trans.* **1989**,2083. (c) K. J. Oberhausen, J. F. Richardson, R. M. Buchanan, J. K. McCusker, D. N. Hendrickson, J.-M. Latour, *Inorg. Chem.* **1991**, 30, 1357. (d) S. S. Tandon, L. K. Thompson, J. N. Bridson, M. Bubenik, *Inorg. Chem.* **1993**, 32,4621. (e)] P. Cheng, D. Liao, S. Yan, J. Cui, Z. Jiang, G. Wang, *Helv. Chim. Acta* **1997**, 80, 213. (f) P. Amudha, M. Kandaswamy, L. Govindasamy, D. Velmurugan, *Inorg. Chem.* **1998**, 37, 4486. (g) P. Dalgaard, A. Hazell, C. J.McKenzie, B. Moubaraki, K. S. Murray, *Polyhedron* **2000**, 19, 1909.

15) J. Reim, K. Griesar, W. Haase, B. Krebs, *J. Chem. Soc., Dalton Trans.* **1995**, 2649.

16) (a) V. H. Crawford, H. W. Richardson, J. R. Wasson, D. H. Hodgson, W. E. Hatfield, *Inorg. Chem.* **1976**, 15, 2107. (b) L. Merz, W. Haase, *J. Chem. Soc., Dalton Trans.* **1980**, 875. (c) L. K. Thompson, S. K. Mandal, S. S. Tandon, J. N.Bridson, M. K. Park, *Inorg. Chem.* **1996**, 35, 3117 and references cited therein.

17) (a) J. A. Bertrand, J. A. Kelly, *J. Am. Chem. Soc.* **1966**, 88, 4746. (b) J. A. Bertrand, *Inorg. Chem.* **1967**, 6, 495.

18) (a) H. Bock, H. tom Dieck, H. Pyttlik, M. Schnöller, *Z. Anorg. Allg. Chem.* **1968,** 357, 54. (b) B. T. Kilbourn, J. D. Dunitz, *Inorg. Chim. Acta* **1967**, 1, 209. (c) F. S. Keij, J. G. Haasnoot, A. J. Oosterling, J. Reedijk, C. J. O'Connor, J. H. Zang, A. L. Spek, *Inorg. Chim. Acta* **1991**, 181, 185. (d) H. M. Haendler, *Acta Crystallogr., Sect. C*, **1990**, 46, 2054. (e) R. E. Norman, N. J. Rose, R. E. Stenkamp, *Acta Crystallogr., Sect. C,***1989**, 45, 1707. (f) S. Brownstein, N.F. Han, E. Gabe, F. Leer, *Can. J.Chem.* **1989**, 67, 551. (g)J. T. Guy, J. C. Cooper, R. D. Gillardi, J. L. Flippen-Anderson, C. F. George, *Inorg. Chem.* **1988***,* 27*,* 635. (h) M. R. Churchill, F. J. Rotella, *Inorg. Chem.* **1979**, 18, 853.(i) R. C. Dickinson, F. T. Helm, W. A. Baker, T. D. Black, W. H. Watson, *Inorg. Chem.* **1977**, 16, 1530 and references therein. (j) J. J. de Boer, D. Bright, J. N. Helle, *Acta Crystallogr., Sect. B*, **1972**, 28, 3436. (k) S. Teipel, K. Griesar, W.

Haase, B. Krebs, *Inorg. Chem.* **1994**, 33, 456. (l) L. Chen, S. R. Breeze, R. J. Rousseau, S. Wang, L. K. Thompson, *Inorg. Chem.* **1995**, 34, 454. (m) S. R. Breeze, S. Wang, L. Chen, *J. Chem. Soc., Dalton Trans.* **1996**, 1341. (n) A. M.Atria, A. Vega, M. Contreras, J. Valenzuela, E. Spodine, *Inorg. Chem.* **1999**, 38, 5681.

19) (a). S. M. Gorun, S. J. Lippard, *Inorg. Chem.,* **1991**, 30, 1625. (b) A. Elmali, Y. Elerman, I. Svoboda, *Z. Naturforsch.,***2001**, 56b, 897. (c) R. Werner, S. Ostrovsky, K. Griesar, W. Haase, *Inorg. Chim. Acta,* **2001**, 326, 78 and references therein. (d) B. Snyder, G.S. Patterson, A. J. Abrahamson, R. H. Holm, *J. Am. Chem. Soc.,* **1989**, 111, 5214 and references therein

20) P. Gütlich, *"Mössbauer Spectroscopy"*, Ed. U. Gonser, Springer-Verlag, Berlin, Heidelberg, New York, 1975; N. N. Greenwood, T. C. Gibb, *"Mössbauer Spectroscopy"*, Chapman and Hall, London, 1971.

21) T. Weyhermüller, T. K. Paine, E. Bothe, E. Bill, P. Chaudhuri, *Inorg. Chim. Acta*, **2002**, 337, 344.

22) S. B. Yu, C. P. Wang, E. P. Day, R. H. Holm, *Inorg. Chem.,* **1991**, 30,4067.

23)(a) E. D. Estes, R. P. Scaringe, W. E. Hatfield, D. J. Hodgson, *Inorg. Chem.,* **1976**, 15, 1179 (b) H. R. Fischer, D. J. Hodgson, E. Pedersen, *Inorg. Chem.,* **1984**, 23, 4755; A. Bencini, M. D. Vaira, F. Manni, *J. Chem. Soc., Dalton Trans.,* **1991**, 41 (c)M. Nakahanda, T. Fujihara, A. Fuyuhiro, S. Kaizaki, *Inorg. Chem.,* **1992**, 31, 1316 (d) A. Böttcher, H. Elias, J. Gleurup, M. Neuburg, C. E. Olsen, J. Springborg, H. Weihe, M. Zehnder, *Acta Chem. Scand.,* **1994**, 48,981(d) M. Ardon, A. Bino, K. Michelsen, E. Pedersen, *J. Am. Chem. Soc.,* **1987**, 109, 5855(e)U. Bossek, K. Wieghardt, B. Nuber, J.Weiss, *Angew. Chem., Int. Ed. Engl.,* **1990**, 29, 1055(f) N. Arulsamy, J. Gleurup, D. J. Hodgson, *Inorg. Chem.,* **1994**, 23, 2066. (g) T. K. Paine, T. Weyhermüller, K. Wieghardt, P. Chaudhuri, *Inorg. Chem.,* **2002**, 41, 6538.

24) For example: C. J. Carrano, C. M. Nunn, R. Quan, J. A. Bonadies, V. L. Pecoraro, *Inorg. Chem.,* **1990**, 29, 944; S. L.Castro, M. E. Cass, F. J. Holländer, S. L. Bartley, *Inorg. Chem.,* **1995**, 34, 466; S. Burojevic, I. Shweky, A. Bino, D. A Summers, R. C.Thompson, *Inorg. Chim. Acta,* **1996**, 251, 75; W. Plass, *Z. anorg. allgem. Chem.,* **1997**, 623, 1290; Y.Sun, M. Melchior, D. A. Summers, R. C. Thompson, S. J. Rettig, C. Orvig, *Inorg. Chem.,* **1988**, 37, 3119; A. S. Cecato, A.Neves, M. A. de Brito, S. M. Drechsel, A. S. Mangrich, R. Werner, W. Haase, A. J. Bortoluzzi, *J. Chem. Soc.,Dalton Trans.,* **2000**, 1573.

25) (a) A. P. Ginsberg, E. Koubeck, H. J. Williams, *Inorg. Chem.,* **1966**, 5, 1656 (b) E. F. Hasty,T. J. Colburn, D. N. Hendrickson, *Inorg. Chem.,* **1973**, 12, 2414 (c) K. Wieghardt, U. Bossek, K. Volckmar, W. Swiridoff, J. Weiss, *Inorg. Chem.,* **1984**, 23, 1387 (d) E. Solari, A. Klose, C. Floriani, N. Re, A. Chiesi-Villa, C. Rizzoli, *Polyhedron,* **1996**, 15, 4103 (e) N. S. Dean, M. R. Bond, C. J. O'Connor, C. J. Carrano, *Inorg. Chem.,* **1996**, 35, 7643.

26) (a) D. C. Crans, H. Chen, O. P. Anderson, M. M. Miller, *J. Am. Chem. Soc.,* **1993**, 115, 6769 (b)M. Bashipoor, H. Schmidt, C. Schutzke, D. Rehder, *Chem. Ber.,* **1997**, 130,651(c) M. Moon, M. Pyo, Y. C. Myoung, C. I. Ahn, M. S. Lah, *Inorg. Chem.,* **2001**, 40, 554 (d) M. S. Palacios, M. J. Rocio, S. Dominguez, P. Gill, C. Ruiz-Perez, F. V. Rodriguez-Romero, J. M. Dance, *Polyhedron,* **1997**, 16, 1143 (e)W. Plass, *Z. anorg. allgem. Chem.,* **1997**, 623, 461 (f)B. Baruah, S. Das, A. Chakravorty, *Inorg. Chem.,* **2002**, 41, 4502.

27)(a)C. R. Cornman, G. J. Colpas, J. D. Hoeschele, J. Kampf, V. L. Pecoraro, *J. Am. Chem.Soc.,* **1992**, 114, 9925 (b) A. Neves, W. Walz, K. Wieghardt, B. Nuber, J. Weiss, *Inorg. Chem.,* **1988**, 27, 2484.

28) D. Rehder, *Angew. Chem., Int. Ed. Engl.,* 1991, **30**, 148.

Chapter 3

TRANSITION METAL COMPLEXES WITH IMINO -BENZOSEMIQUINONE LIGANDS

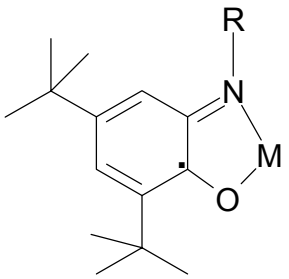

3.1 INTRODUCTION

The reactions catalyzed by radical-dependent proteins are very diverse. The essential tyrosyl radical in ribonucleotide reductase, modified tyrosyl radicals, tryptophan radicals, glycyl radicals and thiyl radicals have been identified and shown to play important roles in enzymes involved in primary metabolic pathways.

Since the report of the redox active ligand by Girgis and Balch (H_2L^N in Chapter1), quite a number of complexes have been synthesized using this ligand[1]. Later on, Pierpont and co-workers used 3,5-di-tert-butylcatechol as another redox active ligand and complexes containing benzosemiquinone radicals were synthesized[1a,2]. This hybridization of organic-inorganic molecules in which paramagnetic ions are coordinated to organic open shell radical ligands helped in studying the development of molecular magnetic materials. [3]

Lately, this field of chemistry interested this group with the synthesis of the ligand 2-anilino-4,6-ditertbutylphenol. Quite a number of complexes have been prepared using this ligand and all have been well characterized[4]. As a natural and obvious progress in this work, a new ligand has been developed based on *m*-phenylenediamine. This ligand can best be described as the dimeric form of 2-anilino-4,6-ditert-butylphenol. [5]

The question, however, arises about ways to discern the presence or absence of radicals in the benzene ring containing the *tert*-butyl substitution. A very powerful tool has been proved to be high quality X-ray crystallography. Figure 3.1 shows the geometrical features observed for i) $[L^{AP}]^-$ containing an aromatic aminophenol (AP) ring with six equivalent C-C bond, a long C-N bond at 1.47 Å and a relatively long C-O bond at 1.35 Å, ii) $[L^{AP}\text{-}H]^{-2}$, where only the shorter C-N bond at 1.37 Å differs significantly from those of $[L^{AP}]^-$, (iii)$[L^{ISQ}]^-$, where the six-membered ring displays a quinoid-type distortion comprising a short, a long, and another short C-C bond followed by three long ones and, in addition, both the C-O and C-N distances are significantly shorter (1.30 and 1.34 Å, respectively) than those in $]L^{AP}]^-$ and $[L^{AP}\text{-}H]^{-2}$ and iv) $[L^{IBQ}]$, where the ring is in a ortho-iminobenzoquinone form.

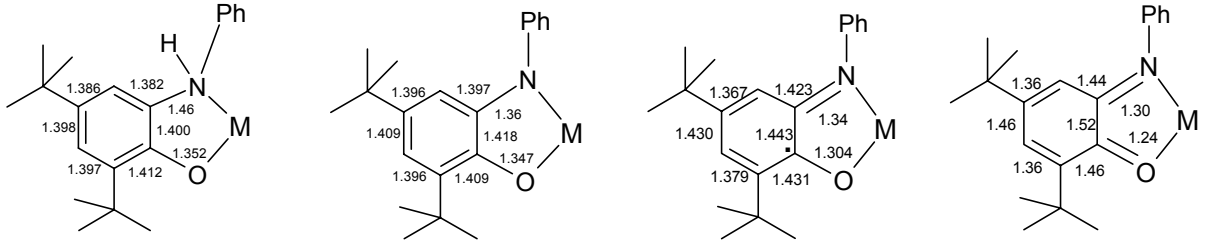

$[L^{AP}]^-$ $[L^{AP}\text{-}H]^{-2}$ $[L^{ISQ}]^-$ $[L^{IBQ}]$

Figure 3.1:- Geometrical features of the ligands.

3.2 SYNTHESIS AND CHARACTERIZATION OF THE LIGANDS

The ligands H_4L^3 and H_4L^4 were synthesized in the same procedure as described for 2-anilino-4,6-ditertbutyl phenol [4a]. Refluxing 1,3 diaminobenzene or 4,4′-diaminodiphenyl methane with 3,5-di-tert-butyl catechol (1:2) in heptane with triethyl amine as base afforded both the ligands [Figure 3.2(a)]. A plausible mechanism for these type of condensation is depicted in Figure 3.2(b).

Although both the ligands are tetradentate, however only dinuclear complexes could be synthesized using this ligand. The –NH and –OH groups easily deprotonate to yield imino-benzosemiquinone radicals in presence of metal and air. These iminobenzosemiquinone radicals are stabilized by the *tert-butyl* groups placed at the 2 and 4 positions to the phenol. For the ligand H_4L^3, the position of the amine group (1,3) necessitates spin polarization

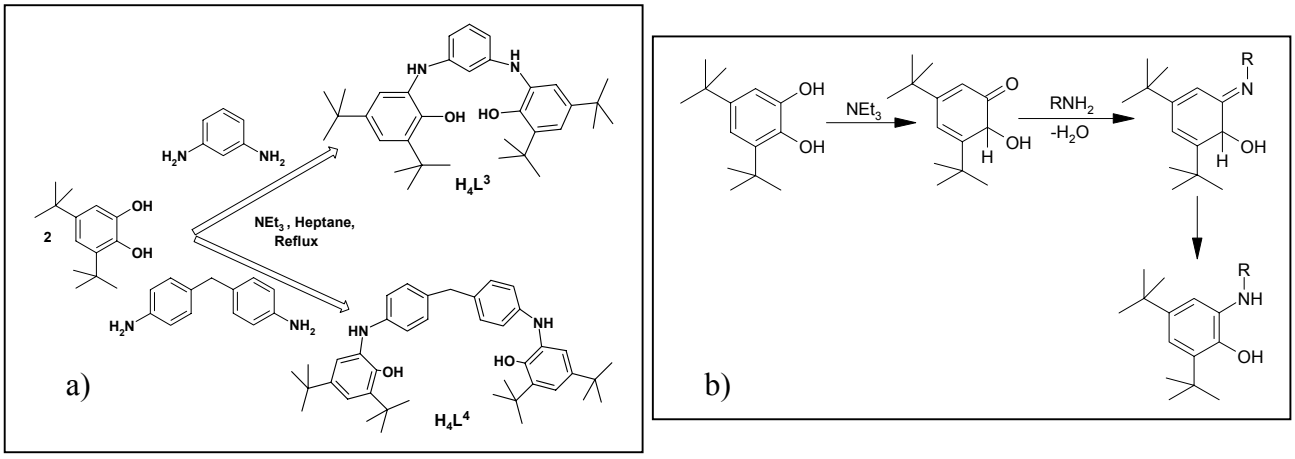

Figure 3.2 :-a) Synthetic procedure for ligands H_4L^3 and H_4L^4. b) Mechanism of the amine condensation with 3,5-di-tert-butyl catechol.

(Chapter 1) and serves as a backbone in attempting to induce ferromagnetic coupling between the dinucleating centers or between the radical centers. However , in H_4L^4 , the presence of –CH_2- group in between the π-conjugation inhibits spin polarization resulting in different magnetic property.

Both the ligands were characterized by different spectroscopic techniques viz. IR, NMR and Mass spectroscopy. The ligands show characteristic peaks in IR due to (-NH) stretch and (-OH) stretch between 3330-3350 cm^{-1} and 3370-3392 cm^{-1} respectively. The peaks at 2960-2860 cm^{-1} are due to the –C-H stretch of the *tert-butyl* groups. The -C-N stretch is between 1610-1615 cm^{-1} and present in both the ligands. Selected IR peaks (in cm^{-1}) are listed in Table 3.1.

	ν(-OH)	ν(-NH)	ν(C-H)	ν(C-N)	ν(C-O)
H_4L^3	3392	3349	2959,2907,2868	1614	1420
H_4L^4	3372	3330	2958,2905,2867	1611	1418

Table 3.1 :- *Characteristic IR bands for H_4L^3 and H_4L^4 (in cm^{-1}).*

NMR spectra of both the ligands are given in the experimental section (Chapter 7). Other than the four exchangeable protons , all the other protons (44 for H_4L^3 and 50 for H_4L^4) are visible for both the ligands. Mass spectroscopy in EI mode clearly confirms the composition of H_4L^3 as $C_{34}H_{48}N_2O_2$ (m/z-516) and for H_4L^4 as $C_{41}H_{54}N_2O_2$ (m/z-606).

3.3 TRANSITION METAL COMPLEXES WITH H_4L^3 and H_4L^4

The ligand H_4L^3 reacts with different metal ions in the presence of base and air to yield dimers with either *four* or *six* iminobenzosemiquinone radicals [Figure 3.3]. With H_4L^4, only the Co^{III}(LS) (**17**) complex has been synthesized in order to study the role played by the radicals in a non-conjugated ligand system. Here L^3 depicts the ligand in the diradical dianionic form and L_A^3 ,the monoradical trianionic form [Figure 3.4].

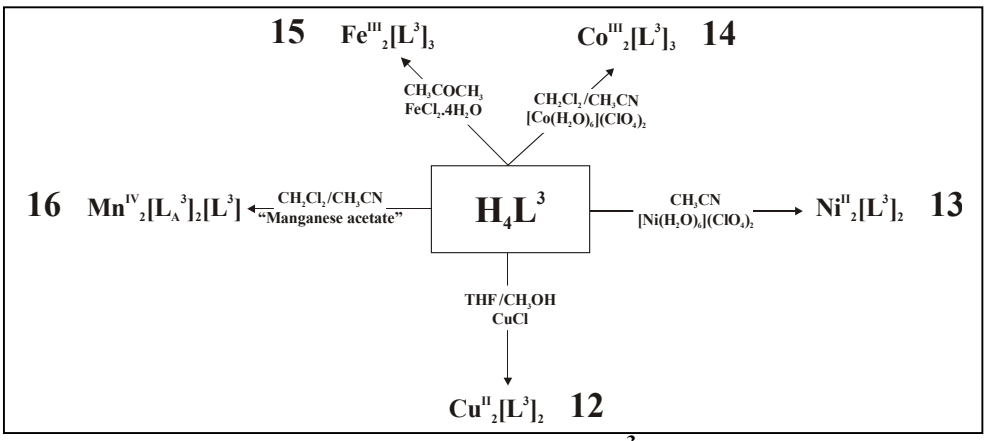

Figure 3.3 :- Complexes prepared with the ligand H_4L^3.

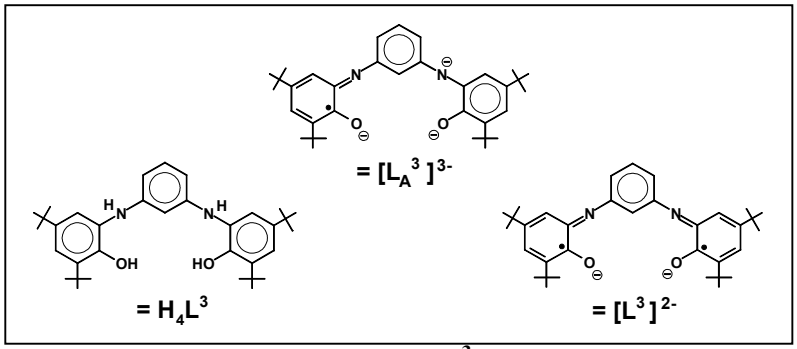

Figure 3.4:- Different forms of the ligand H_4L^3, which have been observed in the complexes.

When the ligand H_4L^3 is reacted with CuCl in presence of triethylamine and air, a dark green microcrystalline compound (**12**) separates out immediately which is recrystallized further from a THF-Methanol solvent mixture. Using Nickel(II) perchlorate hexahydrate as starting material, compound **13** precipitates out as dark green microcrystalline compound. Magnetic data of **13** are given in the Appendix section. If Cobalt(II) perchlorate hexahydrate is used, in an acetonitrile and dichloromethane solvent mixture, crystals of **14** separate out. The cobalt compound with H_4L^4 (**17**) is synthesized using the same procedure. Using this solvent mixture, **15** crystallizes out from solution when iron(II) chloride tetrahydrate is used.

In the synthesis of all these compounds, triethylamine was used as a base. However, when triethylamine is used as base for the preparation of the manganese complex, no precipitation occurs even after addition of tetrabutylammonium perchlorate. When tetrabutylammonium methoxide, a strong base, is used, a dark brown microcrystalline precipitate of **16** is obtained. With a weak base, like triethylamine, an equilibrium between the Mn^{II}, Mn^{III} and Mn^{IV} complexes presumably exists in solution. When a strong base is added, this equilibrium is shifted towards the Mn^{+4} form with the lowering of the oxidation potential.

3.3.1 INFRARED AND MASS SPECTROMETRY OF THE COMPLEXES 12 - 17

Complexes **12-17** were all subjected to infrared and mass spectroscopic studies. The most salient features observed for all the complexes were the absence of the (-NH) and (-OH) peaks of both the ligands. This indicates coordination of the metal sites with the ligands. A medium intense band between 1580-1560 cm^{-1}, assigned to the ν(-C=N) and a sharp peak between 1450-1430 cm^{-1}, due to ν (C-O) appears for all the complexes. List of some of the infrared peaks (in cm^{-1}) are given in Table 3.2.

Complex	ν(C=N)	ν(C-O)	Other characteristic peaks
12	1576m	1473m	1442m,1386m,1265m,1027m,697w
13	1576s	1476s	1437m,1360s,1244s,1024m,698m
14	1575s	1464s	1435s,1359s,1262m,1032w,706s
15	1579m	1478s	1437m,1357w,1262m,1028w,704m
16	1578s	1470s	1520m,1360s,1268s,1021m,703w
17	1578w	1500m	1429s,1358m,1255m,1030w,692w

Table 3.2 :- *Characteristic IR peaks for **12-17** (in cm^{-1}).*

For all the complexes, mass spectroscopy in the EI and/or ESI mode were carried out. The copper(II) complex (**12**) shows a molecular peak in the EI as well as in the ESI-positive mode at m/z-1150 (in dichloromethane for ESI-positive mode) with other characteristic peaks. For the nickel(II) complex (**13**), the peak occurs at m/z-1140 in the EI mode corresponding to the molecular peak. Compounds **14**, **15** and **16** show molecular peaks at 1654,1648 and 1646 respectively [Figure 3.5]. For the cobalt(III) compound (**17**), ESI-positive mode in dichloromethane shows the molecular peak at 1924. The molecular peak along with the characteristic peaks are shown in Table 3.3.

Table 3.3 :- *Characteristic peaks in mass spectroscopy for **12-17**.*

Complex	Molecular Weight	Molecular Peak m/z	Other characteristic Peaks m/z
12	1150	1150[$Cu^{II}_2L^3_2$]	1087, 1047, 791, 616, 575 [CuL^3]$^+$
13	1140	1140[$Ni^{II}_2L^3_2$]	570 [NiL^3]$^+$
14	1654	1654 [$Co_2L^3_3$]	1142 [$Co_2L^3_2$]$^+$
15	1648	1648[$Fe^{III}_2L^3_3$]	1136 [$Fe_2L^3_2$]$^+$, 824 [$CoL^3_{1.5}$]$^+$
16	1646	1646[$Mn^{IV}_2(L^3)(L_A{}^3)_2$]	1134 [$Mn_2L^3_2$]$^+$, 822 [$MnL^3_{1.5}$]$^+$
17	1924	1924[$Co^{III}_2L^4_3$]	1322 [$Co_2L^4_2$]$^+$

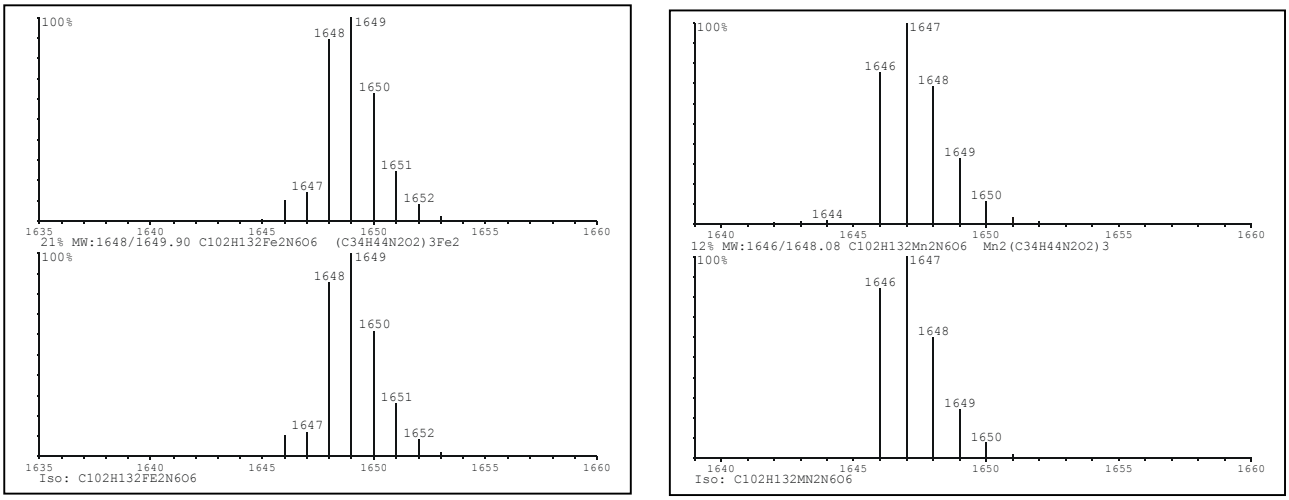

a) b)

Figure 3.5:- Experimental (top) and simulated (bottom) mass spectrum of (a) $Fe_2L^3_3$ (**15**) and (b) $Mn^{IV}_2(L^3)(L_A{}^3)_2$ (**16**).

3.3.2 CRYSTAL STRUCTURE AND CHARACTERIZATION OF COMPLEXES

$[Cu^{II}_2L^3_2]$ (12)

Dark green crystals of **12** were afforded from a solvent mixture of THF-Methanol in the ratio 4:1. The crystal structure [Figure 3.6 (a)]shows the presence of 1.5 THF molecules per unit cell of **12**. The complex consists of two distorted square-planer copper ions co-coordinated to two fully deprotonated ligands. The Cu(1) and Cu(2) centers is 0.457Å and 0.405Å above the plane made by joining the respective donor atoms for each center viz. N(1)N(3)O(1)O(3) and N(2)N(4)O(2)O(4). The distance between the two copper centers is 6.697 Å. The average copper-oxygen bond distance is 1.919(2) Å and that for copper-nitrogen distance is 1.945(2) Å. Therefore the oxidation state of the copper center is (+II) and the copper-donor atom distances values are comparable for other copper complexes [4b]. The two nitrogen and the two oxygen atoms are **cis** co-coordinated to each copper center. In **12*** (the monomeric copper(II) complex with the ligand 2-anilino-4,6-ditertbutyl phenol), the two nitrogen and the two oxygen atoms are in **trans** position[4b]. The geometry of $[L^3]^{2-}$ forces the homo-donor atoms in cis position. The two meta-phenylene rings, which act as the spacer, are in a staggered position and make an angle of 8.5° between them [Figure 3.6(b)].

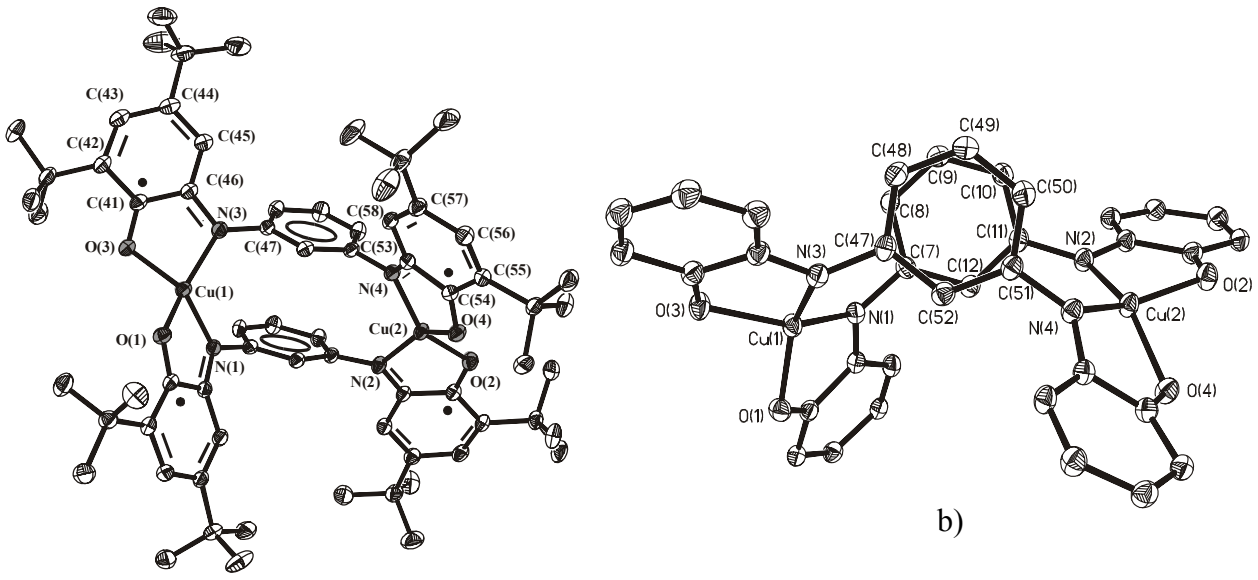

Figure 3.6 :- a) Molecular structure of **12**.b) Perspective view of **12** showing the staggered form of the two meta-phenylene spacers.

Table 3.4:- *Selected bond lengths (Å) and angles (degree) for **12**.*

Cu(1)-O(3)	1.914(2)	C(41)-C(42)	1.439(3)
Cu(1)-O(1)	1.9322(14)	C(42)-C(43)	1.378(3)
Cu(1)-N(1)	1.945(2)	C(42)-C(59)	1.530(3)
Cu(1)-N(3)	1.950(2)	C(43)-C(44)	1.427(3)
Cu(2)-O(2)	1.901(2)	C(44)-C(45)	1.369(3)
Cu(2)-O(4)	1.928(2)	C(44)-C(63)	1.535(3)
Cu(2)-N(4)	1.934(2)	C(45)-C(46)	1.423(3)
Cu(2)-N(2)	1.949(2)	C(47)-C(48)	1.397(3)
O(1)-C(1)	1.292(2)	C(47)-C(52)	1.397(3)
N(1)-C(6)	1.346(3)	C(48)-C(49)	1.386(3)
N(1)-C(7)	1.415(3)	C(49)-C(50)	1.384(3)
O(2)-C(14)	1.290(3)	C(50)-C(51)	1.399(3)
N(2)-C(13)	1.349(2)	C(51)-C(52)	1.392(3)
N(2)-C(11)	1.414(3)	C(53)-C(58)	1.421(3)
O(3)-C(41)	1.294(3)	C(53)-C(54)	1.451(3)
N(3)-C(46)	1.357(3)	C(54)-C(55)	1.432(3)
N(3)-C(47)	1.413(3)	C(55)-C(56)	1.379(3)
O(4)-C(54)	1.284(2)	C(55)-C(67)	1.528(3)
N(4)-C(53)	1.349(3)	C(56)-C(57)	1.435(3)
N(4)-C(51)	1.416(3)	C(57)-C(58)	1.367(3)
	Cu(1)….Cu(2)	6.697	
O(3)-Cu(1)-O(1)	100.16(6)	C(14)-O(2)-Cu(2)	112.50(13)
O(3)-Cu(1)-N(1)	143.83(7)	C(13)-N(2)-C(11)	120.5(2)
O(1)-Cu(1)-N(1)	83.23(6)	C(13)-N(2)-Cu(2)	110.95(14)
O(3)-Cu(1)-N(3)	84.41(7)	C(11)-N(2)-Cu(2)	127.66(13)
O(1)-Cu(1)-N(3)	146.42(7)	C(41)-O(3)-Cu(1)	112.58(13)
N(1)-Cu(1)-N(3)	112.51(7)	C(46)-N(3)-C(47)	120.4(2)
O(2)-Cu(2)-O(4)	95.48(6)	C(46)-N(3)-Cu(1)	111.25(14)
O(2)-Cu(2)-N(4)	149.98(7)	C(47)-N(3)-Cu(1)	126.85(13)
O(4)-Cu(2)-N(4)	83.39(7)	C(54)-O(4)-Cu(2)	112.58(13)
O(2)-Cu(2)-N(2)	84.43(7)	C(53)-N(4)-C(51)	121.6(2)
O(4)-Cu(2)-N(2)	146.87(7)	C(53)-N(4)-Cu(2)	112.63(13)
N(4)-Cu(2)-N(2)	112.57(7)	C(51)-N(4)-Cu(2)	124.10(13)

A closer look at the bond distances and the angles at the tert-butyl substituted rings shows that the average C-O bond distance (1.29 Å) is much shorter than a C-O bond distance for a phenolate oxygen. This distance corresponds to the iminobenzosemiquinone form and is supported by the planer coordination geometry of nitrogen and the C-N bond distance. The nitrogen is deprotonated and three-coordinated (sp^2 hybridization) with average C-N bond distance (carbon of the phenyl ring containing *tert*-butyl as substituent) has shortened considerably (1.35 Å) signifying the formation of a double bond. The phenyl ring with the *tert*-butyl substituents has lost its aromaticity with the formation of long and short bond distances between the six carbon centers describing the phenyl ring (average bond length of C(42)-C(43), C(44)-C(45), C(57)-C(58), C(55)-C(56) is 1.373 Å and average bond length of C(41)-C(42), C(41)-C(46), C(43)-C(44), C(45)-C(46), C(54)-C(55), C(56)-C(57), C(53)-C(58), C(53)-C(54) is 1.434 Å). It is therefore clear that the ligand is rendered in the iminobenzosemiquinone form and the complex contains **four** iminobenzosemiquinone radicals. Thus, **12** can be best described as the dimer containing *m*-phenylene bridges of the

analogous mononuclear Cu(II) complex with the ligand 2-anilino-4,6-di-*tert*-butylphenol [4a]. Selected bond lengths and angles (degree) for **12** are given in Table 3.4.

A magnetic susceptibility study of complex **12** was carried in from the temperature range of 2-290 K. At higher temperatures, the value of μ_{eff} remains almost constant (2.38 μ_B at 30K and 2.51μ_B at 290K). On further decreasing the temperature, a slow decrease in μ_{eff} is observed till 10K (2.22 μ_B) that decreases further at 2K (1.53 μ_B)[Figure 3.7(a)].

The presence of four iminobezosemiquinone radicals along with the copper centers and their interactions between them should be taken into consideration. In order to simplify this complicated magnetic property, the scheme used in simulating the magnetic susceptibility measurement of **12*** (the mononuclear copper complex with the ligand 2-anilino-4,6-ditertbutylphenol)[4a] was taken into consideration. Therefore, in **12**, the environment around each copper center is studied first and then the whole molecule.

Cu(1) or Cu(2) is surrounded by two iminosemiquinone radicals, each having a spin of ½ (S_{Cu}= S_{Rad} = ½). Therefore, it is a three-spin molecule in each metal center. The states corresponding to each metal center are labeled by their total spins $S_t = S_{Cu} + S_{Rad1} + S_{Rad2}$ and a pair subspin $S^* = S_{Rad1} + S_{Rad2}$, ($S_t$, S^*) = ($^3/_2$, 1), (½ ,1), (½ , 0) or in symbolic fashion (↑↑↑), (↑↓↑), (↑↑↓), respectively. The energy of the corresponding states are given by E($^3/_2$,1) = -J-2J′, E(½ ,1) = 2(J-J′) and E(½ ,0) = 0 where J correspond to the coupling between the radical and copper ion and J′ between the two radical centers. It has been shown that the value of J′ override the value of J i.e. the coupling between the radicals is much stronger than the coupling between the radical and copper ion[4a]. The 1st excited state lies at an energy difference of 595 cm^{-1}. This important information is used in simulating the magnetic susceptibility of data of **12**. This indicates that the radical-radical coupling value remains constant throughout the temperature range and is supported by the nickel (II) complex (**13**) which is found to be diamagnetic for the whole temperature range of 2-290K (Appendix).

Incorporating this assumption in **12**, a more simplified model can be drawn up; the interaction which is observed arises from the two copper centers, Cu(1) and Cu(2) with S = ½. From the experimental data it is clear that the value of μ_{eff} between 30K and 290K corresponds to the two uncoupled S = ½ system (μ_{eff} = 2.45 ± 0.07μ_B). The values obtained by simulating this data are J = 0 cm^{-1} (fixed), g_1= g_2 = 2.049 and a Theta-Weiss parameter(θ) of –2.85K. The most plausible reason which can be given for no-coupling is the improper mixing of the p(π) and the metal d(π) orbital. As mentioned earlier (Chapter 1), orthogonal overlap between these types of orbitals is a necessity for the superexchange process. This type of coupling in a *meta*-phenylene bridged system was also observed by Hendrikson, Stucky

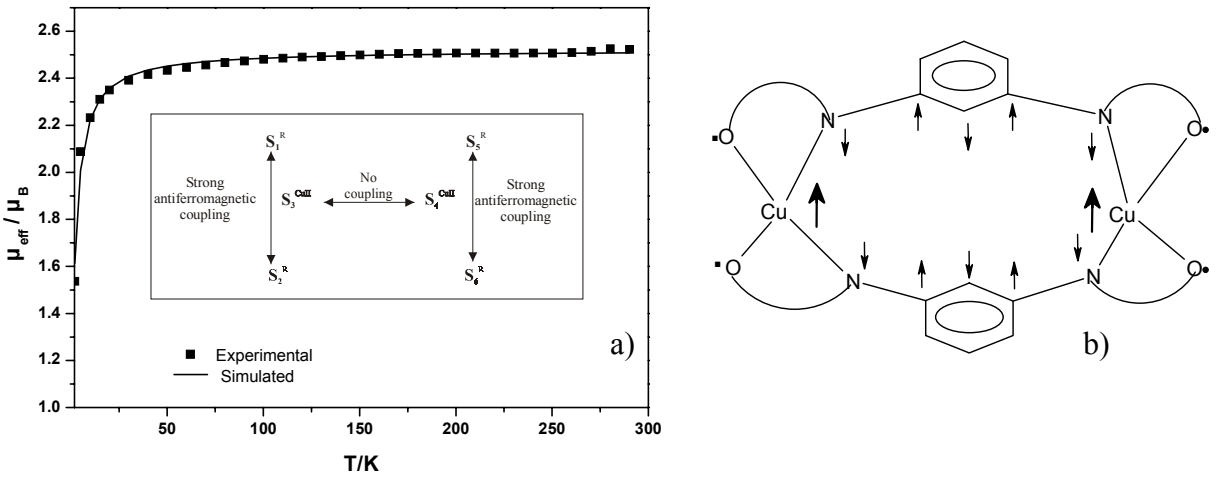

Figure 3.7 :- a) Magnetic data for **12** b) Spin orientation diagram of **12**.

and co-workers[6]. From the crystal structure, it is observed that the Cu(1) and Cu(2) lies about 0.457 A and 0.405 A respectively. This indicates that the geometry surrounding the copper atoms are highly distorted and this leads to improper mixing between the d_{x2-y2} orbital of copper and p(π)-orbital of the nitrogen atom.

In order to understand the electrochemical property of the complexes, the different redox states of the ligand (H_4L^3) should be discussed. Figure 3.8 shows the different states. The de-protonated ligand is oxidized by two electrons to the dianionic diradical form $[L^3]^{-2}$ and further by two electrons to the quinoid form $[L^3]$.

A number of redox waves were observed in the cyclic voltammogram (bold line) and square wave voltammogram(dotted line) of **12** in dichloromethane and in presence of 0.1M $TBAPF_6$ [Figure 3.9(a), Table 3.5]. From coulometric measurements all these waves are single-electron trasfer processes and are assigned to the oxidation and the reduction of the radicals. The two reversible waves at –0.214 V and –0.126 V vs. Fc^+/Fc are assigned to the oxidation to the mono-cation and the di-cation respectively[Figure 3.8(b)].The redox potentials for these oxidations are comparable to **12***(the mononuclear copper complex with the ligand 2-anilino-4,6-ditertbutylphenol).The two reversible reduction peaks at –0.955 V and -1.133V are also comparable to that of **12***. These two peaks are due to the formation of the mono-anionic and di-anionic form of the complex **12**. It is to be noted that the pairwise redox process occurs at a single ligand. The different redox forms are given as

$$[Cu_2(L^3)^{+2}(L^3)] \xleftarrow{-1e^-} [Cu_2(L^3)^{+1}(L^3)] \xleftarrow{-1e^-} [Cu_2L^3_2] \xrightarrow{+1e^-} [Cu_2(L^3)^{-1}(L^3)] \xrightarrow{+1e^-} [Cu_2(L^3)^{-2}(L^3)]$$

The cyclic voltammetry peaks assigned above can be corroborated with the electronic spectrum of the oxidized and reduced form of **12** [Figure 3.9 (b)], generated by coulometry in dichloromethane at –25 °C with 0.2 M $TBAPF_6$. The electronic spectrum of **12** shows peaks at 476nm (ε = 16,400 $M^{-1}cm^{-1}$) which is due to the partial quinone character at the radical site.

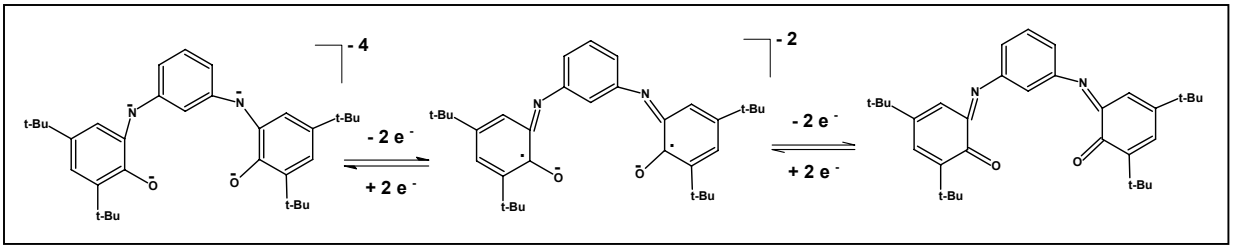

Figure 3.8:- a) Redox states of ligand H_4L^3**.**

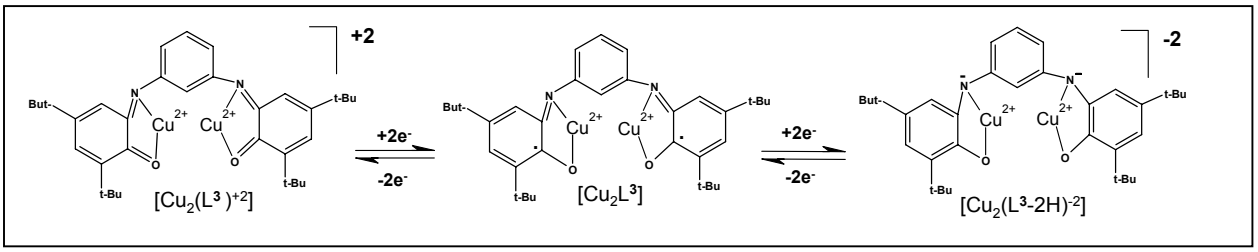

(b) Redox steps of **12** as observed from cyclic voltammetry and square wave voltammetry**.**

Table 3.5 :- *Redox potentials (V) for **12** and **12*** vs. Fc^+/Fc.*

Compound	Oxidation			Reduction		
12	+ 0.440 (irreversible)	- 0.120 (reversible)	- 0.210 (reversible)	- 0.960 (reversible)	- 1.13 (reversible)	- 1.56 (irreversible)
12* (the mononuclear coppercomplex 2-anilino-4,6 ditertbutylphenol)	+ 0.370 (reversible)		-0.260 (reversible)	- 1.02 (reversible)		- 1.32 (reversible)

The broad peak at 815nm (ε = 11,100 $M^{-1}cm^{-1}$) and another peak at 1120nm (ε=9645 $M^{-1}cm^{-1}$) are due to the intense π-π* intra- ligand charge transfer. When **12** is oxidized by one electron, a bathochromic shift of the peak at 476 nm is observed to 509 nm and further to 520 nm upon the 2nd electron oxidation with an increase in the ε value (21,350 M^{-1} cm^{-1}). This agrees with the mechanism given in Figure 3.8b.

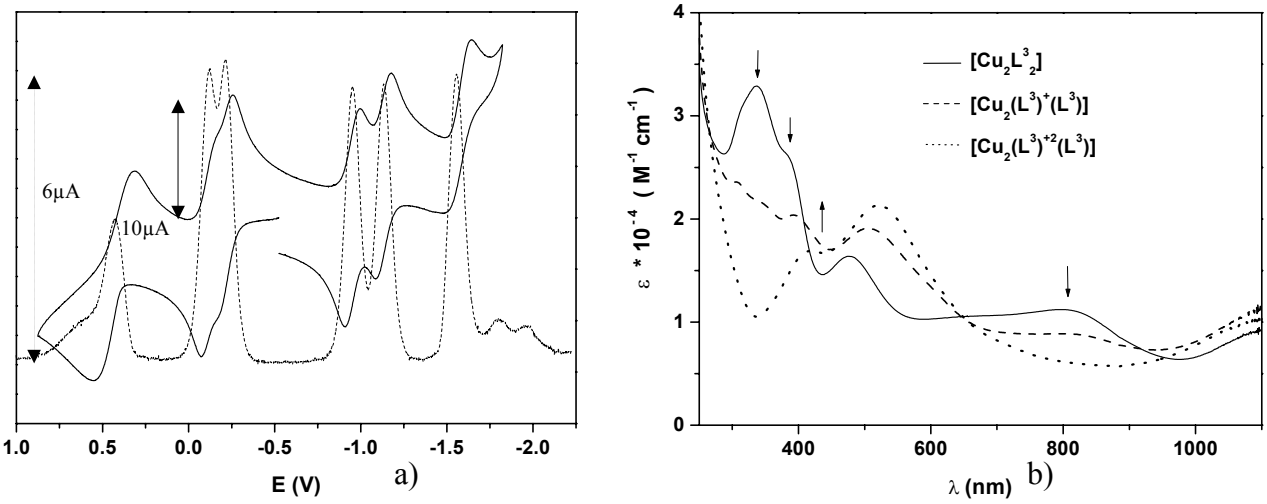

Figure 3.9 :- a) Cyclic (bold line) and square wave (dotted line) voltammogram of **12**.

b) Electronic spectra of **12** (bold line), its $1e^-$ and $2e^-$ oxidized species.

$Co^{III}_2L^3_3$ (14)

The neutral complex $Co_2L^3_3$ (**14**) [Figure 3.10] crystallizes from the reaction medium as deep brown (nearly black) crystals. Each cobalt ion is in a distorted octahedral geometry bounded by three oxygen and three nitrogen. A C_3 axis passes through each of the cobalt center, compared to the complex **14*** (monomer cobalt complex using 2-anilino-4,6-ditert-butylphenol) where a C_2 axis passes through the cobalt center[4a,b]. The six short Co-O distance at 1.899 ± 0.004 Å together with the six short Co-N distance 1.930 ± 0.009Å in **14** are compatible with the low spin d^6 configuration. Here again, it is observed that the ligands has lost their amino-hydrogen atom together with the phenol proton. The coordination geometry around the nitrogen donor atom is planer, showing that it is three coordinated. Each of the phenyl rings containing the *tert*-butyl groups has lost its aromaticity. Thus the average distance between C(3)-C(4), C(5)-C(6), C(15)-C(16), C(17)-C(18), C(43)-C(44), C(45)-C(46), C(55)-C(56), C(57)-C(58), C(83)-C(84), C(85)-C(86), C(95)-C(96) and C(97)-C(98) being 1.374Å which is shorter than the rest 24 C-C bond lengths of the tert-butyl containg phenyl rings; the complex **14** consists of **six** iminobenzosemiquinone radicals. Correspondingly the imino C=N bonds at 1.342 ± 0.012 Å which is shorter than the C-N bonds to the spacer phenyl ring, (1.425 ± 0.012Å) along with the C-O bond length at 1.299 ± 0.012 Å, further supporting the formation of the iminosemiquinone character. Selected bond distances are given in Table 3.6.

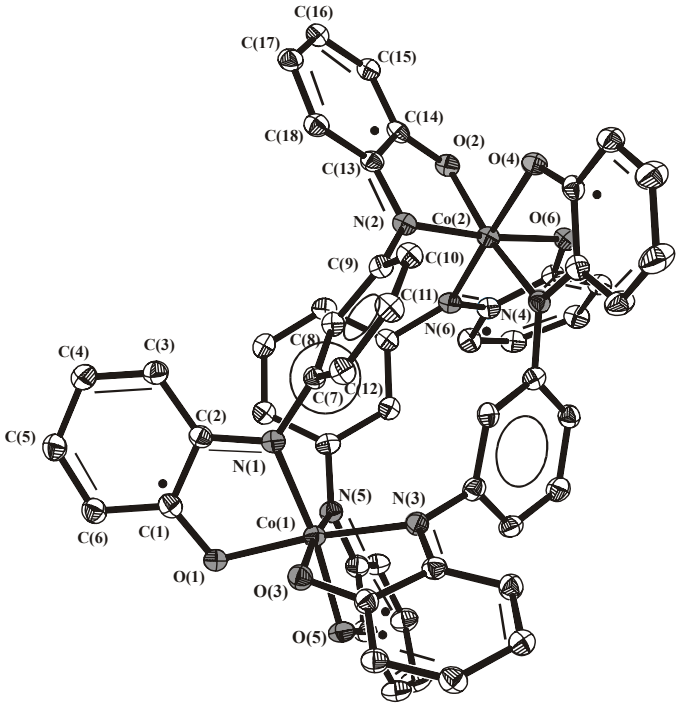

Figure 3.10 :- Molecular structure of **14**.Tert-butyl groups have been removed for clarity.

Table 3.6 :- *Selected bond distances (Å) and bond angles (degree) of **14**.*

Co(1)-O(5)	1.895(2)	N(5)-C(82	1.338(4)
Co(1)-O(3)	1.897(2)	N(5)-C(87)	1.421(4)
Co(1)-O(1	1.905(2)	N(6)-C(9	1.343(4)
Co(1)-N(5)	1.916(3)	N(6)-C(89)	1.421(4)
Co(1)-N(1)	1.926(3)	C(1)-C(6)	1.425(4)
Co(1)-N(3)	1.934(3)	C(1)-C(2)	1.438(5)
Co(2)-O(4)	1.898(2)	C(2)-C(3	1.432(4)
Co(2)-O(2)	1.898(2)	C(3)-C(4)	1.371(5)
Co(2)-O(6)	1.900(2)	C(4)-C(5)	1.425(5)
Co(2)-N(4)	1.927(3)	C(4)-C(23)	1.539(5)
Co(2)-N(2)	1.937(3)	C(5)-C(6)	1.379(5)
Co(2)-N(6)	1.939(3)	C(6)-C(19)	1.531(5)
O(1)-C(1)	1.295(4)	C(7)-C(12)	1.396(5)
O(2)-C(14)	1.301(4)	C(7)-C(8)	1.400(5)
O(3)-C(41)	1.300(4)	C(8)-C(9)	1.389(5)
O(4)-C(54)	1.298(4)	C(9)-C(10)	1.399(5)
O(5)-C(81)	1.299(4)	C(10)-C(1	1.395(5)
O(6)-C(94)	1.301(4)	C(11)-C(1	1.395(5)
N(1)-C(2)	1.343(4)	C(13)-C(18)	1.421(5)
N(1)-C(7)	1.425(4)	C(13)-C(14)	1.436(5)
N(2)-C(13)	1.342(4)	C(14)-C(15)	1.430(5)
N(2)-C(9)	1.429(4)	C(15)-C(16)	1.381(5)
N(3)-C(42)	1.344(4)	C(15)-C(27)	1.539(5)
N(3)-C(47)	1.431(4)	C(16)-C(17)	1.431(5)
N(4)-C(53)	1.344(4)	C(17)-C(18)	1.373(5)
N(4)-C(49)	1.425(4)	C(17)-C(31)	1.531(5)
		C(19)-C(22)	1.536(5)
		C(19)-C(20)	1.543(6)

Co(1)……Co(2) 6.791

O(5)-Co(1)-O(3)	87.64(10)	O(6)-Co(2)-N(6)	83.49(11)
O(5)-Co(1)-O(1)	90.02(10)	N(4)-Co(2)-N(6)	100.15(12)
O(3)-Co(1)-O(1)	90.61(10)	N(2)-Co(2)-N(6)	96.15(12)
O(5)-Co(1)-N(5)	84.10(11)	C(1)-O(1)-Co(1)	113.1(2)
O(3)-Co(1)-N(5)	171.70(11)	C(14)-O(2)-Co(2)	112.8(2)
O(1)-Co(1)-N(5)	88.61(11)	C(41)-O(3)-Co(1)	111.8(2)
O(5)-Co(1)-N(1)	172.92(11)	C(54)-O(4)-Co(2)	113.4(2)
O(3)-Co(1)-N(1)	88.98(11)	C(81)-O(5)-Co(1)	113.2(2)
O(1)-Co(1)-N(1)	83.80(11)	C(94)-O(6)-Co(2)	110.6(2)
N(5)-Co(1)-N(1)	99.14(12)	C(2)-N(1)-C(7)	120.9(3)
O(5)-Co(1)-N(3)	87.03(11)	C(2)-N(1)-Co(1)	112.0(2)
O(3)-Co(1)-N(3)	83.76(11)	C(7)-N(1)-Co(1)	127.1(2)
O(1)-Co(1)-N(3)	173.74(11)	C(13)-N(2)-C(9)	120.8(3)
N(5)-Co(1)-N(3)	96.57(12)	C(13)-N(2)-Co(2)	111.9(2)
N(1)-Co(1)-N(3)	98.78(12)	C(9)-N(2)-Co(2)	126.6(2)
O(4)-Co(2)-O(2)	88.83(11)	C(42)-N(3)-C(47)	120.4(3)
O(4)-Co(2)-O(6)	89.35(11)	C(42)-N(3)-Co(1)	111.0(2)
O(2)-Co(2)-O(6)	87.75(11)	C(47)-N(3)-Co(1)	127.9(2)
O(4)-Co(2)-N(4)	83.96(11)	C(53)-N(4)-C(49)	121.2(3)
O(2)-Co(2)-N(4)	172.75(12)	C(53)-N(4)-Co(2)	112.6(2)
O(6)-Co(2)-N(4)	91.49(11)	C(49)-N(4)-Co(2)	125.9(2)
O(4)-Co(2)-N(2)	90.38(12)	C(82)-N(5)-C(87)	120.6(3)
O(2)-Co(2)-N(2)	84.03(11)	C(82)-N(5)-Co(1)	112.4(2)
O(6)-Co(2)-N(2)	171.78(11)	C(87)-N(5)-Co(1)	126.4(2)
N(4)-Co(2)-N(2)	96.65(12)	C(93)-N(6)-C(89)	120.1(3)
O(4)-Co(2)-N(6)	171.80(11)	C(93)-N(6)-Co(2)	110.6(2)
O(2)-Co(2)-N(6)	86.92(12)	C(89)-N(6)-Co(2)	127.9(2)

Magnetic data for a polycrystalline sample of **14** is displayed in Figure 3.11(b). On lowering the temperature, μ_{eff} (4.21 μ_B at 290 K) decreases rather slowly till 100 K (4.13 μ_B) and then monotonically till it reaches a value of 1.99μ_B at 2K. This data shows that an overall anti-ferromagnetic coupling dominates throughout the whole molecule and needs rationalization for simulating this data.

The mononuclear Co^{III} complex (**14***) prepared with the ligand 2-anilino-4,6-ditertbutyl phenol[4a] with three iminobenzosemiquinone radicals has a quartet ground state arising from the ferromagnetic coupling between the radicals. Out of the three planes possible, two dihedral angles were found to be deviating from orthogonality and the 3rd angle was found to be nearly orthogonal. Therefore, two different coupling constants (J) were needed in order to simulate the data.

In case of **14**, the presence of six radicals complicates the nature of interactions. As Co^{III} (low spin) is a d^6 ion (e_g level is vacant), the interaction must occur through the metal π-orbitals and, the coupling between the radicals in each 'part' can be ferro- or anti-ferromagnetic in nature. When each cobalt center is considered, the dihedral angles made between the two planes (each plane consisting the tert-butyl substituted phenyl rings) containing the O(1) atom [C(1)-C(2)-C(3)-C(4)-C(5)-C(6)] and O(3) [C(41)-C(42)-C(43)-C(44)-C(45)-C(46)] is 121.8°; that between O(1)[C(1)-C(2)-C(3)-C(4)-C(5)-C(6)]-O(5) [C(81)-C(82)-C(83)-C(48)-C(85)-C(86)] and O(3)[C(41)-C(42)-C(43)-C(44)-C(45)- C(46)]-O(5) [C(81)-C(82)-C(83)-C(84)-C(85)-C(86)] being 86.5° and 88.6°, respectively. From these values it is clear that the angles deviate from orthogonality and the coupling between the radicals at each cobalt center is probably anti-ferromagnetic. Examples of anti-ferromagnetic coupling between radicals with cobalt as central ion is known. The dihedral angles made by the phenyl rings between O(2) [C(13)-C(14)-C(15)-C(16)-C(17)-C(18)] - O(4)[C(43)-C(44)-C(45)-C(46)-C(47)-C(48)] is 162°; that between O(2) [C(13)-C(14)-C(15)-C(16)-C(17)-C(18)]-O(6)[C(93)-C(94)-C(95)-C(96)-C(97)-C(98)] and O(4)[C(43)-C(44)-C(45)-C(46)-C(47)-C(48)]-O(6)[C(93)-C(94)-C(95)-C(96)-C(97)-C(98)] being 112° and 121.4°, respectively. In order to simulate the experimental data, it was assumed that since each cobalt center has a symmetric environment, a single coupling constant (J_1) is needed for the radical-radical interaction at each part. It is also to be noted that this coupling constant is the summation of the ferromagnetic (if present) and antiferromagnetic coupling constants ($J = J_{Ferro} + J_{Antiferro}$). This simplifies the problem; the ground state at each 'part' is S = ½ with anti-ferromagnetic coupling between the radicals. Naturally the question arises whether there some interaction between these two residual spins with each other. If these two parts were

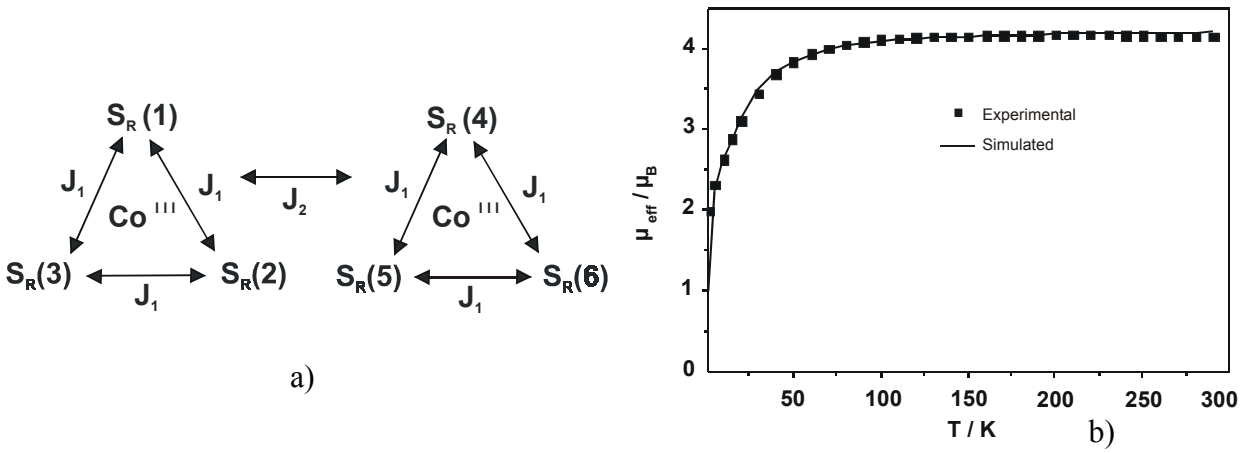

Figure 3.11 :- a) Spin coupling model used in simulating the magnetic data of **14**.
b) Experimental and simulated data of **14**.

assigned as two independent moiety having no interaction between them(as in **12**), the value of μ_{eff} should have reached 5.48 μ_B. This shows that there is some interactions and the nature could be ferromagnetic (S_{total}=1) or anti-ferromagnetic (S_{total}=0). The coupling constant of this interaction is denoted as J_2 and is taken as the coupling between the radicals of the same ligand for sake of simplification.

The spin coupling model is given in Figure 3.11(a). When J_1 is anti-ferromagnetic (negative J value) and J_2 is also taken to be anti-ferromagnetic, a good fit is not obtained. This ensured that by spin polarization mechanism there is ferromagnetic coupling (positive J value) between these two parts. Indeed a good fit is obtained when the value of J_1 is taken to be negative and J_2 positive. The values obtained were J_1 = -9.66 cm^{-1} and J_2 = + 13.03 cm^{-1} with g = 2.0 (fixed) [Figure 3.11(b), bold line].

The complex **14** was subjected to square wave and cyclic voltammetric studies in dichloromethane and in the presence of 0.1M $TBAPF_6$. A number of redox peaks was observed and all inferred to the radical oxidation or reduction process. Figure 3.12(a) depicts the cyclic voltammogram (bold line) and square wave voltammogram (dotted line) of **14**. All the four peaks between –0.75V and 0.5V are due to the oxidation of radicals and each peak correspond to a single electron transfer process, as observed from coulometric measurements. The potentials of **14** and that of the parent mononuclear Co^{III} complex (**14***)[3] are given in Table 3.7. All the anodic peaks are reversible in nature and therefore spectroelectrochemical experiments were performed in order to characterize each of the oxidized species. Coulometric experiments were performed at –25°C in the presence of 0.2M $TBAPF_6$. During the coulometry, the change in the electronic spectrum of **14** was monitored from190-1100 nm.

Table 3.7 :- *Redox potentials (V) for **14** and **14*** vs. Fc^{+}/Fc.*

Compound	$E_{1/2}$ (Oxidation)				$E_{1/2}$ (Reduction)	
14	+ 0.247 (reversible)	0.174 (reversible)	- 0.277 (reversible)	-0.431 (reversible)	-1.214 (irreversible)	
14* (the mononuclear cobalt complex with 2-anilino-4,6 ditert-butylphenol)	+ 0.196 (reversible)		-0.363 (reversible)		- 0.933 (reversible)	- 1.32 (reversible)

The neutral complex **14**, shows a spectrum with absorption maxima at 483 nm (ε = 8230 M^{-1} cm^{-1}), 779 nm (ε = 5536 M^{-1} cm^{-1}) and shoulders at 607 nm (ε =5980 M^{-1} cm^{-1}), 700 nm (ε = 5095 $M^{-1}cm^{-1}$) and 874 nm (ε = 4229 M^{-1} cm^{-1}) [Figure 3.12(b) (bold line)]. It is observed that for each electron oxidation there is an increase in the intensity at 482 nm (ε = 21784 M^{-1} cm^{-1}) which shows the increase in quinoid character of the ligand. The bands lying above 600 nm decreases in intensity and after the 4th electron oxidation, no absorption maxima above 600 nm was observed.

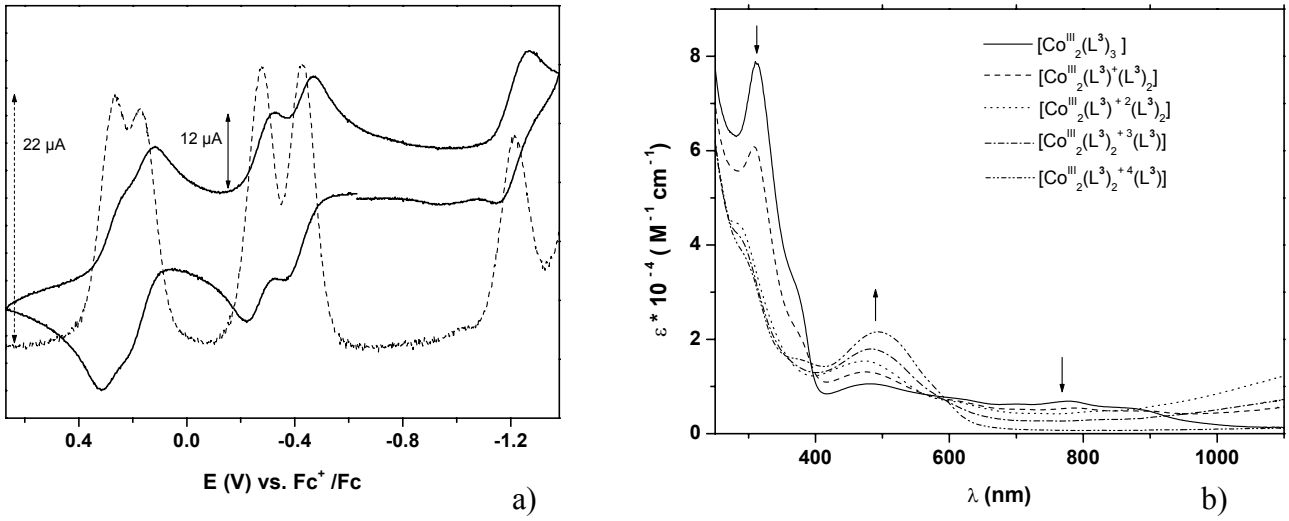

Figure 3.12 :- a) Cyclic voltammogram (bold line) and square wave voltammogram (dotted line) of **14**. b)Electronic spectrum of **14** and the corresponding oxidized products

$Fe^{II}_2L^3_3$ (15)

Although analytical and spectroscopic data are in agreement with the presence of a dinuclear $Fe_2L^3_3$ unit as the smallest unit in **15**, an X-ray analysis was undertaken to remove the doubts. Indeed, the structure analysis shows the presence of two 6-coordinated iron(III) centers. **15** crystallizes in the monoclinic space group $P2_1/n$. The iron center is in a distorted octahedral geometry with three oxygen and three nitrogen donor atoms and a C_3 axis passing through each iron center [Figure 3.13]. The monomer iron complex **15***[4c] (with the ligand 2-anilino-4,6-ditertbutylphenol) possess a C_2 symmetry.

The average Fe-O and Fe-N bond lengths are 2.015 ± 0.009Å and 2.098 ± 0.009Å, respectively. This shows that the complex **15** consists of two high spin ferric centers (d^5) and consequently the Fe-O and Fe-N bonds are larger than that of the Co^{III} complex (**14**). Selected bond lengths are given in Table 3.8. That **15** consists of two high spin ferric centers has also been confirmed by Mössbauer spectroscopy.

The geometrical features of the three ligands are identical within the small experimental error and does not vary appreciably with the nature of the central metal ion (Cu,

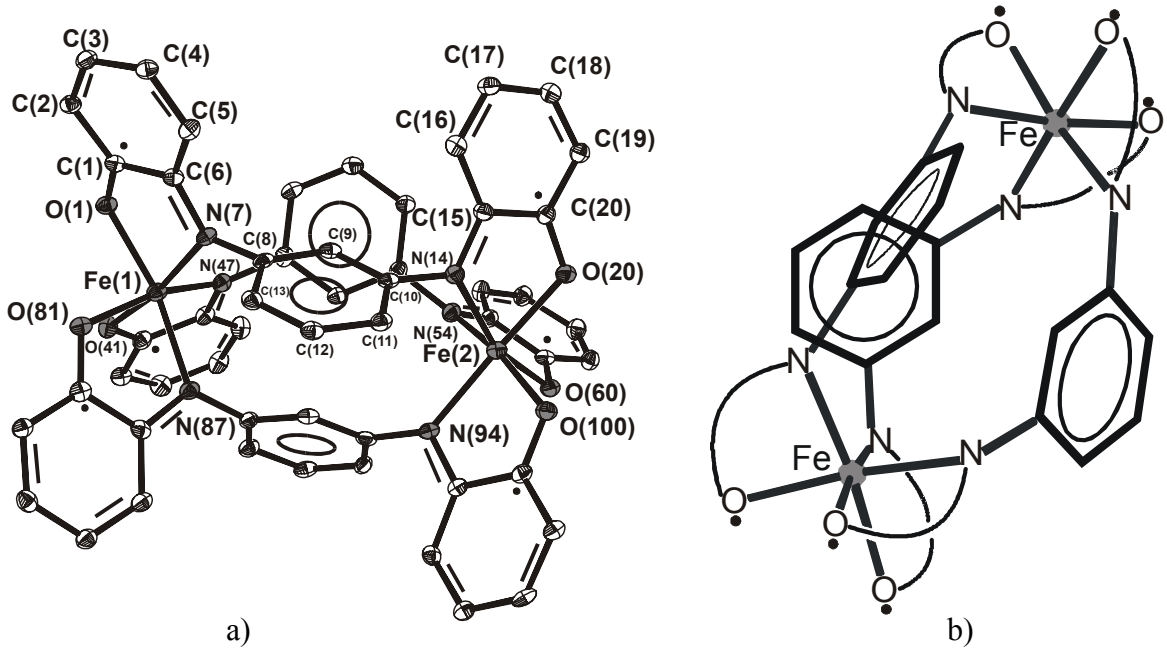

Figure 3.13 :- a) Crystal Structure of **15**. The tert-butyl groups has been removed for clarity. b) A view of **15** highlighting the coordination sphere around the two Fe(III) centers. The tetra-dentate ligand L^3 is denoted by the donor atoms and the meta-phenylene spacer.

Table 3.8 :- *Selected bond distances (Å) and bond angles (degree) of **15**.*

Fe(1)-O(1)	2.006(3)	N(54)-C(55)	1.344(5)
Fe(1)-O(41)	2.013(3)	C(52)-N(54)	1.435(5)
Fe(1)-O(81)	2.019(3)	C(86)-N(87)	1.338(5)
Fe(1)-N(87)	2.070(3)	N(87)-C(88)	1.424(5)
Fe(1)-N(7)	2.083(3)	N(94)-C(95)	1.339(5)
Fe(1)-N(47)	2.124(3)	C(92)-N(94)	1.416(5)
Fe(2)-O(60)	2.004(3)	C(1)-C(2)	1.428(6)
Fe(2)-O(20)	2.004(3)	C(1)-C(6)	1.462(6)
Fe(2)-O(100)	2.046(3)	C(2)-C(3)	1.377(6)
Fe(2)-N(94)	2.073(3)	C(3)-C(4)	1.422(6)
Fe(2)-N(54)	2.097(3)	C(4)-C(5)	1.368(6)
Fe(2)-N(14)	2.139(3)	C(5)-C(6)	1.416(6)
O(1)-C(1)	1.285(5)	C(5)-C(6)	1.416(6)
O(20)-C(20)	1.292(5)	C(8)-C(13)	1.390(5)
O(41)-C(41)	1.287(5)	C(8)-C(9)	1.403(6)
O(60)-C(60)	1.287(5)	C(9)-C(10)	1.375(6)
O(81)-C(81)	1.283(5)	C(10)-C(11)	1.377(6)
O(100)-C(100)	1.290(5)	C(11)-C(12)	1.401(6)
C(6)-N(7)	1.335(5)	C(12)-C(13)	1.383(6)
N(7)-C(8)	1.425(5)	C(12)-N(14)	1.426(5)
N(14)-C(15)	1.326(5)	C(15)-C(16)	1.418(6)
C(12)-N(14)	1.426(5)	C(15)-C(20)	1.459(6)
C(46)-N(47)	1.332(5)	C(16)-C(17)	1.355(6)
N(47)-C(48)	1.429(5)	C(17)-C(18)	1.433(6)
		C(18)-C(19)	1.373(6)
		C(19)-C(20)	1.420(6)

Fe(1)……Fe(2) 6.934

O(1)-Fe(1)-O(41)	88.65(12)	N(94)-Fe(2)-N(14)	93.24(13)
O(1)-Fe(1)-O(81)	92.98(11)	N(54)-Fe(2)-N(14)	95.41(13)
O(41)-Fe(1)-O(81)	86.08(11)	C(1)-O(1)-Fe(1)	115.7(3)
O(1)-Fe(1)-N(87)	170.17(12)	C(6)-N(7)-C(8)	119.6(4)
O(41)-Fe(1)-N(87)	94.49(12)	C(6)-N(7)-Fe(1)	113.5(3)
O(81)-Fe(1)-N(87)	77.97(12)	C(8)-N(7)-Fe(1)	125.4(3)
O(1)-Fe(1)-N(7)	77.68(13)	C(15)-N(14)-C(12)	118.4(3)
O(41)-Fe(1)-N(7)	163.61(13)	C(15)-N(14)-Fe(2)	111.4(3)
O(81)-Fe(1)-N(7)	103.44(12)	C(12)-N(14)-Fe(2)	127.9(3)
N(87)-Fe(1)-N(7)	100.49(13)	C(20)-O(20)-Fe(2)	115.3(2)
O(1)-Fe(1)-N(47)	90.05(12)	C(41)-O(41)-Fe(1)	116.9(3)
O(41)-Fe(1)-N(47)	77.09(12)	C(46)-N(47)-C(48)	119.6(3)
O(81)-Fe(1)-N(47)	162.82(13)	C(46)-N(47)-Fe(1)	112.7(3)
N(87)-Fe(1)-N(47)	99.73(13)	C(48)-N(47)-Fe(1)	126.3(3)
N(7)-Fe(1)-N(47)	93.72(13)	C(55)-N(54)-C(52)	117.5(3)
O(60)-Fe(2)-O(20)	90.51(11)	C(55)-N(54)-Fe(2)	112.6(3)
O(60)-Fe(2)-O(100)	98.66(11)	C(52)-N(54)-Fe(2)	128.7(2)
O(20)-Fe(2)-O(100)	83.14(11)	C(60)-O(60)-Fe(2)	116.9(3)
O(60)-Fe(2)-N(94)	101.26(12)	C(81)-O(81)-Fe(1)	115.2(3)
O(20)-Fe(2)-N(94)	157.97(12)	C(86)-N(87)-C(88)	118.9(3)
O(100)-Fe(2)-N(94)	76.76(12)	C(86)-N(87)-Fe(1)	113.9(3)
O(60)-Fe(2)-N(54)	77.44(12)	C(88)-N(87)-Fe(1)	125.7(2)
O(20)-Fe(2)-N(54)	97.80(12)	C(93)-C(88)-C(89)	120.2(4)
O(100)-Fe(2)-N(54)	175.97(13)	C(95)-N(94)-C(92)	119.9(3)
N(94)-Fe(2)-N(54)	102.87(13)	C(95)-N(94)-Fe(2)	114.5(3)
O(60)-Fe(2)-N(14)	164.92(12)	C(92)-N(94)-Fe(2)	123.7(3)
O(20)-Fe(2)-N(14)	77.19(12)	C(100)-O(100)-Fe(2)	115.5(3)
O(100)-Fe(2)-N(14)	88.62(12)		

Co, Fe). Here again, the ligand is in the deprotonated form and the nitrogen is planer and three coordinated. The average C-O and C-N bond lengths are 1.287 ± 0.009Å and 1.335 ± Å , respectively. The six ring C-C distances of the tert-butyl substituted phenyl rings are not equidistant and a typical pattern of short (1.377 Å), a long (1.422 Å), and a short (1.368 Å) together with three long C-C bonds are observed. This features show that the tert-butyl substituted phenyl rings have lost its aromaticity. Thus, each iron (III) center has three O,N coordinated iminobenzosemiquinone radicals; the complex consists of **six** iminobenzosemiquinone radicals.

Zero-field Mössbauer spectrum of **15** was recorded at 80K and the nonlinear least-squares fit is shown in Figure 3.14. The spectrum was fitted with a single quadrupole split doublet with an isomer shift of δ = 0.56 mms^{-1} and a quadrupole splitting of ΔE_Q = 1.011 mms^{-1}. The isomer shift is consistent with those observed for high spin iron(III) ions in an octahedral or distorted octahedral coordination.

In order to establish the spin ground state of **15**, magnetization measurements at 1, 4 and 7 T was carried out. The field-dependent magnetizations as a function of temperature and their simulations are depicted in Figure 3.15(a). The curve shows the value of magnetization reaches ~1.74 in the temperature range 2.0 - 2.8 K at the highest field of 7 T. The simulated parameters are: S = 2.0, g = 2.0 (fixed), $|D|$= - 2.0 cm^{-1} and a Theta-Weiss parameter (θ) of -1.73K. Complex **15** is X-band EPR silent at 10K, which is in conform with an integer spin system. The magnetic behavior of **15** can be interpreted as the presence of strong antiferromagnetic interactions between the three iminobenzosemiquinone radicals [S_R(total) = $^3/_2$] and the high-spin ferric ion with S_{Fe}= $^5/_2$ resulting in two S = 1 fragments on each side of the *m*-phenylene spacer. The educated guess of strong antiferromagnetic

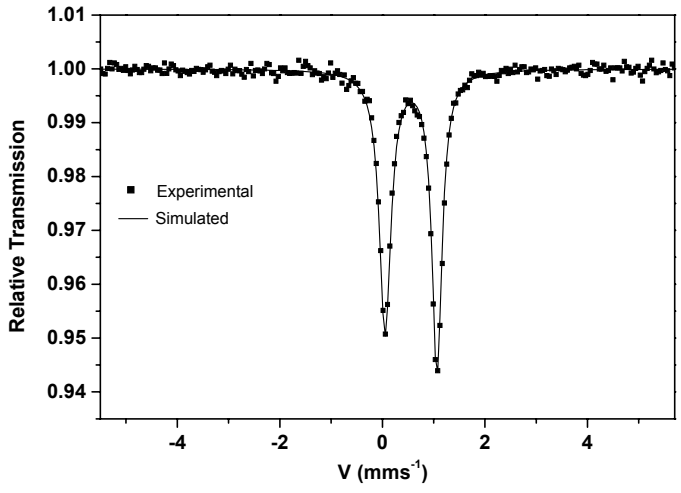

Figure 3.14:- Mössbauer spectrum of **15**.

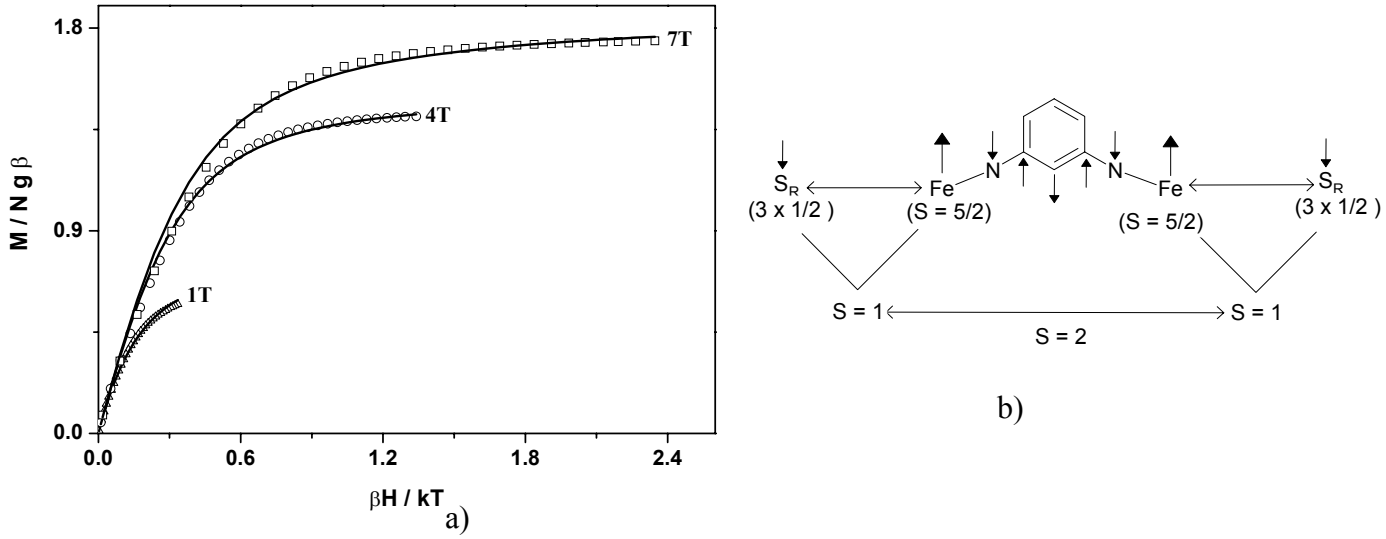

Figure 3.15:- a) Magnetization curve of **15** at 1,4 and 7T. b) Coupling scheme of **15**.

interactions between the radicals and the iron(III) center is strongly supported by the similar antiferromagnetic interactions present in the comparable mononuclear iron(III) compound with the ligand 2-anilino-4,6-ditertbutylphenol(**15***)[4c]. A ferromagnetic interaction arising presumably from the spin-polarization effect due to the topology of the spacer between the S = 1 fragments resulting in the ground state of S_t = 2 for **15**. This quantitative picture is schematically depicted in Figure 3.15(b).

Cyclic voltammograms (CV) and square-wave voltammograms (SQW) in dichloromethane solution of **15** containing 0.1M $TBAPF_6$ as supporting electrolyte was recorded [Figure 3.16(a)]. The nature of the anodic waves are similar to the Co(III) complex (**14**) and consists of four one-electron-transfer reversible waves in the range 0.75 V to – 0.5 V. However the cathodic waves which appear from –0.75 V to –1.75 V shows that two of these waves are reversible in nature and the other is irreversible. Coulometry at –25°C in the presence of 0.2M $TBAPF_6$ supports the assignments of the oxidative and reductive peaks and also shows that the all these peaks consists of a single electron transfer process. The nature of the peak at –1.557V could not be characterized as it was irreversible even in the time scale of CV. The peak potentials ($E_{½}$ in V) vs. Fc^+/Fc for **15** and **15*** (mononuclear iron(III) compound with the ligand 2-anilino-4,6-ditertbutylphenol) is given in Table 3.9.

Table 3.9 :- *Redox potentials (V) for **15** and **15*** vs. Fc^+/Fc.*

Compound	$E_{½}$ (Oxidation)				$E_{½}$ (Reduction)		
15	+ 0.481 (reversible)	+ 0.382 (reversible)	- 0.108 (reversible)	-0.288 (reversible)	-1.114 (reversible)	-1.278 (reversible)	-1.557 (irreversible)
15*	+ 0.27 (reversible)		- 0.35 (reversible)		-1.12 (reversible)	-1.31 (reversible)	-1.51 (irreversible

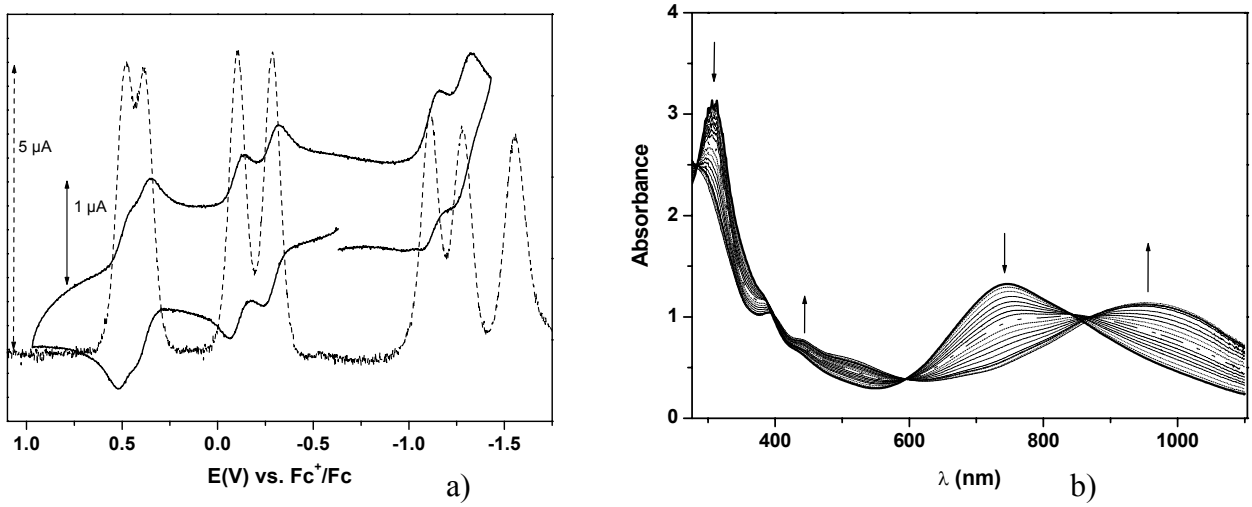

Figure 3.16 :- a) Cyclic (bold line) and square wave voltammogram (dotted line) of **15**.
b) Electronic spectra of **15** (bold line) and its oxidized forms.

In order to characterize the species obtained after each electrochemical oxidation, the UV spectrum was measured for each of the oxidized species. The reduced species were found to be unstable during the time of coulometry. The electronic spectra of **15**, shows a broad but intense peak at 746nm (ε = 35,100 M^{-1} cm^{-1}) with a shoulder at 441nm (ε = 16,100 M^{-1} cm^{-1}). Upon four electron oxidation, the intensity of the peak at 746nm slowly decreases and a new peak at 958nm develops. The intensity of the shoulder peak at 441nm also increases indicating the formation of quinoid character in the ligand [Figure 3.16(b)]. Therefore the four oxidation peaks along with the two reduction peaks are ligand-centered and the peak at –1.557V can be tentatively assigned to the metal centered reduction .

$Mn^{IV}_2(L_A^3)_2L^3$ (16)

Dark brown crystals of **16** were afforded from a dichloromethane-acetonitrile solution mixture. **16** crystallizes in a monoclinic crystal system with a $P2_1/n$ space group, same as that for **15**. This leads to the assumption that manganese has an oxidation state of +3 (d^4 system). However the metal-donor bond length reveals that the average Mn-O and the Mn-N are 1.934 ± 0.009 Å and 1.961 ± 0.009Å, respectively. Each manganese center is in a pseudo-octahedral O_3N_3Mn polyhedron and does not show any Jahn-Teller effect [Figure 3.17] . Thus the oxidation state of each manganese center is +4 (d^3 system).

An intriguing question regarding the neutrality of the complex naturally arises. If all the donor atoms are deprotonated and the oxidation of the three ligands results in six iminobenzosemiquinone radicals, then the complex should be a doubly charged cation! This is

not true and can be corroborated from the bond distances between the tert-butyl substituted rings, and that between the donor atoms and the carbon with which it is attached.

The ligand containing the donor atoms O(41), N(47), O(60) and N(54) has the typical characteristics of the iminobenzosemiquinone form; a short C-N and C-O bond distance together with the loss of aromaticity at the phenyl ring containing the tert-butyl substituent. So, this ligand consists of two iminobenzosemiquinone radicals. The second ligand containing the donor atoms O(1),N(7),O(20) and N(14) consists of the deprotonated ligand and two sp^2 hybridized nitrogen donor atoms. However, the C(1)-O(1) and C(6)-N(7) bond distance are 1.323Å and 1.381Å, respectively which corresponds to the amidophenolate form of the phenyl ring. The six C-C bond distances of this amidophenolate ring are equidistant at 1.404Å [Table 3.10]. Thus, this part of the ligand shows the characteristic of an O,N-coordinated dianion [Figure 3.1]. The other part of the ligand has the typical characteristic of iminobenzosemiquinone ring. So, this ligand consists of a single iminobenzo-semiquinone radical. This features is also observed in the third ligand. One part consists of the amidophenolate ring and the other the iminobenzosemiquinone ring; the complex consists of **four** iminobenzosemiquinone radicals. Thus, each Mn(IV) center is coordinated by i) two oxygen and two imine-nitrogen from two iminobenzosemiquinone rings and ii) one oxygen and one amide-nitrogen from the amidophenolate ring. This renders the complex to be neutral.

Magnetic susceptibility measurement for **16** from 2-290 K for a powdered sample was measured [Figure 3.18(a) as closed square]. The value of μ_{eff} at 290K was found to be

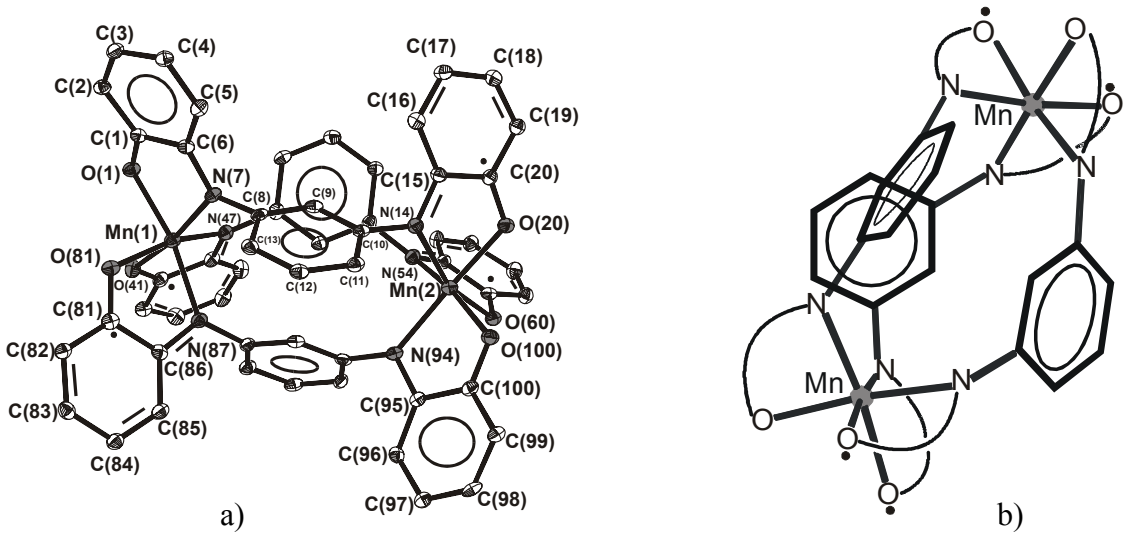

Figure 3.17 :- a) Crystal Structure of **16**. The tert-butyl groups has been removed for clarity. b) A view of **16** highlighting the coordination sphere around the two Mn(IV) centers. The tetradentate ligand L^3 is denoted by the donor atoms and the meta-phenylene spacer.

Table 3.10 :- *Selected bond distances (Å) and bond angles (degree) of **16**.*

Mn(1)-O(1)	1.884(3)	C(15)-C(20)	1.426(6)
Mn(1)-O(41)	1.933(3)	C(16)-C(17)	1.368(6)
Mn(1)-O(81)	1.967(3)	C(17)-C(18)	1.427(6)
Mn(2)-O(100)	1.905(3)	C(18)-C(19)	1.382(6)
Mn(2)-O(20)	1.921(3)	C(19)-C(20)	1.410(6)
Mn(2)-O(60)	1.999(3)	O(41)-C(41)	1.310(5)
Mn(1)-N(7)	1.936(3)	C(41)-C(42)	1.414(6)
Mn(1)-N(47)	1.959(3)	C(41)-C(46)	1.427(6)
Mn(1)-N(87)	1.972(3)	C(42)-C(43)	1.383(5)
Mn(2)-N(94)	1.933(3)	C(42)-C(61)	1.535(6)
Mn(2)-N(14)	1.975(3)	C(43)-C(44)	1.418(6)
Mn(2)-N(54)	1.988(3)	C(44)-C(45)	1.369(6)
O(1)-C(1)	1.323(5)	C(44)-C(65)	1.537(6)
C(6)-N(7)	1.381(5)	C(45)-C(46)	1.414(6)
N(7)-C(8)	1.427(5)	C(46)-N(47)	1.360(5)
C(1)-C(2)	1.415(5)	N(47)-C(48)	1.438(5)
C(1)-C(6)	1.423(6)	C(52)-N(54)	1.440(5)
C(2)-C(3)	1.395(6)	N(54)-C(55)	1.343(5)
C(3)-C(4)	1.410(6)	C(55)-C(56)	1.415(5)
C(4)-C(5)	1.385(6)	C(55)-C(60)	1.445(5)
C(5)-C(6)	1.397(6)	C(56)-C(57)	1.355(5)
O(20)-C(20)	1.318(5)	C(57)-C(58)	1.429(5)
C(12)-N(14)	1.436(5)	C(58)-C(59)	1.367(6)
N(14)-C(15)	1.359(5)	C(59)-C(60)	1.421(6)
C(15)-C(16)	1.406(6)	O(60)-C(60)	1.294(4)

Mn……Mn 6.762

O(1)-Mn(1)-O(41)	87.32(11)	N(94)-Mn(2)-O(60)	95.12(12)
O(1)-Mn(1)-N(7)	82.68(13)	N(14)-Mn(2)-O(60)	168.85(12)
O(41)-Mn(1)-N(7)	169.33(12)	N(54)-Mn(2)-O(60)	78.52(12)
O(1)-Mn(1)-N(47)	90.04(12)	C(1)-O(1)-Mn(1)	113.4(2)
O(41)-Mn(1)-N(47)	81.65(13)	C(6)-N(7)-C(8)	119.4(3)
N(7)-Mn(1)-N(47)	94.59(14)	C(6)-N(7)-Mn(1)	111.7(3)
O(1)-Mn(1)-O(81)	89.69(11)	C(8)-N(7)-Mn(1)	126.4(2)
O(41)-Mn(1)-O(81)	85.84(11)	C(15)-N(14)-C(12)	119.2(3)
N(7)-Mn(1)-O(81)	97.78(12)	C(15)-N(14)-Mn(2)	110.3(3)
N(47)-Mn(1)-O(81)	167.49(13)	C(12)-N(14)-Mn(2)	128.2(3)
O(1)-Mn(1)-N(87)	169.30(13)	C(20)-O(20)-Mn(2)	111.9(2)
O(41)-Mn(1)-N(87)	90.32(12)	C(41)-O(41)-Mn(1)	113.8(2)
N(7)-Mn(1)-N(87)	100.20(13)	C(46)-N(47)-C(48)	118.7(3)
N(47)-Mn(1)-N(87)	99.95(13)	C(46)-N(47)-Mn(1)	112.0(3)
O(81)-Mn(1)-N(87)	79.73(12)	C(48)-N(47)-Mn(1)	128.4(3)
O(100)-Mn(2)-O(20)	84.45(11)	C(55)-N(54)-C(52)	116.6(3)
O(100)-Mn(2)-N(94)	81.86(13)	C(55)-N(54)-Mn(2)	115.3(2)
O(20)-Mn(2)-N(94)	166.03(13)	C(52)-N(54)-Mn(2)	127.7(2)
O(100)-Mn(2)-N(14)	90.69(12)	C(60)-O(60)-Mn(2)	115.8(2)
O(20)-Mn(2)-N(14)	81.85(13)	C(81)-O(81)-Mn(1)	114.4(2)
N(94)-Mn(2)-N(14)	95.53(13)	C(86)-N(87)-C(88)	118.9(3)
O(100)-Mn(2)-N(54)	171.92(12)	C(86)-N(87)-Mn(1)	114.5(3)
O(20)-Mn(2)-N(54)	92.10(12)	C(88)-N(87)-Mn(1)	125.9(2)
N(94)-Mn(2)-N(54)	101.83(13)	C(95)-N(94)-C(92)	119.4(3)
N(14)-Mn(2)-N(54)	96.06(13)	C(95)-N(94)-Mn(2)	112.3(3)
O(100)-Mn(2)-O(60)	94.06(11)	C(92)-N(94)-Mn(2)	125.8(2)
O(20)-Mn(2)-O(60)	88.58(11)	C(100)-O(100)-Mn(2)	113.6(2)

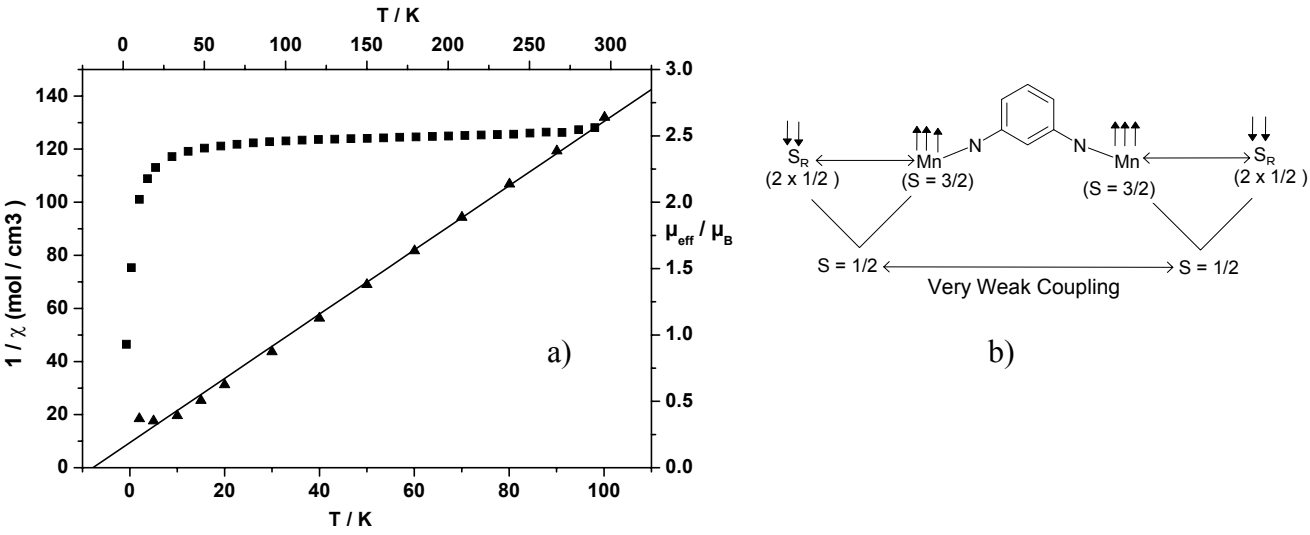

Figure 3.18 :-(a) Magnetic data of **16**. Filled squares shows the μ_{eff} value from 2-290 K and filled triangles denotes $1/\chi$ value from 2-100K. b) Coupling scheme for **16**.

$2.56\mu_B$ which decreases rather slowly till 40 K (2.41 μ_B). A monotonous decrease was then observed till 2K (0.93 μ_B). As seen in **15**, coupling between the two radical centers (S=½) and the metal center is antiferromagnetic. For **16** this also holds true. The two radicals (S = ½) are strongly antiferromagnetically coupled with the electrons of the Mn(IV) ion (S = $^3/_2$) which leaves a residual spin of S = ½ in each part of the complex [Figure 3.18(b)]. The values of μ_{eff} shows that the coupling between these two parts are weak. This data can be simulated with coupling constants (J) between the two S = ½ centers ranging from +5 to –5 cm^{-1} but with a high Theta-Weiss (θ) parameter. The presence of θ can be justified by plotting a $1/\chi$ (χ is the molar susceptibility) vs. Temperature [Figure 3.18(a) as triangle] till 100K. A linear regression fit (bold line) shows that the line makes an intercept at T = - 7.9K i.e. – 5.53 cm^{-1}. This value indicated that the intermolecular interactions exceeds the intramolecular interactions. From the nature of the curve it is probable that coupling between that coupling between the two parts are weakly anti-ferromagnetic. The most plausible reason for antiferromagnetism between the two centers is the non-orthogonal mixing between the d(π) orbitals of the Mn(IV) center with that of the p(π) orbitals of the donor atoms [as seen for the dicopper complex (**12**)].

X-band EPR spectrum of a dichloromethane solution of **16** at 10K in parallel mode is shown in Figure 3.19. The spectrum consists of a broad signal centered at g = 2.0 and a weak 11-line hyperfine signal at g = 4.05. The spectrum needs thorough study and rigorous calculation for simulation.

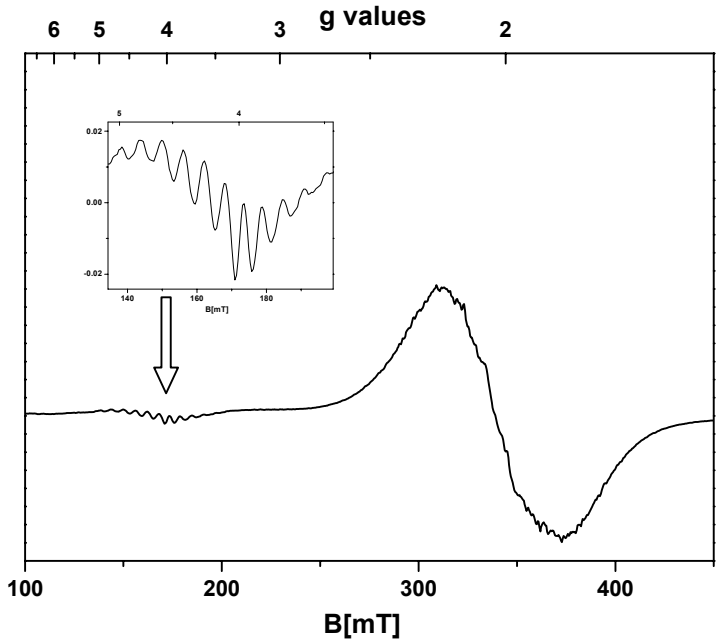

Figure 3.19 :- X-band EPR spectra at 10K of **16**.

Cyclic voltammetry and square wave voltammetry at 50mV/sec and 20Hz., respectively in dichloromethane in the presence of 0.1M $TBAPF_6$ shows waves which are similar to that of the dicopper complex (**12**). Four out of six peaks are reversible and two are irreversible as observed from the variation of scan rate [Figure 3.20(a), Table 3.11]. A broad irreversible peak [not shown] at –1.632V is observed and is probably due to the Mn centered reduction. All the peaks are a single-electron transfer process and that occurring at – 0.12V

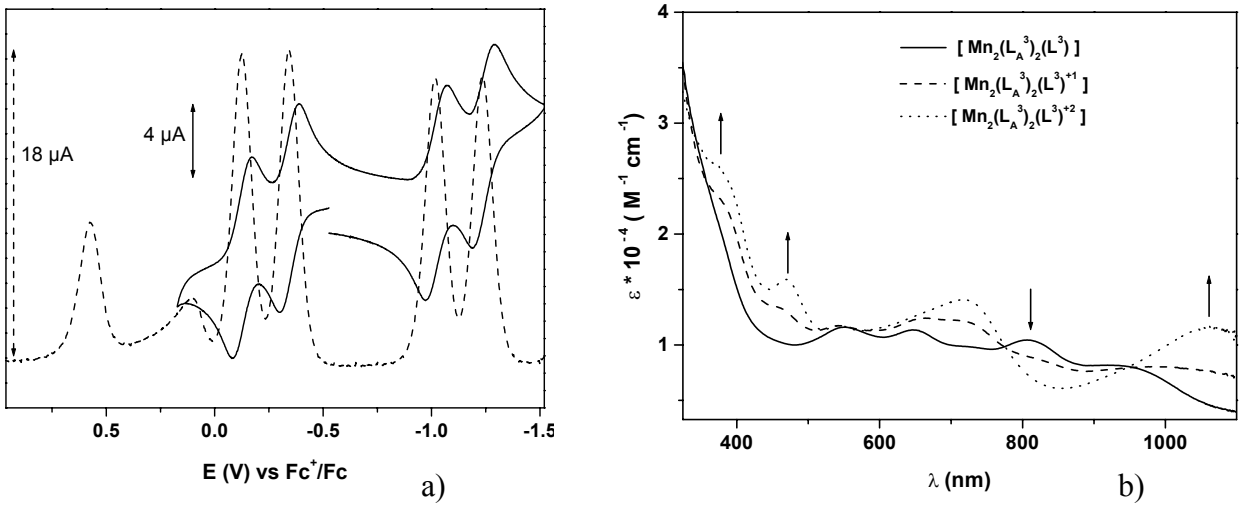

Figure 3.20 :- a) Cyclic (bold line) and square wave voltammogram (dotted line) of **16**.
b) Electronic spectra of **16** (bold line) and its oxidized forms.

and –0.341V corresponds to the oxidation of the ligand to the quinoid form; the peaks observed at –1.019V and –1.234V are due to the reduction of the ligand to the monoanionic and dianionic form of the ligand. These processes has been confirmed from coulometry. The quasi-reversible peaks at +0.101V and +0.575V can be tentatively assigned to the oxidation of ligand but due to its irreversibility in the time scale of coulometry, it was not studied further. The different redox processes are

$$[Mn_2(L^3)^{+2}(L_A^3)_2] \xleftarrow{-1e^-} [Mn_2(L^3)^{+1}(L_A^3)_2] \xleftarrow{-1e^-} [Mn_2(L^3)(L_A^3)_2] \xrightarrow{+1e^-} [Mn_2(L^3)^{-1}(L_A^3)_2] \xrightarrow{+1e^-} [Mn_2(L^3)^{-2}(L_A^3)_2]$$

Table 3.11 :- *Redox potentials (V) for **16** vs. Fc^+/Fc.*

Compound	$E_{½}$ (Oxidation)				$E_{½}$ (Reduction)		
16	+0.575 (Irreversible)	+0.101 (Irreversible)	- 0.120 (Reversible)	- 0.341 (Reversible)	-1.019 (Reversible)	-1.234 (Reversible)	-1.632 (irreversible)

Spectroelectrochemistry of this complex was performed at –25°C in the presence of 0.2M $TBAPF_6$. The electronic spectrum shows a number of waves above 450nm with maximums at 550 nm (ε=11,880 M^{-1} cm^{-1}), 648 nm (ε=11,500 $M^{-1}cm^{-1}$), 807 nm (ε=10,700 $M^{-1}cm^{-1}$) and a shoulder peak at 953nm (ε=8430 $M^{-1}cm^{-1}$) (bold line in Figure 3.20(b)] , all arising due to the strong intra-ligand π-π* transitions. Upon two electron oxidation, these waves disappear and a single maxima is generated at 720nm along with the development of a peak at 420nm, characteristic for the formation of the quinoid form of the ligand.

$Co^{III}_2L^4_3$ (17)

The neutral complex $Co_2L^3_3$ (**17**) crystallizes from a dichloromethane/acetonitrile solution as deep brown crystals. The structure [Figure 3.21] consists of two cobalt atoms in a distorted octahedral geometry with the oxygen and nitrogen atoms. The six short Co-O distance at 1.893Å together with short Co-N distance at 1.923Å shows that the oxidation state of cobalt is (+III) and low spin. Here again, the ligand is deprotonated as evidenced from the planarity of the nitrogen atom. All the tert-butyl substituted phenyl rings has lost its aromaticity with the formation of short (1.387Å), a long (1.444 Å), and a short (1.364 Å) together with three long C-C bonds are observed. The average C-O and the average C-N (N,O-attached to the tert-butyl substituted phenyl rings) bond distances are 1.303Å and 1.346Å which clearly shows that the tert-butyl substituted phenyl rings are in iminobenzosemiquinone form. Thus, the molecule consists of **six** iminobenzosemiquinone

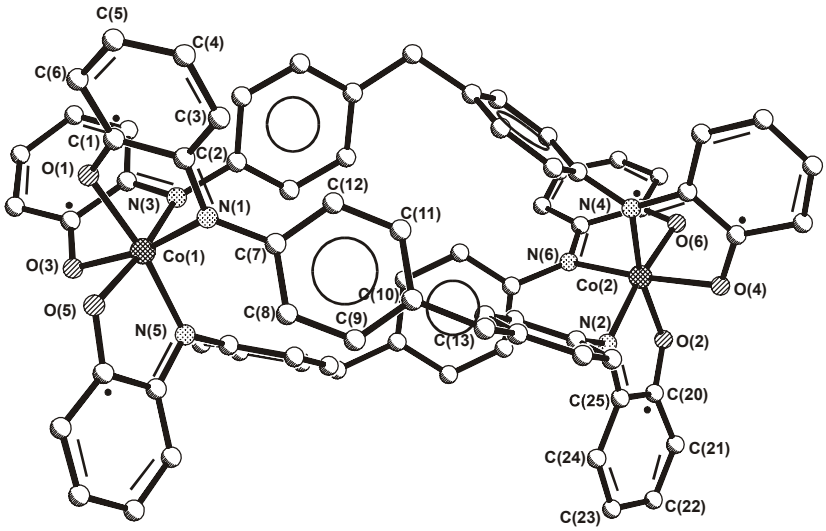

Figure 3.21 :- Molecular structure of **17**. Tert-butyl groups are omitted for clarity.

radicals. Selected bond distances (Å) and bond angles (degree) is given in Table 3.12.

Magnetic data of a polycrystalline sample of **17** is shown in Figure 3.22 (open circle). The value of μ_{eff} at 290K (4.51 μ_B) increases with the decrease in temperature and reaches a maximum at 5.07 μ_B at 30K whereupon it decreases till 4.80 μ_B at 2K. This indicates that an overall ferromagnetic coupling occurs within the molecule. In order to simulate this data, simplification is needed. The value of the magnetic moment at 290K is higher than that of six non-coupled S=½ center (4.24 μ_B) and is due to the presence of temperature independent paramagnetism (TIP) for Co^{III} ion. The value at 30K is however lower than that observed for two uncoupled S = $^3/_2$ spin states (5.24 μ_B) and is probably due to Theta-Weiss parameter (θ) which accounts for the *inter*molecular interactions. Thus, the magnetic data of this molecule can be simulated by calculating the μ_{eff} value for each Co^{III} center. This can be done by dividing the molecular weight and the diamagnetic susceptibility by two. The resultant curve (closed circle) is shown in Figure 3.22 (a). This data can be simulated by using a single coupling constant value between the three iminosemiquinone radicals in each part of the complex and no-coupling between the two parts of the ligand. The presence of a non-conjugated sp^3 carbon atom as a spacer between the two phenyl rings implies that interactions through spin polarization is not possible. Furthermore, the two Co^{III} are at a distance of 11.319 Å which obliterates the possibility of any coupling between the two parts.

Table 3.12 :- *Selected bond distances (Å) and bond angles (degree) of **17**.*

Co(1)-O(1)	1.882(6)	N(6)-C(117)	1.403(10)
Co(1)-O(5)	1.891(5)	O(1)-C(1)	1.293(10)
Co(1)-O(3)	1.903(6)	O(2)-C(21)	1.295(9)
Co(1)-N(3)	1.910(7)	O(3)-C(51)	1.295(9)
Co(1)-N(5)	1.912(7)	O(4)-C(71)	1.309(9)
Co(1)-N(1)	1.928(7)	O(5)-C(101)	1.323(10)
Co(2)-O(6)	1.891(6)	O(6)-C(71)	1.295(10)
Co(2)-O(2)	1.895(6)	C(1)-C(6)	1.410(11)
Co(2)-O(4)	1.900(6)	C(1)-C(2)	1.451(11)
Co(2)-N(2)	1.917(7)	C(2)-C(3)	1.413(11)
Co(2)-N(6)	1.932(7)	C(3)-C(4)	1.382(11)
Co(2)-N(4)	1.943(7)	C(4)-C(5)	1.392(11)
N(1)-C(2)	1.364(10)	C(4)-C(26)	1.513(12)
N(1)-C(7)	1.417(10)	C(5)-C(6)	1.370(12)
N(2)-C(20)	1.337(9)	C(20)-C(21)	1.409(11)
N(2)-C(17)	1.430(10)	C(20)-C(25)	1.444(11)
N(3)-C(52)	1.353(10)	C(21)-C(22)	1.411(11)
N(3)-C(57)	1.429(10)	C(22)-C(23)	1.387(11)
N(4)-C(70)	1.334(10)	C(22)-C(34)	1.535(11)
N(4)-C(67)	1.408(10)	C(23)-C(24)	1.433(11)
N(5)-C(102)	1.343(10)	C(24)-C(25)	1.364(11)
N(5)-C(107)	1.463(10)	C(24)-C(38)	1.534(12)
N(6)-C(120)	1.345(10)		

Co(1) ….. Co(2) 11.319

O(1)-Co(1)-O(5)	87.5(3)	O(4)-Co(2)-N(4)	83.3(3)
O(1)-Co(1)-O(3)	85.3(2)	N(2)-Co(2)-N(4)	99.0(3)
O(5)-Co(1)-O(3)	88.9(2)	N(6)-Co(2)-N(4)	97.9(3)
O(1)-Co(1)-N(3)	88.1(3)	C(2)-N(1)-C(7)	119.3(7)
O(5)-Co(1)-N(3)	171.9(3)	C(2)-N(1)-Co(1)	113.4(6)
O(3)-Co(1)-N(3)	84.0(3)	C(7)-N(1)-Co(1)	127.3(6)
O(1)-Co(1)-N(5)	170.6(3)	C(20)-N(2)-C(17)	120.6(7)
O(5)-Co(1)-N(5)	83.7(3)	C(20)-N(2)-Co(2)	111.7(5)
O(3)-Co(1)-N(5)	91.4(3)	C(17)-N(2)-Co(2)	127.4(6)
N(3)-Co(1)-N(5)	100.3(3)	C(52)-N(3)-C(57)	119.5(7)
O(1)-Co(1)-N(1)	84.0(3)	C(52)-N(3)-Co(1)	108.8(6)
O(5)-Co(1)-N(1)	91.4(3)	C(57)-N(3)-Co(1)	129.0(6)
O(3)-Co(1)-N(1)	169.3(3)	C(70)-N(4)-C(67)	118.7(7)
N(3)-Co(1)-N(1)	94.8(3)	C(70)-N(4)-Co(2)	111.0(6)
N(5)-Co(1)-N(1)	99.3(3)	C(67)-N(4)-Co(2)	130.2(6)
O(6)-Co(2)-O(2)	87.4(3)	C(102)-N(5)-C(107)	119.2(7)
O(6)-Co(2)-O(4)	87.6(3)	C(102)-N(5)-Co(1)	112.2(6)
O(2)-Co(2)-O(4)	86.8(2)	C(107)-N(5)-Co(1)	126.5(6)
O(6)-Co(2)-N(2)	171.3(3)	C(120)-N(6)-C(117)	120.0(8)
O(2)-Co(2)-N(2)	84.0(3)	C(120)-N(6)-Co(2)	111.8(6)
O(4)-Co(2)-N(2)	90.7(3)	C(117)-N(6)-Co(2)	128.2(6)
O(6)-Co(2)-N(6)	84.3(3)	C(1)-O(1)-Co(1)	113.4(5)
O(2)-Co(2)-N(6)	91.4(2)	C(21)-O(2)-Co(2)	112.5(5)
O(4)-Co(2)-N(6)	171.8(3)	C(51)-O(3)-Co(1)	109.6(5)
N(2)-Co(2)-N(6)	97.1(3)	C(71)-O(4)-Co(2)	111.1(5)
O(6)-Co(2)-N(4)	89.3(3)	C(101)-O(5)-Co(1)	113.0(5)
O(2)-Co(2)-N(4)	169.8(3)	C(71)-O(6)-Co(2)	113.0(5)

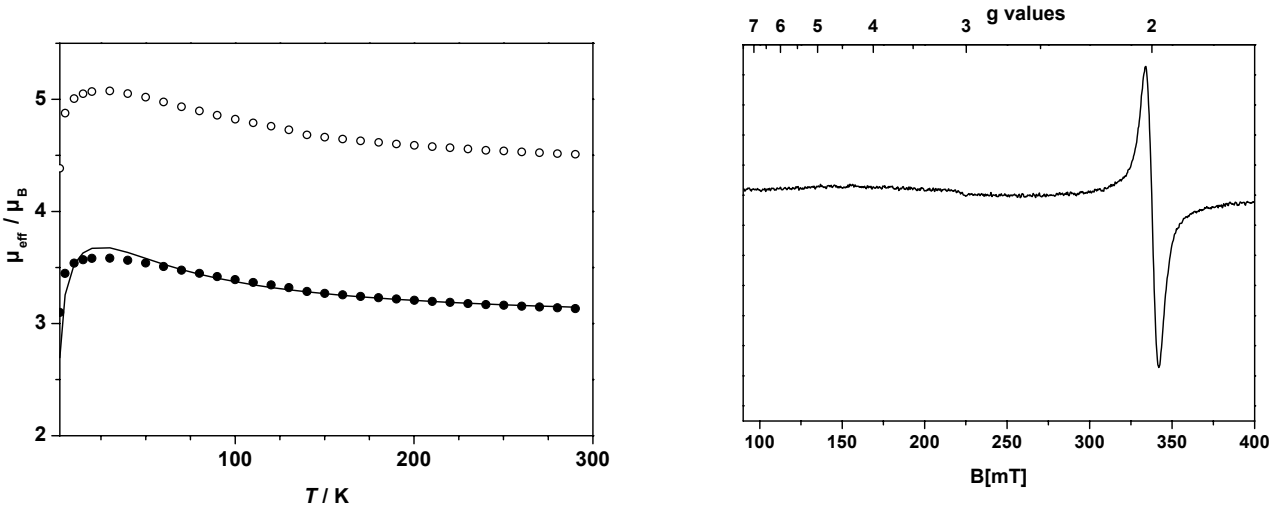

a) b)

Figure 3.22:- a) Magnetic susceptibility data of **17**. The open circle represents the value of μ_{eff} for the total molecule. The closed circle and the bold line represents the calculated and simulated μ_{eff} value for a single Co^{III} center. b) X-band EPR spectrum of **17** at 9.6K.

From the nature of the susceptibility data, it is clear that ferromagnetic interactions is operating between the three radicals in each part of the ligand. When each cobalt center is considered, the dihedral angles made between the two planes (each plane consisting the tert-butyl substituted phenyl rings) O(1) [C(1)-C(2)-C(3)-C(4)-C(5)-C(6)] - O(3)[C(51)-C(52)-C(53)-C(54)-C(55)-C(56)] is 106.6°; that between O(1)[C(1)-C(2)-C(3)-C(4)-C(5)-C(6)]-O(5)[C(101)-C(102)-C(103)-C(104-C(105)-C(106)] and O(3)[C(51)-C(52)-C(53)-C(54)-C(55)-C(56)] - O(5)[C(101)-C(102)-C(103)-C(104-C(105)-C(106)] being 103.4° and 111.4°, respectively. For the other cobalt center, the dihedral angles made between the two planes (each plane consisting the tert-butyl substituted phenyl rings) O(2) [C(21)-C(22)-C(23)-C(24)-C(25)-C(26)] - O(4)[C(71)-C(72)-C(73)-C(74)-C(75)-C(76)] is 114.5°; that between O(2)[C(21)-C(22)-C(23)-C(24)-C(25)-C(26)] - O(6)[C(120)-C(121)-C(122)-C(123-C(124)-C(125)] and O(4)[C(71)-C(72)-C(73)-C(74)-C(75)-C(76)] - O(6)[C(120)-C(121)-C(122)-C(123-C(124)-C(125)] being 100.8° and 93.9°, respectively. The angles do not deviate widely from orthogonality and therefore the interaction between the radicals are taken as ferromagnetic. Therefore, the coupling scheme for **14** [Figure 3.11(a)] can be used in simulating this data. The values obtained are J_1 = +22.0, J_2=0, g =2.0 and a Theta-Weiss parameter (θ) of –2.0 K. where J_1 describes the coupling constant between the radicals at each part and J_2, the interactions between the radicals of each ligand. Therefore the ground state

consists of two quartets (S = $^3/_2$, $^3/_2$) arising from the ferromagnetic coupling of the radicals from each part of the complex.

The X-band EPR spectra of a frozen dichloromethane solution of **17** was measured at 9.6K. Only a sharp signal is observed at g = 2 without any hyperfine structures [Figure 3.22(b)], indicating a very small zerofield splitting for the ground state.

Electrochemistry (cyclic and square wave voltammetry) was carried out with **17**. The peaks consists of three broad waves out of which two, between +0.5V and –0.75V, are reversible and the other (-1.34 V) irreversible [Figure 3.23(a),Table 3.13]. All the reversible redox processes consist of one-electron oxidation as observed from coulometry measurements. The peak at –1.34 V is tentatively assigned to the reduction of the Co^{III} center. The value of the $E_{1/2}$ (oxidation) are similar to that of **14** and therefore can be inferred to the oxidation of the radical centers. Spectroelectrochemistry of **17** also supports this assignment. The electronic spectra of **17** [Figure 3.23(b) (bold line)] shows a similar pattern to that of **14** with maximas at 477nm(ε = 10,765 $M^{-1}cm^{-1}$), 701nm(ε = 5,773 M^{-1} cm^{-1}), 782nm(ε = 6564 $M^{-1}cm^{-1}$) and 857nm(ε = 10,765 $M^{-1}cm^{-1}$). Upon four electron oxidation, the peak corresponding to 477nm increases in intensity along with the decrease in the peak maximas above 650nm, signifying the formation of iminobenzoquinone form of the ligand.

Table 3.13 :- *Redox potentials (V) for **17** vs. Fc^+/Fc.*

Compound	E ½ (Oxidation)		E ½ (Reduction)
17	+ 0.085 (reversible)	- 0.37 (reversible)	-1.34 (irreversible)

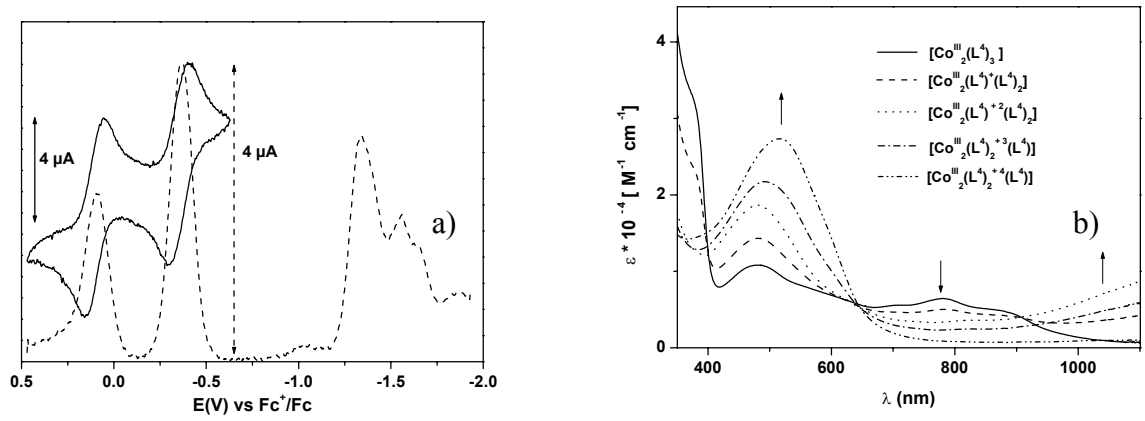

Figure 3.23 :- (a) Cyclic (bold line) and Square Wave voltammetry (dotted line) of **17**.
(b)Electronic spectra of **17** and its oxidized forms.

A novel series of dinuclear (iminosemiquinone)metal complexes is described that provides a suitable basis for further research in a systematic way, especially on the metal-radical interactions. The concept of *spin polarization* was used in an attempt to induce ferromagnetic coupling between the dinulceating centers or between the radical centers.

References :-

1 (a) C. G. Pierpont, C. W. Lange, *Prog. Inorg. Chem.* **1994**, 41, 331. (b) A. Y. Girgis, A. L. Balch, *Inorg. Chem.* **1975**, 14, 2724. (c) S. K. Larsen, C. G. Pierpont, *J. Am. Chem. Soc.* **1988**, 110, 1827. (d) Simpson, C. L.; Boone, S. R.; Pierpont, C. G. *Inorg. Chem.* **1989**, *28*, 4379. (e) A. Caneschi, A. Dei, D. Gatteschi, *J. Chem. Soc., Chem. Commun.* **1992**, 630. (f) S. Bruni, A. Caneschi, F. Cariati, C. Delfs, A. Dei, D. Gatteschi, *J. Am. Chem. Soc.* **1994**, 116, 1388. (g) G. Speier, J. Csihony, A. M. Whalen, C. G. Pierpont, *Inorg. Chem.* **1996**, 35, 3519. (h) B. R. McGarvey, A. Ozarowski, Z. Tian, D. G. Tuck, *Can. J. Chem.* **1995**, 73, 1213. (i) A. Bencini, I. Ciofini, E. Giannasi, C. A. Daul, K. Doclo, *Inorg. Chem.* **1998**, 37, 3719. (j) O.-S. Jung, D. H. Jo, Y. A. Lee, Y. S. Sohn, C. G. Pierpont, *Inorg. Chem.* **1998**, 37, 5875. k) P. Chaudhuri, M. Hess, K. Hildenbrand, E. Bill, T. Weyhermüller, K. Wieghardt, *Inorg. Chem.* **1999,** 38*,* 2781.

2. C. G. Pierpont, *Coord. Chem. Rev.,* **2001**, 216, 99 and references therein.

3 (a) *Magnetic Properties of Organic Materials*, ed. P. M. Lahti, Marcel Dekker, New York, 1999; (b) *Molecular Magnetism: New Magnetic Materials*, ed. K. Itoh, M. Kinoshita and Gordon & Breach, Amsterdam, The Netherlands, 2000; (c) H. Iwamura, K. Inoue , T. Hayamizu, *Pure and Applied Chemistry,* **1996**, 68, 243; (d) O. Kahn, *Molecular Magnetism*, VCH, New York, 1993; (e) D. A. Dougherty, *Acc. Chem. Res.,* **1991**, 24, 88; (f) H. Iwamura , N. Koga, *Acc. Chem. Res.,* **1993**, 26, 346; (g) A. Racja, *Chem. Rev.,* **1994**, 94, 871.

4) (a) C. N. Verani, S. Gallert, E. Bill, T. Weyhermüller, K. Wieghardt, P. Chaudhuri, *Chem. Commun.,***1999**, 1747; (b)P. Chaudhuri, C. N. Verani, E. Bill, E. Bothe, T. Weyhermüller ,K. Wieghardt, *J. Am. Chem. Soc.,* **2001**, 123, 2213; (c) H. Chun, C. N. Verani, P. Chaudhuri, E. Bothe, E. Bill, T. Weyhermüller , K. Wieghardt, *Inorg. Chem.,***2001**, 40, 4157. (d) H. Chun, T. Weyhermüller, E. Bill, K. Wieghardt, *Angew. Chem.,Int. Ed.*, **2001**, 40, 2489. (e)H. Chun, P. Chaudhuri, T. Weyhermüller, K. Wieghardt, *Inorg. Chem.*, **2002**, 41, 790. (f)X. Sun, H. Chun, K. Hildenbrand, E. Bothe, T. Weyhermüller,F. Neese, K. Wieghardt, *Inorg. Chem.*, **2002**, 41, 4295.(g) H. Chun, E. Bill, E. Bothe, T. Weyhermüller ,K. Wieghardt, *Inorg. Chem.*, **2002**, 41, 5091.h) K. S. Min, T. Weyhermüller ,K. Wieghardt, *Dalton Trans.,* **2003**, 1126. (i) C. N. Verani, Dissertation, Bochum, 2001.

5) a)S. Mukherjee, E. Rentschler, T. Weyhermüller, K. Wieghardt , P. Chaudhuri, *Chem. Commun.,***2003**, 1828. b) A. Dei, D. Gatteschi, C. Sangregorio, L. Sorace, M. G. F. Vaz, *Inorg. Chem.* **2003**, 42, 1701. c) A. Dei, D. Gatteschi, C. Sangregorio, L. Sorace, Vaz, M. G. F. *Chem. Phys. Lett*. **2003**, 368, 162.

6) (a)D. R. Corbin, L. C. Francesconi, D. N. Hendrikson, G. D. Stucky; *Inorg. Chem.* **1979**, 18,3069. (b) L. C. Francesconi, D. R. Corbin, D. N. Hendrickson, G. D. Stucky, *Inorg. Chem.* **1979**, 18, 3074.

7) C. W. Lange, B. J. Conklin, C. G. Pierpont ,*Inorg. Chem*. **1994**, 33, 1276.

Chapter 4

Mn^{IV} COMPLEXES WITH IMINO-BENZOSEMIQUINONE LIGANDS; SYNTHESIS, CHARACTERIZATION AND REACTIVITY STUDY

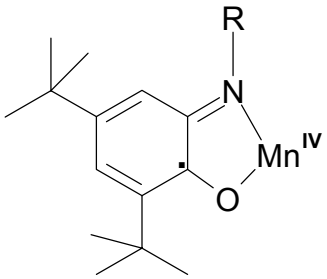

4.1 INTRODUCTION

Out of the several types of metalloenzymes in biochemistry, the oxidase enzymes have been widely studied. The role played by the metal center has always attracted interest and has inspired bioinorganic chemists for synthesizing structural as well as functional models for such type of metalloenzymes [Chapter 1].

One interesting oxidase enzyme is the dicopper containing catechol oxidase [E.C. 1.10.3.1] which catalyzes the two-electron oxidation of catechols to quinones [1]. The different states and the mechanism of catechol oxidase[1] activity are given in Figure 4.1. The crystal structure of catechol oxidase from *I. batatas* (sweet potato) reveals that the two copper centers, in its active form, are at a distance of 3.8 Å.

In order to mimic the structural and functional model of this enzyme, a number of dinuclear copper complexes have been reported. Intensive studies were undertaken so as to elucidate the relationship between structure and reactivity of the natural active sites and to develop new complexes with useful catalytic performance[2].

In the previous chapter, the dinucleating ligand [H_4L^3] along with different transition metal complexes has been described. In an attempt to mimic the function of catechol oxidase, the dinuclear copper complex (**12**) was used as a possible catalyst with 3,5-di-tert-butylcatechol as substrate. 3,5-di-tert-butyl-o-benzoquinone was the expected oxidation

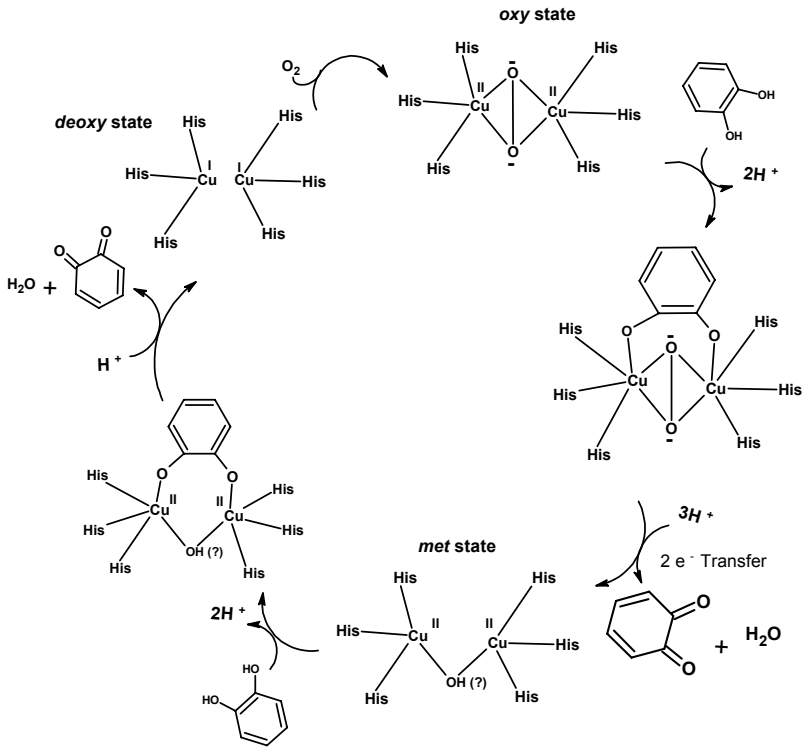

Figure 4.1 :- Catalytic cycle of catechol oxidase [1b].

product. That changing the metal center improves not only the yield but also the turnover number (TON) [expressed in mole product per mole catalyst] will be discussed in this chapter.

4.2 CATECHOL OXIDASE MODEL STUDIES

Among the different catechols used in catechol oxidase model studies, 3,5-di-tert-butylcatechol (3,5-DTBC) is the most widely used substrate due to its low redox potential for the quinone–catechol couple, which makes it easy to be oxidized to the corresponding quinone, 3,5-di-tertbutyl-o-benzoquinone (3,5-DTBQ), and its bulky substitutents which make further oxidation reactions such as ring opening slower. 3,5-DTBQ is considerably stable and has a strong absorption at 408 nm.

To evaluate quantitatively a significant activity, 5 x 10^{-6} mole of catalyst in 25 ml of dichloromethane was treated with 50 equivalents of 3,5-DTBC and stirred in air. It is to be noted that 3,5-DTBC alone does not undergo aerial oxidation. The products were analyzed by liquid chromatography. The retention time in liquid chromatography for 3,5-DTBC and 3,5-DTBQ was found to be 8.0 and 10.5 minutes, respectively, (column:- Luna-5 phenylhexyl; Eluant:- Methanol and Water in ratio 3:1, 0.8 ml/min) as observed from commercially available compound. It was found that for all the oxidative reactions involving 3,5-DTBC as the substrate, 3,5-DTBQ was the only oxidized product.

The dinuclear copper complex (**12**) was used as a catalyst for this oxidation. Stirring a dichloromethane solution of **12** in presence of 3,5-DTBC, in the ratio 1:50, gave at the end of 24 hours 15.6 % of 3,5-DTBQ. The other peaks observed in the liquid chromatography are the decomposed products of **12**, as observed from LC-MS coupling. The turnover number is therefore **eight.** This indicates that although the dicopper complex catalyzes the oxidation of 3,5-DTBC to 3,5-DTBQ, the poor TON obliterates it being a good catalyst for such type of oxidation. A probable reason is the long distance between the two copper centers (~ 6.8 Å). It is observed that several dinuclear copper complexes show catalytic activity if the distance between the two copper centers is around 5Å [3].

The involvement of manganese in biological process and its relevance to oxidation state study, coordination behavior and its role as biological catalyst interested the inorganic chemists in order to synthesize polynuclear high-valent manganese complexes. Several manganese complexes have been studied to demonstrate the mechanism of catalase, superoxide dismutases or photosytem II. The role of the phenoxyl radical during the catalysis process in PS II has also being studied [Chapter 1]. Compound **16**, a high-valent dimanganese

complex may be a suitable complex for catalyzing oxidation reactions. The substrate chosen was 3,5-DTBC for reasons mentioned above.

When **16** was dissolved in dichloromethane and 3,5-DTBC was added in the ratio 1:50, the dark brown color slowly changes, in presence of air, to yellow and then finally red. Analysis of this solution after 24 hours shows a 100 % conversion of 3,5-DTBC to 3,5-DTBQ i.e. the turnover number (TON) of this reaction is 50. On increasing the amount of 3,5-DTBC it was found that the TON increases and the maximum turnover reached after 24 hours is 500. This shows that this complex can act as a good catalyst in catalyzing the oxidation of 3,5-DTBC to 3,5-DTBQ in presence of oxygen. The dimanganese compound (**16**) acts as a much better catalyst than the dicopper complex (**12**), thus mimicking the function of catechol oxidase.[5]

Reaction kinetics was performed by observing the change in absorbance at 408 nm, which is characteristic of 3,5-DTBQ. In a typical reaction the catalyst was dissolved in dichloromethane and the substrate, 3,5-DTBC was added. 1ml from this solution was taken, diluted to 10ml with CH_2Cl_2 and the resultant electronic spectral change was observed in a 1cm cuvette. For calculation of rate constants, initial rate method was used and the velocity of the reaction was obtained by the slope of the tangent to the absorbance vs. time curve. This procedure was taken as standard for all the kinetic measurements.

The kinetic of the oxidative reaction at a constant catalyst concentration was investigated by using 2 x 10^{-7} mole of the catalyst (**16**) in dichloromethane (10ml after dilution) with variation of the substrate concentration from 2 x 10^{-6} to 20 x 10^{-6} moles. The electronic spectra for a catalyst to substrate ratio of 1:30 shows an increase in the intensity of the peak at 408 nm with time [Figure 4.2(a)]. The least square fit plot of the difference in absorbance (absorbance is directly proportional to concentration) vs. time (bold line) [Figure 4.2(b)] gives the velocity(r_0) for that particular catalyst to substrate concentration ratio. The different substrate concentration along with the rate constants are listed in Table 4.1. Plotting the velocity vs. the concentrations shows that the rate of the reaction is first order with respect to the substrate concentration. The best fit line (bold line, Figure 4.3) passes through the origin and the slope is 9.13 x 10^3 $mole^{-1}$ min^{-1}. This value is the rate constant of the reaction at a constant catalyst concentration (k_{sub}).

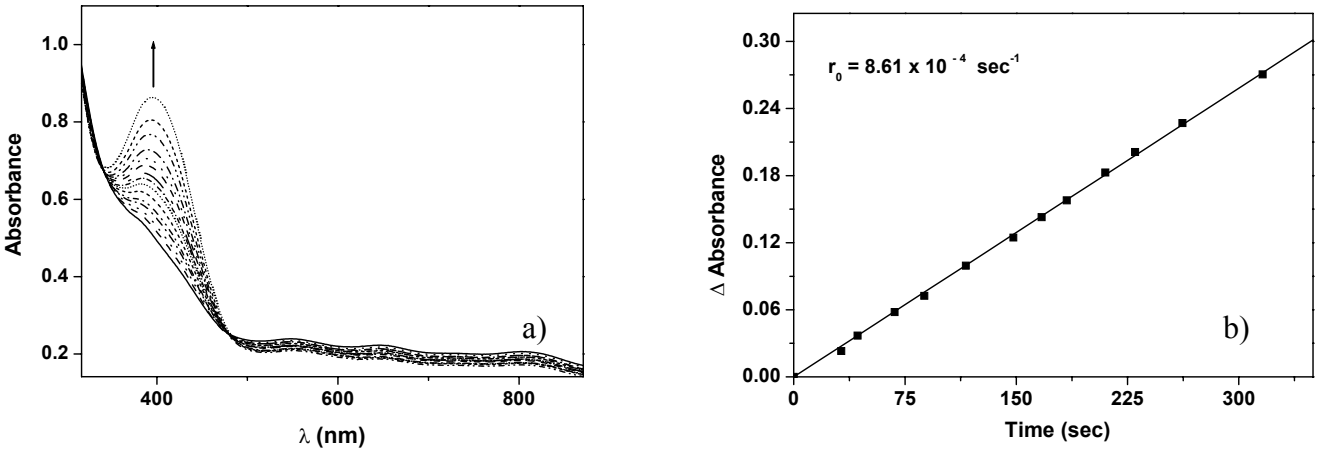

Figure 4.2 :- a) Change in the electronic spectra of **16** after the addition of 3,5-DTBC. b) Plot of the difference in absorbance vs. time for the catalyst to substrate concentration ratio 1:30.

For evaluating the rate constant at a constant substrate concentration, similar reactions were carried out with a constant substrate concentration (5 x 10^{-6} mole) and a varying catalyst concentration in dichloromethane. The different velocities(r_0') obtained [Table 4.2] were plotted against the catalyst concentration [Figure 4.4]. From the plot it is clear that the rate of the reaction is also first order with respect to the substrate concentration. The best fit line (bold line Figure 4.4) passes through the origin with a slope (k_{cat}) of 2.26 x10^5 $mole^{-1}$ min^{-1}.

[Substrate] x 10^6 (mole)	Rate (r_0) x 10^2 (min^{-1})
2	0.8
3.15	1.87
4	3.49
5	4.5
6	5.1
7.6	6
12	10.92
15	13.98
20.6	19.38

Table 4.1:-List of substrate concentration and corresponding rate.

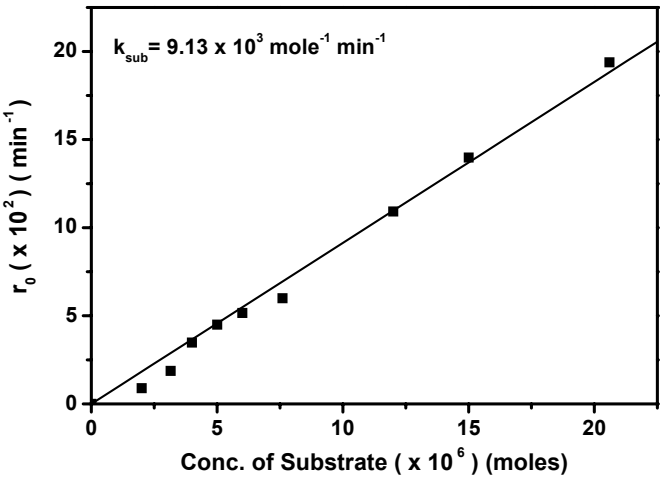

Figure 4.3:-Plot of substrate concentration vs. corresponding rate.

[Catalyst] x 10^6 (mole)	Rate(r_0') x 10^2 (min^{-1})
2.6	2.46
4	3.59
4.5	3.98
5	4.5
5.5	5.02

Table 4.2:-List of catalyst concentration and corresponding rate.

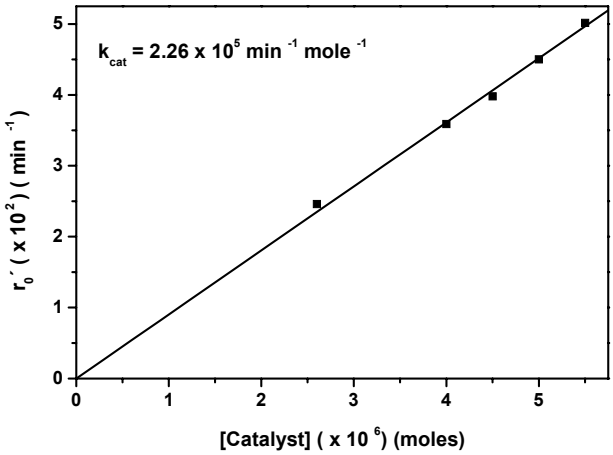

Figure 4.4:- Plot of catalyst concentration vs. corresponding rate.

Thus the evaluated rate law takes the form

Rate = k [Catalyst] [Substrate]

From the rate law, it is probable that each Mn^{IV} center of the dimer (**16)** is catalytically active. A reasonable way to prove this is to synthesize the monomeric Mn^{IV} form (**16***) with two iminobenzosemiquinone radicals and study the similar oxidation reaction. A series of Mn^{IV} compounds were prepared with this type of bidentate ligands, but substituted at the 3,5–position to the amine group, and reactivity with the similar substrate was studied.

The ligands $H_2L^{5\text{-}10}$ [Figure 4.5] were synthesized according to the same procedure used in synthesizing H_2L^5 and all the Mn(IV) complexes were prepared. The complexes were characterized by IR, Mass and EPR spectroscopy together with magnetic susceptibility measurements. From EPR and magnetic susceptibility measurements, it is clear that the oxidation state at the manganese center is +IV. Electrochemical data was also measured for all these compounds. Since these compounds are isostructural, the Mn(IV) complex with ligand H_2L^6 (**18**) has been structurally characterized and will be described in details in this

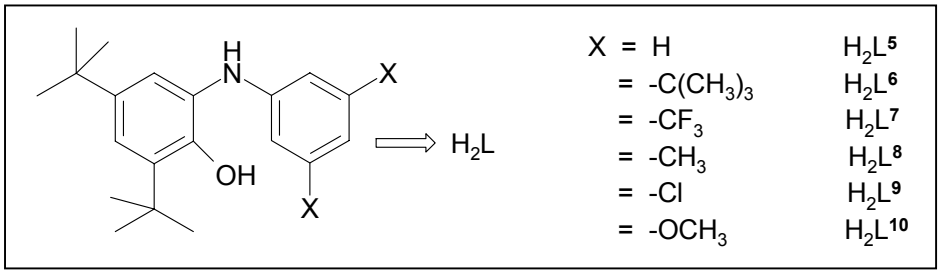

Figure 4.5 :- Ligands used in the synthesis of Mn(IV) complexes.

chapter. The Mn(IV) complex, using the ligand H_2L^5 (**16***) has already been reported.[4] Magnetic susceptibility measurements and EPR data for the complexes **19-23** are given in the Appendix section.

4.3 SYNTHESIS AND CHARACTERIZATION OF $Mn^{IV}(L_A^6)(L^6)_2$ (18)

When H_2L^6 is refluxed in air with "Manganese(III) Acetate" in methanol in the presence of tetrabutylammonium methoxide, a dark brown solution is obtained. On slow cooling, a microcystalline precipitate of **18** is obtained. This was recrystallized from a diethylether and methanol solution mixture. The compound shows the characteristic IR-peaks and EI-MS shows an m/z=1276, which corresponds to three fully deprotonated ligands with a manganese center. Selected IR peaks of H_2L^6 and **18** are given in Table 4.3.

	Characteristic IR peaks (cm^{-1})
H_2L^6	3339s,1598s,1361s,1233s,999m,774m,631b
18	1592w,1478m,1360m,1142b,756w,706w

Table 4.3 :- Characteristic IR bands for H_2L^6 and **18.**

Dark brown crystals afforded by diethylether-methanol solution is subjected to single crystal XRD studies. Selected metal-to-oxygen and metal-to-nitrogen bond lengths are summarized in Table 4.4. The geometrical features of the ligand are within an experimental error of ±0.015 Å identical to those shown in Figure 3.1 (Chapter 3). The neutral molecule in crystals of **18** [Figure 4.6] contains two *O*,*N*-coordinated *o*-iminobenzosemiquinonate(-) π radical ligands, $(L^6)^-$, as is clearly borne out by the observation that (i) both nitrogens are sp^2 hybridized and not protonated, (ii) the six-membered ring of the iminobenzosemiquinonate part displays the typical quinoid distortions, and (iii) the C-O and C-N bond lengths are short, approaching double bonds. The third ligand is *N*-deprotonated. The six C-C bonds of the amidophenolate ring are equidistant at 1.40 (0.009) Å, and the C-O and C-N distances at 1.330 (0.006) and 1.384 (0.006) Å are long. This ligand displays the characteristic features of an *O*,*N*-coordinated aromatic dianion, $(L^6\text{-}H)^{2-}$ [Figure 3.1 (Chapter3)]. If this assignment is correct, the central Mn ion must be ascribed to +IV (d^3) oxidation level. The observed Mn-O and Mn-N bond distances in **18** support this view; they are short (average Mn-O bond distance is 1.904Å, average Mn-N bond distance is 1.945Å) and the pseudooctahedral O_3N_3Mn polyhedron does not show any Jahn-Teller distortion .The crystal structure of **18** is in excellent agreement with the charge distribution of $[Mn^{IV}(L^6)_2(L^6\text{-}H)]$. Selected bond distances for **18** are given in Table 4.4.

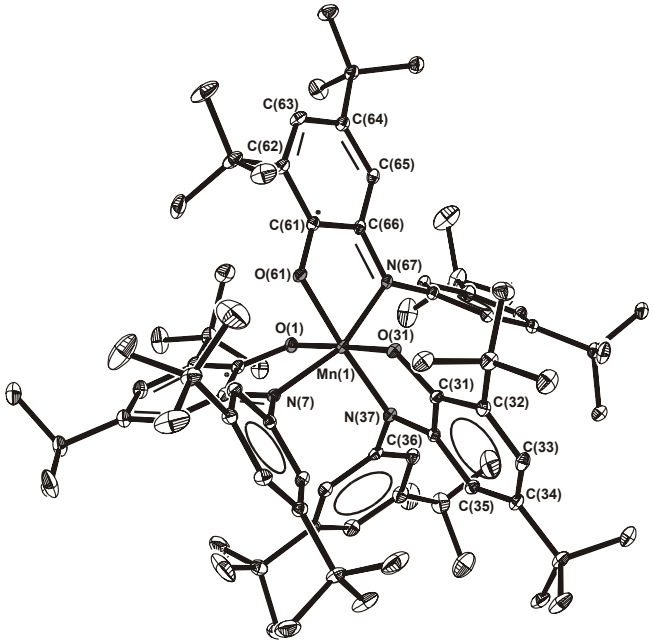

Figure 4.6 :- Crystal structure of **18**.

Table 4.4 :- *Selected bond distances (Å) and angles (degree) of **18***.

Mn(1)-O(31)	1.8676(13)	O(31)-Mn(1)-O(1)	178.12(6)
Mn(1)-O(1)	1.9050(13)	O(31)-Mn(1)-N(37)	83.45(6)
Mn(1)-N(37)	1.9189(16)	O(1)-Mn(1)-N(37)	96.27(6)
Mn(1)-O(61)	1.9394(13)	O(31)-Mn(1)-O(61)	89.43(6)
Mn(1)-N(7)	1.9522(16)	O(1)-Mn(1)-O(61)	90.87(6)
Mn(1)-N(67)	1.9664(17)	N(37)-Mn(1)-O(61)	172.84(6)
O(31)-C(31)	1.330(2)	O(31)-Mn(1)-N(7)	96.61(6)
C(31)-C(32)	1.412(3)	O(1)-Mn(1)-N(7)	81.56(6)
C(31)-C(36)	1.413(3)	N(37)-Mn(1)-N(7)	96.08(7)
C(32)-C(33)	1.390(3)	O(61)-Mn(1)-N(7)	85.44(6)
C(33)-C(34)	1.411(3)	O(31)-Mn(1)-N(67)	96.44(6)
C(34)-C(35)	1.385(3)	O(1)-Mn(1)-N(67)	85.44(6)
C(35)-C(36)	1.404(3)	N(37)-Mn(1)-N(67)	98.95(7)
C(36)-N(37)	1.384(2)	O(61)-Mn(1)-N(67)	81.07(6)
N(37)-C(38)	1.429(2)	N(7)-Mn(1)-N(67)	161.09(7)
C(61)-O(61)	1.297(2)	C(31)-O(31)-Mn(1)	115.33(12)
C(61)-C(62)	1.426(3)	C(36)-N(37)-C(38)	118.18(16)
C(61)-C(66)	1.441(3)	C(36)-N(37)-Mn(1)	113.00(12)
C(62)-C(63)	1.379(3)	C(38)-N(37)-Mn(1)	126.78(12)
C(63)-C(64)	1.424(3)	C(61)-O(61)-Mn(1)	114.57(12)
C(64)-C(65)	1.373(3)	C(66)-N(67)-C(68)	121.10(17)
C(65)-C(66)	1.414(3)	C(66)-N(67)-Mn(1)	113.12(12)
C(66)-N(67)	1.353(2)	C(68)-N(67)-Mn(1)	124.12(13)
N(67)-C(68)	1.422(2)		

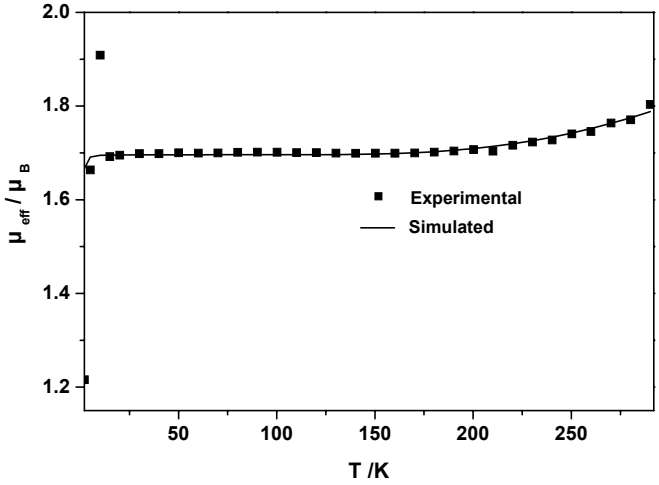

Figure 4.7:- Magnetic data of **18**.

The electronic ground state of **18** have been established from variable-temperature(2-290K) magnetic susceptibility measurements by using a SQUID magnetometer in an external magnetic field of 1.0 T. Figure 4.7 shows the temperature dependence of the magnetic moment, μ_{eff}, for **18**. On lowering the temperature, μ_{eff} of **18** decreases monotonically from 1.8 μ_B at 290 K to 1.7 μ_B at 15 K. This behavior indicates an S = ½ for **18**. As the overall magnetic behavior is dominated by much stronger antiferromagnetic interactions between ligand radicals and metal-based unpaired d-electrons, the decrease of μ_{eff} on lowering the temperature could well be fitted by a single coupling constant **J** [coupling between the radical center (S = ½) and Mn^{IV} center (S = $^3/_2$)] with **J'** [coupling between the radical centers (S = ½)] set to zero. Using the following parameters: $S_1 = S_3 = ½$, $S_2 = {}^3/_2$, g_1=2.0 (fixed), g_2=1.97 (fixed), J_{13} = 0 (fixed), J = -292 cm^{-1} mol^{-1}, a satisfactory fit was obtained (bold line, Figure 4.7). Hence, a strong antiferromagnetic coupling exists between the ligand radicals and the Mn^{IV} ion, similar to that observed for the Mn^{IV} complex with the ligand 2-anilino-4,6-ditertbutylphenol (**16***).[4]

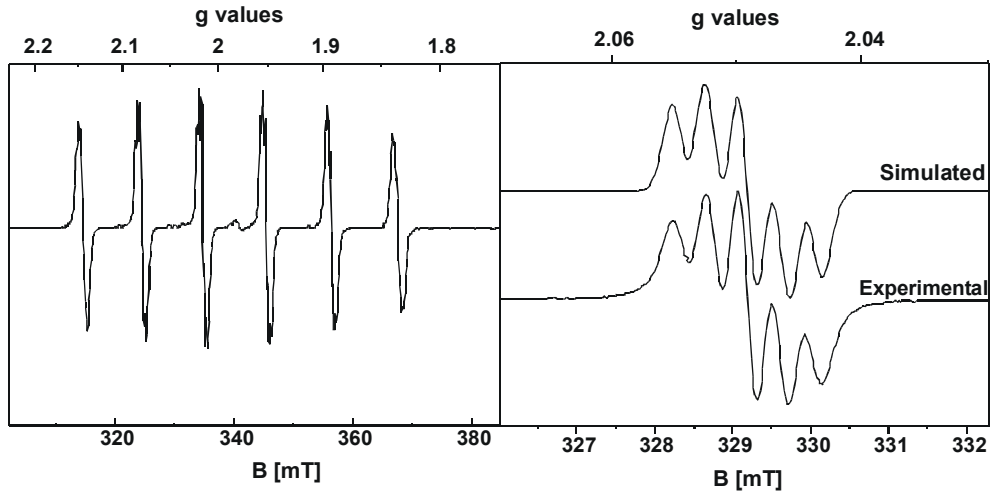

Figure 4.8 :- X-band EPR spectra of **18** at 298K.

The metal-based $S = ½$ ground state of **18** has also been established by X-band EPR spectroscopy. Figure 4.8 shows the EPR spectrum of **18** in CH_2Cl_2 solution at 298K for the X-band. The spectrum displays an isotropic signal at $g_{iso} = 2.009$ with hyperfine coupling to the $I = {}^5/_2$ ^{55}Mn nucleus of A_{iso}=106.6 G , and in addition, superhyperfine coupling to three ^{14}N donor atoms (I = 1) and two protons (I =½) was clearly detected, $A(^{14}N)$ =4.29 G, $A(^{1}H)$ = 5.15G, $A(^{1}H)$ =2.83 G .

Electrochemistry (Cyclic and square wave voltammetry) of **18** shows two reversible waves at -0.508 and –0.953V, which are assigned to the oxidation and reduction at the radical site of the ligand. These redox processes are one-electron transfer processes. The irreversible peak at –1.31V is assigned to the metal centered reduction .

When 3,5-DTBC is added to a CH_2Cl_2 solution of **18**, in the ratio 1:50, the deep red brown color of the solution starts to fade to yellow and then slowly to red. The solution was stirred for one hour and then subjected to Liquid Chromatography. 100% conversion of 3,5-DTBC to 3,5-DTBQ was found and the maximum TON was 169. It is to be pointed out that although the rate of conversion when **18** is used as a catalyst is faster than that of **16**, however the TON is less. The probable reason could be the presence of two metal centers and the presence of four radicals in **16**.

To evaluate the rate constants at a constant catalyst concentration (k_{sub}) and at constant substrate concentration (k_{cat}), the same procedure, when **16** was used as a catalyst, was applied. When the substrate concentration was changed, the amount of catalyst was 2 x 10^{-7} mole in dichloromethane (10ml after dilution) [Table 4.5]. For measuring k_{cat} the amount of substrate taken was 4 x 10^{-6} mole [Table 4.6]. The value of k_{sub} and k_{cat} are 2.8 x 10^4 mole^{-1} min^{-1} and 5.6 x 10^5 mole^{-1} min^{-1}, respectively and are calculated from the slope of the

[Substrate] x 10^6 (moles)	Rate (r_0'') x 10^2 (min^{-1})
1.1	2.78
2.4	6.78
3.2	9.3
4	11.04

Table 4.5:- List of substrate concentration and corresponding rate.

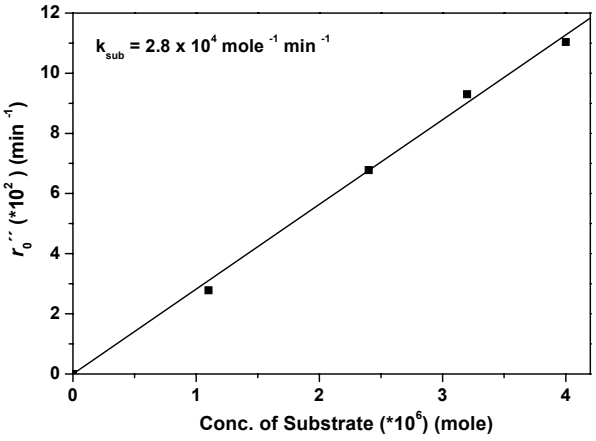

Figure 4.9:-Plot of substrate concentration vs. corresponding rate.

[Catalyst] x 10^8 (moles)	Rate (r_0''') x10^2 (min^{-1})
8	4.38
12	6.96
16	8.94
20	11.04

Table 4.6:- List of catalyst concentration and corresponding rate.

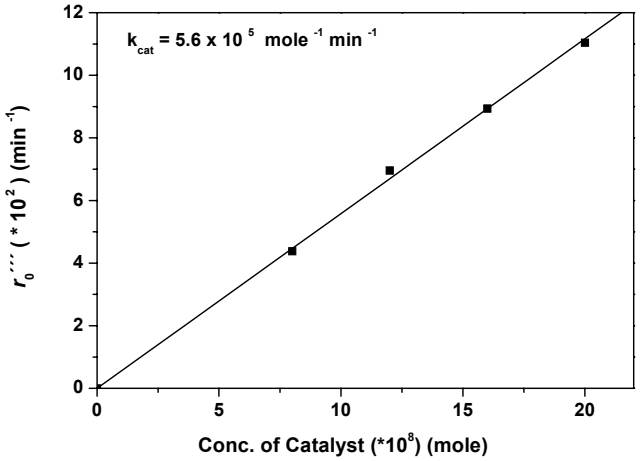

Figure 4.10:-Plot of catalyst concentration vs. corresponding rate.

best fit line. [Figure 4.9 and Figure 4.10]. It is clear that the rate of this reaction is first order to the catalyst and substrate concentration. The rate constant values (k_{sub} as the catalyst concentration is same in both the experiments] obtained show that this reaction is faster than that when **16** is used as a catalyst.

As a natural progress to this work, experiments were carried out with the complexes **16*** and **19-22**. The rate constant (k_{sub}) was calculated by the same procedure as above and the maximum TON was determined. The values are listed in Table 4.7. It is to be noted that only k_{sub} was measured in order to compare the rate of the reaction when the different catalysts were used. From Table 4.7 it is clear that the reaction rate is the slowest when **16** is the catalyst, the fastest being **22**.

In order to understand the mechanism, the knowledge of stoichiometry for this reaction is important. 10 equivalents of 3,5-DTBC was reacted with 1 equivalent of **16** (the

X	Ligands	Mn(IV) complexes with the ligands	E_{red} (Fc^+/Fc) (V)	k_{sub} x 10^{-4} ($mole^{-1}$ min^{-1})	Maximum TON (24 hours)
	H_4L^3	**16**	-1.02, -1.23, -1.63	0.9	500
H	H_2L^5	**16***	-1.03 ,-1.17	1.5	48
$-C(CH_3)_3$	H_2L^6	**18**	-0.95 , -1.31	2.8	169
$-CF_3$	H_2L^7	**19**	-0.68, -1.12, -1.96	4	48
$-CH_3$	H_2L^8	**20**	-1.12, -1.32	4.6	84
-Cl	H_2L^9	**21**	-0.94, -1.20, -1.93	5.3	45
$-OCH_3$	H_2L^{10}	**22**	-1.02, -1.23	9.1	40

Table 4.7 :- Values of E_{red}, k_{sub} and maximum TON obtained for different Mn(IV) complexes used as catalyst .

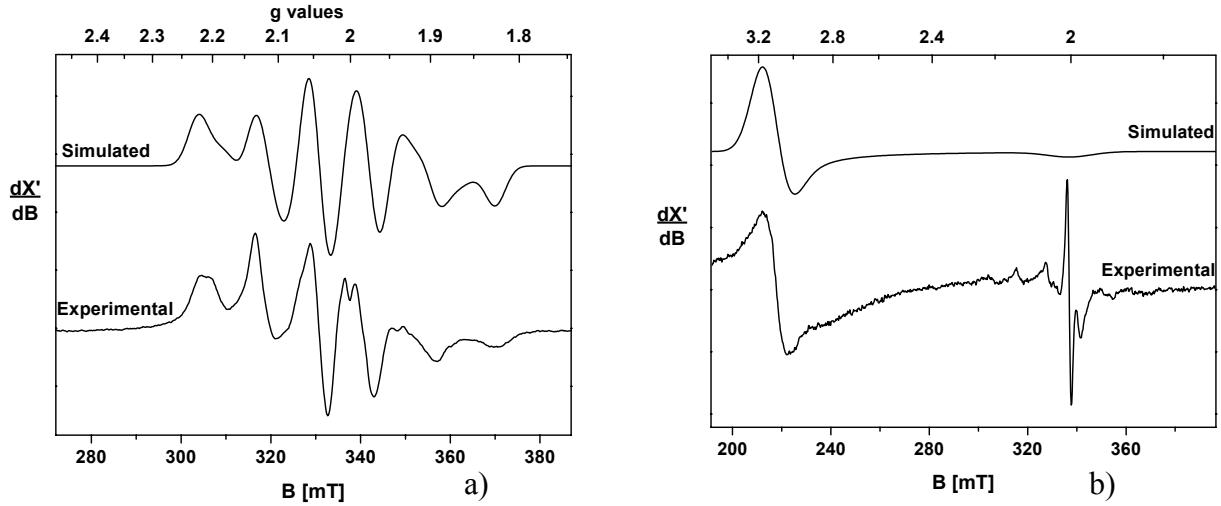

Figure 4.11:- X-band EPR spectrum of **16*** in dichloromethane at 10K (a)before addition of 3,5-DTBC and(b) after the reaction of one equivalent of 3,5-DTBC in glove box.

dimer) or **16*** (the monomer) (as the reaction velocity are slow for both, Table 4.7) in a glove box for 1hour, and divided into two parts. The first portion of the aliquot was subjected to LC study and it was found out that 2 equivalents of 3,5-DTBQ have been formed when **16** was used as catalyst; when **16*** was the catalyst, 1 equivalent of 3,5-DTBQ was formed. Upon exposure to air, it was found out that all the substrate has reacted.

The X-band EPR spectrum of a frozen dichloromethane solution of **16*** was measured at 10K [Figure 4.11(a)]. It shows the characteristic 6 line hyperfine structure with g_{iso} =2.01 [4]. When a frozen solution of the second aliquot, containing **16*** as catalyst, was subjected to X-band EPR studies at 10K, an interesting spectral feature was observed [Figure 4.11(b)]. The spectrum now shows a peak centered at g=3.15 and another low intensity peak centered at g = 2.0. This spectrum is typical for an S $=^3/_2$ system. The spectral feature arising at g=2.0 is probably due to minor amount of Mn^{II}.

When **16** (the dimer) was used as the catalyst, a complicated EPR signal was observed (Figure 4.12, dotted line). The spectrum showed broad peaks between g=20 to g=4 along with another six hyperfine signals centered at 2.0 (probably due to minor amount of Mn^{II}). This spectrum could not be simulated due to the unavailability of corresponding simulation program. However a meaningful interpretation is the formation of S$=^3/_2$ at each Mn center of the dimer.

Oxygen uptake measurements were performed using **18** (**18** was fully characterized and it was assumed that the oxidative reaction mechanism, with **18** as catalyst, was same when **16** or **16*** was used) as catalyst at -25°C and at -10°C (due to high vapour pressure of CH_2Cl_2). It was observed that at -25°C, equivalent amount of oxygen was needed to convert

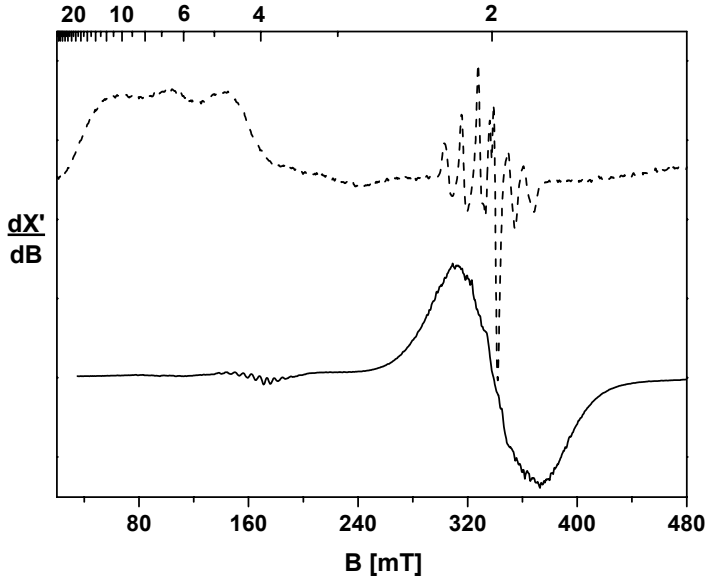

Figure 4.12:- X-band EPR spectrum at 10K of 16 (bold line) before addition of 3,5-DTBC and after the reaction of two equivalents of 3,5-DTBC in glove box (dotted line).

all (0.5 mmole) 3,5-DTBC to 3,5-DTBQ (the reaction was monitored till 320 minutes due to saturation) [Table 4.8]. However, at -10°C, half equivalent of oxygen was required in order to convert all (0.5mmole) of 3,5-DTBC to 3,5-DTBQ (the reaction was monitored till 152 minutes due to saturation) [Table 4.9]. At -25°C, the H_2O_2 formed did not undergo any decomposition to H_2O and O_2. When the reaction was carried out at -10°C, catalase like

Time (mins.)	Vol. of O_2 consumed (ml)
0	0
4	1.1
6	2.5
8	2.7
10	2.9
14	3.5
20	4.5
23	4.8
26	5.1
28	5.3
30	5.5
35	5.9
40	6.5
100	9.6
140	11.5
200	11.7
320	12.9

Table 4.8:- O_2 uptake data when **18** is used as catalyst at –25°C.

Time (mins.)	Vol. of O_2 consumed (ml)
0	0
2	1
3	1.5
10	4
25	4.4
76	4.8
109	4.9
132	4.9
152	5

Table 4.9:- O_2 uptake data when **18** is used as catalyst at –10°C.

activity of **18** decomposed H_2O_2, the oxygen formed being taken up by the reaction medium. The presence of hydrogen peroxide in the catalysis solution was confirmed by addition of water (5ml) to the reaction mixture [5 x 10^{-3} mmole of catalyst was added to 500 x 10^{-3} mmole of 3,5-DTBC in 10ml dichloromethane], extracting the aqueous layer 3 times by dichloromethane (20ml), adding titanyl sulphate solution to the water layer (1ml) and measuring the UV-spectrum of the resulting solution. The absorbance peak due to the titanyl-peroxy complex appears at 400nm. Furthermore, if a freshly prepared, slightly acidic potassium iodide solution is added to the aqueous layer and the resulting solution is extracted with carbon tetrachloride, a violet coloration occurs in the carbon tetrachloride layer. Blank reactions were carried out with **18** as well as with 3,5-DTBC. No H_2O_2 was observed.

Therefore, the stoichiometry of the reaction at lower temperature could be written as

$$\text{3,5-DTBC} + O_2 \xrightarrow[\text{catalyst}]{CH_2Cl_2} \text{3,5-DTBQ} + H_2O_2$$

At room temperature the stoichiometry changes to

$$\text{3,5-DTBC} + \tfrac{1}{2} O_2 \xrightarrow[\text{catalyst}]{CH_2Cl_2} \text{3,5-DTBQ} + H_2O$$

due to incipient decomposition of H_2O_2.

It seems that an outer-sphere mechanism is involved in this reaction. This is supported by the reduction potentials of the catalysts [Table 4.7]. The EPR signal shows that the intermediate could be the two-electron reduced form of the complex. In presence of air, the ligands are re-oxidized to the radical form of the complex which carries out the next turnover. This probable mechanism is shown in Figure 4.13.

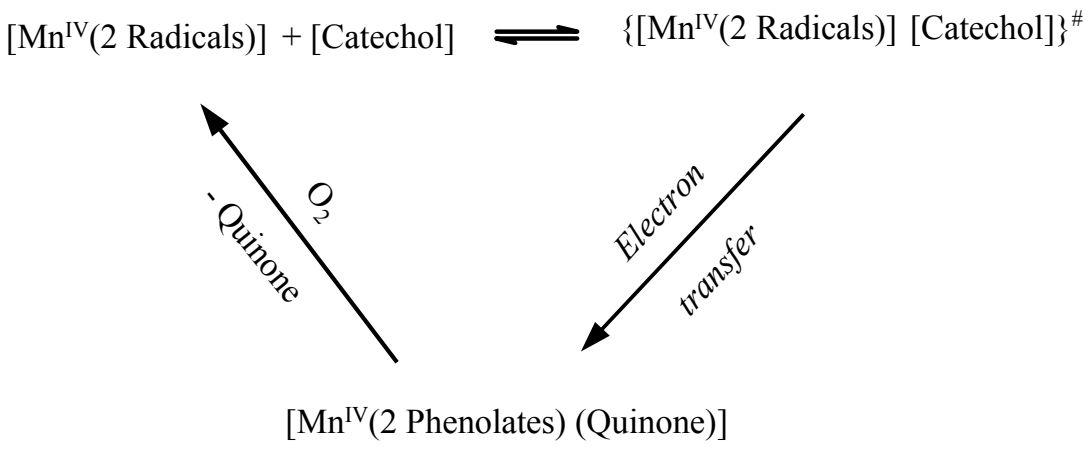

Figure 4.13 :- Tentative mechanism for the oxidation of 3,5-DTBC by the radical containing Mn-complexes.

This type of catalysis, where radicals undergoes an "on-off " mechanism, is observed for the **first time**. More complexes with polyradical species can be synthesized which can act as a better oxidative catalyst.

4.4 OXIDATIVE STUDIES WITH 2,6-DI-TERT-BUTYL-PHENOL

When 2,6-di-tert-butylphenol (DTBP) (412mg; 2mmole) is added to **16** (17mg; 0.01mmole) in dichloromethane/methanol (1:1) solvent mixture (50ml), the dark brown color slowly turns to red. After 48 hours, it was found that 100% of the phenol has converted to 3,3′-5,5′-Tetra-tert-butyldiphenoquinone (TTBD). A maximum turnover number of 1284 was observed.

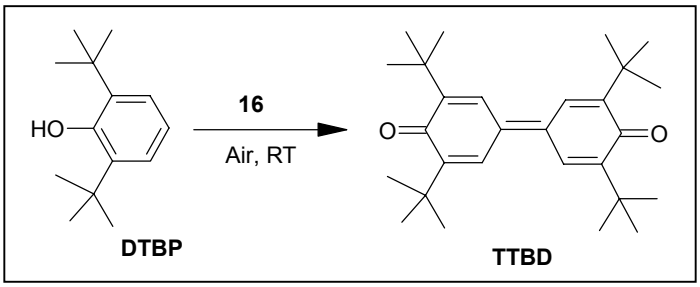

The reaction was monitored by eluting 50µl from the aliquot at different time intervals, passing it through a Amberlyst-resin column to remove the catalyst and then washing it by 10ml of dichloromethane. Electronic spectrum of these solutions were measured. TTBD shows a characteristic peak in the electronic spectrum at 425nm. The resultant change in electronic spectrum and the plot of absorbance vs. time is shown in Figure 4.14(a) and 4.14(b) respectively. From the plot, it could be manifested that the reaction rate is of higher orders and more complicated than that observed for the oxidative catalysis of 3,5-DTBC.

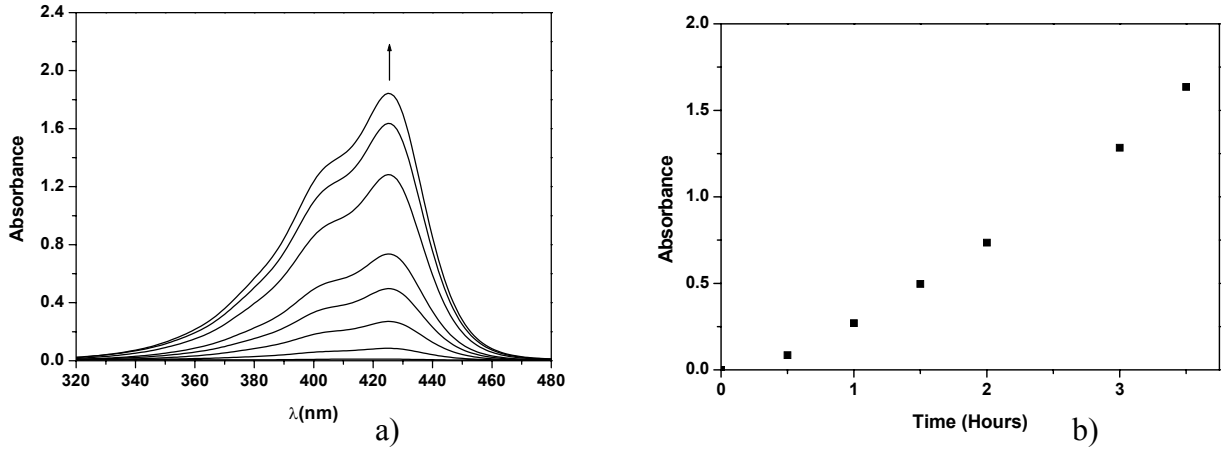

Figure 4.14:-a) Electronic spectrum of the eluted solution at different time.(b) Plot of corresponding absorbance vs. time.

References

1 (a)C. Gerdemann, C. Eicken, B. Krebs, *Acc. Chem. Res.* **2002**, 35, 183. (b) E. I. Solomon, U. M. Sundaram, T. E. Machonkin, *Chem. Rev*.,**1996**, 96, 2563.

2.(a) R. Wegner, M. Gottschaldt, H. Görls, E.-G. Jäger, D. Klemm, *Chem. Eur. J.*, **2001**, 7, 2143.(b) S. C. Cheng , H.H. Wei, *Inorg. Chim. Acta* **2002** , 340,105 and references therein. (c) R. Than, A. A. Feldmann, B. Krebs, *Coord. Chem. Rev.* **1999**, 182, 211. (d) J. Reedijk, Bioinorganic Catalysis, (Ed.: J. Reedijk), 2nd ed., Dekker, New York 1998. (e) J. Reim, B. Krebs, J. Chem. Soc. *Dalton Trans*. **1997**, 3793. f) E. Monzani, G. Battaini, A. Perotti, L. Casella, M. Gullotti, L. Santagostini, G. Nardin, L. Randaccio, S. Geremia, P. Zanello, G. Opromella, *Inorg. Chem*. **1999**, 38, 5359 . g) E. Monzani, L. Quinti, A. Perotti, L. Casella, M. Gullotti, L. Randaccio, S. Geremia, G. Nardin, P. Faleschini, G. Tabbi, *Inorg. Chem*. **1998**, 37, 553. h) L. Casella, E. Monzani, M. Gullotti, D. Cavagnino, G. Cerina, L. Santagostini, R. Ugo, *Inorg. Chem*. **1996**, 35, 7516. i) F. Thaler, C. D. Hubbard, F. W. Heinemann, R. van Eldik, S. Schindler, I. Fabian, A. M. Dittler-Klingemann, F. E. Hahn, C. Orvig, *Inorg. Chem*. **1998**, 37, 4022. j) J. Mukherjee, R. Mukherjee , *Inorg. Chim. Acta* **2002**, 337, 429. k) R. Wegner, M. Gottschaldt, H.Görls, E.-G. Jäger, D. Klemm, *Angew. Chem. Int. Ed*. **2000**, 39. l) M.R. Malachowski, H.B. Huynh, L.J. Tomlinson, R.S. Kelly, J.W. Furbee, jun. *J. Chem. Soc., Dalton Trans*. **1995**, 31. m) M.R. Malachowski, J. Carden, M.G. Davidson, W.L. Driessen and J. Reedijk. *Inorg. Chim Acta* **1997**, 257, 59. n) M.R. Malachowski, B.T. Dorsey, M.J. Parker, M.E. Adams and R.S. Kelly. *Polyhedron* **1998**, 17, 1289.

3. N. Oishi, Y. Nishida, K. Ida, S. Kida, *Bull. Chem. Soc. Jpn.* **1980**, 53, 2847.
4. H. Chun, P. Chaudhuri, T. Weyhermüller, K. Wieghardt, *Inorg. Chem.*, **2002**, 41, 790
5. S. Mukherjee, E. Rentschler, T. Weyhermüller, K. Wieghardt , P. Chaudhuri, *Chem. Comm.*, **2003**, 1828.

Chapter 5

Fe^{III} AND Co^{III} COMPLEXES WITH IMINO-BENZOSEMIQUINONE LIGANDS; EFFECT OF SUBSTITUTION

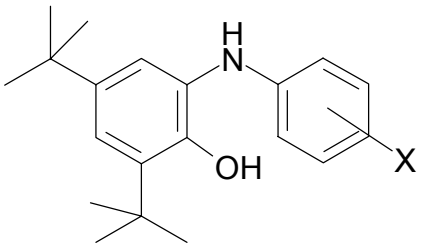

5.1 INTRODUCTION

The existence of imino-benzosemiquinone radical complexes is now well established and quite a few structurally as well as spectroscopically characterized metal complexes containing the imino-benzosemiquinone radicals have been synthesized [Chapter 3]. The parent ligand 2-anilino-4,6-ditert-butylphenol was used in synthesizing complexes with 3d-metal ions. The octahedral iron complex $[Fe^{III}(L^{5})_3]$ (**24***) possesses an S=1 ground state comprising a high-spin Fe^{III} ion ($S_{Fe}=^{5}/_{2}$) coupled antiferromagnetically to three imino-benzosemiquinone π-radical ligands.[1a] This ligand has also been used in synthesizing Fe(III) complexes where the ground state of the iron centers are low spin (LS, $S_{Fe}= ½$)[1b], intermediate spin (IS, $S_{Fe}=^{3}/_{2}$)[1c] or high spin (HS, $S_{Fe}= ^{5}/_{2}$)[1a]. The complex with intermediate Fe^{III} is five coordinated with two ligands and an iodide at the fifth position.[1b] The O,N-donor atoms from each of the ligand occupy the equatorial position with the iodide group in the axial position. On changing the axial halogen group, the spin state of the iron center changes from intermediate spin to high spin. This spin tuning was achieved by the position of the halides in the spectrochemical series.

In this chapter, changing the substituent groups at the meta- or para- position of the aniline ring in the ligand 2-anilino-4,6-ditert-butylphenol results in the formation of Fe(III) complexes with different structural and magnetic property, is discussed.

5.2 SYNTHESIS AND CHARACTERIZATION OF LIGANDS

Refluxing 3,5-ditert-butylcatechol and the respective anilines(1:1) in heptane in the presence of triethylamine as base resulted in the formation of the ligands H_2L^{6}, H_2L^{11} and H_2L^{12}. The IR spectroscopy of the ligands shows characteristic peaks for –OH and –NH stretch from 3500-3200 cm^{-1} along with the typical peaks for –C-H and –C-N stretch. The characteristic IR spectroscopy peaks are given in Table 5.1. The ligands are all characterized by mass spectroscopy in EI-mode[Table 5.1]. NMR spectrum (experimental section, Chapter 7) clearly shows that the number of non-exchangeable hydrogen atoms corroborates to that of the ligand.

Table 5.1 :- *Ligands synthesized and their characterization.*

Ligand	Ligand structure	IR peaks (cm^{-1})	EI-MS (Molecular peak) m/z
H_2L^6	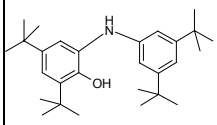	3339s, 1598s, 1361, 1233s, 999m, 774m, 631b.	409
H_2L^{11}	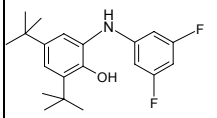	3440s,3363s,1628s,1598s,1478s,1227m,1000s, 830s, 667m.	333
H_2L^{12}	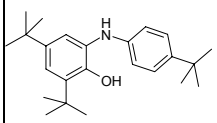	3356m,1614s,1515s,1315m,1232m,825m, 765m.	353

5.3 SYNTHESIS AND CHARACTERIZATION OF COMPLEXES

The iron complex of H_2L^6 was synthesized by refluxing the ligand with $[Fe^{II}(H_2O)_6](ClO_4)_2$ in methanol in the presence of triethylamine as base. Deep green microcrystalline precipitate was obtained in moderate yield and repeated recrystallization from a diethylether-acetonitrile solvent mixture resulted in X-Ray quality crystals of the monomer **24**. With this ligand the cobalt(III) complex, **23**, was prepared in order to understand the nature of interactions between the radical centers. The cobalt salt used was $[Co^{II}(H_2O)_6](ClO_4)_2$ and refluxing with H_2L^6 in the presence of NEt_3 in acetonitrile yields dark brown microcrystalline precipitate of **23**. Recrystallization from a diethylether-acetonitrile solvent mixture affords X-ray quality crystals of **23**. The iron complexes, **25** and **26** using H_2L^{11} and H_2L^{12} as ligand, respectively, were synthesized using the same procedure that for **24**. Recrystallization from dichloromethane-acetonitrile solvent mixture gave crystalline material of **25** and **26**. X-ray quality crystals of **25** were obtained from a saturated acetone solution. **26** was found to be a μ-oxo bridged dimeric Fe^{III} complex with radical containing ligand.

All these complexes have been characterized by various spectroscopic techniques viz. IR, UV-Vis and MS in EI as well as ESI mode. The Infrared spectroscopy of all the complexes shows the absence of the –OH and –NH peaks and appearance of ν(CN) bands between 1615 to 1580 cm^{-1}. Interestingly, for **25**, this band is split into two sharp bands at

Table 5.2:- *Characteristic IR and EI-MS peaks of the complexes **23-26**.*

Ligand	Complex	IR peaks (cm^{-1})	EI-MS (m/z)
H_2L^6	$Co(L^6)_3$ (**23**)	1578,1433,1361,1247,707	1280
H_2L^6	$Fe(L^6)_3$ (**24**)	1581,1468,1362,1247,945	1277
H_2L^{11}	$Fe(L^{11})_3$(**25**)	1612,1591,1468,1116,990	1049
H_2L^{12}	$[\{Fe(L^{12})_2\}_2O]$ (**26**)	1466,1424,1256,842,557	1532

1612 cm^{-1} and 1591cm^{-1}. The peak due to Fe-O-Fe asymmetric stretch, for **26,** appears at 842 cm^{-1} and fits well in the plot of asymmetric stretch frequency vs. the Fe-O-Fe angle.[3] Mass spectroscopy for all the complexes shows the molecular peak in the EI–mode. Selected IR and MS peaks for the complexes **23**-**26** are given in Table 5.2.

$Co^{III}L^6_3$ (23)

The single crystal X-ray structure of **23** (Figure 5.1) at 100K shows that the first coordination sphere of cobalt has a C_2 axis passing through O(61)–Co(1)–N(7); the ligands have lost their aminohydrogen atoms. The structure determination unambiguously shows that cobalt is hexa-coordinated to three deprotonated ligands. The distances C2–C3, C4–C5, C32–C33, C34–C25, C62–C63 and C64–C65 are significantly shorter than the other C–C distances in the original phenol ring[Table 5.3]. Correspondingly, the imino C-N bonds at 1.346 ± 0.006Å are shorter than the C–N bonds to the aniline rings, 1.423 ± 0.006 Å along with the shortened C–O bond distances, 1.30 ± 0.006 Å (average) each of which contains an iminosemiquinone radical anion. The average metal-to-donor atom distance indicates a formal +3 oxidation state at the cobalt centre.

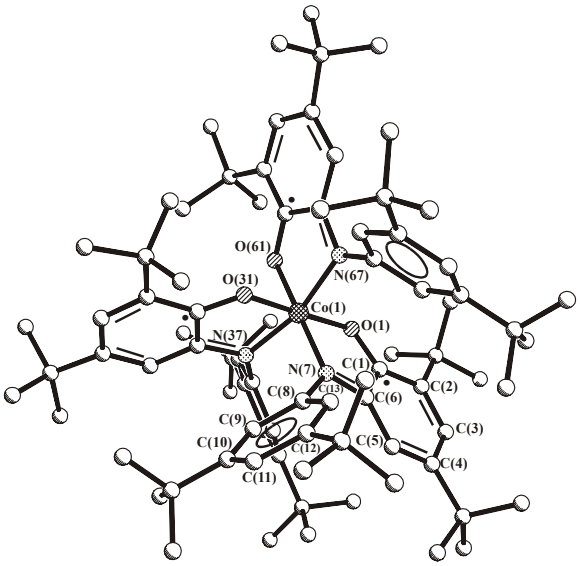

Figure 5.1:- Crystal structure of **23.**

Table 5.3 :- *Selected bond distances (Å) and angles (degree) of **23**.*

Co(1)-O(31)	1.8754(11)		
Co(1)-O(1)	1.8818(11)	O(31)-Co(1)-O(1)	178.65(5)
Co(1)-O(61)	1.8896(11)	O(31)-Co(1)-O(61)	90.19(5)
Co(1)-N(37)	1.9118(14)	O(1)-Co(1)-O(61)	89.64(5)
Co(1)-N(7)	1.9177(13)	O(31)-Co(1)-N(37)	84.68(5)
Co(1)-N(67)	1.9389(14)	O(1)-Co(1)-N(37)	96.64(5)
O(1)-C(1)	1.3007(19)	O(61)-Co(1)-N(37)	85.28(5)
O(31)-C(31)	1.3020(19)	O(31)-Co(1)-N(7)	95.58(5)
O(61)-C(61)	1.296(2)	O(1)-Co(1)-N(7)	84.69(5)
C(6)-N(7)	1.346(2)	O(61)-Co(1)-N(7)	173.17(5)
C(36)-N(37)	1.344(2)	N(37)-Co(1)-N(7)	91.59(6)
C(66)-N(67)	1.347(2)	O(31)-Co(1)-N(67)	85.39(5)
C(1)-C(2)	1.423(2)	O(1)-Co(1)-N(67)	93.26(5)
C(1)-C(6)	1.438(2)	O(61)-Co(1)-N(67)	83.86(5)
C(2)-C(3)	1.375(2)	N(37)-Co(1)-N(67)	165.24(6)
C(3)-C(4)	1.430(2)	N(7)-Co(1)-N(67)	100.22(6)
C(4)-C(5)	1.369(2)		
C(5)-C(6)	1.415(2)		

Such type of electron density distribution in *ortho*-iminosemiquinone has been discussed previously [Figure 3.1, Chapter 3]. Therefore, this complex consists of **three** imino-benzosemiquinone radicals.

Magnetic data (SQUID) with H = 1 T for a polycrystalline sample of **23** are displayed in Figure 5.2 as μ_{eff} *vs*. T. On lowering the temperature, μ_{eff} ($3.20\mu_B$ at 290 K) increases monotonically approaching a maximum around 30K with a value of $3.76\mu_B$, which is close to the spin-only value for $S_t = {}^3/_2$, expected as the ground state for three ferromagnetically coupled iminosemiquinone radicals. Below 15 K there is a decrease in μ_{eff}, which reaches a value of $2.79\mu_B$ at 2 K due to saturation effects and/or intermolecular antiferromagnetic interactions. The experimental data could not be fitted with only one coupling constant (J) as satisfactorily as with two 'J' values. Two exchange coupling constants have to be considered for the simulation based on the Hamiltonian

$$\hat{H} = -2J(\vec{S}_1\vec{S}_2 + \vec{S}_2\vec{S}_3) - 2J_{13}(\vec{S}_1\vec{S}_3)$$

with $S_1 = S_2 = S_3 = ½$ and the best fit shown as the solid line in Figure 5.2 yields $J = J_{12} = J_{23}$ = +26.7 cm^{-1}, J_{13} = +53.2 cm^{-1}, $g_1 = g_2 = g_3 = 2.0$ (fixed) and a Theta-Weiss parameter (Θ) of –0.908K . Thus the quartet ground state is separated from the first doublet state by ~ 80 cm^{-1} owing to the exchange interactions. The coupling constants, J and J_{13}, of **23*** (mononuclear Co^{III} complex with the ligand 2-anilino-4,6-ditert-butylphenol) were found to be +9.0 cm^{-1} and +59.5cm^{-1}, respectively. Here the quartet ground state is separated from the first doublet state by 27 cm^{-1}.[1d]

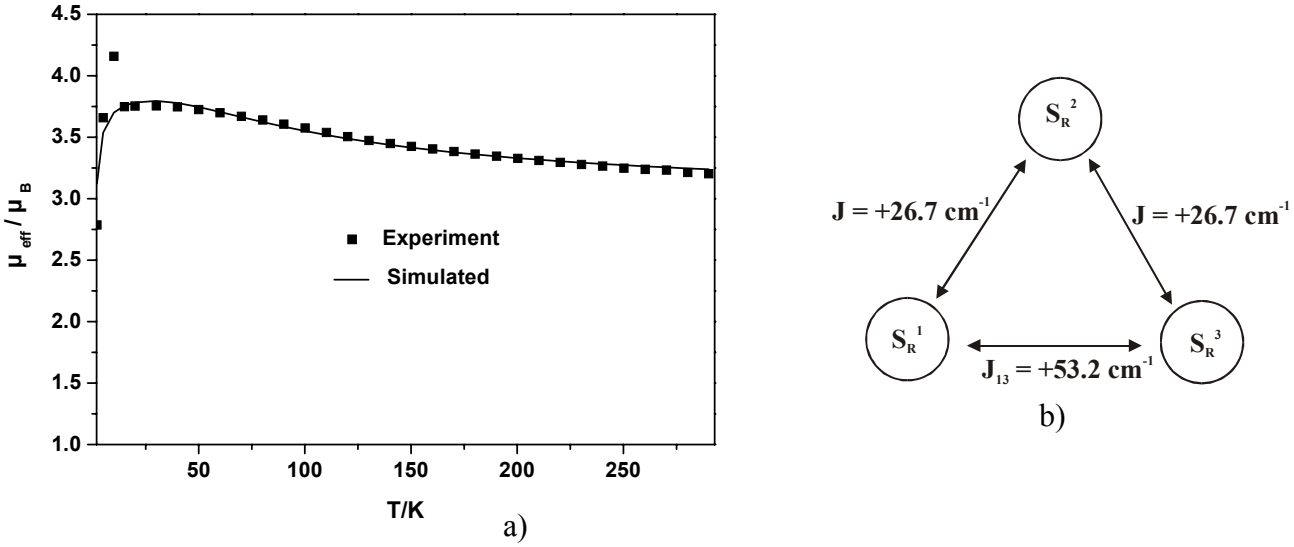

Figure 5.2 :- (a) Magnetic data of **23**. (b) Spin coupling model used in simulating the data.

Optical spectrum of **23** in CH_2Cl_2 consist of a series of intense bands and shoulders [Figure 5.3(a)]; in particular two intense absorptions at low energies are noteworthy: λ/nm (ε/M^{-1} cm^{-1}) 883(7559) and 661(6916). A peak with weaker intensity at 477 nm (ε = 5716 M^{-1} cm^{-1}) is assigned to the quinone to metal charge transfer band. The intensity suggests that allowed electronic transitions are the ligand-to-ligand π-π* charge transfer bands, which has also been observed with **23***(mononuclear Co^{III} complex with the ligand 2-anilino-4,6-ditert-butylphenol)[1d] that dominate the spectra.

Cyclic voltammetric experiments at high scan rates exhibit three reversible one-electron redox waves for **23** in CH_2Cl_2 [0.1M $(NBu)_4PF_6$]: $E^{1}{}_{½}$ = 0.225, $E^{2}{}_{½}$ = - 0.386, and $E^{3}{}_{½}$ = -1.464 V *vs.* Fc^+/Fc [Figure 5.3(b)]. The first two redox potentials are associated with two ligand centered oxidation processes and $E^{3}{}_{½}$ is assigned to the Co(III)–Co(II) couple.

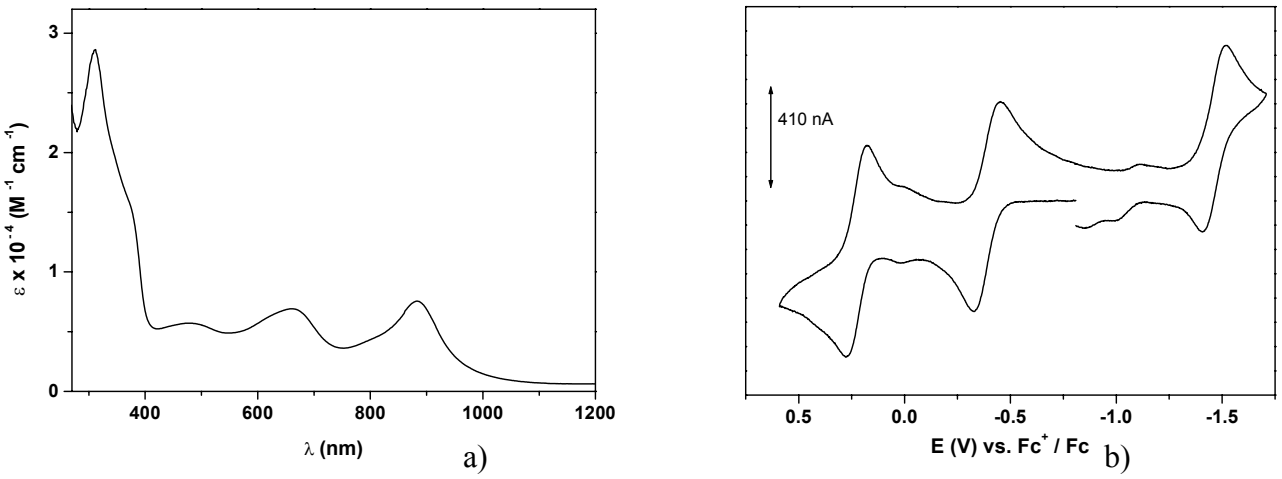

Figure 5.3:- a) Electronic spectrum of **23**. b) Cyclic voltammogram of **23**.

$Fe^{III}L^{6}_{3}$ (24)

Dark green single crystals of **24,** obtained from a diethylether-acetonitrile solvent mixture, was subjected to X-Ray diffractometric studies at 100K (as well as at 293K for reasons mentioned later) and it was found that the complex was iso-structural with the cobalt complex (**23**) [Figure 5.4]. A C_2 axis passes through O(1)-Fe(1)-N(37). Here again, it was observed that the three phenyl rings containing the tert-butyl as substituents have lost their aromaticity with the presence of two long and four short C-C bond distances for each of these rings. The C-N as well as the C-O bond distances have shortened (Average C-O bond distance is 1.30Å; average C-N bond distance is 1.351 Å); the three rings adopts a quinoid-type structure. Thus the complex consists of **three** imino-benzosemiquinone radicals. Selected bond distances are given in Table 5.4.

The most interesting structural feature of this complex is the metal-to-donor bond distances. The average Fe-O and Fe-N bond distances are 1.904 and 1.922 Å, respectively which are much shorter than the reported iron(III) complex with the ligand 2-anilino-4,6-ditertbutylcatechol.[1a] Thus, the iron in **24** has a oxidation state of +3 but probably not in a high spin state. In order to discern the spin state, magnetic susceptibility measurements as well as Mössbauer spectroscopy were performed with this complex.

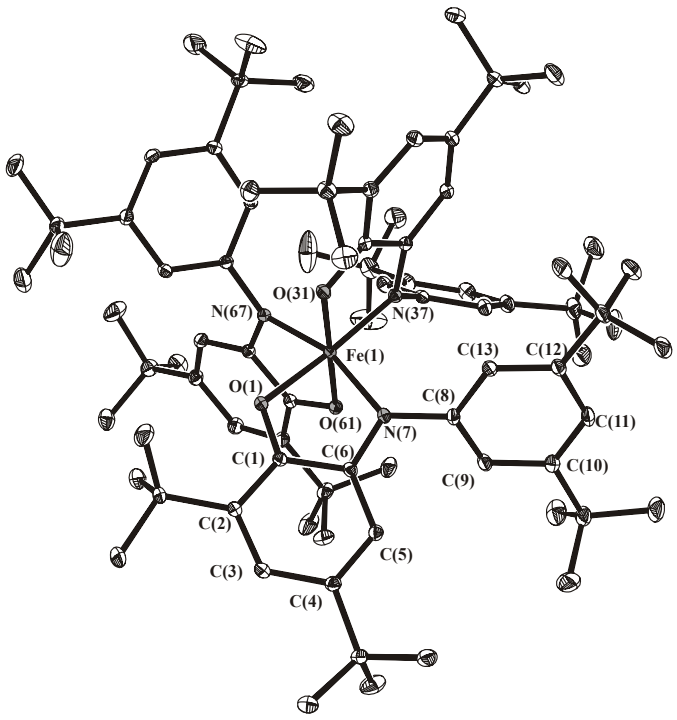

Figure 5.4:- Crystal structure of **24.**

Table 5.4:- *Selected bond distances(Å) and angles (degree) of **24** at 100K and 293K.*

100K		293K	
Fe(1)-O(31)	1.8869(11)	Fe(1)-O(31)	1.987(2)
Fe(1)-O(61)	1.9013(11)	Fe(1)-O(61)	1.995(2)
Fe(1)-N(37)	1.9083(13)	Fe(1)-N(37)	2.067(3)
Fe(1)-N(67)	1.9144(13)	Fe(1)-N(67)	2.078(3)
Fe(1)-O(1)	1.9228(11)	Fe(1)-O(1)	2.006(2)
Fe(1)-N(7)	1.9429(13)	Fe(1)-N(7)	2.079(3)
O(1)-C(1)	1.2950(19)	O(1)-C(1)	1.287(4)
C(6)-N(7)	1.352(2)	C(6)-N(7)	1.336(4)
C(1)-C(2)	1.429(2)	C(1)-C(2)	1.423(5)
C(1)-C(6)	1.442(2)	C(1)-C(6)	1.453(5)
C(2)-C(3)	1.381(2)	C(2)-C(3)	1.368(5)
C(3)-C(4)	1.426(2)	C(3)-C(4)	1.420(5)
C(4)-C(5)	1.373(2)	C(4)-C(5)	1.355(5)
C(5)-C(6)	1.421(2)	C(5)-C(6)	1.416(5)
O(31)-Fe(1)-O(61)	178.55(5)	O(31)-Fe(1)-O(61)	173.53(10)
O(31)-Fe(1)-N(37)	83.42(5)	O(31)-Fe(1)-N(37)	78.29(10)
O(61)-Fe(1)-N(37)	95.81(5)	O(61)-Fe(1)-N(37)	96.04(10)
O(31)-Fe(1)-N(67)	95.94(5)	O(31)-Fe(1)-N(67)	99.17(10)
O(61)-Fe(1)-N(67)	82.91(5)	O(61)-Fe(1)-N(67)	78.08(10)
N(37)-Fe(1)-N(67)	96.29(6)	N(37)-Fe(1)-N(67)	95.08(11)
O(31)-Fe(1)-O(1)	89.74(5)	O(31)-Fe(1)-O(1)	91.88(10)
O(61)-Fe(1)-O(1)	91.03(5)	O(61)-Fe(1)-O(1)	93.76(10)
N(37)-Fe(1)-O(1)	173.16(5)	N(37)-Fe(1)-O(1)	170.16(10)
N(67)-Fe(1)-O(1)	84.54(5)	N(67)-Fe(1)-O(1)	86.04(10)
O(31)-Fe(1)-N(7)	95.86(5)	O(31)-Fe(1)-N(7)	97.95(10)
O(61)-Fe(1)-N(7)	85.47(5)	O(61)-Fe(1)-N(7)	86.33(10)
N(37)-Fe(1)-N(7)	98.62(6)	N(37)-Fe(1)-N(7)	103.05(11)
N(67)-Fe(1)-N(7)	161.92(5)	N(67)-Fe(1)-N(7)	156.90(10)
O(1)-Fe(1)-N(7)	81.87(5)	O(1)-Fe(1)-N(7)	78.01(10)

Figure 5.5 shows the magnetic data of a powdered sample of **24** from 2 to 290K. The value of μ_{eff} at 290K (3.017 μ_B) decreases monotonously till 260 K (2.89 μ_B). A sharp decrease was then observed till 140 K (1.23μ_B) and then again a monotonous decrease till 2K (0.64 μ_B). The nature of the curve clearly shows that spin transition occurs on raising or lowering the temperature. This spin transition occurs rather rapidly between the temperature range of 140K to 260K .The value of μ_{eff} at low temperatures corroborated to a S_t (total spin)=0. The residual magnetic moment at 2K is probably due to the presence of a temperature independent paramagnetism(TIP) (Mössbauer spectroscopy fortifies the purity of **24**). The value at 290K shows that at room temperature S_t=1. The diamagnetic ground state of this complex can be explained by the antiferromagnetic coupling of one radical center with the low spin iron center (S_{Fe}=½) and very weak anti-ferromagnetic coupling between the two residual radical centers. At higher temperature, the iron center changes its spin state to high spin (S_{Fe}= $^5/_2$) and its strong anti-ferrromagnetic interactions with the radicals renders a total spin of S_t = 1. No hysteresis effect was observed [Figure 5.5].

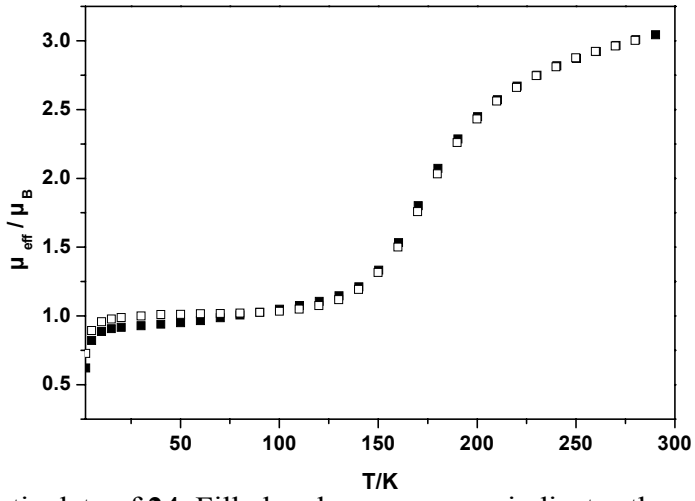

Figure 5.5 :- Magnetic data of **24**. Filled and open squares indicates the values of μ_{eff} on increasing and decreasing the temperature, respectively.

In order to establish that the iron(III) center in **24** has a high spin character, X-Ray diffratometric studies were also carried out at 293K. It was observed that all the three ligands retain their imino-benzosemiquinone character. However the average metal-to-donor bond distance increases; average Fe-O bond distance is 1.996Å and average Fe-N bond distance is 2.075Å. The bond distances are comparable to high spin Fe(III) complex synthesized with the ligand 2-anilino-4,6-ditertbutylcatechol. Thus, the complex at room temperature consists of a high spin Fe(III) ($S_{Fe} = {}^5/_2$) with three radicals (S_R = ½). At temperature below ~140K, the iron center is in an low spin ground ($S = {}^1/_2$) with three imino-benzosemiquinone radicals. Table 5.5 compares the iron-to-donor bond distances for this complex at 100K and 293K and for the iron complex with the ligand 2-anilino-4,6-ditertbutylcatechol (**24***).

Mössbauer spectroscopy was also carried out with **24** both at 80K and at 297K (Figure 5.6(a) and(b)). At 80K, the doublet obtained could be simulated by using an isomer shift (IS) value of 0.13 mms^{-1} and a quadrupole split (ΔE_Q) of 1.37 mms^{-1} indicating a low spin ground state for iron. At 297K , the isomer shift value changes to 0.391mms^{-1} and ΔE_Q changes to 0.917mms^{-1}. The value of isomer shift and ΔE_Q at room temperature shows that the Fe(III) center in **24** is in a high spin state.

Table 5.5 :- *Average Fe-O and Fe-N bond lengths (Å) for **24** at 100K and 293K and corresponding average bond length of **24***.

	24 at 100K	**24** at 293K	**24***(iron complex with the ligand 2-anilino-4,6-ditert- butylcatechol) at 100K
Fe-O	1.904	1.996	2.014
Fe-N	1.922	2.075	2.099

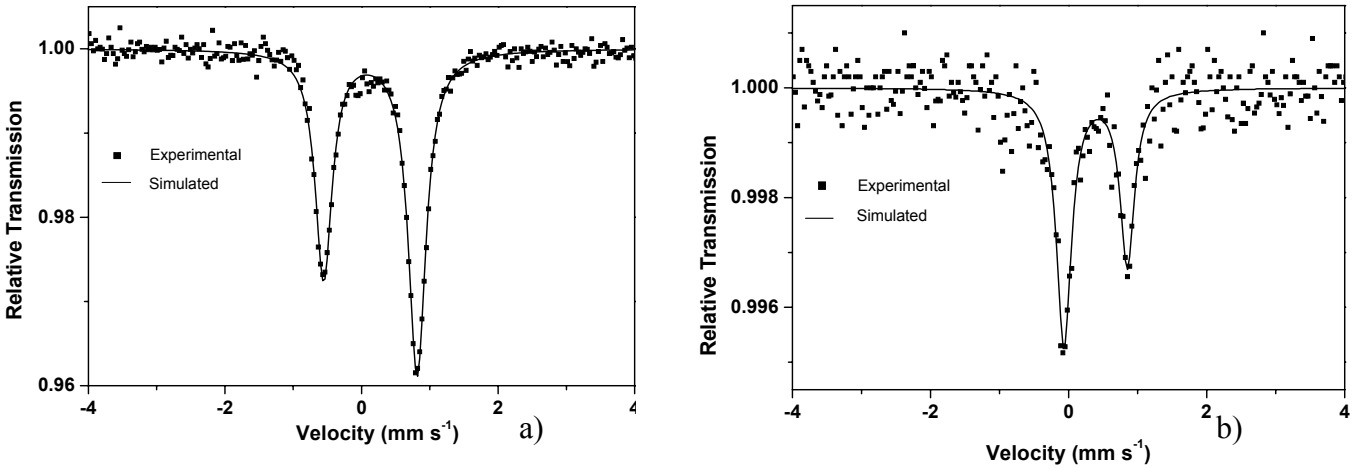

Figure 5.6:- Mössbauer spectrum of **24** at a) 80K and b) 297K.

Electronic spectrum of **24** in a dichloromethane solution at room temperature is shown in Figure 5.7(a). Absorption maxima were obtained at 750nm (ε = 9217 $M^{-1}cm^{-1}$) and 441nm (ε =6571 $M^{-1}cm^{-1}$) and the spectrum is similar to that obtained for **24***.

The CV of a dichloromethane solution of **24** in the presence of 0.1M $TBAPF_6$, shown in Figure 5.7 (b), has been recorded at fast scan rates because the reduced form is quite labile. The CV is essentially identical to that of **24***- (iron complex with the ligand 2-anilino-4,6-ditertbutylcatechol) the oxidation potentials are +0.294V and -0.422V and the reduction potential is at –1.293V vs. Fc^+/Fc. All these redox-processes comprise a single electron transfer as witnessed by coulometric studies.

It is probable that steric reasons are responsible for this behavior of **24**. As a natural progress, the iron complexes with the other two ligands, where the tert-butyl group has been replaced by the fluro-substituent (H_2L^{11}) and where the tert-butyl group is now at the para-position (H_2L^{12}), were synthesized.

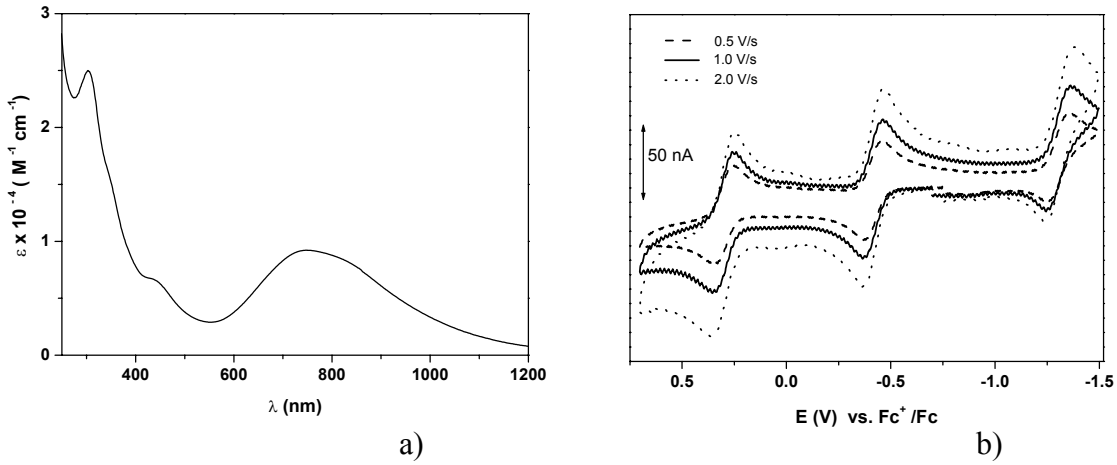

Figure 5.7 :- a) Electronic spectra of **24**. b) Cyclic voltammogram of **24** at fast scan rates.

$Fe^{III}L^{11}{}_3$ (25)

The crystal structure of **25** at 100K is shown in Figure 5.8. A C_2 axis passes through O(31)-Fe(1)-N(7) and the donor atoms are in a meridional coordination sphere. Here again, it was observed that the three phenyl rings containing the tert-butyl as substituents have lost their aromaticity with the presence of two long and four short C-C bond distances for each of these rings. The C-N as well as the C-O bond distances have shortened (Average C-O bond distance is 1.30Å; average C-N bond distance is 1.351 Å); the three rings adopts a quinoid-type structure. Thus the complex consists of **three** imino-benzosemiquinone radicals. The

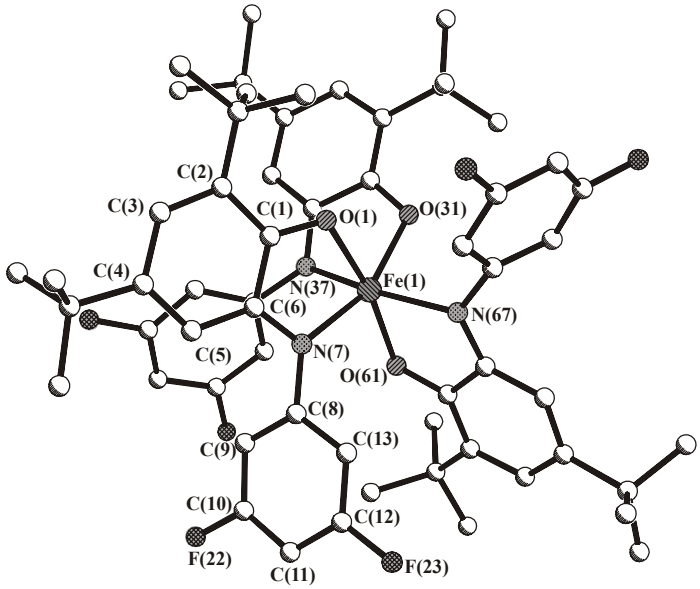

Figure 5.8:- Crystal Structure of **25**.

Table 5.6:- *Selected bond distances(Å) and angles (degree) of **25** at 100K* .

Fe(1)-O(31)	1.9932(8)	C(10)-F(22)	1.3524(18)
Fe(1)-O(61)	2.0008(8)	C(10)-C(11)	1.371(2)
Fe(1)-O(1)	2.0368(8)	C(11)-C(12)	1.376(2)
Fe(1)-N(67)	2.0692(9)	C(12)-F(23)	1.3508(17)
Fe(1)-N(7)	2.0934(10)	C(12)-C(13)	1.3883(18)
Fe(1)-N(37)	2.0956(9)		
O(1)-C(1)	1.2841(13)	O(31)-Fe(1)-O(61)	108.25(3)
C(6)-N(7)	1.3391(14)	O(31)-Fe(1)-O(1)	82.40(3)
O(31)-C(31)	1.2874(13)	O(61)-Fe(1)-O(1)	168.92(3)
C(36)-N(37)	1.3347(14)	O(31)-Fe(1)-N(67)	89.52(3)
O(61)-C(61)	1.2892(13)	O(61)-Fe(1)-N(67)	77.87(3)
C(66)-N(67)	1.3406(13)	O(1)-Fe(1)-N(67)	105.89(3)
		O(31)-Fe(1)-N(7)	157.74(3)
C(1)-C(2)	1.4371(14)	O(61)-Fe(1)-N(7)	92.73(4)
C(1)-C(6)	1.4564(14)	O(1)-Fe(1)-N(7)	76.33(3)
C(2)-C(3)	1.3753(15)	N(67)-Fe(1)-N(7)	102.45(4)
C(3)-C(4)	1.4339(15)	O(31)-Fe(1)-N(37)	77.38(4)
C(4)-C(5)	1.3694(15)	O(61)-Fe(1)-N(37)	91.05(3)
C(5)-C(6)	1.4230(15)	O(1)-Fe(1)-N(37)	88.28(3)
C(8)-C(9)	1.3924(18)	N(67)-Fe(1)-N(37)	159.39(4)
C(8)-C(13)	1.3951(17)	N(7)-Fe(1)-N(37)	95.31(4)
C(9)-C(10)	1.3864(17)		

average Fe-O and Fe-N bond distances are 2.010Å and 2.086Å which correspond to a high spin Fe(III) center (Table 5.6). Magnetic susceptibility measurements and Mössbauer spectroscopy supports this assignment. Selected bond distances are given in Table 5.6.

The iron containing species **25** contains a high-spin ferric ion (d^5) as was clearly established by its zero-field Mössbauer spectrum recorded at 80 K [Figure 5.9(a)]. An isomer shift, δ, of 0.545 mms^{-1} and a quadrupole splitting parameter, $|\Delta E_Q|$, of 1.035 mms^{-1} are diagnostic for octahedral high-spin ferric species.

Figure 5.9(b) displays the temperature dependence of the effective magnetic moments, μ_{eff}, of **25**. Complex **25** possesses an S =1 ground state. In the temperature range 30-200 K, **25** display nearly temperature-independent spin-only value of 2.80-2.84 μ_B for S =1. Above 200 K the magnetic moments increase monotonically: At 290 K the magnetic moment is 4% larger than that at 200 K. Strong intramolecular antiferromagnetic coupling between a high-spin ferric ion ($S = {}^5/_2$) with three organic radical ligands (S=½) prevails yielding the observed ground states of S = 1. It is possible to fit this temperature dependence by using antiferromagnetic coupling constants for the coupling between the paramagnetic metal ion and three semiquinonate ligand radicals. The fits in Figure 5.9(b) was obtained by using the following parameters: $J_{12}= J_{13} = J_{14}$ = -184 cm^{-1}, g = 2.0 (fixed) and a Theta-Weiss parameter (θ) of –0.8K.

Electronic spectra of **25** , in a dichloromethane solution at room temperature is shown in Figure 5.10(a). Absorption maximas were obtained at 745nm (ε = 9260 $M^{-1}cm^{-1}$) and 435nm (ε =7015 $M^{-1}cm^{-1}$) and the spectrum is very similar to that obtained for **24**.

The CV of the ferric complex **25** in dichloromethane, in the presence of 0.1M $TBAPF_6$ is shown in Figure 5.10(b). The oxidation potentials are at +0.531V and -0.103V and the reduction potential is at –0.874V vs. Fc^+/Fc. The nature of the voltammogram is similar to

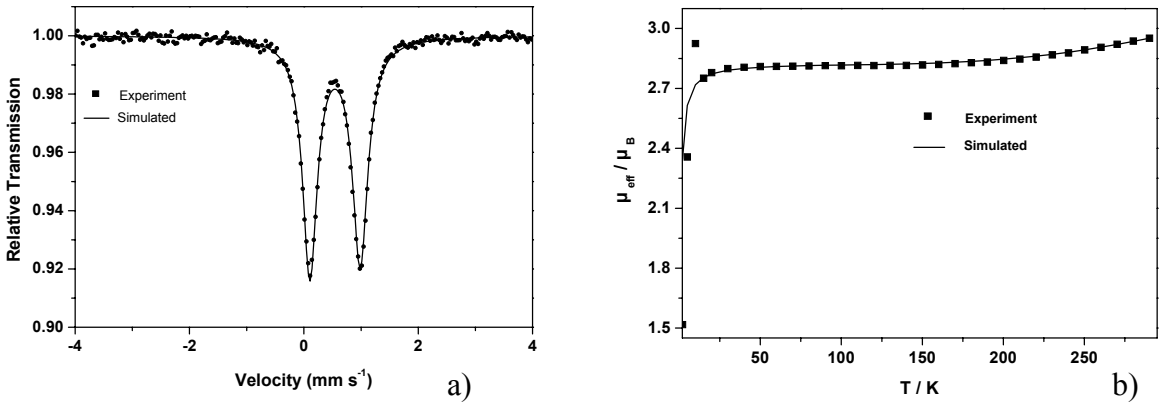

Figure 5.9:- (a) Mössbauer spectroscopy of **25**. b) Magnetic data of **25**.

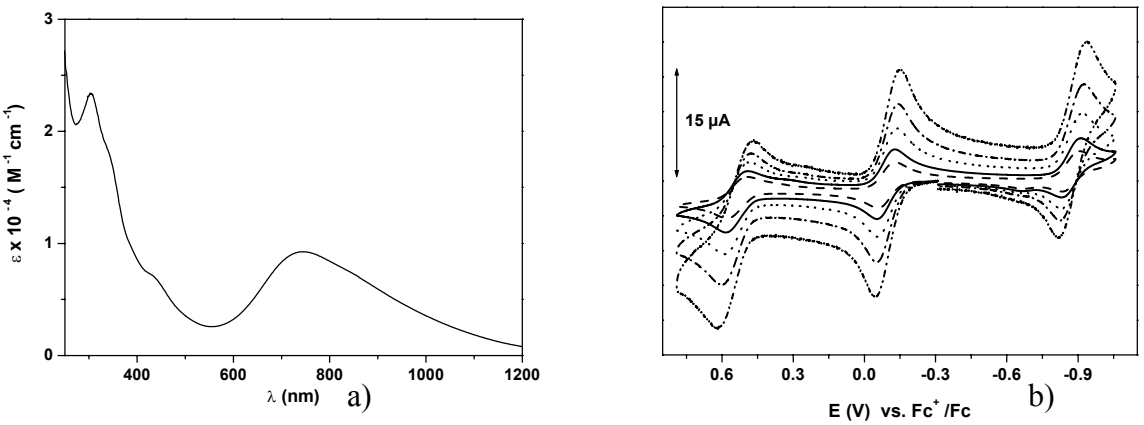

Figure 5.10:-a)Electronic spectra of **25**. b) Cyclic voltammogram at different scan rates of **25**.

that of **24**- however a shift of the waves to more positive values is observed for all three processes. In **25,** due to the strong -I effect of the fluro-group, the radical becomes less viable for oxidation to the quinone form and more viable for reduction to amino-phenolate. A fourth irreversible wave at -1.268 V (not shown) may involve a metal-centered reduction generating the Fe^{II} species.

$[(Fe^{III}L^{12}{}_2)_2(\mu\text{-}O)]$ (26)

Figure 5.11 shows the structure at 100K of a neutral complex in crystals of **26**•2.75CH_2Cl_2.[4] Both ferric ions are coordinated to two *o*-imino benzosemiquinonate(1-) π radical anions. This is conclusively deduced from the average C-N, C-C, and C-O distances which are identical within experimental error in each of the four ligands. They are the same as observed for the above iron complexes. The two halves $Fe^{III}(L^{ISQ})_2$ in dinuclear **26** are bridged by a nearly linear oxo group (Fe-O-Fe 175.2(2)^o) which is substantiated by the presence of asymmetric stretch peak in the IR at 842 cm^{-1}. This value fits well in the asymmetric stretch frequency vs. Fe-O-Fe angle plot from literature.[3] The two Fe-O_{oxo} distances are short at 1.775(2) Å and indicative of a strongly covalent bond with double bond character. This bonding situation has been observed in many dinuclear μ-oxo bridged complexes containing two high spin ferric ions (S_{Fe} = $^5/_2$).[3c] Table 5.7 summarizes Fe-O and Fe-N bond lengths in **26**. The average Fe-O_{rad} distance is 1.964 Å whereas the average Fe-N bond length is 2.061 Å. These data are in excellent agreement with the notion that complex **26** contain high spin ferric ions. *Complex **26** provides the **first example** of a structurally characterized μ-oxo(diferric) complex containing four organic ligand radicals.*

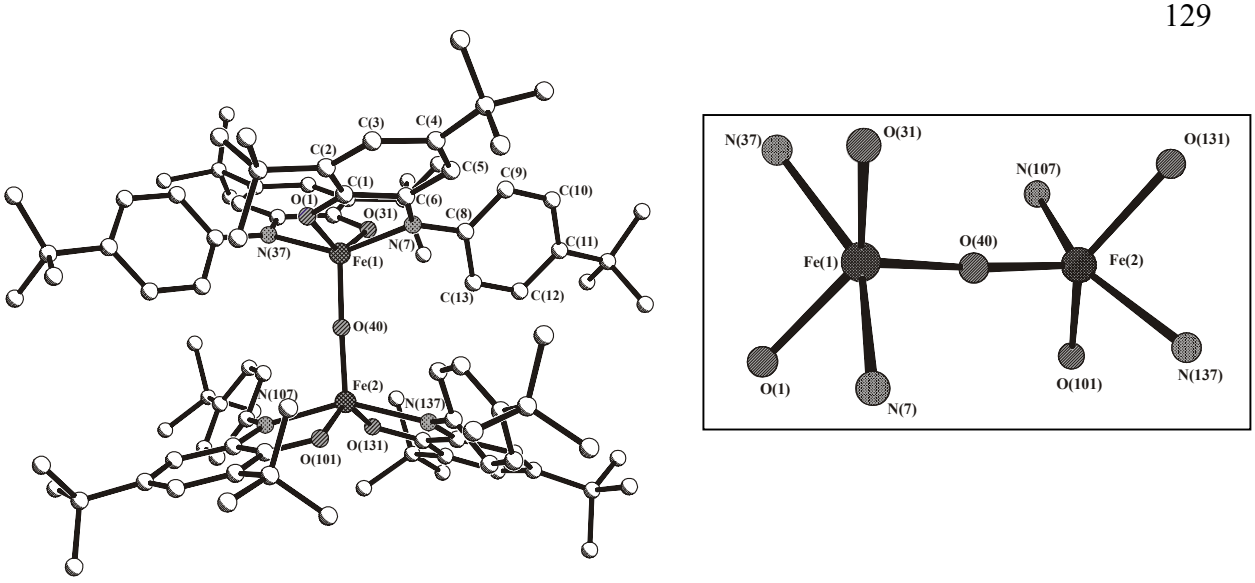

a) b)

Figure 5.11:-a)Molecular structure of **26**. b) Bonding environment at the Fe(III) centers in **26**.

Table 5.7:- *Selected bond distances(Å) and angles (degree) of **26**.*

Fe(1)-O(40)	1.776(2)		
Fe(1)-O(31)	1.968(2)	C(5)-C(6)	1.422(4)
Fe(1)-O(1)	1.970(2)	C(1)-C(6)	1.447(5)
Fe(1)-N(37)	2.051(3)	C(2)-C(3)	1.375(5)
Fe(1)-N(7)	2.057(3)	C(3)-C(4)	1.426(5)
Fe(2)-O(40)	1.775(2)	C(4)-C(5)	1.374(5)
Fe(2)-O(131)	1.958(2)		
Fe(2)-O(101)	1.961(2)	Fe(2)-O(40)-Fe(1)	175.21(15)
Fe(2)-N(107)	2.066(3)		
Fe(2)-N(137)	2.069(3)	O(40)-Fe(1)-O(31)	112.40(10)
O(1)-C(1)	1.296(4)	O(40)-Fe(1)-O(1)	110.92(10)
C(6)-N(7)	1.348(4)	O(31)-Fe(1)-O(1)	136.68(10)
O(31)-C(31)	1.300(4)	O(40)-Fe(1)-N(37)	106.84(11)
C(36)-N(37)	1.340(4)	O(31)-Fe(1)-N(37)	78.84(10)
O(101)-C(101)	1.299(4)	O(1)-Fe(1)-N(37)	88.94(10)
C(106)-N(107)	1.349(4)	O(40)-Fe(1)-N(7)	105.10(10)
O(131)-C(131)	1.292(4)	O(31)-Fe(1)-N(7)	90.04(10)
C(136)-N(137)	1.345(4)	O(1)-Fe(1)-N(7)	78.76(10)
C(1)-C(2)	1.434(4)	N(37)-Fe(1)-N(7)	148.04(11)

The notion of the presence of high spin ferric ions in **26** is corroborated by their Mössbauer spectra at 80 K . From simulation of this spectra, an isomer shift, δ, of 0.38 mms^{-1} and quadrupole splitting, ΔE_Q, of 1.105 mms^{-1} [Figure 5.12(a)] was obtained. The fact that the isomer shift decreases from 0.545 mms^{-1} for octahedral **25** to 0.38 mms^{-1} for five-coordinate **26** is rationalized by an increasingly covalent character of the iron-to-ligand bonds; in **26** it is dominated by the covalently bound oxo bridge.

Figure 5.12(b) exhibits the temperature dependence of the magnetic moment of dinuclear **26** in the range 2 - 290 K. It has been possible to fit the behavior successfully by using a model which invokes very strong intramolecular antiferromagnetic coupling between high spin ferric ions ($S_{Fe}= {}^5/_2$) and - in each case - two o-iminosemiquinonate π radicals

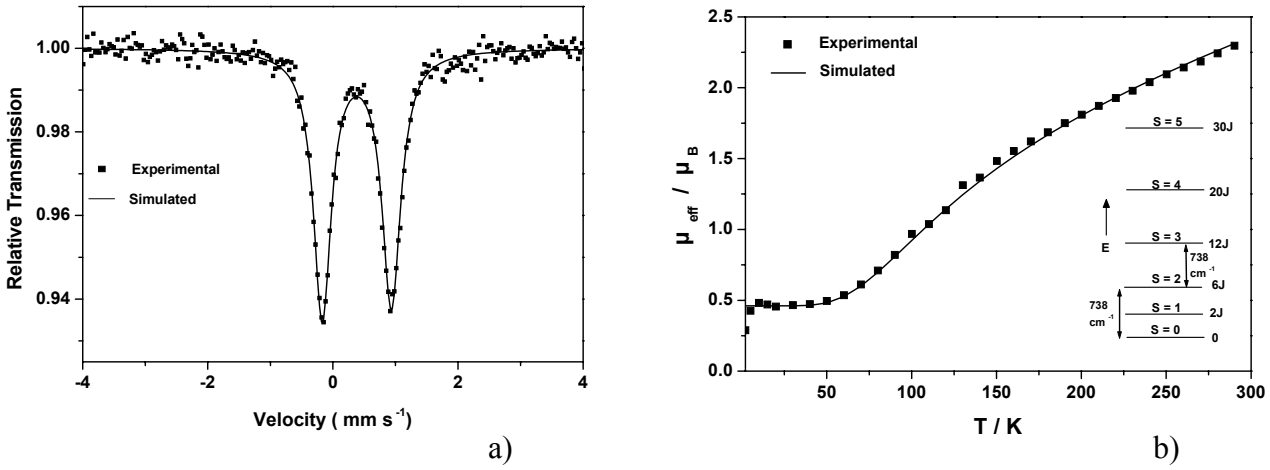

Figure 5.12:- a) Mössbauer spectrum of **26**. b) Magnetic data of **26** (inset: Energy levels of the spin states).

yielding a fictitious S* = $^3/_2$ state at each iron ion. The two halves of **26** are then coupled through the μ-oxo group. Thus, using the spin Hamiltonian H= -2J $S_1 \bullet S_2$ ($S_1 = S_2 = {}^3/_2$), yields the following parameters: J = - 123(5) cm^{-1}, g = 2.0 (fixed). A mononuclear paramagnetic impurity of 0.6% (S = $^5/_2$) was included. Thus, a moderately strong antiferromagnetic coupling between the two halves in **26** prevails yielding the observed singlet ground state.

That the S = 3 state remains depopulated even at the highest temperature of the susceptibility measurement and only upto the S =2 state is populated is established by simulating the magnetic data considering another fictitious S* = 1 (S_t = 0, 1, 2) state at each iron centre. A good fit can be obtained (not shown). However, if S* = ½ is considered at each iron center (S_t = 0,1), no reasonable fit was obtained. Thus population occurs till S = 2, which is separated at 738 cm^{-1} from the singlet state [Figure 5.12(b) (Inset)].

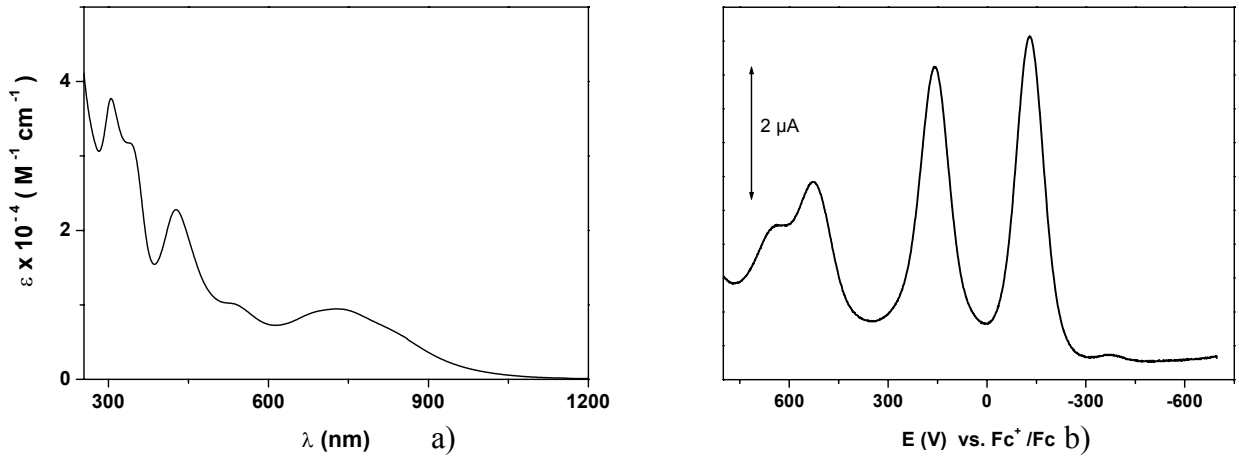

Figure 5.13 :- a) Electronic spectra of **26**. b) Square wave voltammogram of **26**.

Figure 5.13(a) displays the electronic spectrum of **26** in CH_2Cl_2 solution. Interestingly, the spectrum is very similar to **24** and **25** and indicates the presence of $Fe^{III}(L^{ISQ})_x$ units (ISQ-imino-benzosemiquinone ; x = 2 or 3).

A few electrochemical experiments with a dichloromethane solution of **26** in presence of 0.1M $TBAPF_6$ were performed. The square wave voltammogram [Figure 5.13(b)] shows two reversible oxidation peaks at –0.26V, +0.153V and broad peaks at 0.512V and 0.617V vs. Fc^+/Fc. All these processes can be attributed to ligand centered radical oxidations. An irreversible peak (not shown) appears at –1.219V vs. Fc^+/Fc and is ascribed to the metal centered reduction.

In this chapter, the aniline ring of the ligand 2-anilino-4,6-ditert-butylphenol is substituted at different position by different groups and the synthesis and characterization of transition metal complexes is discussed. Although the difference in structural as well as spectroscopic property could be attributed to the stereochemical effects, electronic effects could also play a significant role for such a behavior. Theoretical study is needed in order to explain the results.

References

1. a)H. Chun, C. N. Verani, P. Chaudhuri, E. Bothe, E. Bill, T. Weyhermüller, K. Wieghardt, *Inorg. Chem.,* **2001**, 40, 4157. b) K. S. Min, T. Weyhermüller ,K. Wieghardt, *Dalton Trans.,* **2003**, 1126. c) H. Chun, T. Weyhermüller, E. Bill, K. Wieghardt, *Angew. Chem.,Int. Ed.*, **2001**, 40, 2489.d) C. N. Verani, S. Gallert, E. Bill, T. Weyhermüller, K. Wieghardt ,P. Chaudhuri, *Chem. Commun.,***1999**,1747.
2. a) D. A. Summerville, I. A. Cohen, K. Hatano, W. R. Scheidt, *Inorg. Chem.* **1978**, 17, 2906.b) W. R. Scheidt, C. A. Reed, *Chem. Rev.* **1981**, 81, 543; c) M. M. Maltempo, *J. Chem. Phys.* **1974**, 61, 2540; d) M. E. Kastner, W. R. Scheidt, T. Mashiko, C. A. Reed, *J. Am. Chem. Soc.* **1978**, 100, 666; e) P. Gans, G. Buisson, E. Duée, J.-R. Regnard, J.-C. Marchon, *J. Chem. Soc. Chem. Commun.* **1979**, 393.
3. a)J. Sanders-Loehr, W. D. Wheeler, A. K. Shiemke, B. A. Averill, T. M. Loehr, *J. Am. Chem. Soc.* **1989**, 111, 8084. b) J. E. Plowman, T. M. Loehr, C. K. Schauer, O. P. Anderson, *Inorg. Chem.* **1984**, 23, 3553. c) D. M. Kurtz, Jr., *Chem. Rev.* **1990**, 90, 585.
4. S. Mukherjee, T. Weyhermüller, K. Wieghardt, P. Chaudhuri, *Dalton Transactions* , **2003**, 3483.

Chapter 6
CONCLUSIONS AND PERSPECTIVES

6.1 Conclusions

The attempt to coalesce two different subjects viz. bio-inorganic chemistry and molecular magnetism have been the main goal of this work. The complexes have interesting magnetic properties and some act as structural as well as functional models for some metalloenzymes. The main information and conclusions concerning this work are summarized and some perspectives are suggested.

Chapter 2

The ligands H_3L^1 and H_3L^2 act as a backbone for the synthesis of polynuclear complexes. The ligand H_2L^1 was found to be "non-innocent" and form radicals in air. With H_2L^1

- Two new tetrameric, isostructural nickel(II)(**1**) and copper(II)(**2**) complexes have been synthesized with the metals in a *butterfly*-formation. The imidazolate-group acts as a bridge between the two metal centers.
- The nickel complex (**1**) is diamagnetic.
- The magnetic data of the copper complex (**2**) exhibits anti-ferromagnetic coupling between the copper centers with the coupling constant of -49 cm^{-1}. This value is relatively high from other reported imidazolate-bridged copper complexes.
- The EPR spectrum of **2**, at different temperatures, were recorded. A plot of IT vs. T and its fit show that the value of the coupling constant is -42 cm^{-1} close to that obtained from the magnetic susceptibility measurements (-49 cm^{-1}).

With the dinucleating ligand H_2L^2, ten new dinuclear and tetranuclear complexes with 3d-transition metal ions were synthesized.

- The dinuclear nickel (II) complex(**3**) has been synthesized where a single-atom oxygen of urea bridges the two nickel atoms. The Ni…Ni bond distance at 2.966(1) Å is significantly shorter than those observed in comparable complexes. This complex acts as a structural model for the dinickel containing enzyme *urease*.
- Electronic spectra of **3** shows the three lower energy bands along with intense π-π* transitions below 480 nm, attributable to the ligand.
- The magnetic susceptibility data for **3** exhibits an antiferromagnetic exchange coupling between two paramagnetic Ni(II) ($S_{Ni} = 1$) centers ($J = -3.5$ cm^{-1}).
- However, **3** is not able to catalyze the ethanolysis of urea presumably because of the hydrogen bonding network involving urea in **3**, which is also maintained in solution.

- **4** consist of a low-symmetry cubane core with differing Ni•••Ni distances and Ni-O-Ni angles.
- The couplings in **4** is dominated by a ferromagnetic exchange interaction between four $^3A_2$ nickel(II) ions. The observation of three discrete exchange parameters for **4** is consistent with the lower symmetry of the cubane. A plot of J vs Ni-O-Ni angles indicates that the symmetry of the cubane core has a profound effect on the magnetostructural correlation. Thus more such distorted cubanes of Ni(II) are warranted to solve this open question.
- Complex **5** consists of a (μ-methoxo)(μ-phenoxo)dicopper(II) unit and belongs to an ubiquitous class of coordination complexes for copper(II).
- The magnetic properties of **5** are antiferromagnetic with J value of -192 cm^{-1} and are in agreement with the paramagnetic copper(II) centers with the ($d_{x^2-y^2}$) magnetic orbitals.
- The redox processes as observed from the cyclic voltammograms were assigned to ligand-centered oxidation yielding phenoxyl radical in the complex.
- Complex **6**, [$L^2_2Cu_4(\mu_4$-O)] is the ***first example*** of a (μ_4-oxo)tetranuclear copper(II) without any bridging ligand between the tetrahedral edges.
- The simulation of the magnetic data affords an overall anti-ferromagnetic interaction in **6**. In accordance with the three averaged Cu-O-Cu angles of 90°, 99.5° and 121.3°, a three-J model was used to analyze the magnetic data. It is interesting to note that an exchange coupling constant J_{14} corresponding to the Cu-O-Cu angle of 90° could not be evaluated. The other J values are -122 cm^{-1} and –90 cm^{-1}.
- Cyclic voltammetry of **6** shows a redox wave at +0.523 V which is assigned to the oxidation of the ligand to phenoxyl radical.
- This ligand can adapt itself to various metal ion sizes to yield dinuclear complexes. It makes a versatile building block for the construction of dimetal complexes, which might be models for the study of biologically relevant dinuclear complexes as has been shown from complexes **7-11**. Although this dinucleating ligand has the intrinsic property to complex metal ions of the first transition series mostly in a six-coordinate fashion, however electronic preferences, e.g., Jahn-Teller effect, absence of LFSE, can override this proclivity as is evidenced by the square-pyramidal 5-coordinated V(IV) (**10**) and V(V) (**11**) complexes.
- The magnetic exchange values for complexes **7-11** show that the coupling is anti-ferromagnetic between the paramagnetic centers.

- The electrochemical results for **7-11** suggest the generation of ligand-centered oxidation processes attributable to the phenoxyl radicals, rather than the formation of unusually high oxidation states at the central metal centers.

Chapter 3.

The ligand H_4L^3 is dinucleating and "non-innocent" with the amine groups at 1,3 positions. This serves as a backbone in attempting to induce ferromagnetic coupling between the dinucleating centers or the radical centers by ***spin polarization***. For H_4L^4, the methylene bridge between the two phenyl rings inhibits spin polarization. The complexes synthesized contain either ***four*** or ***six*** imino-benzosemiquinone radicals.

- The copper(II)(**12)** and Mn(IV)(**16**) complex consists of ***four*** imino-benzosemiquinone radicals. Thus **12** and **16** are the dimers containing *m*-phenylene bridges of the analogous mononuclear Cu(II) and Mn(IV) complexes with the ligand 2-anilino-4,6-di-*tert*-butylphenol.
- The magnetic data simulation for **12** shows that the antiferromagnetic coupling between the radicals are strong throughout the whole temperature range. However, no coupling was observed between the two copper centers. For **16**, the coupling between the radicals and the 3d-electrons at each 'part' is anti-ferromagnetic; very weak coupling was observed between the residual fictitious two S= ½ centers. Improper mixing between the respective d-orbitals with that of the p(π)-orbitals of the nitrogen atom is a probable reason.
- Electrochemistry of both the dimers show interesting redox properties, all ascribed to the oxidation or reduction of the radical centers.
- The dimeric cobalt(III)(**14**) and iron(III)(**15**) complexes consist of ***six*** imino-benzosemiquinone radicals. Each metal center is six-coordinated with three radicals residing at each 'part' of the dimer.
- Magnetic susceptibility studies show that for **14**, the interaction between the three radical centers at each 'part' is anti-ferromagnetic and a fictitious spin of ½ is obtained. These two parts couple ferromagnetically giving a ground state of S_t=1. For **15**, the coupling between the radical and the d-electrons of Fe(III) is strongly anti-ferromagnetic. The residual $S_{Residual}$=1 spin at each part interacts with each other ferromagnetically and a ground state of S = 2 is obtained. Thus molecules with high spins are possible using the ligand H_4L^3.

- Electrochemistry of **14** and **15** shows a number of oxidation and reduction peaks, all attributed to radical centered oxidation or reduction.

Chapter 4.

A reactivity study using **12** and **16** as catalyst and 3,5-ditert-butylcatechol as substrate is discussed in this chapter.

- **12** and **16** can catalyze the aerial oxidation of catechol to quinone; **16**, is a better catalyst than, **12**, for the aerial oxidation of catechol to quinone, thus mimicking the function of catechol oxidase.
- The maximum turnover number obtained when **16** was used as a catalyst is 500. For **12**, it is only 8.
- The rate law for this reaction was found to be first order for the catalyst concentration and first order for the substrate concentration; rate = k [catalyst][substrate].
- The monomeric Mn(IV) complexes(**16*,18-22**), containing two imino-benzo-semiquinone radicals, also catalyze the oxidation of 3,5-ditert-butylcatechol to 3,5-ditert-butyl-ortho-benzoquinone. The rate constants (k_{sub}) were measured and it was found out that the velocity was the fastest, when **22** was used as catalyst.
- An outer sphere reaction mechanism is probable and is in conform with the electrochemical data.

Chapter 5.

The substitution effect at the meta- and para- positions of the aniline ring of the parent ligand 2-anilino-4,6-di-*tert*-butylphenol have been discussed in this chapter. A Co(III) along with three Fe(III) complexes have been synthesized using these ligands.

- The cobalt(III) complex with the ligand H_2L^6(**23**), consists of three imino-benzosemiquinone radicals. Magnetic susceptibility data and its simulation show that the radicals are coupled ferromagnetically with a total spin of $S_t = {}^3/_2$.
- The crystal structure for the iron(III) complex with H_2L^6(**24**) at 100K, again shows the presence of three imino-benzosemiquinone radicals; however the metal-donor bond lengths are much shorter than that for high spin Fe(III) complex with the ligand 2-anilino-4,6-di-*tert*-butylphenol.
- Magnetic susceptibility data of **24** exhibits a thermally induced HS $\Leftrightarrow$ LS spin transition. The ground state is $S_t = 0$ and that at room temperature is $S_t = 1$. The crystal structure of **24**, at room temperature, shows that the bond distance between the metal-donor atoms is consistent for a high spin Fe(III).

- Mössbauer measurements at 80K as well as 297K for **24** supports the spin transition phenomenon.
- The Fe(III) complex with the ligand H_2L^{11}(**25**), shows the typical characteristics of the iron(III) complex with the ligand 2-anilino-4,6-di-*tert*-butylphenol. The complex consists of three imino-benzosemiquinone radicals and the ground state is S = 1 arising due to the antiferromagnetic coupling of the three radicals with the d^5 electron at the iron center.
- A μ-oxo diferric complex (**26**) was obtained when H_2L^{12} was used as the ligand. Each iron center is in the high spin state and is five coordinated. The complex consists of four imino-benzosemiquinone radicals. Magnetic data and its simulation afford a coupling constant value of -123 cm^{-1} which is comparable with those of other μ-oxo diferric complexes. *Complex **26** provides the **first example** of a structurally characterized* μ*-oxo(diferric) complex containing four organic ligand radicals.*
- Electrochemistry of all the above complexes show mainly ligand centered redox processes.

6.2 Perspectives.

A few ideas and perspectives, in the continuation of this work, are outlined below.

- The synthesis of complexes with redox-active ligands play a very important role in bio-inorganic chemistry as well as in molecular magnetism. The "Robson type" of ligands, which have been used for synthesizing homo- and hetero- polynuclear complexes, can be modified in order to synthesize complexes which can act as structural model for various metalloenzymes.
- The knowledge of radical-metal interactions can be widened by synthesizing complexes where the number of radicals, as well as metal centers, may be increased. Conjoining *spin polarization* may help in synthesizing molecules with larger spins. The ligand, obtained by the condensation of 1,3,5-triamino-benzene with 3,5-ditert-butylcatechol may serve both a ferromagnetic coupler (1,3,5 position) and as a redox active ligand.
- The radical complexes can be tested further as catalyst for oxidative reactions.
- Several different ligands could be synthesized by the condensation with 3,5-ditert-butylcatechol with the ring substituted anilines. Transition metal complexes with these ligands will probably show interesting structural as well as spectroscopic characteristics.

Chapter 7

EQUIPMENT AND EXPERIMENTAL WORK

7.1 METHODS AND EQUIPMENTS

All the analyses were performed at the Max-Planck-Institut für Bioanorganische Chemie, Mülheim an der Ruhr, unless otherwise mentioned. Commercial grade chemicals were used for the synthetic purposes and solvents were distilled and dried before use.

Infrared Spectroscopy

Infrared spectra were measured from 4000 to 400 cm^{-1} as KBr pellets at room temperature on a '*Perkin-Elmer* FT-IR-Spectrophotometer 2000'.

NMR Spectroscopy

^{1}H- and ^{13}C- NMR spectra were measured using a '*Bruker* ARX 250, DRX 400 or DRX 500'. The spectra were referenced to TMS, using the ^{13}C or residual proton signals of the deuterated solvents as internal standards. $VOCl_3$ was used as reference in ^{51}V NMR spectra.

Mass Spectroscopy

Mass spectra in the Electron Impact mode (EI; 70 eV) were recorded on a Finnigan MAT 8200 mass spectrometer. Only characteristic fragments are given with intensities. The spectra were normalised against the most intense peak having intensity 100. Electron Spray Ionization (ESI) mass spectra were recorded either on a Finnigan Mat 95 instrument or a Hewlett-Packard HP 5989 mass spectrometer. ESI- and EI- spectra were measured by the group of Dr. W. Schrader at the Max-Planck-Institut für Kohlenforschung, Mülheim an der Ruhr.

Elemental Analysis

The determination of the C, H, N and metal content of the compounds was performed by the ' Mikroanalytischen Labor H. Kolbe', Mülheim an der Ruhr, Germany.

UV-vis Spectroscopy

UV-Vis spectra were recorded on a '*Perkin-Elmer* UV-vis Spectrophotometer Lambda 19'or on a Hewlett-Packard HP 8452A diode array spectrophotometer in the range 200-1200 nm. For UV-vis spectro-electrochemical investigations the HP 8452A diode array spectrophotometer was used, by employing a coulometry cuvette and Bu_4NPF_6 as supporting electrolyte.

Electrochemistry

Cyclic voltammetry, square wave voltammetry and linear sweep voltammetry experiments were performed using an 'EG&G Potentiostat / Galvanostat 273A'. A standard three-electrode-cell was employed with a glass-carbon working electrode, a platinum-wire auxiliary electrode and Ag/AgCl (saturated LiCl in EtOH) reference electrode. Measurements were made under an inert atmosphere at room temperature. The potential of the reference electrode was determined using Fc^{+}/Fc as the internal standard.

Magnetic Susceptibility Measurements

The measurements of the temperature or field dependent magnetization of the sample were performed in the range 2 to 295 K at 1,4 or 7 T on a '*Quantum Design* SQUID-Magnetometer MPMS'. The samples were encapsulated in gelatin capsules and the response functions were measured four times for each given temperature, yielding a total of 32 measured points. The resulting volume magnetization from the samples had its diamagnetic contribution compensated and was recalculated as volume susceptibility. Diamagnetic contributions were estimated for each compound by using Pascal's constants. The experimental results were fitted with the programme JULIUS calculating through full-matrix diagonalzation of the Spin-Hamiltonian. The following Hamiltonian-operators were used:

$H_{ZE} = \mu_B \sum g_i \hat{S}_i \,.\mathbf{B}$

$H_{HDVV} = -2 \sum J_{ij} \hat{S}_i \,.\, \hat{S}_j$

$H_{ZFS} = \sum D_i[\hat{S}_{iz}^2 - \{S_i(S_i+1)/3\} + E_i/D_i(\hat{S}_{ix}^2 - \hat{S}_{iy}^2)]$

Indexes i,j indicate individual spins. For the magnetic measurement the calculated g values obtained during simulation is the isotropic.

EPR Spectroscopy

First derivative X-Band EPR spectra of powdered or frozen solution samples were measured with a '*Bruker* ESP 300 Spectrometer' coupled to an '*Oxford Instruments* ESR 910-Cryostat'. Spin-Hamiltonian simulations of the EPR spectra were performed with a program which was developed from the S = 5/2 routines of Gaffney and Silverstone and which specifically makes use of the resonance search procedure based on a Newton-Raphson algorithm as described therein.

^{57}Fe-Mössbauer Spectroscopy

^{57}Fe-Mössbauer spectra were measured with an *Oxford Instruments* Mössbauer spectrometer in the constant acceleration mode. ^{57} Co/Rh was used as the radiation source. The minimum experimental linewidths were 0.24 mm/s. The temperature of the sample was controlled by an '*Oxford Instruments* Variox Cryostat'. Isomer shifts were determined relative to α-iron at 300K. The measurements were carried out at 80K and 100K with solid samples containing the isotope ^{57}Fe.

Crystallography

X-ray diffraction data were collected on an '*Enraf-Nonius* CAD4 Diffractometer' or on a '*Siemens* Smart System'. Graphite-monochromatized Mo-Kα with λ = 0.71073 Å was employed. Data were collected by the 2θ-ω scan method ($3 \leq 2\theta \leq 50°$). The data were corrected for absorption and Lorenz polarization effects.The structures were solved by direct methods and subsequent Fourier-difference techniques, and refined anisotropically by full-matrix least-squares on F^2 with the program SHELXTL PLUS. Hydrogen atoms were included at calculated positions with $U < 0.08$ Å^2 in the last cycle of refinement.

GC / GC-MS Analysis

GC of the organic products were performed either on HP 6890 instruments using RTX-5 Amine 13.5 m S-63 columns respectively. GC-MS was performed using the above column coupled with a HP 5973 mass spectrometer with mass selective detector.

LC Analysis

LC of the complexes were performed on HPLC instrumentation using a Gilson M305 pump, and the Diode-Array-Detector (DAD) SPDM 10 AV (Shimadzu corporation). MeOH and water in the ratio 3:1 with flow velocity 0.8 ml/ min was used as eluent through a Luna-5 phenylhexyl column.

7.2 SYNTHESIS

7.2.1 LIGANDS

Preparation of 2,4-Di-tert-butyl-6-[(5-methyl-3H-imidazol-4-ylmethyl)-amino]-phenol [H_3L^1]

To de-aerated methanol (50 ml),2.2 gms (10 mmole) of 2-Amino-4,6-di-tert-butyl-phenol and 1.1 gms (10 mmole) of 5-Methyl-3H-imidazole-4-carbaldehyde was added and the whole solution was refluxed for 2 hours under Argon. The red solution was cooled and $NaBH_4$ was added portion wise till the solution turns faint yellow. Drop wise addition of water initiates the precipitation of a white solid . The white solid was collected and dried under vacuum.

Yield : 2.8 gms (89 %)

MP: 186°C

Molecular Weight: 315.46 g/mol $C_{19}H_{29}N_3O$

Elemental Analysis:

	%C	%H	%N
Calculated	72.34	9.27	12.84
Found	71.0	8.2	12.8

Infrared Spectrum:

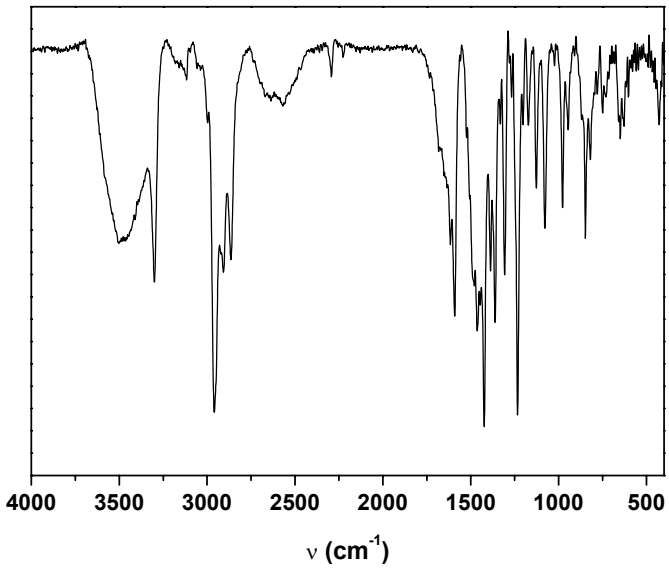

^{1}H NMR (DMSO-d6): δ 1.21(s, 9H), 1.31(s,9H), 2.15(s,3H), 4.02(s,2H), 6.5(t,2H), 7.4 (s, 1H)

^{13}C-NMR (DMSO-d6) : δ 30.0 (s), 31.6 (s), 34.1 (s), 34.5(s), 48.6(s), 107.5(s), 111.1(s), 133.2(s), 136.3(s), 140.3(s), 141.9(s)

Synthesis of 2,6-Bis-iminomethyl-(4,6-di-tertbutyl-2-iminophenol)-4-methyl-phenol (H_3L^2)

In 70 ml of de-aerated methanol, 2,6-Diformyl p-cresol (1.6 gm, 10 mmole) and 2,4 Di-tert Butyl-o-amino phenol (4.4 gm, 20 mmole) was added and the whole solution was refluxed for 1 hour. The solution colour changes to deep red from where yellow microcrystalline compound precipitates. The solution was cooled , filtered and the residue was washed with cold methanol.

Yield: 5.1 gm (90 %).

MP: 192 °C

Molecular Weight :- 570.82 $C_{37}H_{50}N_2O_3$

Elemental Analysis:

	%C	%H	%N
Calculated	77.85	8.83	4.91
Found	77.7	8.7	4.8

Infrared Spectrum:

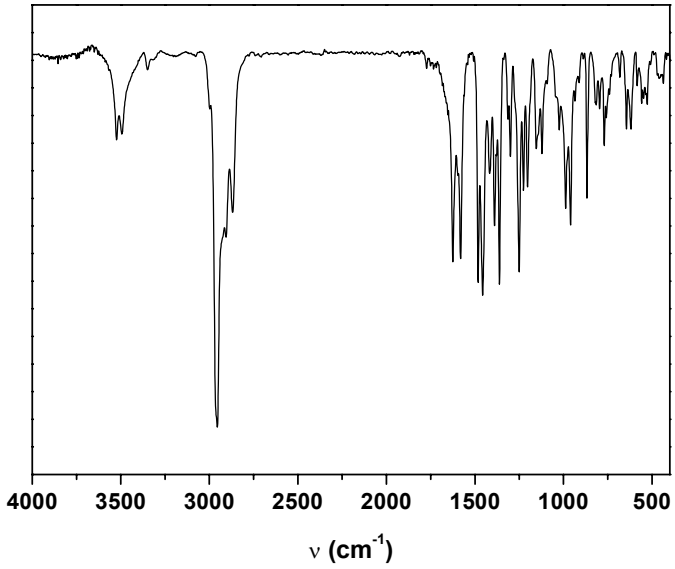

^{1}H NMR Data ($CDCl_3$):

δ 1.32 (s,18H), 1.43 (s,18H), 2.38 (s,3H,), 8.94(s,2H), 7.26 (m,4H), 7.12(d,2H).

^{13}C NMR ($CDCl_3$):

δ 29.4 (s), 51.6 (s), 34.6 (s,), 35.0(s,),111.4(s), 121.9(s), 123.4(d), 128.8(s), 133.8(s), 135.1(d), 142.1(s), 147.5(s), 158.8(s)

Preparation of 1,3-bis-(4,6-di-tert-butyl-2-iminophenol)benzene (H_4L^3)

To 150 ml of n-heptane, 3,5 Di-tert-Butyl Catechol (14.4 gm; 65 mmole) was added along with 2 ml of NEt_3.To this stirred solution, 1,3 phenylene diamine (3.24 gm; 30 mmole) was added and the whole solution was refluxed for three hours. It was cooled and stirred in a closed vessel for 2 days. It was filtered and the light grey solid residue was washed with cold n-pentane.

Yield : 15 gm (96 %)

MP : above 200°C

Molecular Weight : 516.77 $C_{34}H_{48}N_2O_2$

Elemental Analysis:

	%C	%H	%N
Calculated	79.02	9.36	5.42
Found	79.0	9.4	5.3

Infrared Spectrum :

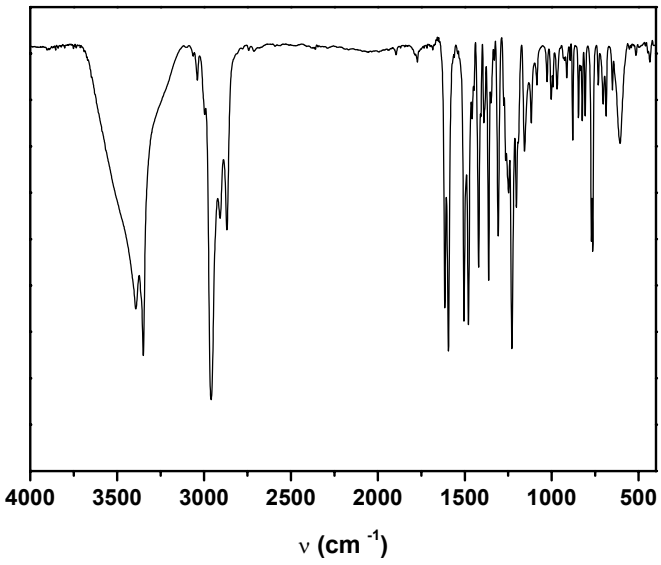

^{1}H NMR ($CDCl_3$):

δ 1.22 (s, 18H), 1.37 (s, 18H), 6.12 (s, 1H), 6.25 (d, 2H), 7.02 (d, 3H), 7.18 (d, 2H).

^{13}C-NMR ($CDCl_3$):

δ 29.28, 31.33, 34.12, 34.74, 121.27, 122.20, 126.86, 141.1, 148.83

Preparation of 4,4´-bis-(4,6-di-tert-butyl-2-iminophenol)diphenyl methane (H_4L^4)

To 90 ml of n-heptane, 3,5 Di-tert-Butyl Catechol (6.6 gm; 30 mmole) was added along with 0.8 ml of NEt_3.To this stirred solution, 4,4´-diaminodiphenyl methane(2 gm; 10 mmole) was added and the whole solution was refluxed for three hours. It was cooled and stirred in a closed vessel for 2 days. It was filtered and the light grey solid residue was washed with cold n-pentane.

Yield :- 5 gms (89 %)

MP: above 200°C

Formula Weight :- 606.89 $C_{41}H_{54}N_2O_2$

Elemental analysis:

	%C	%H	%N
Calculated	81.14	8.97	4.62
Found	80.7	9.0	4.7

Infrared Spectrum:

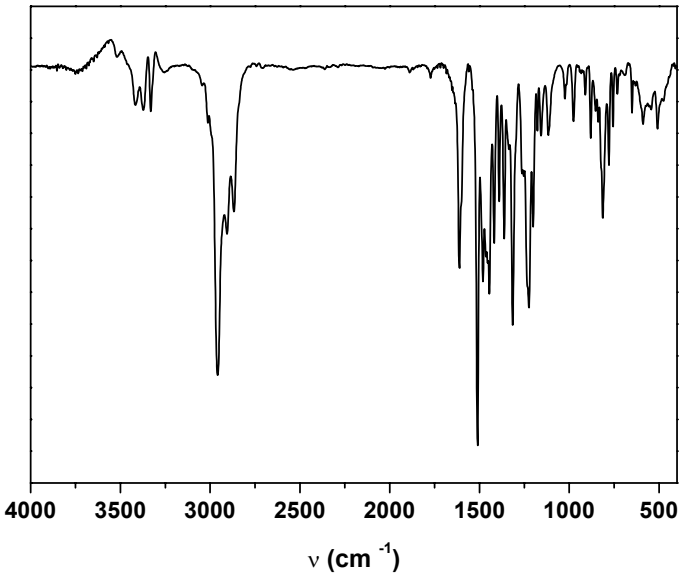

^{1}H NMR ($CDCl_3$):

δ 1.24 (s, 18H), 1.41 (s, 18H), 3.77 (d, 2H), 6.60 (p, 4H), 7.0 (p , 6H), 7.18 (d, 2H)

^{13}C-NMR ($CDCl_3$)

δ 29.5(s), 30.1(s), 31.6(s), 34.3(s), 34.9(s),115.2(d), 121.3(s), 121.8(s), 129.6(s), 142.1(s), 144.8(s), 149.3(s).

Preparation of H_2L^{6-12}

As the di-substituted or mono-substituted ligands were prepared by similar protocol, a representative method is only described. A solution containing 3,5-di-tertbutylcatechol, the substituted anilines(1:1) and triethylamine in n-heptane was refluxed for 3 hours, cooled, filtered and then concentrated. Colorless crystalline solid precipitates which was filtered and washed with cold n-pentane.

	Yield (gms)/(%)	Melting point (°C)	Molecular Weight	Molecular formula
H_2L^6	6.20 (75 %)[a]	180	409.66	$C_{28}H_{43}NO$
H_2L^7	3.42 (40%)[a]	158	433.44	$C_{22}H_{25}F_6NO$
H_2L^8	4.25(65%)[a]	164	325.49	$C_{22}H_{31}NO$
H_2L^9	4.49(61%)[a]	175	366.33	$C_{20}H_{25}Cl_2NO$
H_2L^{10}	10.99(77%)[b]	132	357.49	$C_{22}H_{31}NO_3$
H_2L^{11}	9.09(68%)[b]	154	333.42	$C_{20}H_{25}F_2NO$
H_2L^{12}	12 (68%)[c]	173	353.55	$C_{24}H_{35}NO$

a) 3,5-ditert-butylcatechol (4.4gm;20mmole), substituted aniline (20mmole),0.2ml NEt_3, 40ml heptane.

b) 3,5-ditert-butylcatechol (8.8gm;40mmole), substituted aniline (40mmole),0.5ml NEt_3, 40ml heptane.

c) 3,5-ditert-butylcatechol (11.1gm;50mmole), 4-tertbutylaniline (7.46gm;50mmole),0.5ml triethylamine, 60ml heptane.

Synthesis of H_2L^5 is already described [Reference 4(a), Chapter 3].

NMR Data

[^{1}H ($CDCl_3$)]

	δ
H_2L^6	1.26(s, 27H), 1.44(s ,9H), 5.02(s, 1H), 6.23(s, 1H), 6.54(s, 1H), 6.92(m, 1H), 7.06(m, 1H), 7.17(s, 1H)
H_2L^7	1.26(s ,9H), 1.43(s, 9H), 5.44(s, 1H), 5.94(b, 1H), 7.06(m, 3H), 7.28(s, 2H)
H_2L^8	1.38(s,9H), 1.57(s,9H), 2.32(s, 6H), 4.93(b,1H), 6.4(s,2H), 6.61(s,1H), 7.15(s,2H), 7.35(s,1H)
H_2L^9	1.26(s, 9H), 1.42(s, 9H), 5.08(s, 1H), 6.06(s, 1H), 6.52(m, 2H), 6.81(b, 1H), 6.96(b, 1H), 7.24(s, 1H)
H_2L^{10}	1.24(s, 9H), 1.41(s, 9H), 3.70(s, 6H), 5.01(s, 1H), 5.83(b, 2H), 5.98(b, 1H), 7.02(b, 1H), 7.18(b, 1H)
H_2L^{11}	1.26(s, 9H), 1.42(s, 9H), 5.15(s, 1H), 6.1(m, 3H), 6.26(m, 1H), 6.98(d, 1H), 7.24(s, 1H)
H_2L^{12}	1.33 (s, 9H), 1.38 (s, 9H), 1.56 (s,9H), 4.95 (s, 1H), 6.70 (d, 2H), 7.14 (d, 1H), 7.33 (s, 1H), 7.34 (m, 2H)

7.2.2 COMPLEXES

Synthesis of $Ni^{II}_4L^1_4$ (1)

The ligand (1 mmole; 315 mg) was dissolved in 25 ml of de-aerated methanol. Solid $[Ni(H_2O)_6](ClO_4)_2$ (1mmole;365mg) was added along with NEt_3 (0.15 ml).The light orange-red solution was refluxed for 1 hour under Argon, cooled and then stirred in air for 30 minutes from where orange-red microcrystalline solid precipitated .The solid was filtered, dried and recrystallised from Dichloromethane-Methanol.

Yield: 210mg (58%)

Molecular Weight: 1480.47 $C_{76}H_{100}N_{12}O_4Ni_4$

Elemental Analysis:

	%C	%H	%N	%Ni
Calculated	61.66	6.81	11.35	15.86
Found	58.74	5.83	10.71	14.47

Infrared spectrum:

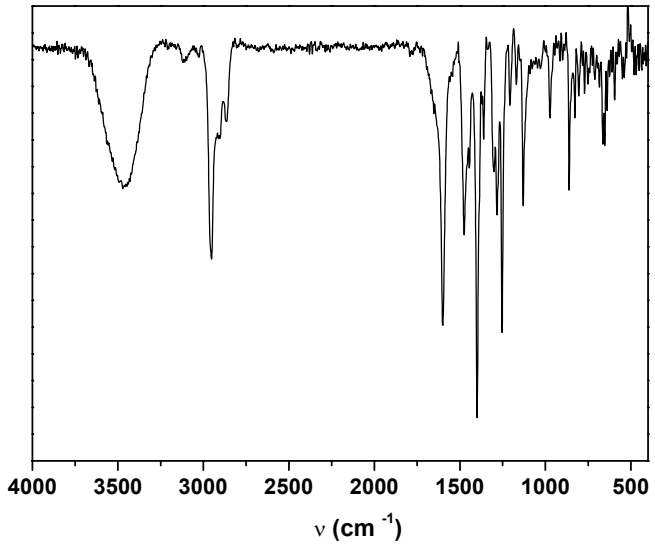

Synthesis of $Cu^{II}_4L^1_4$ (2)

The ligand (155 mg;0.5 mmole) was dissolved in 15 ml of methanol. Solid $Cu(OAc)_2.4H_2O$ (0.5mmole;100mg) was added along with NEt_3 (0.15 ml).The light orange-red solution was refluxed for 1 hour under Argon, cooled and then stirred in air for 30 minutes from where orange-red microcrystalline solid precipitated .The solid was filtered, dried and recrystallised from THF-Methanol.

Yield: 120mg (64%)

Formula Weight: 1499.89 $C_{76}H_{100}N_{12}O_4Cu_4$

Elemental Analysis:

	%C	%H	%N	%Cu
Calculated	60.86	6.72	11.21	16.95
Found	59.8	6.6	11.1	17.3

Infrared spectrum:

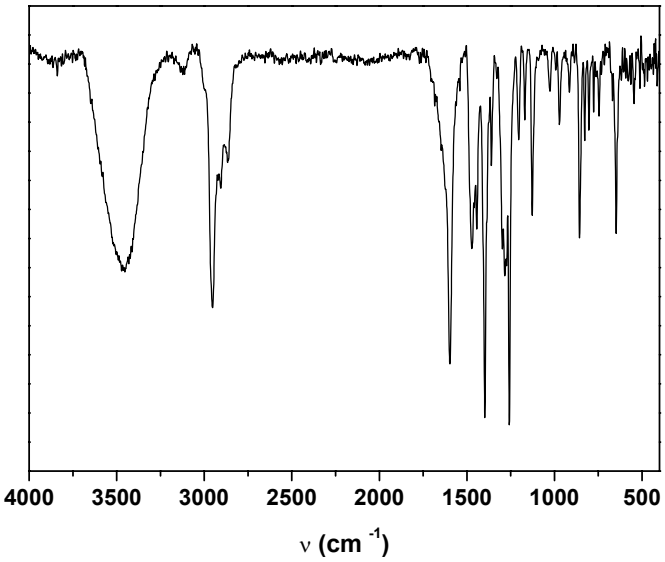

Synthesis of $[Ni^{II}_2 (L^2)(NH_2CONH_2)(OAc)(MeOH)_2]$ (3)

Method 1.

Ni acetate (240mg, 1mmole), sodium acetate (160 mg, 2 mmole) and urea (180mg, 3 mmole) were dissolved in methanol (15ml). Dichloromethane (30ml) was added along with the ligand H_3L (280 mg, 0.5 mmole). The solution was refluxed for 15 minutes in air and allowed to cool. It was filtered and the solution was allowed to evaporate slowly giving orange red crystals.

Yield: 240 mg (60 %)

Molecular Weight : 1012.54 $C_{46.5}H_{80}N_4O_{12.5}Ni_2$

Elemental Analysis:

	%C	%H	%N	%Ni
Calculated	55.16	7.91	5.53	11.59
Found	55.8	7.4	6.0	11.7

Infrared spectrum:

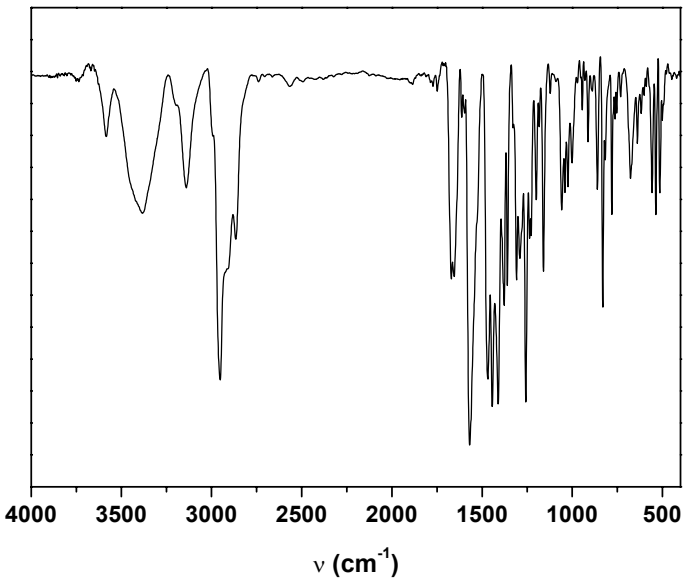

Method 2

The same compound (**3**) can be prepared from (**4**) by addition of urea and refluxing the resulting solution.

Synthesis of $[Ni^{II}_4 (LH)_2(OMe)_2(OAc)_2(OHMe)_2]$ (4)

Nickel acetate (240 mg, 1mmole) and sodium acetate (240 mg, 3 mmole) was dissolved in methanol (15ml). Dichloromethane was added along with H_3L (280 mg, 0.5 mmole) and the solution was refluxed for 15 minutes. It was then cooled and filtered. The volume of the filtrate was reduced till orange red microcrystalline precipitation occurs. It was filtered and washed with methanol. The compound was recrystallised from dichloromethane and methanol.

Yield: 188 mg (47%)

Molecular Weight : 1616.60 $C_{82}H_{116}N_4O_{14}Ni_4$

Elemental Analysis:

	%C	%H	%N	%Ni
Calculated	61.02	7.25	3.47	14.37
Found	58.9	7.0	3.2	13.1

Infrared Spectrum:

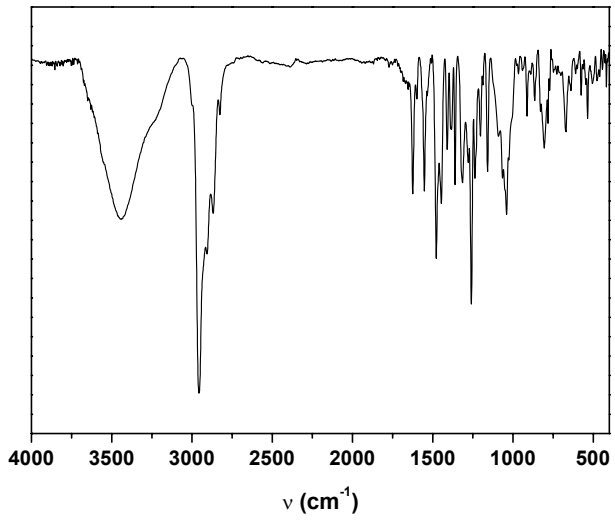

Synthesis of $[Cu^{II}_2\ L^2\ (\mu\text{-MeO})\ (THF)_2]$ (5)

To a Methanol/Dichloromethane solvent mixture(1:3), the ligand (0.5mmole; 290mg), $[Cu(H_2O)_6](ClO_4)_2$ (1.0 mmole ; 370 mg) and NEt_3 (0.3 ml) was added and refluxed for ½ hour in air. The deep red solution was cooled , filtered and the filtrate was concentrated by slow evaporation of the solvent. Orange-red microcrystalline solid precipitates after a few days. Single crystals was grown from a THF-MeOH solvent mixture.

Yield :130 mg (70%)

Formula Weight: 725.92 $C_{38}H_{50}N_2O_4Cu_2$

Elemental Analysis:

	%C	%H	%N	%Cu
Calculated	62.96	6.96	3.87	17.38
Found	63.1	6.9	3.8	17.4

Infrared spectrum:

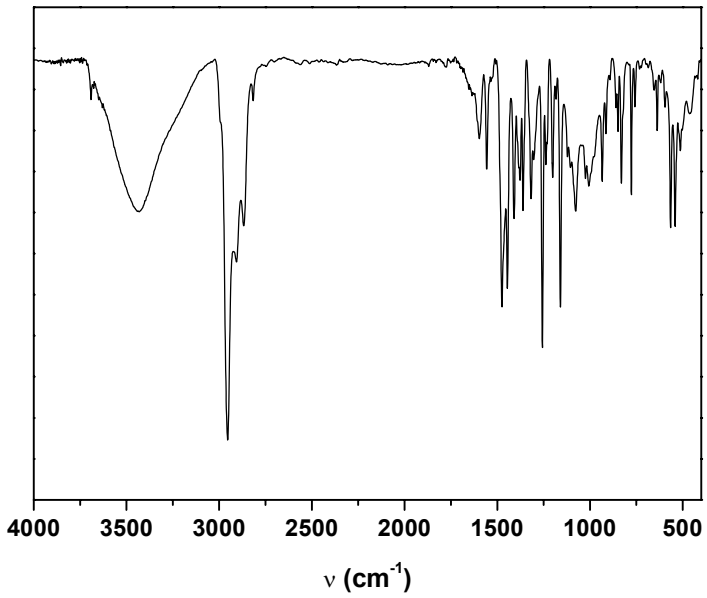

Synthesis of $[Cu^{II}_4 L^2_2 (\mu_4\text{-}O)]$ (6)

To a Acetonitrile / Dichloromethane solvent mixture (1:3) , the ligand (0.5mmole ; 290mg),$[Cu(H_2O)_6](ClO_4)_2$ (1.0 mmole ; 370 mg) and NEt_3 (0.3 ml) was added and refluxed for ½ hour in air. The deep red solution was cooled, filtered and the filtrate was concentrated by slow evaporation of the solvent. Orange-red microcrystalline solid precipitates after a few days. Single crystals was grown from a MeCN-DCM solvent mixture.

Yield : 210 mg (60%)

Molecular Weight: 1405.76 $C_{74}H_{94}N_4O_7Cu_4$

Elemental Analysis :

	%C	%H	%N	%Cu
Calculated	63.23	6.74	3.99	18.08
Found	62.4	6.9	4.0	17.8

Infrared Spectrum:

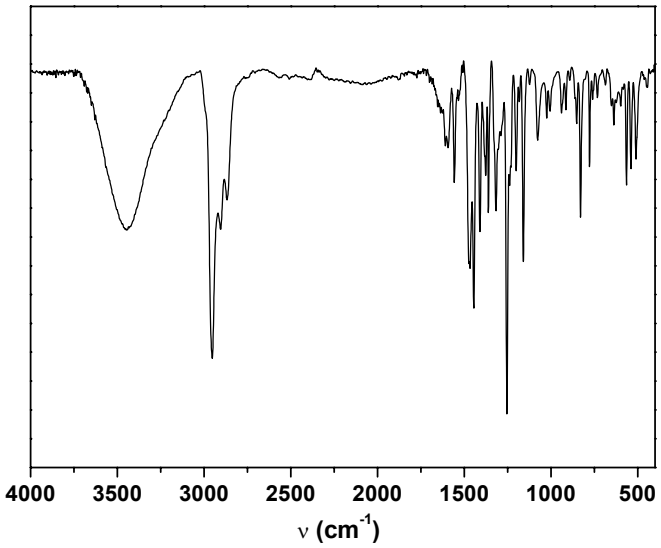

Synthesis of $Fe^{III}_2 L^2_2$ (7)

To a degassed solution of the ligand H_3L^2 (0.29 g; 0.5 mmol) and NEt_3 (0.12 ml) in an acetonitrile-dichloromethane solvent mixture (10 ml:15ml), $Fe(ClO_4)_2.6H_2O$ (0.18 g; 1 mmol) was added. The resulting solution was refluxed for 0.5 h under argon, cooled and stirred in air for an hour. The resulting deep reddish-brown solution was kept at ambient temperature for crystallization. After two days red-brown microcrystals were collected by filtration and air-dried.

Yield: 140 mg(45 %)

Molecular Weight : 1247.28 $C_{74}H_{94}O_6N_4Fe_2$

Elemental Analysis:

	%C	%H	%N	%Fe
Calculated	71.27	7.54	4.49	8.98
Found	71.3	7.5	4.4	9.0

Infrared Spectrum:

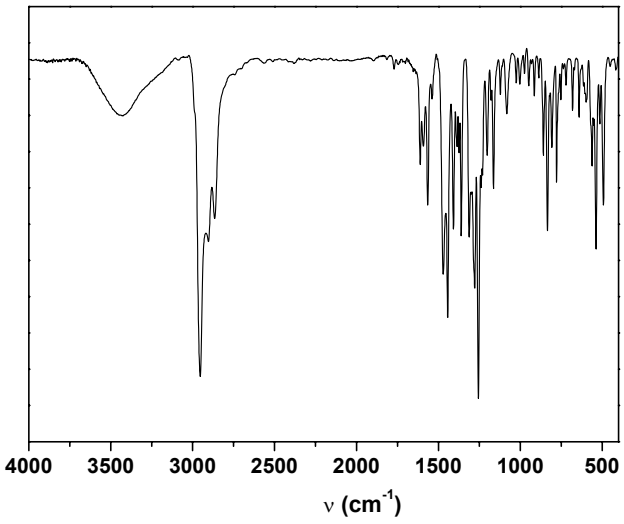

Synthesis of $Mn^{III}_2L^2_2$ (8a)

A methanolic solution (25 ml) of the ligand H_3L (0.29 g; 0.5 mmol), manganese(III) acetate (0.13 g; 0.2 mmol) and tetrabutylammonium methoxide (0.2 ml) was refluxed for 1 h, which on cooling and furthur concentration at room temperature yielded red-brown microcrystals of **8a**. The solid was collected by filtration and air-dried.

Yield : 70 mg (23 %)

Molecular Weight : 1245.46 $C_{74}H_{94}O_6N_4Mn_2$

Elemental Analysis:

	%C	%H	%N	%Mn
Calculated	71.36	7.61	4.50	8.82
Found	71.5	7.5	4.5	8.7

Infrared Spectrum :

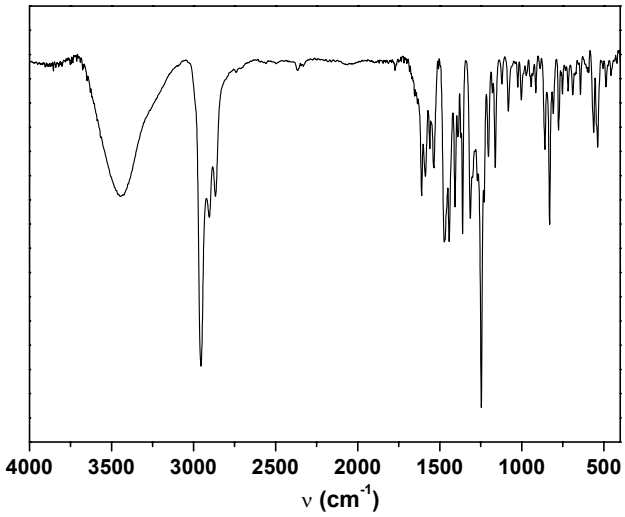

$[Mn^{III}_2L^2_2(THF)_2]$ (8b).

X-ray quality crystals of **8b**•4 CH_3CN were obtained by crystallizing **8a** from a tetrahydrofuran-acetonitrile solution.

Elemental Analysis :

	%C	%H	%N	%Mn
Calculated	69.57	7.91	7.21	7.07
Found	69.7	7.9	6.7	7.3

Synthesis of $Cr^{III}_2L^2_2$ (9)

A solution of the ligand (0.29 g; 0.5 mmol), NEt_3 (0.1 ml) and $CrCl_2$ (0.12 g; 0.5 mmol) in tetrahydrofuran (25 ml) was refluxed under argon for 15 min and the refluxing was continued further for 1 h in air. The resulting deep red solution was filtered and the filtrate was evaporated to dryness in a rotary evaporator. The solid was dissolved in 5 ml of THF and the solution was filtered to remove any solid particle. After addition of 2 ml of acetonitrile to the filtrate, the solution on slow evaporation at room temperature yielded orange-red microcrystalline solid of **9**.

Yield : 130 mg (42 %)

Molecular Weight: 1239.58 $C_{74}H_{94}O_6N_4Cr_2$

Elemental Analysis:

	%C	%H	%N	%Cr
Calculated	71.70	7.64	4.52	8.39
Found	71.4	7.6	4.5	8.3

Infrared Spectrum:

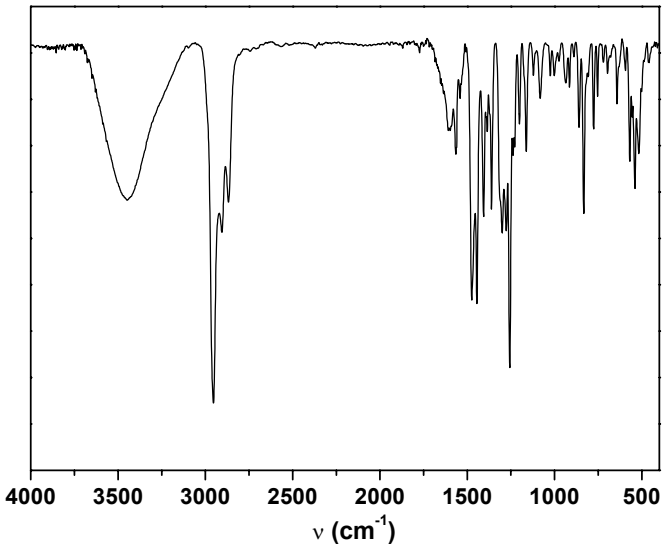

Synthesis of $[(V^{IV}=O)_2\ (\mu\text{-}O^{isoprop})\ L^2)]$ (10)

A solution of the ligand H_3L^2 (0.29 g; 0.5 mmol), vanadyltris(isopropoxide) (0.25 ml; 1 mmol) and Et_3N (0.3 ml) in a deaerated acetonitrile-dichloromethane (10ml:10ml) solvent mixture was refluxed under argon for 1 h and then stirred in air for further 1 h. The solution was filtered to remove any solid particle and the filtrate was allowed to evaporate slowly at ambient temperature to provide deep red crystals.

Yield: 180 mg (47 %)

Molecular Weight : 760.76 $C_{40}H_{54}O_6N_2V_2$

Elemental Analysis:

	%C	%H	%N	%V
Calculated	63.13	7.16	3.68	13.40
Found	63.1	7.1	3.6	13.4

Infrared Spectrum:

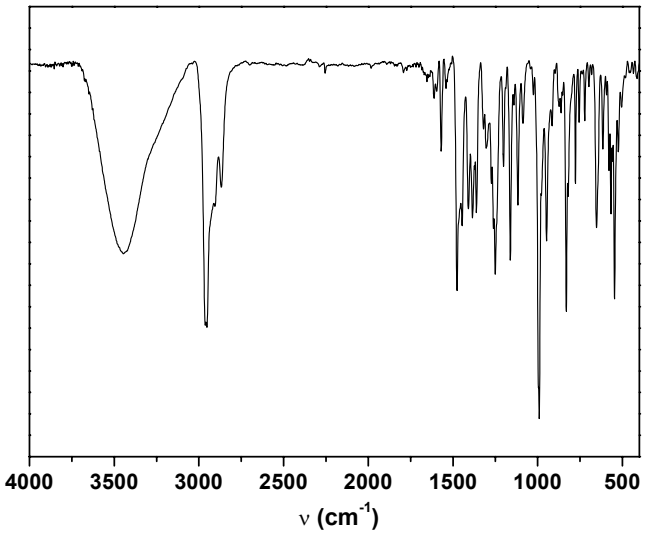

Synthesis of $[(V^{V}=O)_2\ L^{2}_{2}]$ (11)

To a de-aerated solvent mixture of Acetonitrile/DCM (30 ml:10 ml),the ligand (290 mg; 0.5 mmole), $V(THF)_3Cl_3$ (190 mg;0.5 mmole) and NEt_3 (0.25 ml) was added and refluxed under Argon for 1 hour, cooled and then stirred in air for 1 hour. It was filtered and the filtrate was allowed to evaporate slowly. Dark brown crystals appear after some days.

Yield: 200 mg (63 %)

Molecular Weight:1269.47 $C_{74}H_{94}O_8N_4V_2$

Elemental Analysis:

	%C	%H	%N	%V
Calculated	70.00	7.47	4.42	8.03
Found	69.8	7.3	4.4	7.9

Infrared spectrum:

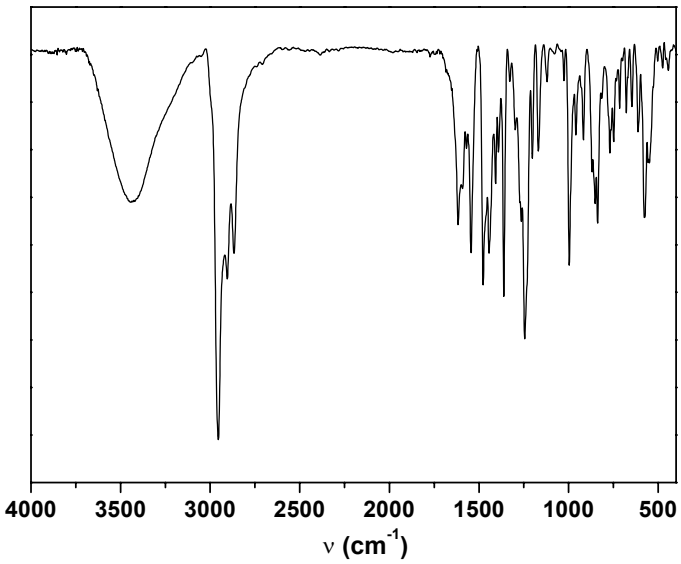

Synthesis of $Cu^{II}_2L^3_2$ .THF(12)

The ligand H_4L^3 (0.3 g, 0.6 mmol), CuCl (0.06 g, 0.6 mmol) and NEt_3 (0.4 cm^3) were dissolved under argon in CH_3CN/CH_3OH (1:1) and the resulting solution was refluxed for 1 h and filtered in the air. Slow evaporation of the filtrate afforded green microcrystals of **12**. Recrystallization from THF/CH_3OH (4:1) afforded X-ray quality crystals.

Yield: 400 mg (53%)

Molecular Weight : 1258.62 $C_{74}H_{100}Cu_2N_4O_{5.5}$

Elemental Analysis:

	%C	%H	%N	%Cu
Calculated	70.50	8.00	4.44	10.08
Found	69.1	8.1	4.4	9.8

Infrared Spectrum:

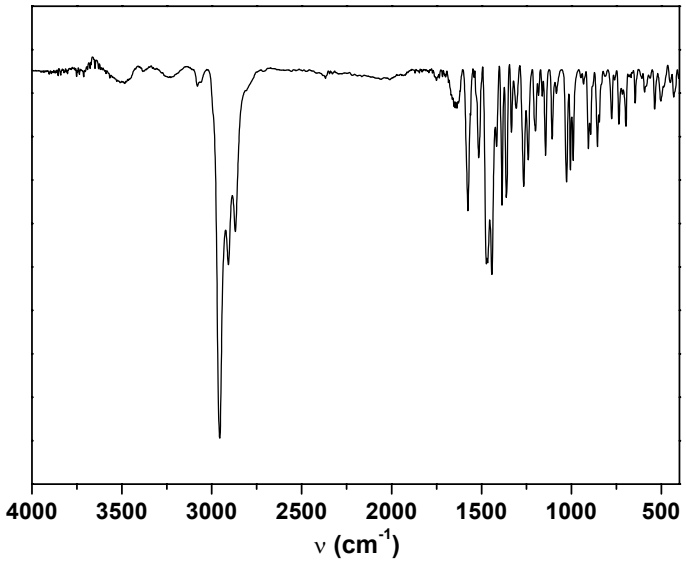

Synthesis of $Co^{III}_2L^3_3$ (14)

To a solvent mixture of dichloromethane and acetonitrile (4:5),the ligand (H_4L^3) (300 mg ; 0.6 mmole) and $[Co(H_2O)_6](ClO_4)_2$ (160 mg ;0.44 mmole) was added. Addition of NEt_3 (0.4 ml) turns the solution dark green. The solution was refluxed for 30 minutes, cooled and then filtered. Slow evaporation of the filtrate afforded dark brown crystals of **14**.

Yield: 265 mg(80%)

Molecular Weight : 1654.89 $C_{102}H_{132}Co_2N_6O_6$

Elemental Analysis:

	%C	%H	%N	%Co
Calculated	73.96	8.04	5.08	7.12
Found	73.8	8.0	5.1	7.2

Infrared Spectrum:

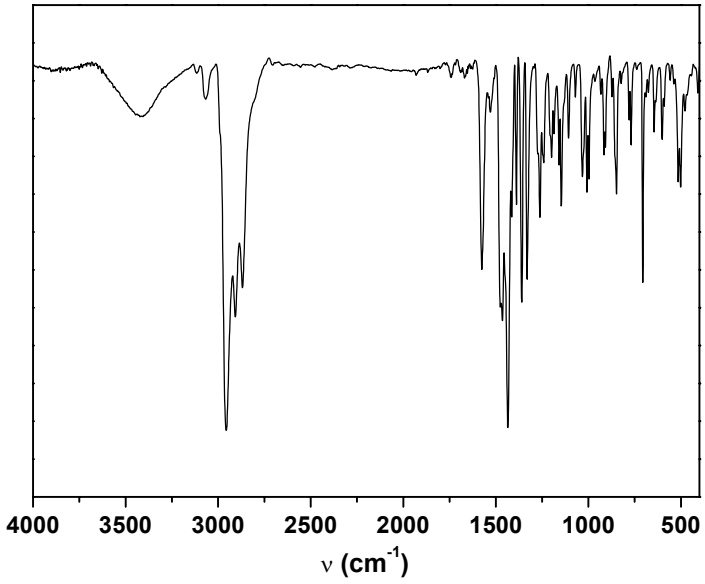

Synthesis of $Fe^{III}_2L^3_3$ (15)

The ligand H_4L^3 (0.3 g, 0.6 mmol), $FeCl_2.4H_2O$ (0.08 g, 0.44 mmol) and NEt_3 (0.4 cm^3) were dissolved in a solvent mixture (40 cm^3) of CH_2Cl_2/CH_3CN (4:5) and the resulting solution was refluxed for 0.5 h and filtered. Slow evaporation of the filtrate afforded green crystals of **15**. Recrystallization from acetone afforded X-ray quality crystals.

Yield: 180 mg(54%)

Molecular Weight : 1648.89 $C_{102}H_{132}Fe_2N_6O_6$

Elemental Analysis:

	%C	%H	%N	%Fe
Calculated	74.23	8.07	5.10	6.78
Found	74.2	7.8	5.1	6.8

Infrared Spectrum:

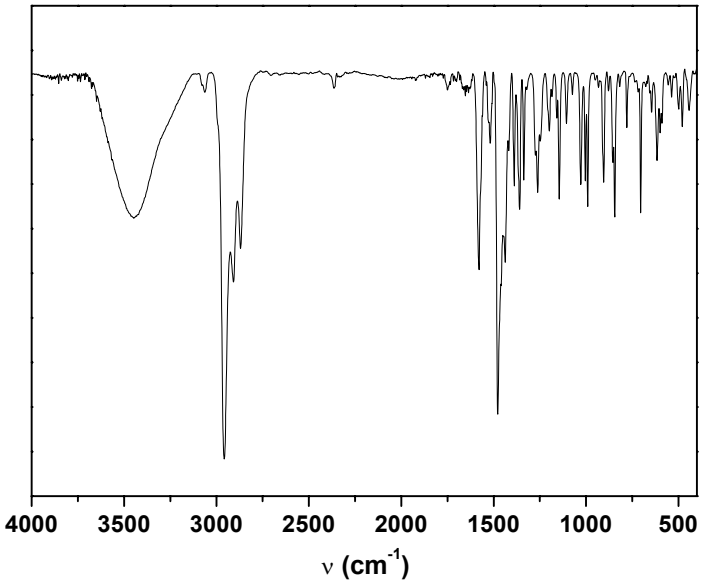

Synthesis of $Mn^{IV}_2(L_A^3)_2(L^3)$ (16)

To a solution of the ligand (0.52 g, 1 mmol) in CH_3OH (25 cm^3) containing $[Bu_4N]OCH_3$ (0.9 cm^3, 2.5 mmol) "manganese(III) acetate" (0.13 g, 0.2 mmol) was added to produce to a brown solution, which was refluxed in air for 0.5 h and filtered to remove any solid particles. The deep brown microcrystalline solid, separated after cooling was recrystallized from CH_2Cl_2/ CH_3CN (1:1).

Yield: 320 mg (60%)

Molecular Weight : 1646.89 $C_{102}H_{132}Mn_2N_6O_6$

Elemental Analysis:

	%C	%H	%N	%Mn
Calculated	74.34	8.07	5.10	6.67
Found	74.3	8.0	5.0	6.5

Infrared spectrum:

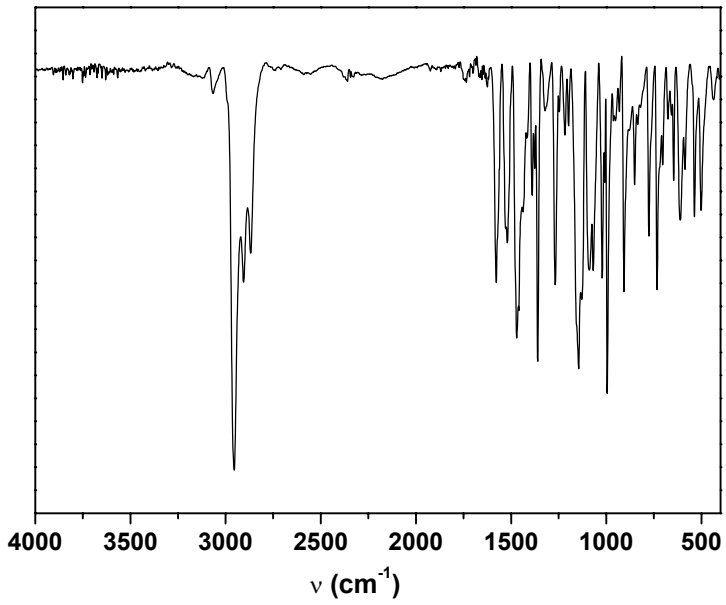

Synthesis of $Co^{III}_2L^4_3$ (17)

To a solvent mixture of Dichloromethane and Acetonitrile (4:5),the ligand (H_4L^4) (360 mg ; 0.6 mmole) and $[Co(H_2O)_6](ClO_4)_2$ (160 mg ;0.44 mmole)was added. Addition of NEt_3 (0.4 ml) turns the solution dark green. The solution was refluxed for 1 hour, cooled and then filtered. Slow evaporation of the filtrate afforded dark brown crystals.

Yield: 170 mg(45%)

Molecular Weight : 1925.02 $C_{123}H_{150}Co_2N_6O_6$

Elemental Analysis:

	%C	%H	%N	%Co
Calculated	76.67	7.85	4.36	6.12
Found	76.6	7.8	4.5	6.2

Infrared Spectrum:

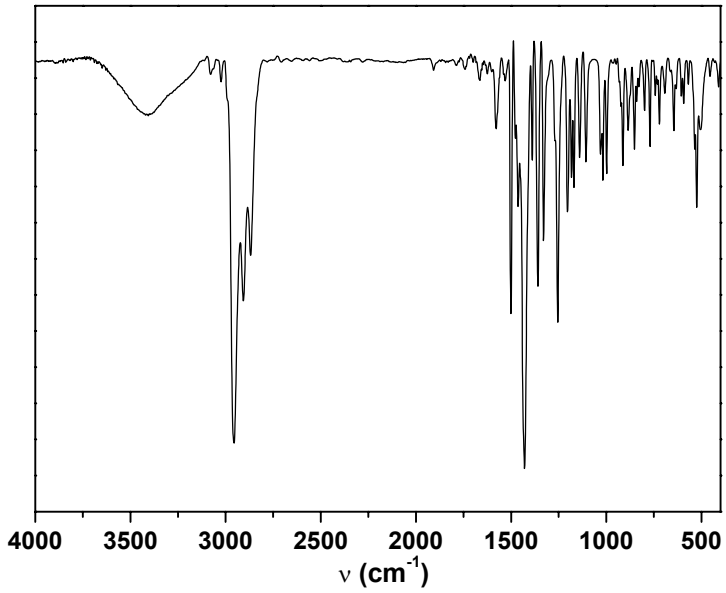

Synthesis of $Mn^{IV}(L_A^6)(L^6)_2$ (18)

The ligand H_2L^6 (0.82 g; 2.0 mmol) and "manganese(III) acetate" (0.13 g, 0.2 mmol) were dissolved in methanol (25 mL). Upon addition of $[Bu_4N]OCH_3$ (0.9 cm^3, 2.5 mmol) the color of the solution turned deep red. The solution was heated to reflux for 1 h in the presence of air. From the cooled and filtered solution black microcrystals crystallized upon slow evaporation of the solvent. The crude material was recrystallized from a Et_2O-CH_3OH solvent mixture.

Yield: 430 mg (60%)

Molecular Weight : 1276.89 $C_{84}H_{123}MnN_3O_3$

Elemental Analysis:

	%C	%H	%N	%Mn
Calculated	78.95	9.70	3.29	4.30
Found	78.8	9.8	3.2	4.3

Infrared Spectrum:

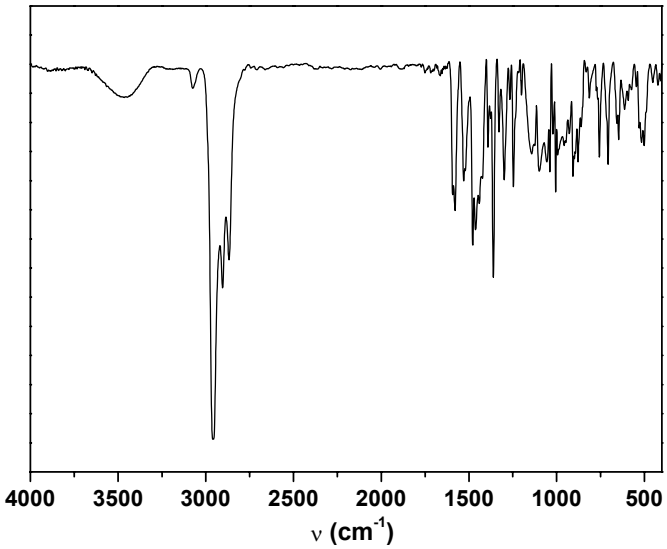

Synthesis of $Co^{III}L^{6}_{3}$ (23)

The ligand H_2L^{6} (0.41 g; 1.0 mmol) and $[Co^{II}(H_2O)_6](ClO_4)_2$ (0.12 g, 0.33 mmol) were dissolved in deaerated acetonitrile (25 mL) under argon. Upon addition of NEt_3 (0.5 cm^3) the color of the solution turned light blue. The solution was heated to reflux for 1h under argon. It was then cooled and stirred in air for ½ hour. From the solution deep blue microcrystals crystallized upon slow evaporation of the solvent. The crude material was recrystallized from a Et_2O-CH_3CN solvent mixture.

Yield: 280 mg (66%)

Molecular Weight : 1280.89 $C_{84}H_{123}CoN_3O_3$

Elemental Analysis:

	%C	%H	%N	%Co
Calculated	77.90	9.32	3.06	5.06
Found	78.7	9.7	3.3	4.6

Infrared Spectrum:

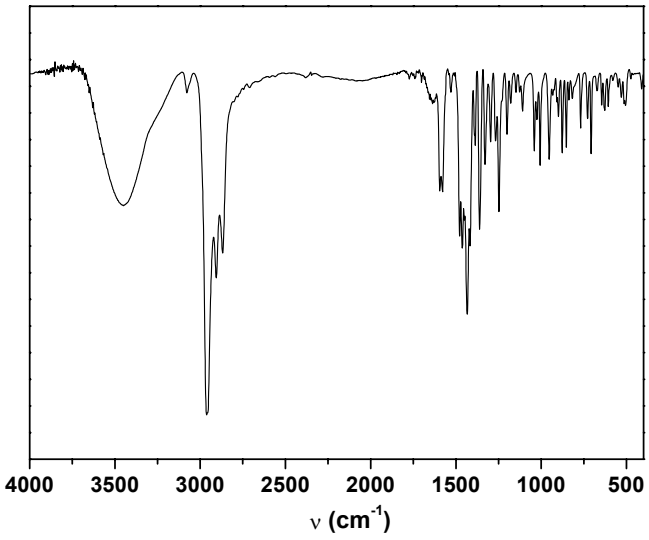

Synthesis of $Fe^{III}L^{6}_{3}$ (24)

The ligand H_2L^{6} (0.41 g ;1.0 mmol) and $[Fe^{II}(H_2O)_6](ClO_4)_2$ (0.06 g; 0.25 mmol) were dissolved in methanol (25 mL). Upon addition of NEt_3 (0.5 mL) the color of the solution turned deep green. The solution was heated to reflux for 1 h in the presence of air. From the cooled and filtered solution deep green microcrystals crystallized upon slow evaporation of the solvent. The crude material was recrystallized several times from a Et_2O-CH_3CN solvent mixture.

Yield: 220 mg (69%)

Molecular Weight : 1277.89 $C_{84}H_{123}FeN_3O_3$

Elemental Analysis:

	%C	%H	%N	%Fe
Calculated	78.88	9.7	3.29	4.38
Found	76.9	9.0	3.0	4.9

Infrared Spectrum:

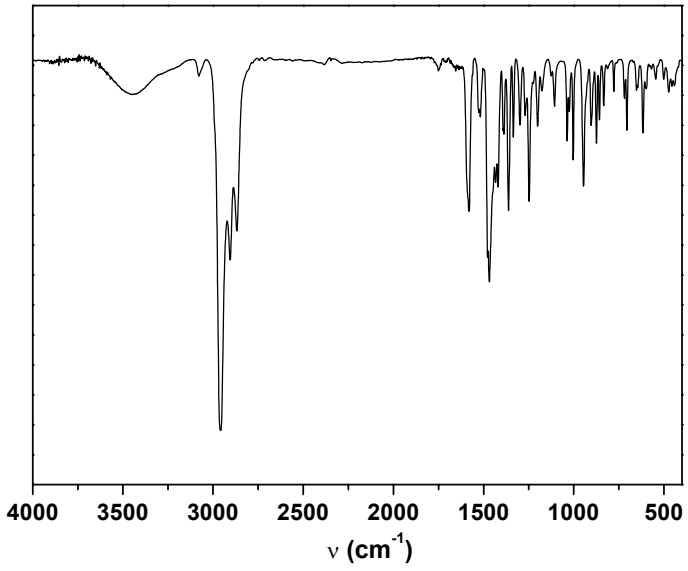

Synthesis of $Fe^{III}L^{11}_3$ (25)

The ligand H_2L^{11} (0.34g ;1.0 mmol) and $[Fe^{II}(H_2O)_6](ClO_4)_2$ (0.06 g; 0.25 mmol) were dissolved in methanol (20 mL). Upon addition of NEt_3 (0.4 mL) the color of the solution turned deep green. The solution was heated to reflux for 1 h in the presence of air. From the cooled and filtered solution deep green microcrystals crystallized upon slow evaporation of the solvent. The crude material was recrystallized several times from a CH_2Cl_2-CH_3CN solvent mixture.

Yield: 165mg (63%)

Molecular Weight : 1049.46 $C_{60}H_{69}F_6FeN_3O_3$

Elemental Analysis:

	%C	%H	%N	%Fe
Calculated	68.61	6.63	4.0	5.33
Found	68.5	6.75	3.9	5.28

Infrared Spectrum:

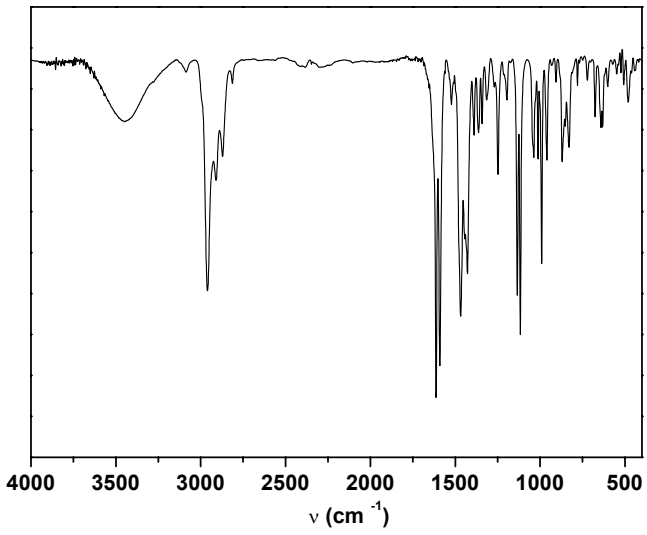

Synthesis of $[Fe^{III}_2(\mu\text{-}O)(L^{12})_4]$ (26)

The ligand H_2L^{12} (0.36 g; 1.0 mmol) and $[Fe^{II}(H_2O)_6](ClO_4)_2$ (0.06 g; 0.25 mmol) were dissolved in methanol (25 mL). Upon addition of NEt_3 (0.5 mL) the color of the solution turned deep red. The solution was heated to reflux for 1 h in the presence of air whereupon a color change to deep green was observed. From the cooled and filtered solution black microcrystals crystallized upon slow evaporation of the solvent within 2 days. The crude material was recrystallized from a CH_2Cl_2-CH_3CN (3:1) mixture.

Yield: 120 g (63 %).

Molecular Weight : 1532.89 $C_{96}H_{132}N_4O_5Fe_2$

Elemental Analysis:

	%C	%H	%N	%Fe
Calculated	75.15	8.68	3.65	7.30
Found	75.0	8.6	3.5	7.4

Infrared spectrum:

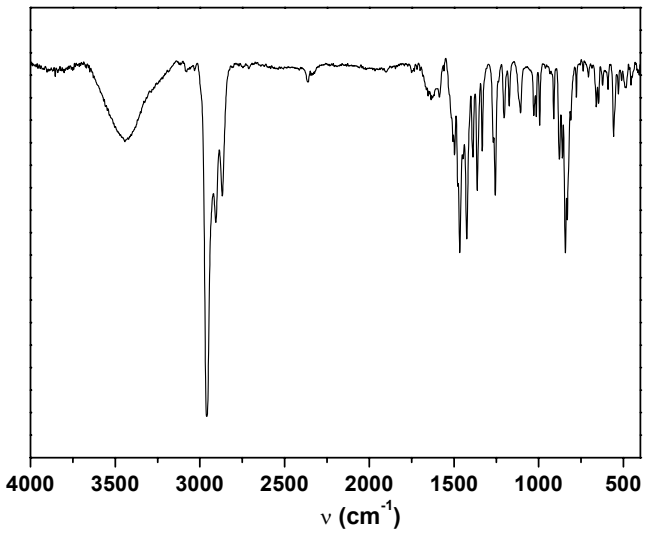

7.3 REACTIVITY STUDIES

Catalytic oxidation of 3,5-di-tert-butylcatechol

In dichloromethane (25ml), the Mn(IV) complexes were dissolved and 3,5-ditertbutylcatechol was added and the solution was stirred in room temperature for 24hours. The solution was then subjected to liquid chromatography studies.

For kinetic measurements, 1ml from this solution was taken and diluted to 10ml with dichloromethane. The change in the concentration of the product, 3,5-di-tert-butyl-o-benzoquinone, was measured by UV-spectroscopy.

Catalytic oxidation of 2,6-di-tert-butylphenol

In a dichloromethane/methanol solvent mixture (1:1; 50ml), **16** was dissolved. To it 2**,**6-di-tert-butylphenol was added and the solution was stirred for 48 hours. The solution was then filtered, and the filtrate was evaporated to dryness. 5ml of methanol was added to dissolve the excess 2**,**6-di-tert-butylphenol (**16** is insoluble in methanol) and the methanolic solution was subjected to GC studies with the presence of hexadecane (C_{16}) as standard.

For measuring the progress of the reaction, 50µl from the aliquot was passed through an Amberlyst cationic ion-exchanger and washed with 10ml dichloromethane. The change in the concentration of product, 3,3´-5,5´-Tetra-tert-butyldiphenoquinone, was measured by UV-spectroscopy.

Appendices

1. **Crystallographic data**
2. **Magnetochemical data**
3. **Magnetic and EPR data**
4. **Curriculum vitae**

1) Crystallographic data

Crystal data and structure refinement for 1, 2.

	1	**2**
Empirical formula	$C_{76}H_{100}N_{12}Ni_4O_4.9CH_2Cl_2$	$C_{76}H_{100}N_{12}Cu_4O_4.xTHF$
Formula weight	2244.85	1499.xTHF
Temperature (K)	100(2)	100(2)
Wavelength (Å)	0.71073	0.71073
Crystal system	Tetragonal	Monoclinic
Space group	P-42_1/c (No. 114)	$P2_1$/c
Unit cell dimensions	a = 20.74(3) Å	a = 24.916(5) Å
	b = 20.74(3) Å	b = 17.296 (4) Å
	c = 12.1538 (10) Å	c = 33.004(7) Å
	α = 90 deg.	α = 90 deg.
	β = 90 deg.	β = 91.72 deg.
	γ = 90 deg.	γ = 90 deg.
Volume ($Å^3$);Z	5227.9(12); 2	14216
Density (cal.) (Mg/m^3)	1.426	1.401
Absorp. coeff. (mm^{-1})	1.220	1.24
F(000)	2324	6304
θ range for data collection	1.94 to 25.00 deg.	1.94 to 21.18 deg.
Index ranges	-31<=h<=32,	-21<=h<=21,
	-10<=k<=31,	-17<=k<=12,
	-18<=l<=17	-33<=l<=33
Reflections collected	39793	13608
Independent reflections	4608	10569
Absorption correction	SADABS	
Data / restraints / parameters	4591 / 16 / 289	10212 / 0 / 1137
Goodness-of-fit on F^2	1.048	2.895
Final R indices	R1 = 0.0786, wR2 = 0.2180	R1 = 0.1513,
[I>2σ(I)]		
R indices (all data)	R1 = 0.0982, wR2 = 0.2366	R1 = 0.2162, wR2 = 0.4469

Crystal data and structure refinement for 3, 4, 5, 6.

	3	**4**	**5**	**6**
Empirical formula	$C_{42}H_{62}N_4O_8Ni_2$ •4.5CH_3OH	$C_{82}H_{116}N_4O_{14}Ni_4$ •3CH_2Cl_2	$[C_{38}H_{50}N_2O_4Cu_2$. (2THF)] • 2THF	$C_{74}H_{94}N_4O_7Cu_4$ •3.3CH_2Cl_2•0.7CH_3CN
Formula weight	1012.57	1871.41	1014.35	1715.56
Temperature	100(2) K	100(2) K	100(2) K	100(2) K
Wavelength (MoKα)	0.71073 Å	0.71073 Å	0.71073	0.71073 Å
Crystal System	Triclinic	Triclinic	Monoclinic	Triclinic
Space group	P-1	P-1	P2(1)/n	P-1
Unit cell dimensions	a = 12.099(2) Å	a = 19.9102(12) Å	a = 11.7479 Å	a = 16.4678(9) Å
	b = 12.128(2) Å	b = 21.545(2) Å	b = 30.236 Å	b = 17.2675(12) Å
	c = 18.800(3) Å	c = 22.076(2) Å	c = 15.64 Å	c = 17.3208(12) Å
	α = 95.90(2)°	α = 80.45(2)°	α = 90.0(2)°	α = 106.03(1)°
	β = 104.16(2)°	β = 80.88(2)°	β = 110.19(2)°	β = 112.14(1)°
	γ = 91.48(2)°	γ = 83.43(2)°	γ = 90.0(2)°	γ = 102.71(1)°
Volume ($Å^3$); Z	2656.9(8); 2	9182.7(13); 4	5213.2; 4	4083.9(5); 2
Density (calc.) Mg/m^3	1.266	1.354	1.292	1.395
Absorp. coeff. (mm^{-1})	0.769	1.043	0.87 mm^{-1}	1.298
F(000)	1086	3944	2168	1785
Crystal size (mm)	0.20 x 0.19 x 0.10	0.18 x 0.10 x 0.09	0.13 x 0.09 x 0.06	0.33 x 0.24 x 0.15
θ range for data collect.	1.69 to 23.27°	3.13 to 22.50°	4 to 26°	2.87 to 30.0°
Reflections collected	18237	57320	27492	49175
Independent reflect.	7534	23751	17225	23491
	[R(int.) = 0.1014]	[R(int.) = 0.0845]	[R(int.) = 0.0918]	[R(int.) = 0.0452]
Absorpt. correction	Gaussian, face indexed	Gaussian, face indexed	not measured	not measured
Data/restraints/param.	7524 / 25 / 672	23751 / 112 / 2033	5150 / 62 / 492	23356 / 166 / 964
Goodness-of-fit on F^2	0.877	1.051	1.214	1.019
Final R indices[I>2σ(I)]	R_1 = 0.0508	R_1 = 0.0837	R_1 = 0.0919	R_1 = 0.0569
	wR_2 = 0.0971	wR_2 = 0.1851	wR_2 = 0.2172	wR_2 = 0.1434
R indices (all data)	R_1 = 0.1113	R_1 = 0.1412	R_1 = 0.2092	R_1 = 0.0803
	wR_2 = 0.1134	wR_2 = 0.2173	wR_2 = 0.4007	wR_2 = 0.1602

Crystal data and structure refinement for 7, 8(b), 10, 11.

	7	**8(b)**	**10**	**11**
Empirical formula	$C_{74}H_{94}Fe_2N_4O_6$ •2.5 CH_3CN	$C_{82}H_{110}Mn_2N_4O_8$ •4 CH_3CN	$C_{42}H_{59}N_3O_6V_2$	$C_{74}H_{94}N_4O_8V_2$ •2 CH_3CN
Formula weight	1349.87	1553.84	803.80	1351.52
Temperature	100(2) K	100(2) K	100(2) K	100(2) K
Wavelength (MoKα)	0.71073 Å	0.71073 Å	0.71073 Å	0.71073 Å
Crystal system	Triclinic	Triclinic	Triclinic	Triclinic
Space group	P-1	P-1	P-1	P-1
Unit cell dimensions	a = 16.887(2) Å	a = 11.6088(8) Å	a = 8.456(1) Å	a = 14.8895(8) Å
	b = 17.026(2) Å	b = 12.6390(8) Å	b = 16.087(2) Å	b = 16.047(1) Å
	c = 17.040(2) Å	c = 31.802(2) Å	c = 16.685(2) Å	c = 16.881(1) Å
	α = 115.63(2)°	α = 79.41(1)°	α = 71.35(2)°	α = 77.47(1)°
	β = 113.09(2)°	β = 83.17(1)°	β = 89.26(2)°	β = 79.50(1)°
	γ = 90.69(2)°	γ = 72.87(1)°	γ = 79.26(2)°	γ = 81.47(1)°
Volume ($Å^3$); Z	3964.7(8); 2	4372.7(5); 2	2110.2(4); 2	3846.5(4); 2
Density (calc.) Mg/m^3	1.131	1.180	1.265	1.167
Absorp. coeff. (mm^{-1})	0.417	0.346	0.490	0.298
F(000)	1442	1664	852	1440
Crystal size (mm)	0.39 x 0.37 x 0.34	0.44 x 0.36 x 0.24	0.33 x 0.14 x 0.09	0.35 x 0.11 x 0.10
θ range for data collect.	1.69 to 26.00°	2.31 to 27.11°	2.16 to 22.50°	4.21 to 32.50°
Reflections collected	26505	31923	13369	44652
Independent reflect.	13350	18622	5434	27516
	[R(int.) =0.0419]	[R(int.) = 0.0482]	[R(int.) = 0.0852]	[R(int.) = 0.0452]
Absorpt. correction	SADABS	Gaussian, face indexed	Gaussian, face indexed	Gaussian, face indexed
Data/restraints/param.	13308 / 36 / 805	18622 / 6 / 1000	5430 / 0 / 479	27259 / 34 / 839
Goodness-of-fit on F^2	1.057	1.065	1.012	1.014
Final R indices	R1 = 0.0862,	R1 = 0.0747,	R1 = 0.0527,	R1 = 0.0681,
[I>2σ(I)]	wR2 = 0.2532	wR2 = 0.1899	wR2 = 0.1194	wR2 = 0.1539
R indices (all data)	R1 = 0.1223,	R1 = 0.0933,	R1 = 0.0963,	R1 = 0.1102,
	wR2 = 0.2875	wR2 = 0.2020	wR2 = 0.1345	wR2 = 0.1814

Crystal data and structure refinement for 12, 14, 15, 16.

	12	**14**	**15**	**16**
Empirical formula	$C_{74}H_{100}Cu_2N_4O_{5.5}$	$C_{102}H_{132}Co_2N_6O_6$ *$3CH_2Cl_2$	$C_{102}H_{132}Fe_2N_6O_6$ * 0.5 C_3H_6O	$C_{102}H_{132}Mn_2N_6O_6$ * 0.5 CH_2Cl_2
Formula weight	1260.66	1910.77	1678.88	1690.48
Temperature (K)	100(2)	100(2)	100(2)	100(2)
Wavelength (Å)	0.71073	0.71073	0.71073	0.71073
Crystal system	Monoclinic	Triclinic	Monoclinic	Monoclinic
Space group	$P2_1/c$	P-1	$P2_1/n$	$P2_1/n$
Unit cell dimensions	a = 15.2345(12) Å	a = 15.5627(8) Å	a = 25.374(2) Å	a = 25.0716(9) Å
	b = 18.903 (2) Å	b = 16.2417(12) Å	b = 15.7754(12) Å	b = 15.7152(6) Å
	c = 24.840 (3) Å	c = 23.594(2) Å	c = 26.287(2) Å	c = 26.2842(12) Å
	α = 90 deg.	α = 74.09(1) deg.	α = 90 deg.	α = 90 deg.
	β = 90.51(2) deg.	β = 76.48(1) deg.	β = 106.40(1) deg.	β = 105.43(1) deg.
	γ = 90 deg.	γ = 66.45(1) deg.	γ = 90 deg.	γ = 90 deg.
Volume ($Å^3$);Z	7153.1(13); 4	5205.1(6); 2	10094.2(13); 4	9982.8(7); 4
Density (cal.) (Mg/m^3)	1.171	1.219	1.105	1.125
Absorp. coeff. (mm^{-1})	0.645	0.526	0.340	0.332
F(000)	2696	2028	3608	3620
Crystal size (mm)	0.33 x 0.31 x 0.31	0.28 x 0.27 x 0.24	0.11 x 0.06 x 0.04	0.25 x 0.20 x 0.16
θ range for data collection	2.15 to 30.00 deg.	3.50 to 30.00 deg.	3.06 to 23.50 deg.	2.06 to 22.50 deg.
Index ranges	-23<=h<=14,	-23<=h<=22,	-29<=h<=15,	-27<=h<=27,
	-29<=k<=27,	-19<=k<=24,	-18<=k<=15,	-16<=k<=17,
	-38<=l<=30	-33<=l<=36	-30<=l<=30	-29<=l<=23
Reflections collected	46103	47876	33764	56918
Independent reflections	19375	29002	14847	13020
	[R(int) = 0.0438]	[R(int) = 0.0441]	[R(int) = 0.0768]	[R(int) = 0.0922]
Absorption correction	Not measured	Gaussian, face indexed	Gaussian, face-indexed	Not measured
Data / restraints / parameters	19318 / 0 / 808	26325 / 0 / 1105	14670 / 0 / 1081	12926 / 0 / 1072
Goodness-of-fit on F^2	1.033	1.034	1.045	1.027
Final R indices	R1 = 0.0472,	R1 = 0.0881,	R1 = 0.0658,	R1 = 0.0592,
[I>2σ(I)]	wR2 = 0.1196	wR2 = 0.2329	wR2 = 0.1120	wR2 = 0.1236
R indices (all data)	R1 = 0.0755,	R1 = 0.1275,	R1 = 0.1303,	R1 = 0.1005,
	wR2 = 0.1307	wR2 = 0.2708	wR2 = 0.1372	wR2 = 0.1444

Crystal data and structure refinement for 17, 18, 23.

	17	**18**	**23**
Empirical formula	C_{123} H_{150} Co_2 N_6 O_6 * CH_3CN	C_{84} H_{123} Mn N_3 O_3	C_{84} H_{123} Co N_3 O_3
Formula weight	1967.40	1277.79	1281.78
Temperature (K)	100(2)	100(2)	100(2)
Wavelength (Å)	0.71073	0.71073	0.71073
Crystal system	Monoclinic	Monoclinic	Monoclinic
Space group	$P2_1/c$	$P2_1/c$	$P2_1/c$
Unit cell dimensions	a = 15.077(1) Å	a = 16.6726(4) Å	a = 16.1355(4) Å
	b = 35.459(4) Å	b = 14.5993(4)Å	b = 14.5516(4) Å
	c = 21.803(3) Å	c = 33.4362(12)Å	c = 34.0664(8) Å
	α = 90 deg.	α = 90 deg.	α = 90 deg.
	β = 105.53(2) deg.	β = 97.20(1)deg.	β = 97.77(1) deg.
	γ = 90 deg.	γ = 90 deg.	γ= 90 deg.
Volume ($Å^3$);Z	11230(2); 4	8074.5(4); 4	7925.3(3); 4
Density (calculated) (Mg/m^3)	1.164	1.051	1.074
Absorption coefficient (mm^{-1})	0.352	0.209	0.263
F(000)	4216	2788	2796
Crystal size (mm)	0.56 x 0.50 x 0.16	0.22 x 0.14 x 0.14	0.48 x 0.17 x 0.09
θ range for data collection	1.58 to 20.00 deg.	2.96 to 27.50	3.01 to 27.50 deg.
Index ranges	-16<=h<=16,	-21<=h<=21,	-20<=h<=20,
	-39<=k<=30,	-18<=k<=18,	-18<=k<=18,
	-24<=l<=22	-43<=l<=43	-44<=l<=44
Reflections collected	31610	35212	86147
Independent reflections	10466 [R(int) = 0.1036]	18437 [R(int) = 0.0410]	18094 [R(int) = 0.0676]
Absorption correction	SADABS	Not measured	Gaussian, face-indexed
Data / restraints / parameters	10429 / 0 / 1232	18437 / 0 / 856	18094 / 0 / 856
Goodness-of-fit on F^2	1.037	1.062	1.046
Final R indices	R1 = 0.0779,	R1 = 0.0590,	R1 = 0.0480,
[I>2σ(I)]	wR2 = 0.1872	wR2 = 0.1285	wR2 = 0.0954
R indices (all data)	R1 = 0.1470,	R1 = 0.0830,	R1 = 0.0674,
	wR2 = 0.2231	wR2 = 0.1394	wR2 = 0.1027

Crystal data and structure refinement for 24, 24 (at room temperature), 25, 26.

	24	**24 (at RT)**	**25**	**26**
Empirical formula	C_{84} H_{123} Fe N_3 O_3	C_{84} H_{123} Fe N_3 O_3	C_{60} H_{69} F_6 Fe N_3 O_3	C_{96} H_{132} Fe_2 N_4 O_5 * 2.75 CH_2Cl_2
Formula weight	1278.70	1278.70	1050.03	1767.30
Temperature (K)	100(2)	293(2)	100(2)	100(2)
Wavelength (Å)	0.71073	0.71073	0.71073	0.71073
Crystal system	Monoclinic	Monoclinic	Monoclinic	Triclinic
Space group	$P2_1/c$	$P2_1/c$	C2/c	P-1
Unit cell dimensions	a = 16.656(2) Å	a = 17.0012(2) Å	a = 25.6710(4) Å	a = 11.9826(6) Å
	b = 14.648(2) Å	b = 14.8159(2) Å	b = 24.8786(4) Å	b = 15.9612(9) Å
	c = 33.433(3) Å	c = 33.897(3) Å	c = 17.9867(3) Å	c = 27.5321(15) Å
	α = 90 deg.	α = 90 deg.	α = 90 deg.	α = 84.48(1) deg.
	β = 97.32(1) deg.	β = 96.76(1) deg.	β = 105.50(1) deg.	β = 82.47(1) deg.
	γ = 90 deg.	γ = 90 deg.	γ = 90 deg.	γ = 77.64(1) deg.
Volume ($Å^3$);Z	8090.4(16) ; 4	8478.9(16) ; 4	11069.6(3); 8	5086.7(5); 2
Density (calc.) (Mg/m^3)	1.050	1.002	1.260	1.154
Absorp. coeff. (mm^{-1})	0.232	0.221	0.339	0.479
F(000)	2792	2792	4432	1887
Crystal size (mm)	0.32 x 0.11 x 0.08	0.32 x 0.11 x 0.08	0.27 x 0.19 x 0.18	0.16 x 0.13 x 0.12
θ range for data collection	2.95 to 28.32 deg.	2.91 to 23.50 deg.	2.97 to 31.07	3.35 to 27.50
Index ranges	-22<=h<=22,	-19<=h<=19,	-37<=h<=37,	-15<=h<=15,
	-19<=k<=19,	-16<=k<=15,	-36<=k<=36,	-14<=k<=20,
	-44<=l<=44	-38<=l<=38	-26<=l<=26	-35<=l<=35
Reflections collected	92357	47308	138510	38197
Independent reflections	20013	12467	17667	21829
	[R(int) = 0.0493]	[R(int) = 0.0586]	[R(int) = 0.0479]	[R(int) = 0.0482]
Absorption correction	Gaussian, face-indexed	Gaussian, face-indexed	Gaussian, face-indexed	Gaussian, face-indexed
Data / restraints / parameters	20013 / 0 / 820	12467 / 216 / 893	17667 / 30 / 700	21829 / 38 / 1065
Goodness-of-fit on F^2	1.037	1.023	1.038	1.043
Final R indices	R1 = 0.0485,	R1 = 0.0688,	R1 = 0.0384,	R1 = 0.0682,
[I>2σ(I)]	wR2 = 0.1093	wR2 = 0.1563	wR2 = 0.0946	wR2 = 0.1562
R indices (all data)	R1 = 0.0690,	R1 = 0.1024,	R1 = 0.0458,	R1 = 0.1066,
	wR2 = 0.1195	wR2 = 0.1748	wR2 = 0.0989	wR2 = 0.1799

2) Magnetochemical data

Complex $Cu_4L^1_4$ (2)

MW= 1498 gm/mol; λ_{dia}= -1000 x 10^{-6} cm^3mol^{-1} ;

m=32.12 mg ; H = 1T

	Temp.(K)	λ_mT(exp.)	λ_mT(theo.)	μ_{eff} (exp.)	μ_{eff}(theo.)
1	1.998	0.00402	0.00753	0.17998	0.24639
2	5	0.00591	0.00753	0.21828	0.24639
3	10.003	0.00766	0.00753	0.24851	0.24643
4	14.999	0.00963	0.00778	0.27866	0.25043
5	20.001	0.01442	0.01014	0.34099	0.28591
6	30.001	0.04634	0.03463	0.61139	0.52853
7	39.998	0.1115	0.09353	0.9483	0.86854
8	50.005	0.19708	0.17669	1.26079	1.19378
9	060.01	0.29136	0.26936	1.53298	1.47397
10	70.044	0.38413	0.36179	1.76017	1.70823
11	80.073	0.46943	0.44847	1.94584	1.90189
12	90.09	0.54592	0.52734	2.09838	2.06237
13	100.11	0.61319	0.59818	2.2239	2.19651
14	110.13	0.67235	0.66137	2.32871	2.30961
15	120.15	0.72541	0.71764	2.41885	2.40586
16	130.16	0.77136	0.76775	2.49429	2.48844
17	140.18	0.81147	0.81256	2.55832	2.56004
18	150.19	0.84747	0.85269	2.61446	2.62248
19	160.19	0.88167	0.88874	2.66668	2.67736
20	170.21	0.91385	0.92136	2.71491	2.72605
21	180.22	0.94286	0.95089	2.75768	2.76938
22	190.23	0.96988	0.97774	2.7969	2.80822
23	200.24	0.99383	1.00225	2.83122	2.84319
24	210.23	1.01628	1.02464	2.86302	2.87478
25	220.2	1.03612	1.04518	2.89084	2.90345
26	230.24	1.05326	1.06423	2.91465	2.92979
27	240.26	1.07078	01.0818	2.93879	2.95387
28	250.25	1.08718	1.09803	2.96121	2.97595
29	260.27	1.10477	1.11315	2.98507	2.99637
30	270.25	1.12177	1.12717	3.00795	3.01518
31	280.29	1.13854	1.14033	3.03035	3.03273
32	290.25	1.15384	1.15254	3.05064	3.04892

Complex $[Ni_2(L^2)(NH_2CONH_2)(OAc)(MeOH)_2]$ (3)

MW= 866 gm/mol; λ_{dia}= -450 x 10^{-6} cm^3mol^{-1} ;

m=40.4 mg ; H = 1T

	Temp.(K)	λ_mT(exp.)	λ_mT(theo.)	μ_{eff} (exp.)	μ_{eff}(theo.)
1	1.998	0.27169	0.02841	1.48032	0.47869
2	5	0.61728	0.35823	2.2313	1.69981
3	10.003	0.9786	0.89348	2.80944	2.68449
4	15	1.21507	1.26015	3.13054	3.18808
5	20.002	1.38996	1.4917	3.34826	3.46864
6	30.001	1.62955	1.74783	3.62537	3.75464
7	40	1.78154	1.88131	3.79067	3.89537
8	50.002	1.88122	1.96201	3.89528	3.97804
9	60.032	1.94994	2.01587	3.96578	4.03227
10	70.046	2.0008	2.05415	4.01717	4.07037
11	80.067	2.04218	2.08277	4.0585	4.09863
12	90.091	2.07292	2.10495	4.08893	4.1204
13	100.11	2.09862	2.12263	4.1142	4.13767
14	110.09	2.11771	2.137	4.13287	4.15165
15	120.15	2.1372	2.14904	4.15184	4.16333
16	130.16	2.15098	2.15916	4.16521	4.17312
17	140.18	2.16485	2.16781	4.17861	4.18147
18	150.19	2.17675	2.1753	4.19008	4.18869
19	160.2	2.18789	2.18183	4.20079	4.19497
20	170.21	2.19893	2.18759	4.21138	4.2005
21	180.22	2.20801	2.19271	4.22006	4.20542
22	190.22	2.21813	2.19727	4.22972	4.20979
23	200.22	2.22626	2.20138	4.23747	4.21372
24	210.23	2.23375	2.20509	4.24459	4.21727
25	220.24	2.24198	2.20847	4.2524	4.2205
26	230.24	2.24904	2.21154	4.25909	4.22343
27	240.27	2.26024	2.21437	4.26968	4.22614
28	250.24	2.26586	2.21695	4.27499	4.2286
29	260.25	2.27094	2.21934	4.27978	4.23088
30	270.24	2.27934	2.22155	4.28769	4.23298
31	280.14	2.28173	2.22358	4.28993	4.23492
32	290.25	2.29061	2.22551	4.29827	4.23675

Complex $[Ni_4 (LH)_2(OMe)_2(OAc)_2(OHMe)_2]$ (4)

MW= 1612 gm/mol; λ_{dia}= -860 x 10^{-6} cm^3mol^{-1} ;

m=12.27 mg ; H = 1T

	Temp.(K)	λ_mT(exp.)	λ_mT(theo.)	μ_{eff} (exp.)	μ_{eff}(theo.)
1	2	1.99243	3.02359	4.00876	4.93833
2	4.999	3.46621	4.01102	5.28744	5.68782
3	9.996	4.56533	4.65646	6.06812	6.12839
4	15	4.96198	4.94213	6.32624	6.31358
5	20.003	5.09559	5.05135	6.41085	6.38296
6	30.001	5.10728	5.07334	6.4182	6.39684
7	40	5.0382	5.02374	6.37465	6.36549
8	50	4.96035	4.9668	6.3252	6.32931
9	60.031	4.89486	4.91575	6.28331	6.2967
10	70.052	4.84391	4.87261	6.25052	6.26901
11	80.071	4.80548	4.83651	6.22568	6.24575
12	90.081	4.77253	4.80622	6.2043	6.22616
13	100.07	4.7401	4.78062	6.18318	6.20955
14	110.12	4.71522	4.75861	6.16693	6.19524
15	120.14	4.69132	4.7397	6.15129	6.18292
16	130.16	4.67169	4.72325	6.1384	6.17218
17	140.17	4.6551	4.70885	6.12749	6.16277
18	150.19	4.64667	4.69611	6.12194	6.15442
19	160.19	4.6361	4.6848	6.11498	6.14701
20	170.2	4.63168	4.67468	6.11206	6.14037
21	180.21	4.62484	4.66557	6.10755	6.13438
22	190.15	4.61775	4.65738	6.10286	6.12899
23	200.23	4.61749	4.64984	6.10269	6.12403
24	210.23	4.61483	4.64302	6.10093	6.11954
25	220.24	4.61881	4.63677	6.10356	6.11542
26	230.24	4.62173	4.63103	6.10549	6.11163
27	240.26	4.62821	4.62572	6.10977	6.10813
28	250.25	4.63203	4.62083	6.11229	6.1049
29	260.25	4.63361	4.61628	6.11333	6.10189
30	270.24	4.63972	4.61206	6.11736	6.0991
31	280.24	4.63367	4.60812	6.11337	6.0965
32	290.26	4.62858	4.60442	6.11001	6.09405

Complex $[Cu^{II}_2(\mu\text{-MeO})L^2(THF)_2]$ (5)

MW= 724 gm/mol; λ_{dia}= -375 x 10^{-6} cm^3mol^{-1} ;

m=25.53 mg ; H = 1T

	Temp.(K)	λ_mT(exp.)	λ_mT(theo.)	μ_{eff} (exp.)	μ_{eff}(theo.)
1	1.999	2.38659E-4	5.997E-5	0.04387	0.02199
2	5.002	4.48819E-4	1.5006E-4	0.06017	0.03479
3	10.003	6.13843E-4	3.0009E-4	0.07036	0.0492
4	15	7.08861E-4	4.5E-4	0.07561	0.06025
5	20.002	7.85329E-4	6.0006E-4	0.07959	0.06957
6	30	9.31086E-4	9.00031E-4	0.08666	0.0852
7	39.999	0.00111	0.0012	0.09447	0.09851
8	50.01	0.0026	0.00155	0.14478	0.11182
9	60.03	0.00516	0.00212	0.20402	0.13069
10	70.048	0.00493	0.00328	0.19944	0.16273
11	80.065	0.00636	0.00557	0.22647	0.21192
12	90.092	0.00996	0.00951	0.28345	0.27691
13	100.1	0.0158	0.0155	0.35694	0.35361
14	110.12	0.02385	0.02381	0.43861	0.4382
15	120.13	0.0341	0.03445	0.52447	0.5271
16	130.15	0.04631	0.04732	0.61119	0.61781
17	140.18	0.06049	0.0622	0.69847	0.7083
18	150.18	0.07555	0.0787	0.78063	0.7967
19	160.19	0.09095	0.09652	0.85649	0.88232
20	170.13	0.10514	0.11517	0.92088	0.96382
21	180.09	0.15125	0.1345	1.1045	1.04153
22	190.22	0.12857	0.1545	1.01833	1.1163
23	200.24	0.18132	0.17438	1.20932	1.18595
24	210.23	0.20026	0.19409	1.27091	1.25118
25	220.24	0.22112	0.21356	1.33545	1.31244
26	230.24	0.23972	0.23261	1.3905	1.36971
27	240.26	0.25684	0.25119	1.43931	1.42338
28	250.24	0.27393	0.26913	1.48642	1.47333
29	260.26	0.28833	0.28653	1.52498	1.52021
30	270.25	0.30181	0.30324	1.56021	1.5639
31	280.24	0.31502	0.31929	1.59399	1.60477
32	290.25	0.32557	0.33473	1.62047	1.6431

Complex $[L^2{}_2Cu^{II}{}_4(\mu_4\text{-}O)]$ (6)

MW= 1402 gm/mol; λ_{dia}= -800 x 10^{-6} cm^3mol^{-1} ;

m=30.85 mg ; H = 1T

	Temp.(K)	λ_mT(exp.)	λ_mT(theo.)	μ_{eff} (exp.)	μ_{eff}(theo.)
1	1.999	0.0022	0.00311	0.13308	0.15849
2	4.999	0.00371	0.00383	0.17301	0.17586
3	10.002	0.00522	0.00503	0.20511	0.20152
4	15	0.00659	0.00623	0.2306	0.22424
5	20.002	0.00812	0.00744	0.25587	0.24495
6	30.001	0.01206	0.01023	0.31192	0.28719
7	40	0.01984	0.01593	0.40001	0.3584
8	50.007	0.03558	0.02881	0.53567	0.48208
9	60.031	0.06053	0.05171	0.69869	0.64584
10	70.05	0.09999	0.08475	0.89805	0.82678
11	80.07	0.13952	0.12628	1.06082	1.0092
12	90.081	0.18582	0.17387	1.22424	1.18422
13	100.06	0.23476	0.22505	1.37604	1.34729
14	110.13	0.28524	0.27849	1.51679	1.49873
15	120.14	0.33583	0.33188	1.64581	1.63609
16	130.16	0.38596	0.3845	1.76438	1.76103
17	140.17	0.43497	0.43554	1.87304	1.87427
18	150.18	0.48179	0.48461	1.97128	1.97704
19	160.2	0.52705	0.53152	2.06178	2.07051
20	170.2	0.57019	0.57602	2.14451	2.15544
21	180.22	0.61144	0.61827	2.22073	2.23309
22	190.22	0.65108	0.65816	2.29159	2.30401
23	200.25	0.6884	0.69598	2.35635	2.36928
24	210.24	0.72414	0.73156	2.41674	2.42909
25	220.24	0.75845	0.76522	2.47333	2.48434
26	230.24	0.79234	0.79704	2.52798	2.53546
27	240.25	0.82178	0.82717	2.57453	2.58294
28	250.24	0.85384	0.85564	2.62426	2.62702
29	260.26	0.88109	0.8827	2.66581	2.66824
30	270.26	0.90834	0.90832	2.70672	2.70669
31	280.25	0.93295	0.93264	2.74314	2.74268
32	290.25	0.95817	0.95579	2.77997	2.77651

Complex $Fe^{III}_2 L^2_2$ (7)

MW= 1246 gm/mol; λ_{dia}= -800 x 10^{-6} cm^3mol^{-1} ;

m=27.76 mg ; H = 1T

	Temp.(K)	λ_mT(exp.)	λ_mT(theo.)	μ_{eff} (exp.)	μ_{eff}(theo.)
1	1.999	0.00938	0.01317	0.27506	0.32595
2	4.998	0.01856	0.01519	0.38687	0.35002
3	10	0.06601	0.08544	0.72965	0.83012
4	15	0.22492	0.22808	1.34688	1.35632
5	20.003	0.36954	0.37543	1.72642	1.74013
6	30.001	0.64667	0.65673	2.28381	2.3015
7	40.001	0.9198	0.93253	2.72373	2.74251
8	50.007	1.193	1.20706	3.10198	3.1202
9	60.032	1.46667	1.48139	3.43941	3.45663
10	70.053	1.74184	1.7546	3.7482	3.7619
11	80.069	2.01492	2.02567	4.03132	4.04206
12	90.088	2.2852	2.29317	4.29319	4.30067
13	100.11	2.55122	2.55521	4.5362	4.53975
14	110.12	2.80876	2.80954	4.75966	4.76032
15	120.15	3.05992	3.05538	4.96791	4.96422
16	130.17	3.29905	3.29081	5.15837	5.15193
17	140.18	3.52759	3.5151	5.33405	5.3246
18	150.19	3.74458	3.7281	5.49566	5.48355
19	160.19	3.94848	3.92953	5.6433	5.62974
20	170.21	4.14351	4.12013	5.78099	5.76466
21	180.21	4.3233	4.29948	5.90508	5.88879
22	190.22	4.4954	4.46858	6.02147	6.00348
23	200.24	4.65671	4.6279	6.12855	6.10957
24	210.23	4.80675	4.77739	6.2265	6.20746
25	220.24	4.95209	4.91838	6.31993	6.29839
26	230.24	5.08527	5.05099	6.40435	6.38273
27	240.27	5.21458	5.17628	6.48527	6.46141
28	250.25	5.3312	5.2938	6.55739	6.53435
29	260.26	5.44199	5.405	6.62517	6.60262
30	270.25	5.54933	5.50978	6.69019	6.66631
31	280.23	5.65361	5.60871	6.75276	6.72589
32	290.26	5.75484	5.70276	6.81295	6.78205

Complex $Mn^{III}_2L^2_2$ (8a)

MW= 1244gm/mol; λ_{dia}= -600 x 10^{-6} cm^3mol^{-1} ;

m=26.89 mg ; H = 1T

	Temp.(K)	λ_mT(exp.)	λ_mT(theo.)	μ_{eff}(exp.)	μ_{eff}(theo.)
1	1.998	0.25211	0.04311	1.42597	0.58966
2	5.001	0.63175	0.40159	2.25731	1.79974
3	10	1.22521	0.98777	3.14357	2.82258
4	15.001	1.74069	1.5593	3.74696	3.54636
5	20.002	2.198	2.09149	4.21049	4.1072
6	30.003	2.94746	2.94793	4.87576	4.87615
7	39.998	3.49126	3.54096	5.30652	5.34415
8	50.01	3.88691	3.95348	5.59913	5.64687
9	60.031	4.18325	4.25001	5.80865	5.85482
10	70.052	4.4134	4.47086	5.9663	6.00501
11	80.073	4.59476	4.64077	6.08765	6.11805
12	90.084	4.74048	4.77496	6.18343	6.20588
13	100.11	4.85597	4.88366	6.2583	6.27612
14	110.12	4.94917	4.97313	6.31807	6.33335
15	120.11	5.02472	5.04796	6.36611	6.38082
16	130.16	5.08928	5.1119	6.40688	6.4211
17	140.18	5.14118	5.16669	6.43946	6.45542
18	150.19	5.1893	5.21422	6.46953	6.48505
19	160.2	5.2266	5.25589	6.49274	6.51091
20	170.22	5.26353	5.29273	6.51564	6.53369
21	180.21	5.2912	5.32542	6.53274	6.55383
22	190.24	5.31924	5.3548	6.55003	6.57189
23	200.24	5.34432	5.38119	6.56545	6.58806
24	210.23	5.36357	5.40505	6.57726	6.60265
25	220.25	5.3856	5.42681	6.59076	6.61593
26	230.24	5.40325	5.44663	6.60155	6.628
27	240.27	5.41758	5.46488	6.6103	6.63909
28	250.24	5.43033	5.48156	6.61807	6.64922
29	260.27	5.44188	5.49706	6.62511	6.65861
30	270.26	5.45774	5.51136	6.63475	6.66727
31	280.25	5.46841	5.52463	6.64124	6.67529
32	290.26	5.47791	5.53702	6.647	6.68277

Complex $[Mn^{III}_2L^2_2(THF)_2]$ (8b).

MW= 1388 gm/mol; λ_{dia}= -650 x 10^{-6} cm^3mol^{-1} ;

m=3.15 mg ; H = 1T

	Temp.(K)	λ_mT(exp.)	λ_mT(theo.)	μ_{eff} (exp.)	μ_{eff}(theo.)
1	1.998	0.47003	0.93522	1.94706	2.74647
2	4.999	1.67597	2.41695	3.67664	4.41522
3	10.001	3.44863	3.85251	5.27402	5.5743
4	15	4.26771	4.51283	5.867	6.03313
5	20.003	4.69551	4.871	6.15403	6.26798
6	30.001	5.13289	5.24137	6.43427	6.50191
7	39.994	5.35646	5.42935	6.5729	6.61747
8	50.005	5.49297	5.54274	6.65613	6.68622
9	60.024	5.5823	5.61841	6.71004	6.7317
10	70.046	5.64892	5.67243	6.74996	6.76399
11	80.071	5.70341	5.71291	6.78243	6.78808
12	90.084	5.75149	5.74434	6.81096	6.80673
13	100.11	5.78237	5.76949	6.82922	6.82161
14	110.13	5.81254	5.79003	6.84702	6.83374
15	120.14	5.83062	5.80713	6.85766	6.84383
16	130.16	5.84936	5.8216	6.86867	6.85235
17	140.12	5.86428	5.83392	6.87742	6.8596
18	150.18	5.8784	5.84471	6.8857	6.86594
19	160.2	5.88611	5.85411	6.89021	6.87146
20	170.21	5.89856	5.86238	6.89749	6.87631
21	180.21	5.90393	5.86973	6.90063	6.88062
22	190.22	5.90934	5.87631	6.90379	6.88447
23	200.23	5.9171	5.88223	6.90833	6.88794
24	210.23	5.91841	5.88758	6.90909	6.89107
25	220.25	5.93376	5.89246	6.91804	6.89393
26	230.23	5.93129	5.89689	6.9166	6.89652
27	240.26	5.95107	5.90097	6.92813	6.8989
28	250.26	5.94699	5.90471	6.92575	6.90109
29	260.25	5.93893	5.90816	6.92106	6.9031
30	270.25	5.957	5.91136	6.93158	6.90497
31	280.16	5.95511	5.91431	6.93048	6.9067
32	290.25	6.02226	5.9171	6.96944	6.90833

Complex $Cr^{III}_2L^2_2$ (9)

MW= 1238 gm/mol; λ_{dia}= -700 x 10^{-6} cm^3mol^{-1} ;

m=10.09 mg ; H = 1T

	Temp.(K)	λ_mT(exp.)	λ_mT(theo.)	μ_{eff} (exp.)	μ_{eff}(theo.)
1	2	0.05736	0.01887	0.68017	0.39013
2	5.001	0.11509	0.05192	0.96345	0.64712
3	10.003	0.31612	0.25705	1.59677	1.43989
4	15	0.52389	0.47098	2.0556	1.94904
5	20.002	0.72819	0.67751	2.42348	2.33764
6	30.002	1.11131	1.07116	2.99389	2.93931
7	40.002	1.43313	1.4142	3.39986	3.37733
8	50.005	1.6906	1.6933	3.69266	3.6956
9	60.023	1.89877	1.91498	3.9134	3.93007
10	70.051	2.06498	2.09091	4.08109	4.10663
11	80.065	2.20015	2.23167	4.21254	4.24261
12	90.072	2.31339	2.34597	4.31959	4.3499
13	100.12	2.40744	2.44056	4.40652	4.43673
14	110.14	2.48994	2.51936	4.48139	4.50779
15	120.15	2.55765	2.58597	4.54191	4.56699
16	130.16	2.61839	2.64297	4.59553	4.61705
17	140.18	2.66825	2.69229	4.63908	4.65993
18	150.18	2.71428	2.73523	4.67892	4.69694
19	160.2	2.75576	2.77306	4.71454	4.72931
20	170.21	2.79317	2.80653	4.74643	4.75777
21	180.22	2.82974	2.83637	4.7774	4.78299
22	190.23	2.86029	2.86313	4.80312	4.8055
23	200.25	2.88934	2.88728	4.82745	4.82573
24	210.23	2.9176	2.90908	4.851	4.84391
25	220.25	2.93991	2.929	4.86951	4.86047
26	230.26	2.96553	2.94719	4.89068	4.87554
27	240.25	2.98076	2.96384	4.90323	4.88929
28	250.15	3.00401	2.97903	4.92231	4.9018
29	260.26	3.01805	2.99336	4.9338	4.91358
30	270.25	3.03828	3.00647	4.95031	4.92433
31	280.25	3.05423	3.01866	4.96328	4.9343
32	290.26	3.06364	3.03003	4.97092	4.94358

Complex [(V^{IV}=O)$_2$ (μ-$O^{isoprop}$) L^2)] (10)

MW= 924 gm/mol; λ_{dia}= -450 x 10^{-6} cm^3mol^{-1} ;

m=44.21 mg ; H = 1T

	Temp.(K)	λ_mT(exp.)	λ_mT(theo.)	μ_{eff} (exp.)	μ_{eff}(theo.)
1	1.999	0.00312	0.00711	0.1586	0.23952
2	5	0.0038	0.00735	0.17503	0.24353
3	10.004	0.00457	0.00775	0.19192	0.25007
4	15	0.00515	0.00815	0.20386	0.25643
5	20.004	0.00566	0.00855	0.21366	0.26266
6	30.004	0.00668	0.00939	0.23212	0.27514
7	40.004	0.00864	0.01061	0.264	0.29251
8	50.008	0.01604	0.01329	0.35966	0.32736
9	60.03	0.02703	0.01886	0.4669	0.38999
10	70.042	0.03884	0.02837	0.55972	0.47839
11	80.029	0.05328	0.04214	0.65552	0.583
12	90.043	0.07076	0.05989	0.75544	0.69501
13	100.12	0.08783	0.08095	0.84168	0.80805
14	110.13	0.10569	0.10411	0.9233	0.91636
15	120.15	0.12487	0.12859	1.00358	1.01842
16	130.16	0.1464	0.15356	1.08664	1.11292
17	140.17	0.16992	0.17842	1.17067	1.19962
18	150.18	0.19442	0.20272	1.25224	1.27869
19	160.2	0.2188	0.22617	1.32845	1.35062
20	170.21	0.24233	0.24854	1.39804	1.41584
21	180.2	0.26531	0.26971	1.46282	1.4749
22	190.23	0.28632	0.28976	1.51965	1.52875
23	200.24	0.30672	0.30858	1.57284	1.57763
24	210.24	0.3257	0.32623	1.62079	1.62211
25	220.27	0.34264	0.34282	1.66241	1.66286
26	230.25	0.36043	0.3583	1.70502	1.69996
27	240.26	0.37345	0.37284	1.73555	1.73412
28	250.25	0.391	0.38645	1.77585	1.76548
29	260.26	0.40419	0.39924	1.80555	1.79447
30	270.25	0.41793	0.41123	1.83598	1.82122
31	280.27	0.43277	0.42254	1.86831	1.84608
32	290.24	0.44296	0.43313	1.89016	1.86908

Complex $Cu^{II}_2L^3_2$ (12)

MW= 1150 gm/mol; λ_{dia}= -688 x 10^{-6} cm^3mol^{-1} ;

m=23.83 mg ; H = 1T

	Temp.(K)	λ_mT(exp.)	λ_mT(theo.)	μ_{eff} (exp.)	μ_{eff}(theo.)
1	2	0.29294	0.32292	1.53711	1.61386
2	5.003	0.54075	0.50075	2.08841	2.00969
3	10	0.61789	0.6125	2.23241	2.22266
4	14.998	0.66212	0.66162	2.31093	2.31005
5	20.001	0.68506	0.68923	2.35062	2.35777
6	30.001	0.70903	0.71919	2.39139	2.40847
7	39.997	0.72393	0.73515	2.41639	2.43504
8	50.008	0.73466	0.74507	2.43423	2.45142
9	60.027	0.74195	0.75184	2.44628	2.46253
10	70.048	0.74804	0.75675	2.4563	2.47055
11	80.047	0.75442	0.76046	2.46675	2.4766
12	90.086	0.7588	0.76338	2.4739	2.48136
13	100.11	0.76307	0.76573	2.48086	2.48517
14	110.14	0.76605	0.76767	2.48568	2.48831
15	120.15	0.769	0.76928	2.49048	2.49092
16	130.11	0.77044	0.77065	2.4928	2.49314
17	140.17	0.7727	0.77183	2.49646	2.49505
18	150.18	0.77451	0.77286	2.49937	2.49671
19	160.19	0.7764	0.77376	2.50242	2.49816
20	170.2	0.77793	0.77455	2.50489	2.49945
21	180.21	0.77876	0.77526	2.50623	2.50059
22	190.22	0.77929	0.7759	2.50708	2.50161
23	200.23	0.77943	0.77647	2.5073	2.50253
24	210.24	0.77952	0.77699	2.50745	2.50337
25	220.25	0.77914	0.77746	2.50683	2.50413
26	230.24	0.7794	0.77789	2.50726	2.50482
27	240.25	0.77965	0.77829	2.50766	2.50546
28	250.14	0.77919	0.77865	2.50691	2.50604
29	260.26	0.78075	0.77899	2.50943	2.50659
30	270.24	0.78392	0.7793	2.51452	2.50709
31	280.25	0.79093	0.77959	2.52573	2.50756
32	290.24	0.78914	0.77986	2.52287	2.50799

Complex $Co^{III}_2L^3_3$ (14)

MW= 1654gm/mol; λ_{dia}= -1026 x 10^{-6} cm^3mol^{-1} ;

m=55.39 mg ; H = 1T

	Temp.(K)	λ_mT(exp.)	λ_mT(theo.)	μ_{eff} (exp.)	μ_{eff}(theo.)
1	2	0.12429	0.49797	1.99594	0.99717
2	5	0.61984	0.67461	2.32311	2.22681
3	10	0.85717	0.86468	2.6301	2.61865
4	15	1.04218	1.03844	2.88227	2.88746
5	20	1.22355	1.2039	3.10342	3.12864
6	30	1.51795	1.48728	3.44938	3.48477
7	40	1.71275	1.69612	3.68361	3.70162
8	50.01	1.83917	1.83994	3.83661	3.8358
9	60.03	1.92401	1.93759	3.93709	3.92327
10	70.05	1.98323	2.0062	4.0062	3.98319
11	80.05	2.02614	2.05755	4.05714	4.02605
12	90.08	2.05843	2.09089	4.08988	4.058
13	100.11	2.08332	2.11482	4.11322	4.08247
14	110.13	2.10298	2.12936	4.12734	4.10169
15	120.15	2.11883	2.14215	4.13971	4.11712
16	130.16	2.13183	2.14959	4.14689	4.12973
17	140.18	2.14267	2.15611	4.15318	4.14021
18	150.19	2.15181	2.15898	4.15594	4.14903
19	160.21	2.15961	2.16235	4.15919	4.15655
20	170.22	2.16634	2.1652	4.16192	4.16302
21	180.22	2.17219	2.16715	4.16379	4.16863
22	190.15	2.17728	2.16771	4.16433	4.17352
23	200.24	2.18186	2.1732	4.16961	4.1779
24	210.24	2.18589	2.17556	4.17187	4.18176
25	220.25	2.18949	2.17611	4.1724	4.18521
26	230.25	2.19273	2.17374	4.17013	4.1883
27	240.25	2.19566	2.17119	4.16767	4.1911
28	250.25	2.19832	2.16294	4.15975	4.19363
29	260.26	2.20075	2.15769	4.15469	4.19595
30	270.24	2.20296	2.15338	4.15055	4.19805
31	280.26	2.205	2.15181	4.14903	4.2
32	290.23	2.20686	2.15055	4.14781	4.20177

Complex $Fe^{III}_2L^3_3$ (15)

MW= 1648 gm/mol; λ_{dia}= -1026 x 10^{-6} cm^3mol^{-1} ;

m=39.23 mg ; H = 1T, 4T and 7T

Field(T)	Temp. (K)	λ_MT (exp.)	λ_MT (calc.)	Field(T)	Temp. (K)	λ_MT (exp.)	λ_MT (calc.)
1	2	1.2814	1.32305	4	4.227	1.49312	1.47348
1	2.072	1.31592	1.35379	4	4.526	1.56467	1.54571
1	2.134	1.3449	1.37954	4	4.868	1.64043	1.62298
1	2.203	1.37737	1.40743	4	5.265	1.71871	1.70588
1	2.286	1.41386	1.43996	4	5.734	1.80019	1.79506
1	2.366	1.44711	1.47029	4	6.294	1.88313	1.89023
1	2.456	1.4847	1.50326	4	6.975	1.96641	1.99134
1	2.553	1.52373	1.53749	4	7.82	2.05028	2.0979
1	2.659	1.56482	1.57341	4	8.899	2.13159	2.20941
1	2.773	1.60681	1.61039	4	10.324	2.21394	2.3247
1	2.898	1.65117	1.64909	4	12.289	2.28835	2.44201
1	3.034	1.69721	1.68913	4	15.182	2.37049	2.55969
1	3.184	1.74504	1.73095	4	19.858	2.45989	2.67526
1	3.349	1.79436	1.77431	4	28.688	2.59474	2.78592
1	3.533	1.84599	1.81966	4	51.676	2.86958	2.88875
1	3.738	1.89948	1.86677	4	260.01	3.48723	2.98021
1	3.967	1.95316	1.91552	7	1.999	0.55623	0.56193
1	4.23	2.00777	1.96699	7	2.071	0.57576	0.58073
1	4.526	2.06555	2.01979	7	2.14	0.59429	0.59866
1	4.868	2.12686	2.07489	7	2.203	0.61123	0.61494
1	5.265	2.18697	2.132	7	2.285	0.63313	0.63602
1	5.734	2.24849	2.19146	7	2.365	0.65436	0.65646
1	6.293	2.30945	2.25295	7	2.456	0.67844	0.67956
1	6.973	2.37004	2.31668	7	2.553	0.70393	0.70401
1	7.819	2.43414	2.38271	7	2.658	0.73135	0.73026
1	8.9	2.49972	2.45101	7	2.772	0.76088	0.75851
1	10.324	2.57539	2.5213	7	2.897	0.79302	0.78919
1	12.289	2.65165	2.59361	7	3.033	0.82759	0.82222
1	15.182	2.75825	2.66796	7	3.183	0.86526	0.85821
1	19.859	2.90029	2.74414	7	3.349	0.90644	0.89749
1	28.689	3.11649	2.82184	7	3.533	0.95127	0.94037
1	51.679	3.43761	2.9009	7	3.738	1.00025	0.9873
1	260.01	3.74699	2.9809	7	3.968	1.05425	1.03887
4	2	0.78639	0.79131	7	4.229	1.11229	1.09601
4	2.072	0.81346	0.81717	7	4.527	1.17745	1.15942
4	2.133	0.83621	0.83891	7	4.869	1.24899	1.22974
4	2.203	0.86223	0.86365	7	5.267	1.32733	1.30827
4	2.286	0.89267	0.89269	7	5.734	1.41299	1.39587
4	2.369	0.92277	0.92142	7	6.295	1.50684	1.49465
4	2.456	0.954	0.95118	7	6.973	1.60728	1.60485
4	2.553	0.98846	0.98394	7	7.818	1.71529	1.72881
4	2.659	1.02553	1.01921	7	8.897	1.82814	1.86721
4	2.773	1.0647	1.05653	7	10.322	1.94655	2.02016
4	2.898	1.10687	1.09669	7	12.289	2.05885	2.18621
4	3.034	1.1517	1.13949	7	15.182	2.17588	2.36187
4	3.184	1.1999	1.18558	7	19.858	2.28822	2.54053
4	3.349	1.25121	1.23491	7	28.691	2.41846	2.712
4	3.533	1.30644	1.28825	7	51.67	2.65287	2.86321
4	3.738	1.36544	1.34558	7	260.01	3.38497	2.97932
4	3.967	1.4277	1.40701				

Complex $Mn^{IV}_2(L_A^3)_2L^3$ (16)

MW= 1646 gm/mol; λ_{dia}= -1026 x 10^{-6} cm^3mol^{-1} ;

m=46.01 mg ; H = 1T

	Temp. (K)	λ_M	$\lambda_M T$	μ_{eff}
1	2	0.02426	0.44046	1.45348
2	5.001	0.24774	1.40759	1.87883
3	10.003	0.48633	1.97216	2.13161
4	15	0.57824	2.15048	2.24132
5	20.002	0.624	2.23394	2.30295
6	30.001	0.66924	2.31351	2.36986
7	40.002	0.6921	2.35269	2.40557
8	50.004	0.70662	2.37723	2.42777
9	60.034	0.71705	2.39472	2.44295
10	70.053	0.72588	2.40941	2.45395
11	80.076	0.73448	2.42365	2.4623
12	90.09	0.74113	2.43459	2.46884
13	100.09	0.74665	2.44365	2.47411
14	110.13	0.7518	2.45205	2.47845
15	120.16	0.75601	2.45891	2.48209
16	130.17	0.75957	2.4647	2.48517
17	140.17	0.76271	2.46979	2.48782
18	150.19	0.76559	2.47444	2.49013
19	160.14	0.76791	2.47819	2.49214
20	170.22	0.77051	2.48239	2.49394
21	180.21	0.77307	2.48651	2.49553
22	190.23	0.77588	2.49101	2.49696
23	200.24	0.77931	2.49651	2.49824
24	210.24	0.78424	2.5044	2.49941
25	220.25	0.7896	2.51295	2.50047
26	230.24	0.77319	2.4867	2.50144
27	240.25	0.80057	2.53034	2.50233
28	250.26	0.80787	2.54185	2.50315
29	260.28	0.81605	2.55468	2.50391
30	270.26	0.82373	2.56668	2.50461
31	280.26	0.83497	2.58413	2.50526
32	290.25	0.84273	2.59611	2.50587

Complex $Co^{III}_2L^4_3$ (17)

MW/2= 962 gm/mol; $\lambda_{dia}/2$= -610 x 10^{-6} cm^3mol^{-1} ;

m=35.04 mg ; H = 1T

	Temp.(K)	λ_mT (exp.)	λ_mT (theo.)	μ_{eff} (exp.)	μ_{eff} (theo.)
1	1.999	1.20088	0.90888	3.09905	2.69608
2	4.999	1.48573	1.32593	3.44706	3.25641
3	10	1.56517	1.55712	3.53802	3.52891
4	15.001	1.59172	1.64722	3.5679	3.62957
5	20.002	1.60308	1.6855	3.58061	3.6715
6	30.002	1.60473	1.68889	3.58245	3.67519
7	39.999	1.58877	1.65107	3.56459	3.63381
8	50.007	1.56656	1.60318	3.53959	3.58072
9	60.017	1.53916	1.55685	3.5085	3.5286
10	70.045	1.51082	1.51551	3.47605	3.48144
11	80.071	1.48645	1.47974	3.4479	3.44011
12	90.058	1.46145	1.44915	3.41878	3.40436
13	100.1	1.43819	1.42272	3.39147	3.37318
14	110.13	1.4174	1.39996	3.36686	3.34609
15	120.16	1.39838	1.3802	3.3442	3.32239
16	130.11	1.37794	1.36307	3.31967	3.30171
17	140.17	1.34986	1.34784	3.28567	3.28321
18	150.18	1.33625	1.33442	3.26906	3.26682
19	160.19	1.32542	1.32248	3.25579	3.25218
20	170.2	1.31445	1.31179	3.24229	3.239
21	180.22	1.30508	1.30216	3.23071	3.22709
22	190.23	1.29528	1.29346	3.21856	3.2163
23	200.23	1.28665	1.28557	3.20782	3.20647
24	210.24	1.27879	1.27837	3.198	3.19748
25	220.25	1.27137	1.27177	3.18871	3.18921
26	230.16	1.26307	1.26577	3.17829	3.18168
27	240.25	1.2554	1.26014	3.16862	3.1746
28	250.26	1.25063	1.25497	3.1626	3.16808
29	260.27	1.24408	1.25018	3.1543	3.16203
30	270.23	1.23859	1.24576	3.14734	3.15643
31	280.27	1.23284	1.2416	3.14002	3.15116
32	290.26	1.22827	1.23773	3.1342	3.14624

Complex $Mn^{IV}(L_A^6)(L^6)_2$ (18)

MW= 1276 gm/mol; λ_{dia}= -750 x 10^{-6} cm^3mol^{-1} ;

m=43.71 mg ; H = 1T

	Temp.(K)	λ_mT(exp.)	λ_mT(theo.)	μ_{eff} (exp.)	μ_{eff}(theo.)
1	1.999	0.18322	0.34439	1.21563	1.66664
2	5.004	0.34322	0.3546	1.66381	1.69117
3	10.004	0.45162	0.35612	1.90855	1.69478
4	15.001	0.35495	0.3564	1.69201	1.69546
5	20.002	0.35628	0.3565	1.69517	1.6957
6	30.003	0.35768	0.35657	1.69851	1.69587
7	39.994	0.35764	0.3566	1.6984	1.69594
8	50.012	0.35837	0.35662	1.70015	1.69597
9	60.036	0.35818	0.35663	1.69969	1.69599
10	70.036	0.35835	0.35663	1.70008	1.69601
11	80.062	0.35888	0.35664	1.70135	1.69602
12	90.099	0.35905	0.35664	1.70174	1.69604
13	100.11	0.35896	0.35666	1.70153	1.69607
14	110.13	0.35867	0.35668	1.70085	1.69613
15	120.16	0.35865	0.35674	1.7008	1.69626
16	130.16	0.35816	0.35684	1.69964	1.69651
17	140.18	0.35794	0.35703	1.69912	1.69696
18	150.18	0.35806	0.35734	1.6994	1.69769
19	160.2	0.35806	0.35781	1.69941	1.69881
20	170.2	0.35829	0.35849	1.69994	1.70041
21	180.22	0.35902	0.35942	1.70167	1.70262
22	190.23	0.36001	0.36065	1.70402	1.70553
23	200.23	0.36133	0.36222	1.70713	1.70924
24	210.15	0.35991	0.36415	1.70379	1.71379
25	220.25	0.36526	0.36653	1.71641	1.71939
26	230.24	0.36819	0.36934	1.72327	1.72596
27	240.26	0.37009	0.37262	1.72772	1.7336
28	250.26	0.37562	0.37637	1.74057	1.74231
29	260.03	0.37788	0.38052	1.74581	1.75188
30	270.27	0.38572	0.38537	1.76383	1.76303
31	280.24	0.38876	0.39061	1.77076	1.77497
32	290.22	0.40336	0.39635	1.80371	1.78796

Complex $Co^{III}(L^6)_3$ (23)

MW= 1282 gm/mol; λ_{dia}= -750 x 10^{-6} cm^3mol^{-1} ;

m=33.01 mg ; H = 1T

	Temp.(K)	λ_mT(exp.)	λ_mT(theo.)	μ_{eff} (exp.)	μ_{eff}(theo.)
1	2	0.97157	1.21805	2.78751	3.12113
2	5.003	1.67421	1.56491	3.65919	3.53773
3	10.002	2.16215	1.71231	4.15836	3.70059
4	15	1.75745	1.76464	3.74905	3.75671
5	20.003	1.76257	1.78928	3.7545	3.78285
6	30.001	1.76313	1.80106	3.7551	3.79528
7	40.008	1.75495	1.7848	3.74638	3.77811
8	50	1.73579	1.7541	3.72587	3.74547
9	60.026	1.7113	1.71715	3.6995	3.70581
10	70.052	1.6844	1.67895	3.6703	3.66436
11	80.094	1.65758	1.64202	3.64097	3.62384
12	90.097	1.62726	1.60772	3.60751	3.58579
13	100.1	1.59816	1.57631	3.57511	3.55059
14	110.14	1.56591	1.54772	3.53886	3.51824
15	120.18	1.53605	1.52189	3.50495	3.48876
16	130.16	1.50892	1.49872	3.47386	3.4621
17	140.18	1.48782	1.47771	3.44949	3.43775
18	150.19	1.46745	1.45872	3.42579	3.41559
19	160.2	1.4495	1.44149	3.40478	3.39536
20	170.21	1.43161	1.42582	3.3837	3.37685
21	180.14	1.4143	1.41164	3.36318	3.36002
22	190.23	1.39951	1.39846	3.34555	3.34429
23	200.23	1.38437	1.38648	3.3274	3.32994
24	210.24	1.37037	1.37545	3.31054	3.31667
25	220.25	1.35768	1.36527	3.29517	3.30437
26	230.26	1.34468	1.35586	3.27936	3.29296
27	240.25	1.33336	1.34715	3.26553	3.28237
28	250.26	1.31966	1.33903	3.24871	3.27246
29	260.27	1.31133	1.33147	3.23844	3.26321
30	270.26	1.30753	1.32443	3.23374	3.25457
31	280.27	1.2909	1.31783	3.21311	3.24645
32	290.16	1.28257	1.31171	3.20273	3.23891

Complex $Fe^{III}(L^6)_3$ (24)

MW= 1277 gm/mol; λ_{dia}= -750 x 10^{-6} cm^3mol^{-1} ;

m=36.24 mg ; H = 1T

	Temp.(K)	λ_m(exp.)	λ_mT(exp.)	μ_{eff} (exp.)
1	2	0.02597	0.05193	0.6445
2	5.001	0.01737	0.08689	0.8336
3	10.003	0.01016	0.10161	0.9015
4	14.999	0.00708	0.10621	0.9216
5	20.003	0.00543	0.1087	0.9324
6	29.999	0.00372	0.11169	0.9451
7	40	0.00286	0.11428	0.956
8	50.009	0.00234	0.11718	0.9681
9	60.023	0.00202	0.12138	0.9853
10	70.041	0.00182	0.12719	1.0086
11	80.034	0.00166	0.13257	1.0297
12	90.083	0.00153	0.13821	1.0513
13	100.1	0.00144	0.14408	1.0735
14	110.12	0.00137	0.15099	1.0989
15	120.17	0.00133	0.15941	1.1291
16	130.16	0.00131	0.17066	1.1683
17	140.18	0.00135	0.18933	1.2305
18	150.19	0.00151	0.22696	1.3473
19	160.2	0.00185	0.29656	1.54
20	170.21	0.00238	0.40525	1.8003
21	180.09	0.00296	0.53316	2.0649
22	190.23	0.00339	0.64459	2.2705
23	200.23	0.00369	0.73845	2.4302
24	210.24	0.00387	0.81323	2.5503
25	220.27	0.00397	0.8751	2.6455
26	230.25	0.00402	0.92676	2.7225
27	240.26	0.00404	0.97116	2.7869
28	250.24	0.00404	1.0101	2.8423
29	260.25	0.00402	1.0469	2.8936
30	270.24	0.00399	1.0794	2.9381
31	280.26	0.00397	1.1121	2.9824
32	290.25	0.00392	1.1382	3.0171

Complex $Fe^{III}(L^{11})_3$ (25)

MW= 1049 gm/mol; λ_{dia}= -550 x 10^{-6} cm^3mol^{-1} ;

m=40.29 mg ; H = 1T

	Temp.(K)	λ_mT(exp.)	λ_mT(theo.)	μ_{eff} (exp.)	μ_{eff}(theo.)
1	1.999	0.28784	0.68833	1.51724	2.34627
2	5	0.69449	0.85478	2.35674	2.6146
3	10.005	1.0698	0.92394	2.92503	2.71832
4	15.001	0.94635	0.94859	2.7511	2.75435
5	20.001	0.96578	0.96124	2.77919	2.77265
6	30.003	0.9801	0.97409	2.79972	2.79113
7	40.002	0.98448	0.98059	2.80597	2.80042
8	50.006	0.98696	0.98452	2.80949	2.80602
9	60.028	0.98787	0.98715	2.8108	2.80977
10	70.039	0.9881	0.98903	2.81112	2.81244
11	80.087	0.98936	0.99045	2.81291	2.81446
12	90.099	0.99038	0.99157	2.81437	2.81605
13	100.08	0.98995	0.9925	2.81375	2.81738
14	110.15	0.99095	0.99336	2.81517	2.8186
15	120.16	0.99075	0.99422	2.81489	2.81982
16	130.16	0.99099	0.99519	2.81524	2.8212
17	140.18	0.99122	0.99637	2.81555	2.82287
18	150.19	0.99309	0.99786	2.81821	2.82497
19	160.19	0.9946	0.99975	2.82035	2.82764
20	170.21	0.99723	1.00214	2.82408	2.83102
21	180.22	1.00039	1.0051	2.82855	2.8352
22	190.14	1.00311	1.00868	2.83239	2.84025
23	200.23	1.0085	1.01304	2.83999	2.84638
24	210.23	1.01346	1.01813	2.84697	2.85352
25	220.25	1.02078	1.02404	2.85723	2.86179
26	230.23	1.02851	1.03075	2.86803	2.87115
27	240.25	1.03558	1.03835	2.87787	2.88172
28	250.26	1.04655	1.04681	2.89307	2.89343
29	260.26	1.05587	1.05614	2.90593	2.9063
30	270.26	1.06704	1.06634	2.92126	2.9203
31	280.25	1.07877	1.07739	2.93727	2.93539
32	290.26	1.08966	1.08931	2.95206	2.95158

Complex $[Fe^{III}_2(\mu\text{-}O)(L^{12})_4]$ (26)

MW= 1532 gm/mol; λ_{dia}= -820 x 10^{-6} cm^3mol^{-1} ;

m=25.28 mg ; H = 1T

	Temp.(K)	λ_mT(exp.)	λ_mT(theo.)	μ_{eff} (exp.)	μ_{eff}(theo.)
1	2	0.01033	0.02634	0.28863	0.46096
2	5.004	0.02255	0.02634	0.42645	0.46096
3	9.999	0.02871	0.02634	0.48121	0.46096
4	15.003	0.02738	0.02634	0.46992	0.46096
5	20.003	0.02573	0.02634	0.45556	0.46096
6	30.003	0.02689	0.02637	0.46569	0.46115
7	39.996	0.02776	0.02676	0.47322	0.46455
8	50.009	0.03036	0.02878	0.49485	0.48181
9	60.037	0.03566	0.03429	0.53627	0.52589
10	70.048	0.04639	0.04467	0.61166	0.60023
11	80.062	0.06261	0.06037	0.71065	0.6978
12	90.107	0.08344	0.08103	0.82034	0.80841
13	100.11	0.11627	0.10552	0.96839	0.92254
14	110.14	0.13358	0.13291	1.03797	1.03536
15	120.15	0.15994	0.16205	1.13578	1.14327
16	130.16	0.21356	0.19223	1.31242	1.24515
17	140.18	0.23133	0.22289	1.36596	1.34079
18	150.19	0.27284	0.25361	1.48344	1.43022
19	160.2	0.29906	0.28422	1.55309	1.51407
20	170.2	0.3259	0.31457	1.62129	1.59286
21	180.22	0.35259	0.34472	1.68637	1.66744
22	190.22	0.37975	0.37453	1.75012	1.73805
23	200.25	0.40613	0.40419	1.80989	1.80555
24	210.23	0.43451	0.43347	1.87205	1.86981
25	220.25	0.46061	0.46268	1.92746	1.93179
26	230.25	0.4855	0.49167	1.97885	1.99138
27	240.26	0.51565	0.52055	2.03937	2.04903
28	250.25	0.54393	0.54925	2.09454	2.10477
29	260.26	0.56956	0.57791	2.14332	2.15898
30	270.26	0.59213	0.60645	2.18538	2.21165
31	280.27	0.6237	0.63494	2.24288	2.263
32	290.26	0.6542	0.66329	2.29706	2.31298

Complex $Ni_2L^3{}_2$ (13) and $Mn^{IV}(L_A{}^8)(L^8)_2$ (20)

MW= 1140 (**13**) and 1024 (**20**) gm/mol; λ_{dia}= -680 x 10^{-6} (**13**) and -560 x 10^{-6} (**20**) cm^3mol^{-1} ; m=36.40(**13**) and 23.09(**20**) mg ; H = 1T

	Temp.(K) (**13**)	μ_{eff}(exp.) (**13**)		Temp.(K) (**20**)	μ_{eff}(exp.) (**20**)	μ_{eff}(theo.) (**20**)
1	1.998	0.3282	1	1.999	1.30222	1.68697
2	5.001	0.4292	2	5	1.68037	1.71264
3	10.003	0.5007	3	10.005	1.70354	1.71642
4	15	0.5269	4	14.999	1.70483	1.71712
5	20.002	0.5334	5	20.001	1.70684	1.71737
6	29.999	0.533	6	30.002	1.70944	1.71755
7	40	0.5295	7	39.999	1.71132	1.71761
8	50.007	0.5376	8	50.008	1.71349	1.71764
9	60.032	0.5502	9	60.029	1.71362	1.71766
10	70.047	0.5648	10	70.054	1.71521	1.71766
11	80.071	0.5799	11	80.071	1.71717	1.71767
12	90.084	0.5937	12	90.096	1.71848	1.71768
13	100.13	0.6055	13	100.1	1.71955	1.71768
14	110.13	0.6148	14	110.18	1.72112	1.71768
15	120.16	0.6247	15	120.13	1.72147	1.71769
16	130.17	0.6359	16	130.11	1.72069	1.7177
17	140.17	0.646	17	140.17	1.72094	1.71772
18	150.19	0.6547	18	150.19	1.71989	1.71776
19	160.2	0.6609	19	160.2	1.71847	1.71784
20	170.21	0.6627	20	170.2	1.71563	1.71797
21	180.18	0.6676	21	180.21	1.71226	1.71817
22	190.22	0.6727	22	190.21	1.71075	1.71849
23	200.24	0.6776	23	200.22	1.70885	1.71895
24	210.24	0.6858	24	210.15	1.70883	1.71958
25	220.26	0.6946	25	220.26	1.7137	1.72045
26	230.25	0.6983	26	230.26	1.7119	1.72157
27	240.28	0.7087	27	240.26	1.71445	1.72299
28	250.26	0.7193	28	250.25	1.72128	1.72475
29	260.27	0.7213	29	260.27	1.72563	1.72691
30	270.25	0.7293	30	270.26	1.73009	1.72947
31	280.25	0.7546	31	280.26	1.73354	1.73249
32	290.24	0.7425	32	290.24	1.74971	1.73599

Complex $Mn^{IV}(L_A^9)(L^9)_2$ (21) and $Mn^{IV}(L_A^{10})(L^{10})_2$ (22)

MW= 1147 (**21**) and 1120 (**22**) gm/mol; λ_{dia}= -600 x 10^{-6} (**21**) and -600 x 10^{-6} (**22**) cm^3mol^{-1} ; m=44.83(**21**) and 32.44(**22**) mg ; H = 1T

	Temp.(K) (**21**)	μ_{eff}(exp.) (**21**)	μ_{eff}(theo.) (**21**)		Temp.(K) (**22**)	μ_{eff}(exp.) (**22**)	μ_{eff}(theo.) (**22**)
1	1.999	1.09263	1.77633	1	1.998	1.44496	1.6941
2	5.023	1.66037	1.80614	2	5.001	1.69474	1.71991
3	10.003	2.02483	1.81049	3	10.005	1.71419	1.7237
4	15.001	1.78425	1.81132	4	15.001	1.71721	1.72441
5	20.002	1.77662	1.81162	5	20.003	1.72004	1.72466
6	29.999	1.78627	1.81184	6	30	1.72276	1.72484
7	40	1.79329	1.81193	7	39.998	1.72462	1.7249
8	50.006	1.80006	1.81198	8	50.009	1.72716	1.72493
9	60.037	1.80532	1.81202	9	60.024	1.72783	1.72494
10	70.063	1.80889	1.81205	10	70.057	1.72878	1.72496
11	80.063	1.81462	1.81207	11	80.071	1.73104	1.72496
12	90.106	1.81937	1.8121	12	90.086	1.73266	1.72497
13	100.1	1.82295	1.81214	13	100.09	1.73375	1.72497
14	110.12	1.82677	1.8122	14	110.13	1.7348	1.72499
15	120.14	1.82987	1.81233	15	120.15	1.73499	1.72503
16	130.16	1.83263	1.81257	16	130.16	1.73429	1.7251
17	140.12	1.83465	1.81297	17	140.18	1.73264	1.72525
18	150.19	1.83761	1.81364	18	150.19	1.7302	1.72551
19	160.2	1.84008	1.81466	19	160.19	1.72753	1.72594
20	170.2	1.84221	1.81613	20	170.21	1.72569	1.72661
21	180.22	1.84389	1.81815	21	180.22	1.72672	1.72757
22	190.23	1.84542	1.82083	22	190.23	1.72604	1.72891
23	200.23	1.84685	1.82425	23	200.15	1.73008	1.73068
24	210.25	1.84882	1.82851	24	210.24	1.72997	1.73301
25	220.24	1.84798	1.83365	25	220.25	1.73436	1.73591
26	230.25	1.85139	1.83977	26	230.24	1.73374	1.73946
27	240.26	1.85403	1.8469	27	240.26	1.73623	1.74373
28	250.26	1.85907	1.85506	28	250.25	1.74067	1.74875
29	260.17	1.85601	1.86418	29	260	1.73667	1.75441
30	270.24	1.85992	1.8745	30	270.24	1.75211	1.76119
31	280.27	1.87352	1.88584	31	280.27	1.76335	1.76869
32	290.24	1.87872	1.89813	32	290.27	1.79002	1.77703

3) Magnetic and EPR data.

The complexes **19-22** exhibit similar EPR spectra within the range 310mT to 370mT (Figure 4.8, Chapter 4). The simulation of the spectra between 326 mT and 332 mT are shown below along with the parameters used.

19

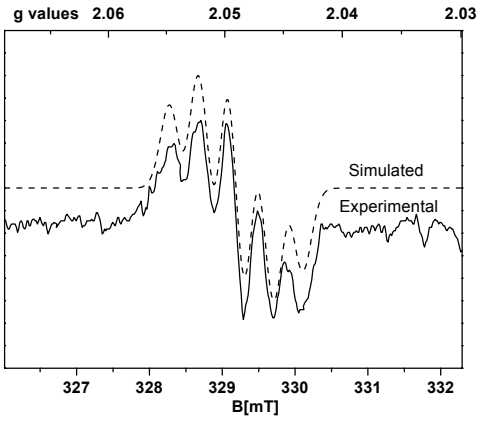

A_{Mn} = 106.7 G

A_N = 4.20 G

A_H = 4.62 G

A_H = 2.71 G

20

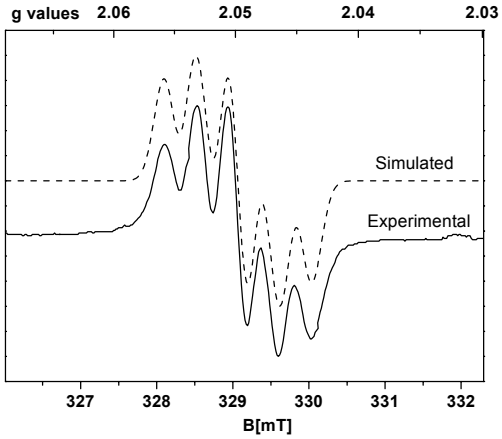

A_{Mn} = 106.6 G

A_N = 4.36 G

A_H = 5.15 G

A_H = 2.83 G

21

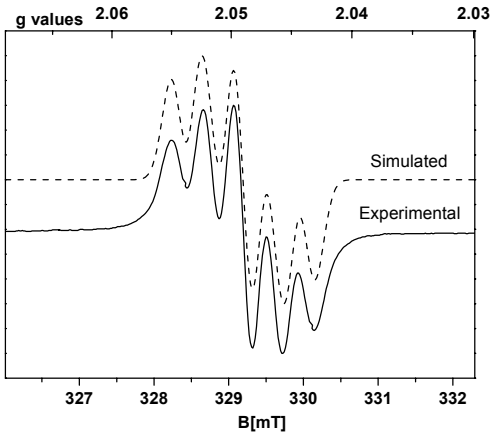

A_{Mn} = 106.7 G

A_N = 4.29 G

A_H = 5.15 G

A_H = 2.83 G

22

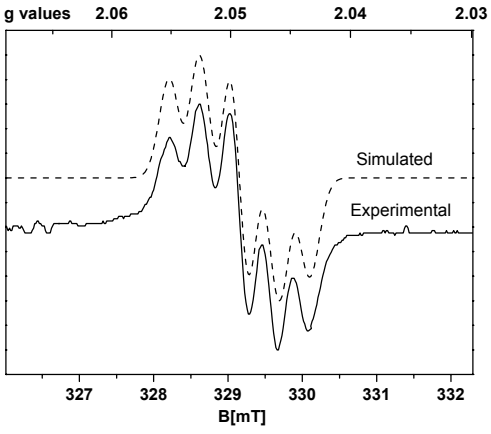

A_{Mn} = 106.9 G

A_N = 4.23 G

A_H = 5.02 G

A_H = 2.78 G

The magnetic data for complexes **13**, **20-23** is given below together with the parameters used for simulation.

13

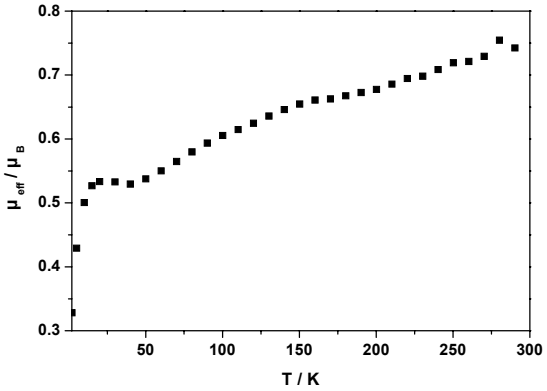

20

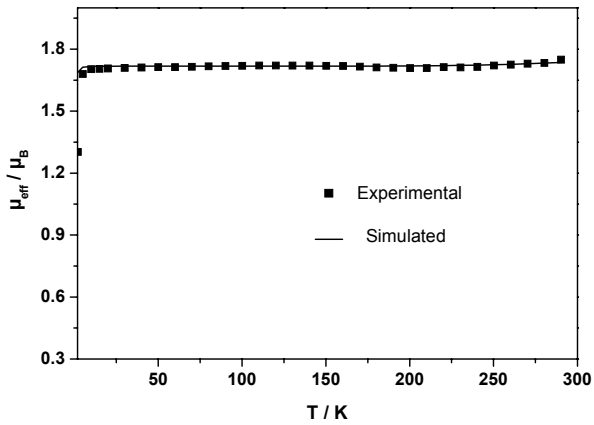

$J_{12} = J_{23} = -400\ cm^{-1}$

$g_1 = g_3 = 2.00$

$g_2 = 1.99$

21

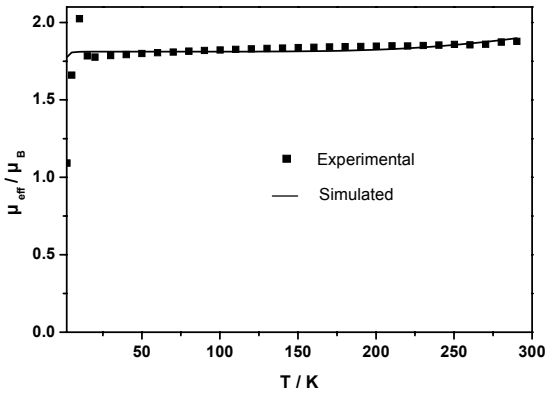

$J_{12} = J_{23} = -295\ cm^{-1}$

$g_1 = g_3 = 2.0$

$g_2 = 2.05$

22

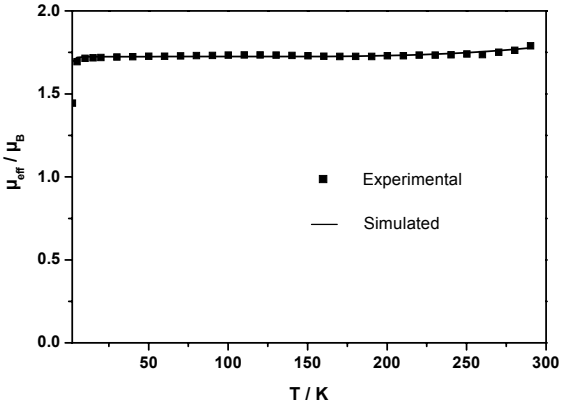

$J_{12} = J_{23} = -330\ cm^{-1}$

$g_1 = g_3 = 2.00$

$g_2 = 1.99$